Modelling Baroreceptors Function

MICHEL EDWAR KHALIL MICKAEL

School of Engineering

And Computing Sciences

Michel Edwar Michael

Durham University

Department of Engineering

November 2011

Abstract

Cardiovascular diseases form one of the most dangerous events that affect human life. They are usually the result of high blood pressure. Thus controlling blood pressure within patient specific healthy limits is a goal that we must target. There are two control loops for blood haemostasis inside the body either long term or short term. Baroreceptors control the short term blood pressure regulation. They are nerve ending that exist in certain locations within the blood vessels walls and they report blood pressure into the brain and the central nervous system. However the basics of their function are not yet known. We propose here that the baroreceptors work by converting circumferential and axial pressure into a stress into their respective direction and they start to send nerve signals based on a threshold of strain energy of the location they are embedded in. Thus baroreceptors A fibre is highly likely to exist in the stiffer adventitia, while the media will contain C fibres. This explains the reason behind having identical fibres with different threshold. We were able to arrive to this solution by getting a relationship between stress–strain relationship for the whole wall and for the arterial vessels. These findings are quiet significant as they allow a method to identify different stress in the arterial wall layers using whole wall experimental data and also as they were able to differentiate between different fibres based on their locations inside the arterial wall. A complete modelling of the baroreceptors function might lead to the formation of biosynthetic material that could interact with the body on the cellular level, so as to give humans the mean to the control of short term blood regulation thus preventing hypertension and its accompanying diseases such as atherosclerosis.

Modelling Baroreceptors Function

By

Michel Edwar Khalil Mickael

Submitted in accordance with requirements for the degree of doctor of philosophy

DURHAM UNIVERSITY

DEPARTMENT OF ENGINEERING

NOVEMBER 2011

Contents

Nomenclature

Symbol	Definition	Unit
E_{ym}	Young's modulus	N/m²
H_{radf}	Radial load on the wall	N
I_1	First strain invariant	
I_4	Fourth strain invariant	
I_{cur}	Current	A
R_{res}	Resistance	Ω
$\overline{W}$	Strain-energy	J
$W_{elastin}$	Elastin strain energy	J
$W_{icaniso}$	Collagen strain energy	J
α_{ext}	External work	J
α_{int}	Internal work	J
η_{rd}	Radius deformation.	m
η_d	Virtual displacement	
ρ_{disp}	Dispersion factor	
$\sigma_{viscoelastic}$	Stress viscoelastic	N/m²
$\mathbf{A_1}$	Direction of one family of collagen	
$\mathbf{V_i}$	Velocity in the undeformed configuration	m/s
$\boldsymbol{A_{acc}}$	Acceleration in the undeformed configuration	m/s^2
$\mathbb{C}_{ABCD}$	Elastic modulus	
a	Material parameter	Nm^{-2}
a_1 to a_7	Material parameter	Nm^{-2}
$a_{\theta\theta}$, a_{zz}, $a_{\theta z}$	Material constants	
b	Dimensionless material parameter	Nm^{-2}
b_f	Body force	N/kg
b_1, b_2, b_3	Material constants	
C	Right Cauchy-green tensor	
c_1	Material parameter	Nm^{-2}
D	Material matrix	
E	Green Lagrange strain tensor	
e_1, e_2, e_3,	Ortho-normal vectors	
E_{inc}	Incremental elasticity modulus	N/m^2
F	Deformation gradient	
F_a	Axial force	N
F_{res}	Resultant force	N
G_m	Shear modulus	N/m²
G	Elasticity	Pa
H	Thickness	m
h	Deformed thickness	m
F	Deformation gradient	
F_a	Axial force	N
F_{res}	Resultant force	N
G_m	Shear modulus	N/m²
G	Elasticity	Pa
H	Thickness	m

h	Deformed thickness	m
J	Jacobian	
K	Timoshenko shear correction factor	
k_1	Material parameter	Nm^{-2}
k_2	Dimensionless material parameter	
L	Linear momentum	kg m/s
m	Mass	Kg
n	Unit vector	
P	Pressure	N/m2
r	Deformed radius	m
R_i	Inner radius	m
R_{or}	Original vessel radius	m
R_o	Outer radius	m
S	Second piola kirchhoff stress tensor	N/m^2
s_{sa}	Area in the deformed state	m^2
S_{sa}	Area in the undeformed state	
t	Time	
t	Cauchy or true traction	N/m^2
T	First piola-kirchhoff (nominal) traction vector	N/m^2
U	Displacement	m
U	Displacement in the undeformed configuration	m
u	Displacement in the deformed configuration	m
U_{volt}	Voltage	V
v	Volume in the undeformed configuration	m^3
V	Volume in the deformed configuration	m^3
$\mathbf{v_i}$	Velocity in the deformed configuration	m/s
X	Point in th undeformed configuration	
x	Point in the deformed configuration	
x	Certain configuration	
α_i	Dimensionless material parameter	
η	Dynamic viscosity	Pa·s
η	Virtual displacement	
λ_1, λ_2 and λ_3	Three principal stretches	
μ_i	Material parameter	Nm^{-2}
ν	Poisson's ratio	
ρ	Density in the deformed state	Kgm/ m^3
ρ_o	Density in the undeformed state	Kgm/ m^3
ρ_w	Density of the wall material	kg/m^3
σ	Cauchy stress tensor	N/m^2
ρ_{disp}	Dispersion factor	
φ	Angle between collagen fibres and the circumferential direction	degree
ψ	Opening angle	degree
ϵ_1	Elastic strain	
ϵ_2	Viscoelastic strain	
ϵ_{total}	Total strain	
Γ	A certain curve	
a_o	Unit vector	
$\mathbf{P_i}$	Piola Kirchoff stress	N/m^2

Statement of Copyright

Acknowledgement

I would like to acknowledge the effort and the dedication of my main supervisor Dr Sherri Johnstone. Through her understanding, encouragement, discremnt and directing, new perspectives of scientific way of thinking were opened to me. Also I would like to thank Dr Susan Pyner for her help and direction.

CHAPTER 1

INTRODUCTION

1.1 Introduction

The purpose of this study is to model the relationship between applied blood pressure and the resulting stress and strain in arterial walls, such that the function of baroreceptors (biological pressure sensors located in the arterial tissue) can be studied. The first novelty of this research is the use of the thin wall theory method to find a relationship between the layer responses of the arterial wall and the whole wall response. Specifically, this study investigates whether it is possible to determine the model parameters used to estimate the elastin and collagen response of each arterial layer using whole wall experimental data. Secondly, the model was extended to calculate strain-energy of each layer constituting the arterial wall. This model was then used to investigate the relationship between baroreceptors location and its firing rate.

Baroreceptors play an important role in controlling blood pressure. It is well known that blood pressure problems are one of the main causes of cardiovascular diseases. According to the world health organization[1],cardiovascular diseases have the highest contribution to death rates worldwide. 18 million people died because of cardiovascular diseases in 2005, which is about 30% of the total deaths which happened in the same year. This is shown in figure 1.1.

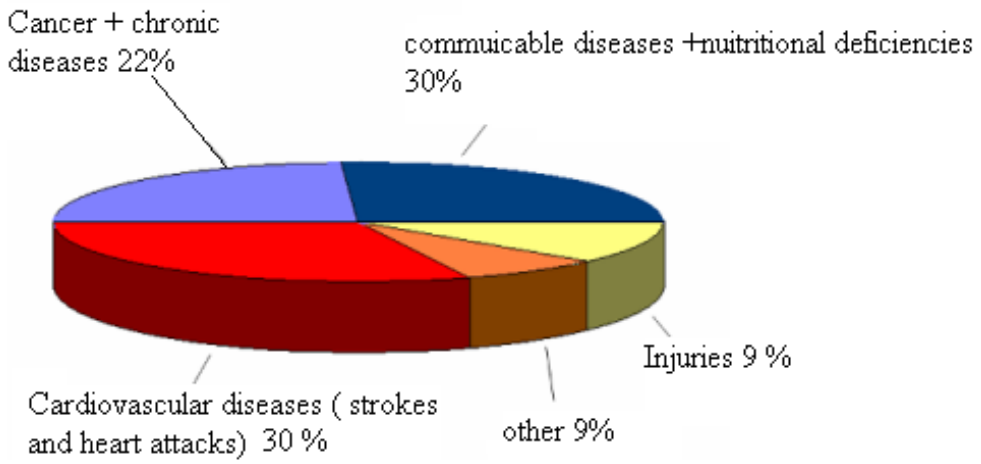

Figure 1.1: Death ratio divided according to cause [1].

Strokes and heart attacks usually happen because of arthrosclerosis (thickening of blood vessels). One of the risk factors of arthrosclerosis is high blood pressure, which is also known as hypertension. According to national UK statistics more than 20 % of the population in England is affected by hypertension at a stage of their life [2]. Thus, using better methods of controlling blood pressure will result eventually in decreasing death rates, both worldwide and on the national level.

In the next section, the process of controlling blood pressure inside humans or animal bodies will be covered. There are two types of regulation of normal blood pressure. The first is called short term regulation and is done through cardiovascular receptors and their reflexes; the other is called long term regulation and is achieved through the kidney. Only short term regulation will be covered in this research [3].

1.2 Short term regulation

The heart actions (blood pressure and filling) are controlled through the activity of sympathetic and parasympathetic nerves. These nerve activities are controlled by the brain which makes its decision based on the sensory information gained from peripheral receptors (in and outside the circulatory system). The main control loop is shown in figure 1.2.

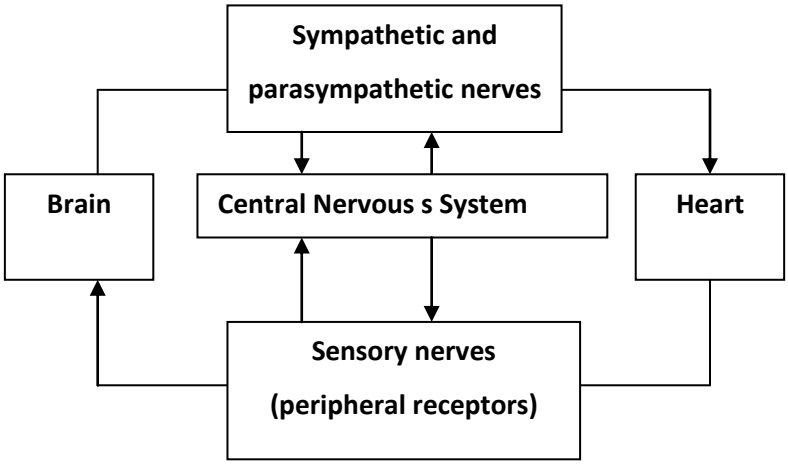

Figure 1.2: Schematic of the control loop between the brain and the heart.

There are 2 main types of sensory nerves both of which act as pressure receptors: The first is known as an arterial baroreceptor and is found in the walls of systematic arteries. The second type is called a cardiopulmonary receptor and is located in the wall of the heart. These two types transmit a signal to the brain indicating certain information such as the arterial pressure and the cardiac filling rate. It is worth noting that their principle of operation is the same. They are accompanied by two other types of receptors that carry relevant information to the brain known as arterial chemoreceptors and muscle receptors. The above mechanisms are summarised in figure 1.3. Only baroreceptors will be the focus of this research.

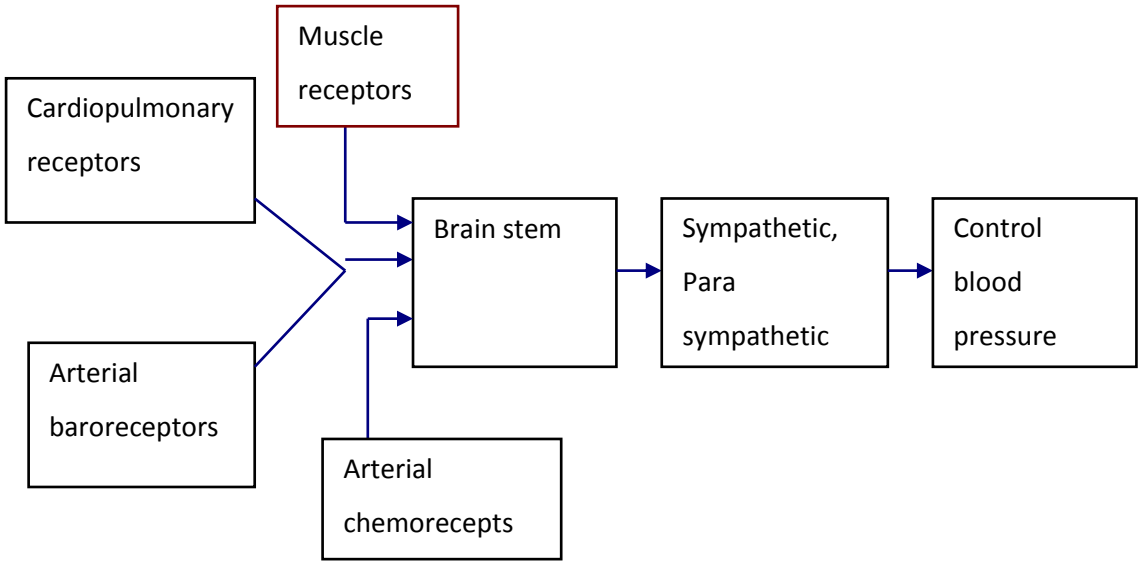

Figure 1.3: Schematic of the detailed control mechanism.

As an intelligent control system, the body has different responses to every interruption to the system. Generally there are three main types of responses which aim to stabilise the system.

(i)The negative feedback reflex is defined as any positive change blood pressure that leads to the generation of a depressor reflex to return blood pressure to its set point.
(ii) The positive feedback reflex is defined as any negative change in blood pressure that leads to a generation of a pressor reflex to return blood pressure to its set point.
(iii) The feed forward process initiates a non reflex cardiovascular order through sending a signal from the cerebral cortex which helps to increase the heart rate instantly. This usually occurs during exercise.

It might be clear from the above three situations, that baroreceptors play a major role in decreasing blood pressure. In the next section, the baroreceptors function and process of operation will be discussed in more detail.

1.3 Arterial baroreceptors

Baroreceptors are literally pressure receptors as the word "baro" means "pressure". They are sprayed nerve endings packed with mitochondria and connected to an axon. They can be found in two main locations, the carotid sinus and the aortic arch as shown in figure 1. 4.

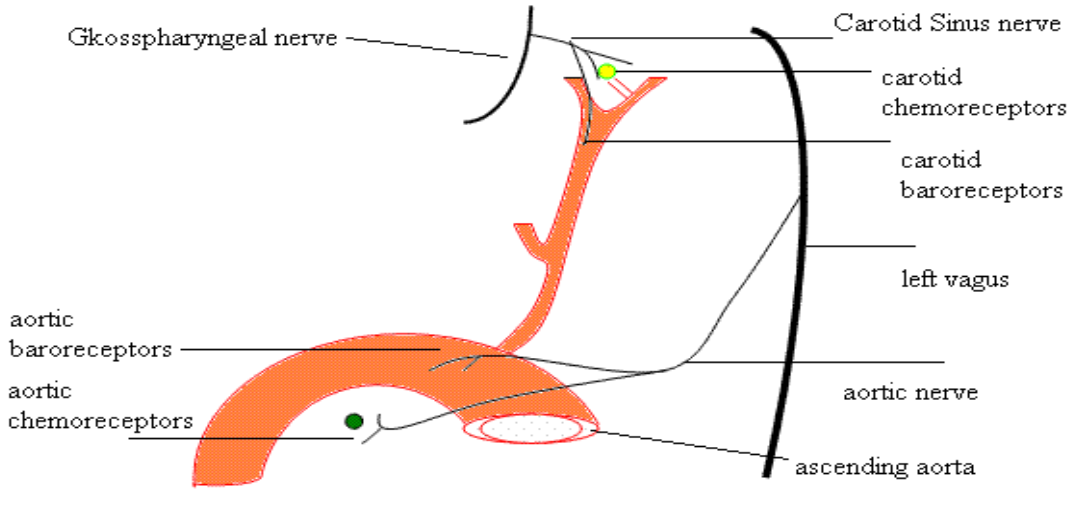

Figure 1.4: Schematic diagram of locations of the arterial baroreceptors [4].

The baroreceptors of the carotid sinus are located at the start of the internal carotid artery. The afferent fibres from these baroreceptors form the sinus carotid nerve. The sinus carotid nerve meets the glossopharyngeal nerve (the nerve responsible for the tongue and pharynx) at the petrous ganglion which is the parent neuron. The petrous ganglion is extended to the brain stem where it terminates at the nucleus tractus solitarius. The baroreceptors of the aorta are located around the transverse arch of the aorta. Its fibres form the aortic depressor nerve then they are connected to the vagus. Their neuron lies in the nodose ganglion. Their central axon terminates in the nucleus tractus solitarius.

1.3.1 Characteristics of baroreceptors

They are mechanoreceptors which mean that they respond to stretch such that a rise in pressure causes a stretch in the arterial wall; for example the diameter of the carotid sinus oscillates by 15 % with each arterial pulse but it does not respond to change if a plaster is applied around the sinus to prevent it from stretching [3].

The baroreceptors have both static and dynamic sensitivity. The static sensitivity is the firing rate of the baroreceptors due to the magnitude of the pressure stimulus. The dynamic sensitivity is the firing rate due to the rate of increase of the pressure stimulus; for example if the carotid sinus faces a rapid rise in the blood pressure the baroreceptors respond by firing an initial burst of action potentials. Then the fibre activity declines and settles down so as to adapt to the new level of blood pressure. When the pressure drops the fibres fall silent and then adapt with the slower rate as shown in figure 1. 5.

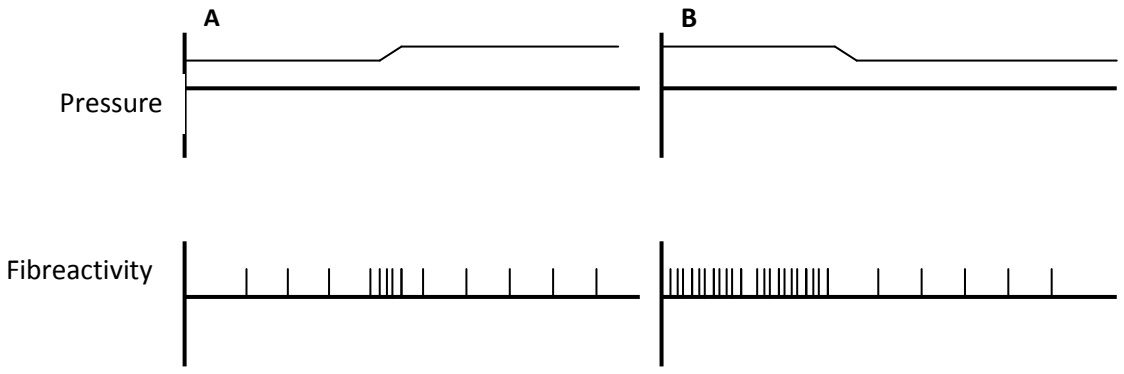

Figure 1.5: a) A pressure rise results in initial burst of action potential followed by decline in the activity known as adaptation. B) A pressure drop results in full silent phase followed by adaptation with a slower rate [3].

In vivo the baroreceptors usually act in the same way as above where the baroreceptors fire a burst of action potential in systole and fall silent in diastole. There are two types of baroreceptor fibres which are classified according to their threshold range (the lowest pressure that triggers an action potential), A - fibre and C-fibre. Both types will be examined fully in chapter 8.

1.3.2 Fibre recruitment

Recruitment means that when blood pressure rises, the discharge frequency of active fibre increases and fibres of higher threshold begin to fire[3]. Fibre recruitment extends the signalling range of multi- fibre nerve such that the nerve would be able to signal a wider operating range to the brain.

1.3.3 Pulsatile versus steady signals

The carotid baroreceptors signal the pulse size (the pulse pressure and the mean pressure) to the brain. The pulsed signal has greater oscillation than the steady signal[3]. The greater the pressure oscillation, the greater the aggregate activity in the nerve (as shown in figure 1.6) which leads to a greater depressor reflex than the steady state pressure (As shown in figure 1.7).

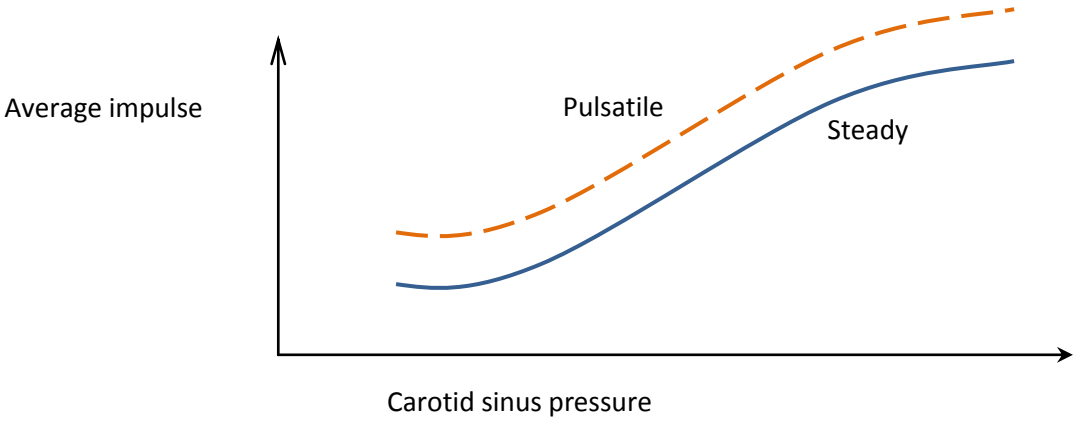

Figure 1.6: Pulsatile signal produce more nerve activity than the steady signal at the same carotid pressure[3].

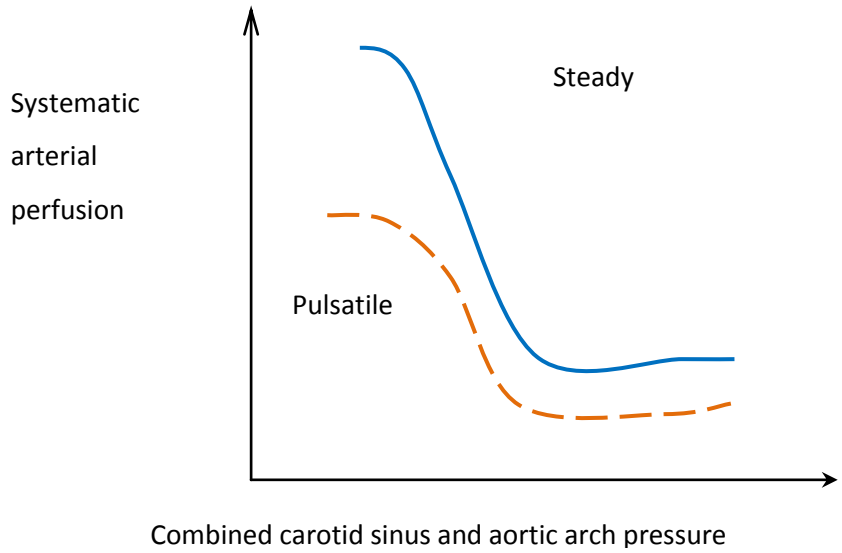

Figure 1.7: Reflex falls in systemic pressure, the pulsatile strengthens the depressor reflex [3].

1.3.4 Baroreceptor reflex (Baroreflex)

The carotid and the aortic baroreceptors have been found to have similar reflex properties [3].Hence, the term baroreflex could be used to describe the reflex caused by any of them. Baroreflex is defined as a pressure reflex that cause changes in the heart and circulation to stabilise arterial pressure[3]. One of the main functions of the baroreflex is to provide protection against acute rises in pressure. This is shown in figure 1.8. This shows that stimulating the nerve initiates a reflex that results in a drop in blood pressure.

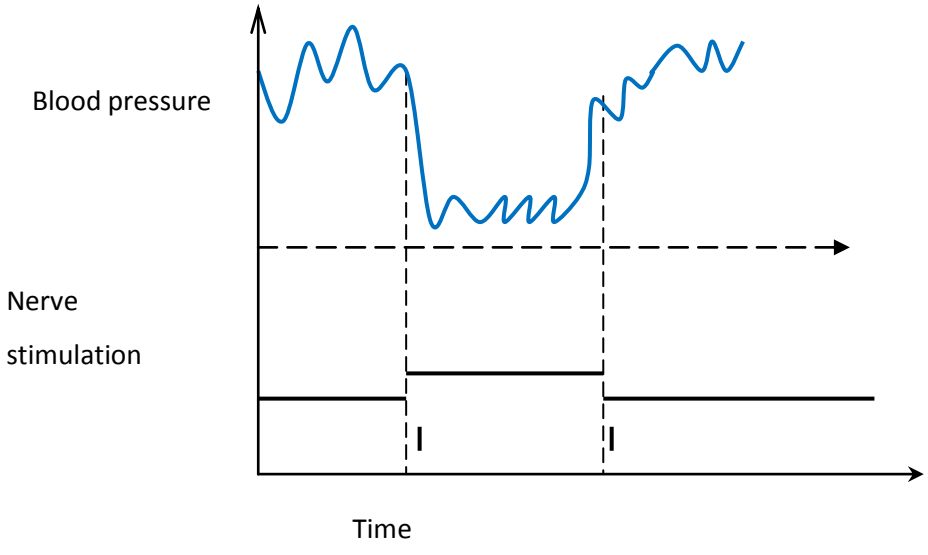

Figure 1.8: Stimulating the nerve causes a drop in the pressure (Adapted from [3]).

The steps in reducing blood pressure are summarised. The input activates the polysynaptic central pathway which enhances the vagus parasympathetic output to inhibit the sympathetic output to the heart. This causes vasodilatation, a decrease in the total peripheral resistance, bradycardia and reduced myocardial contractility. This results in the arterial blood pressure returning to its normal range[3]. Other features of the baroreflex includes a variable gain, given by the slope of the response curve as shown in figure 1.9 and the ability of the gain to reset when the gain is a maximum.

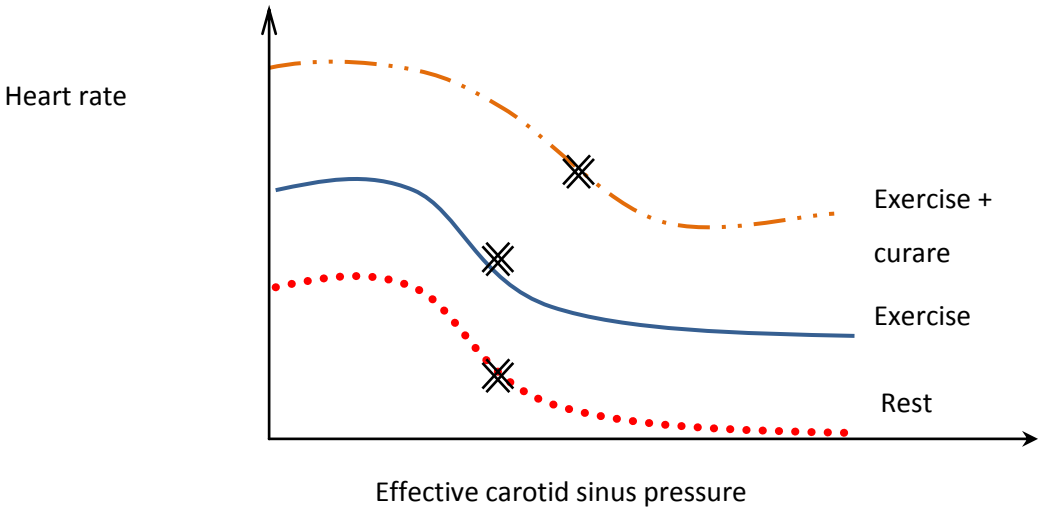

Figure 1.9: Resetting of human baroreflex during exercise [3].

If all baroreflexes were denervated (removed), the mean pressure would increase with increasing fluctuations about the mean[3]. For example when a dog walks on an inclined surface of 21°, the blood pressure fluctuates in the range of 10 mm of Hg. When this dog is deprived from the carotid sinus and walks on the same inclined surface the blood pressure fluctuates by about 50 mm of Hg. The effect of denervation of the baroreflex is shown in the figure 1.10.

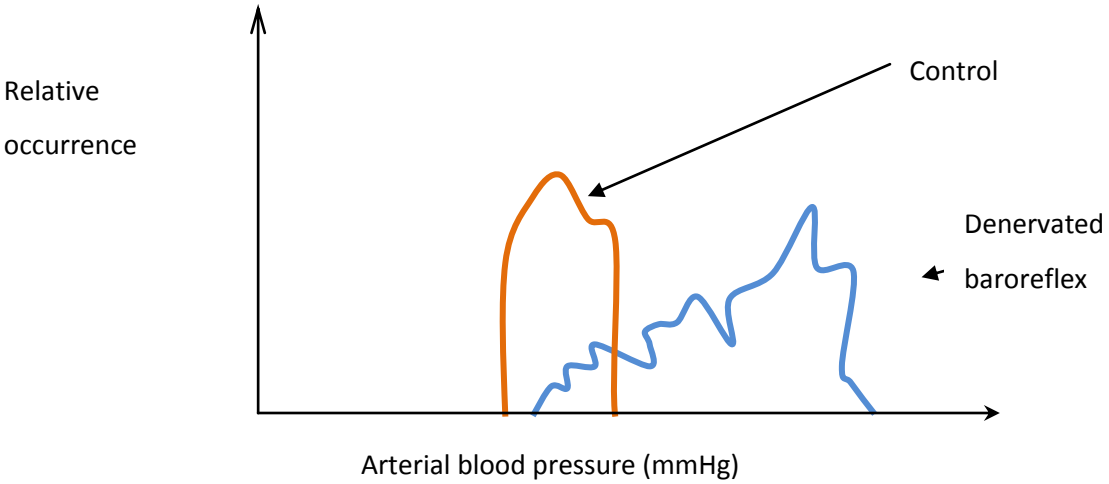

Figure 1.10: Denervating baroreflex result in an increase in the mean pressure accompanied by pressure instability [3].

Thus the baroreflex is considered to buffer acute changes in the arterial pressure over short term. However, the baroreflex do not provide the brain with reliable information about absolute blood pressure over long periods of time. This is because if the blood pressure is raised for a long period of time the baroreceptors threshold is reset to a new higher pressure.

Baroreceptors belong to the short term group regulators as mentioned in the previous section. This is based on the experiments done by Guyton et al [5],where they showed that after denervation of the arterial baroreceptors , the average 24-hours mean was increased for few weeks, but returned to its normal level later, nevertheless the variability in the pressure values remained high.

This section reviewed baroreceptor position, type and reflex. In the next section its stages of operation will be introduced, and then the main aims of this research will be restated.

1.3.5 Stages of operation

The control loop of the baroreceptor is shown in figure 1.11.

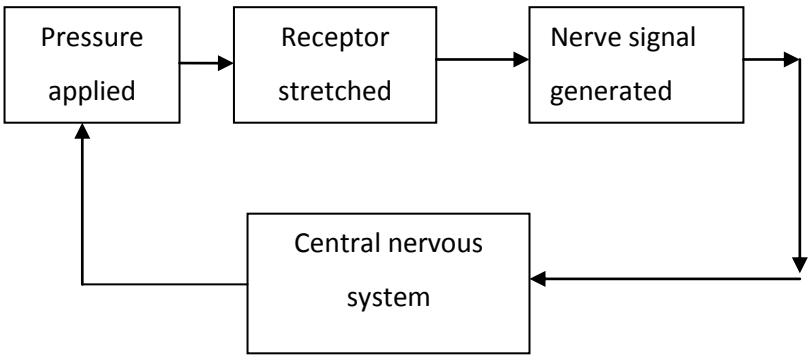

Figure 1.11: Different stages of the receptors function.

There are two main stages covering the function of pressure sensors: the first stage is where the pressure is applied on the blood vessel wall and the wall is stretched along with the receptors embedded in it. The second stage covers the conversion between the stretch of receptors and the generation of the action potential inside the nerve[6]. Both of these two stages will be covered in the following section from the anatomical and physiological point of view.

1.3.6 Blood pressure conversion to stress

From an engineering point of view, the heart may be considered as a pump that pushes fluids into vascular vessels i.e. the arteries, the arterioles and the capillaries then to the veins and back to the heart again. Human blood vessels can be classified according to their function to elastic arteries, muscular arteries, resistance arteries and exchange arteries. These types will explained more in chapters 2 and 3. However, in this study only elastic arteries, such as the aorta will be considered. Blood passes through the aorta in two phases, systolic and diastolic as shown in figure 1.12. During the systolic phase blood and its pulse exerts a pressure on the arterial wall that causes stress and strain in the arterial walls. This will be explained in more detail in chapters 2, 3 and 4.

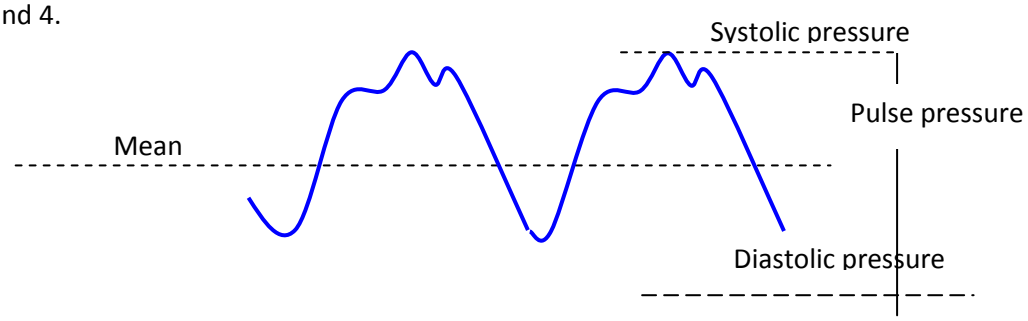

Figure 1.12: Pressure curve for the aorta during 2 cardiac cycles [3].

Thus the question arises, how do the baroreceptors convert blood pressure to nerve signal?

It is generally accepted that the arterial baroreceptors convert stress/strain in the radial direction into a nerve signal, as shown in figure 1.13. Complete analysis of this phenomenon will be discussed in details chapters 6-8. At the end of this stage pressure has been converted to stress, the next section covers the stress conversion to action potential.

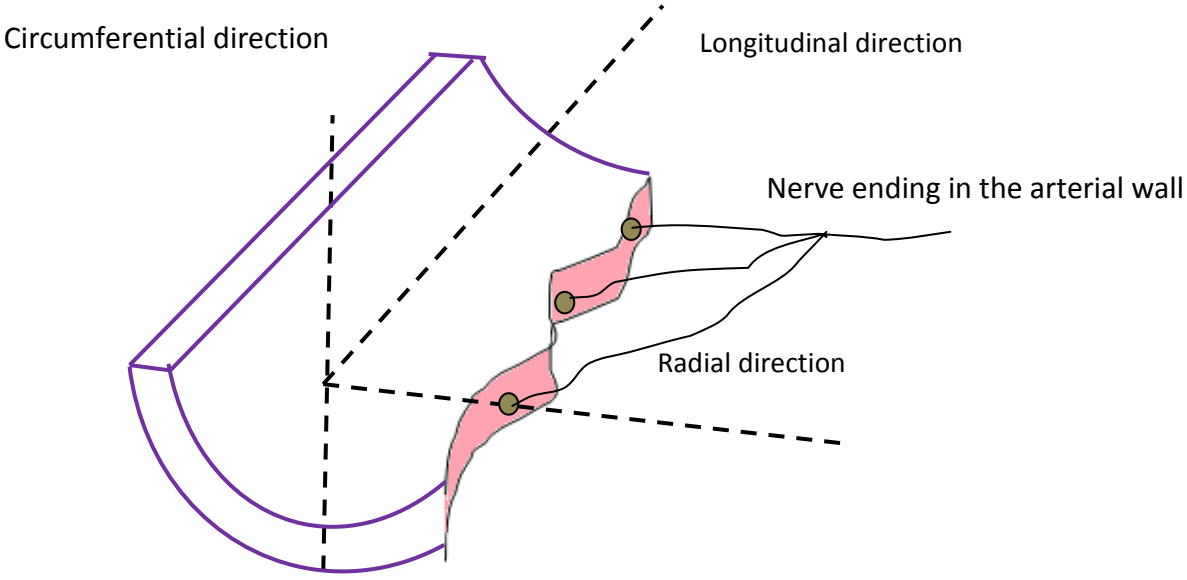

Figure 1.13: Schematic diagram with a cut made through the arterial wall, showing nerve endings subjected to axial, radial and circumferential stress.

1.3.7 Stress to spike frequency relationship

The central nervous system is an unresting assembly of cells that continually receives analyses and perceives information. This is done through neurons (nerve cells) which are the building block for the central nervous system, CNS and the brain. The neurons do the required task by generating or conducting a form of an electric signal in the form of an electric spike of amplitude 0.1 v and 1ms duration which is identical in all the nerve cells of the body. When a baroreceptors nerve ending is stimulated, the cell membrane depolarises rapidly and then the membrane returns to its resting state. This is the action potential. It occurs when the nerve cell is depolarized to a certain critical level called threshold[7]. The action potential is shown in figure 1. 14.

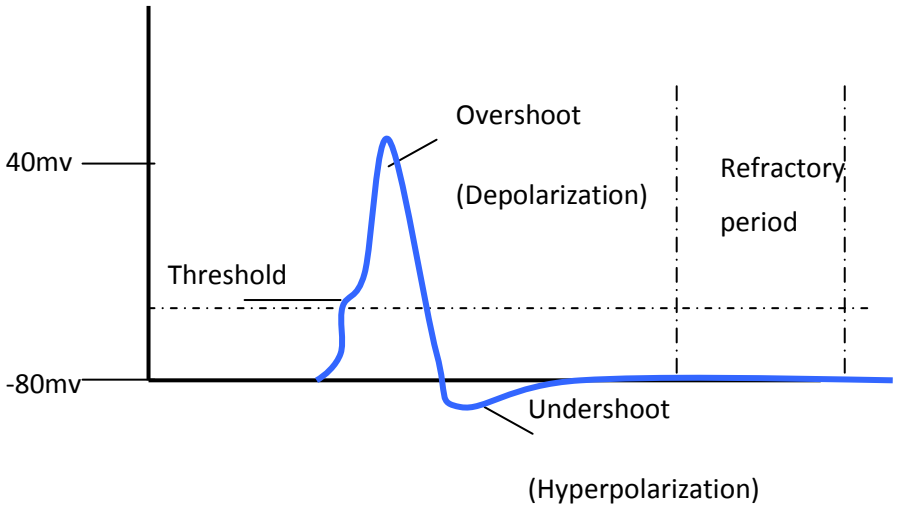

Figure 1.14: The action potential generated by injecting a depolarizing current into an axon [7].

When the baroreceptors nerve ending is stimulated, the membrane potential is reversed in what is called over shoot. Afterwards the action potential reverses its polarization action and ends with hyperpolarization (undershoot). The refractory period is the period between two subsequent action potentials at which the nerve cannot be further stimulated to produce an action potential. The action potential propagates along the axon and arrives at the distant end unaltered in size and in form.

In the last section two phases of the function of the baroreceptors were covered. This thesis will only concentrate on the first phase i.e the effect of arterial pressure on the arterial wall in which the baroreceptors are embedded. A model (chapter 4 and 5) was constructed to establish a relationship between pressure applied and stress and strain induced both in the whole wall, and in the layers. This allowed us to suggest a relationship between the location of a receptor inside the wall and its frequency response as will be discussed more in chapter 8. That enabled us in achieving the research aims. The research aims are summarised as follows:

1.4 Research aims

a) Understand various types of experimental data applied to arterial wall
b) Calculate whole wall stress response using nonlinear solid mechanics
c) Calculate layer arterial wall stress response using nonlinear solid mechanics
d) Propose a simple model that connects the whole wall and the layer response using thin wall theory

e) Using gained knowledge to try to differentiate various baroreceptors types based on their location

It is worth noting that the finite element method is well known for its applications and advantages. It is not be used here, basically because this is a probing research that aims to put principles of neurophysiology with continuum mechanics and electronics. This research is concerned with understanding the base functions in this interdisciplinary field. Finite element analysis studies in this field are underway by other groups[8-9].

Experimental investigations reported in the literature will be reviewed in chapter 2 and related to the current understanding of the anatomy and physiology of arterial and venous tissue. Specifically, the histology and the mechanical properties of the tissue will be discussed. Chapter 3 will cover existing mathematical models. Chapter 4 will cover the nonlinear continuum mechanics basis for the proposed model. Chapter 5 will discuss the optimisation techniques suitable for this type of research. It will consider the rationale behind the novel method proposed in this thesis. It will also cover the principles of Monte Carlo simulation. Chapter 6 is concerned with analysis of the model estimation. Chapter 7 will show the application of the model to other types of vascular vessels. Chapter 8 will investigate the relationship between strain-energy and receptor response together with its implication on the location of the nerve endings within each layer. Chapter 9 will summarise the conclusion of the research and finally chapter 10 will show basic ideas for future research.

1.5 References

1. Molnar S, *Human Variations: Races, Types and Ethnic Groups*. 2005: Prentice Hall College Div.
2. Hardill I, Graham DT, and Kofman E, *Human Geography of the Uk: An Introduction* 2001, London: Routledge. iii.
3. Levick JR, *An Introduction to Cardiovascular Physiology*. 2003, London: Hodder. 384.
4. Stanfield CL and Germann WJ, *Principles of Human Physiology*. 3rd ed. 2008: Pearson Benjamin Cummings.
5. GUYTON AC, *Arterial Pressure and Hypertension*. 1980, Philadelphia: Saunders.
6. Srinivasan R and Nudelman H, *Modeling the Carotid Sinus Baroreceptor.* Biophysical journal, 1972. **12**: p. 1172-1182.
7. Nicholis J , Martin AR, Wallace BG , and Fuchs PA, *From Neuron to Brain: A Cellular and Molecular Approach to the Function of the Nervous System*. 4th ed. 1993 Sunderland: Sinauer 679.
8. Ogden RW Gasser TC, Holzapfel GA *Hyperelastic Modelling of Arterial Layers with Distributed Collagen Fibre Orientations.* J R Soc Interface, 2006. **3**(6): p. 15-35.
9. Holzapfel GA, *Structural and Numerical Models for the Viscoelastic Response of Arterial Walls with Residual Stresses*, in *Biomechanics of Soft Tissue in Cardiovascular System*, Holzapfel GA and Ogden RW, Editors. 2003, Springer: New York. p. 109-184.

CHAPTER 2

REVIEW OF EXPERIMENTAL INVESTIGATIONS

---

2 Overview

Arterial baroreceptors and cardiopulmonary receptors are concerned with short term blood regulation. They have been shown to have a high degree of similarity [1]. One of the main similarities is that they both convert a pressure signal into a nervous signal. A major factor in the conversion process is the role of the vascular wall itself whether it is an artery or a vein. Thus this section reviews the experimental evidence that underpins the descriptions of the anatomy and physiology of these vascular structures. However in order to be able to appreciate different mechanical concepts here , various mechanical concepts will be simplified then they will covered in detailed in chapter 4. Stress and strain here are defined according to a continuum mechanics basis. The basic idea behind the strain concept is the deformation gradient and it is defined as the ratio of length of a certain curve on a certain body before and after deformation. Stretch here would be used to mean a product of deformation gradient and a unit vector. Based on this Right Cauchy strain tensor (Green deformation tensor) is defined as the product of the transpose of the deformation gradient by itself. While the Green strain tensor is the right Cauchy strain tensor minus unity divided by half. Stress is based on traction force acting on a certain area of a body. Traction force is defined as the product of Cauchy stress and the norm to the surface, where as

second Piola Kirchoff stress tensor does not admit a physical interpretation in terms of surface traction. Nevertheless it is a symmetrical matrix and parameterised by material coordinates. Thus it is often used to represent stress measure in computational mechanics. Having defined the main mechanical concepts that will be used in this chapter, the following section will describe different characteristics of arteries and veins.

2.1 Arteries and veins

Human body vessels whether they are arteries or veins can be classified according to their function as shown in table 2.1.

Table 2.1

Classification of vessels according to their function[1]

Vessel type	Function
Elastic arteries	Transfer of blood to muscular arteries
Muscular arteries	Deliver blood to organs
Resistance veins	High resistance veins that decrease the pressure and the flow of blood
Exchange vessels	Transfer of oxygen carbon dioxide from and to cells
Capacitance vessels	Veins are considered as capacitance vessels that store blood

The aorta receives blood from the left ventricle and it branches down reducing its size (smaller size arteries are called arterioles). Arterioles carry blood to thin capillaries where the exchange of nutrients and oxygen takes place (table 2.2). After that, capillaries carry deoxygenated blood to veins that end finally with the vena cava. The vena cava carries deoxygenated blood to the right atrium of the heart.

Thus, in general, arteries are the vessels that carry blood from the heart to the body organs, while veins are the vessels that carry blood from body organs to the heart. As a result, blood pressure in the arteries is high and the walls are thick, while the pressure in veins is smaller and the walls are thin as shown in [1]. Veins are more distensible than arteries and they are more compliant[2-3]. Arteries distend during systole and retreat during diastole; veins are more in rhythm with the

cardiac cycle[1] [4]. When arteries or veins are pressurised they extend into all directions, i.e. circumferentially and longitudinally, but almost no twisting happens, this implies that negligible shear forces exit[5-6].

In this chapter, a description of the main building blocks of vascular tissue is given, followed by the general histology of the wall tissue structure. This is followed by a review of a series of experiments used to characterise the mechanical properties of the vascular walls in terms of their constituents.

Table 2.2
Comparison of the various sizes of arteries [6]

Vessel	Internal diameter	Wall thickness	Thickness/diameter ratio
Aorta	1-3 cm	2-3 mm	0.125
Main branches	0.5-2.25 cm	2 mm	0.182
Large arteries	4-5 mm	1 mm	0.222
Medium arteries	2.5-4 mm	0.75 mm	0.231
Small arteries	1-2.5 mm	0.5 mm	0.286
Tributaries	0.5-1mm	0.25 mm	0.333
Small rami	250-500 µm	125 µm	0.333
Terminal arteries	100-250 µm	60 µm	0.342
Arterioles	25-100 µm	20-30 µm	0.400
Metaarterioles	1-25µm	5-15µm	0.571

2.2 Arterial wall main components

In this section the basic components of vascular wall tissue are firstly introduced. Histological studies are then presented detailing evidence about the types and proportions and distributions of these biological structures such that the concept of vascular wall layers is derived. The three main components elastin, collagen and smooth muscle cells are firstly covered.

2.2.1 Elastin

Elastin is a linearly elastic protein with a low elastic modulus. It can endure large amounts of stress or strain [7]. It is an extracellular matrix protein which is responsible for the resilience (ability to recover to its original shape) of tissues found in the skin, arteries and lungs. It is insoluble and hydrophobic. Its fibres consist of extensively cross-linked proteins such as glycine, valine, alanine, and proline, which are present in variable amounts depending on the tissue [7-8]. The arrangement of elastin inside the different arterial wall layers will be discussed later in this chapter. Figure 2.1 shows intimal and medial bovine aorta stained with Vierhoeff-van Gieson for elastin [8]. It can be seen that the elastin fibrils formed by elastin and a protein called fibrillin are regular and oriented [8].

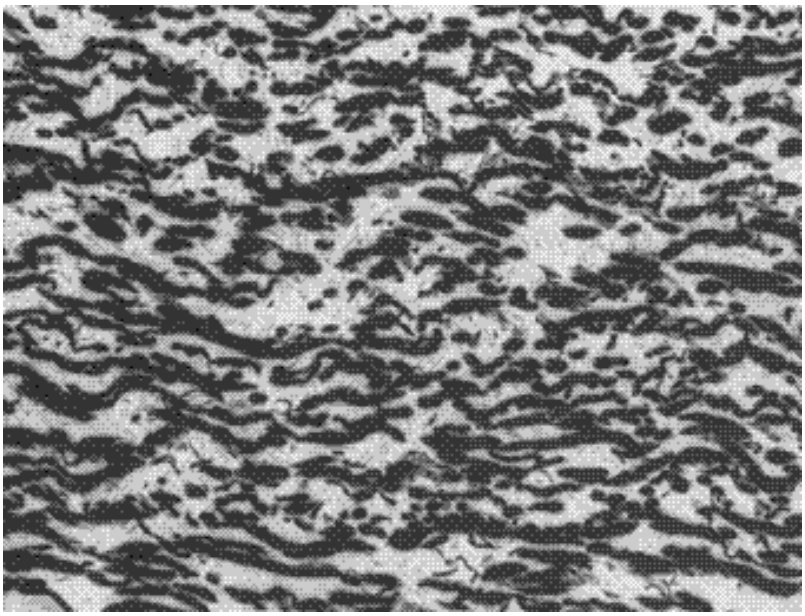

Figure 2.1: A cross section in the arterial wall stained only for elastin showing elastin fibres organised and oriented [8]. The photomicrograph was taken from the ascending aorta just above the aortic valve. It is worth noting that elastin fibres (in black) are regular in size and oriented.

Elastin is reported to have a linear relationship between stress and strain [9]. It is found in complex structures along with other proteins in the form of connective tissues. To study it, the elastin needs to be extracted. The method of extraction involves the following: Purification of elastin; this is done it using cycles of autoclaving and treatment in guanidine hydrochloride. This technique is used to get rid of collagen and proteoglycans without causing damage to the peptide bonds in elastin [9]. Mechanical tests indicate that elastin is extensible over a long range as shown in figure 2.2.

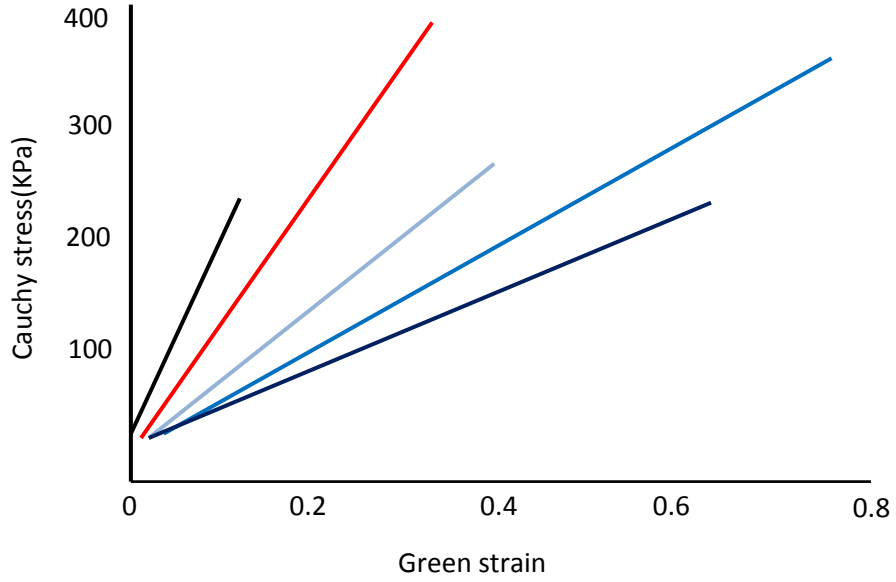

Figure 2.2: Measured stress-strain characteristics for arterial walls with only elastin present. Linear relationships were observed for 5 different samples, where sample one to five colours are black, red navy blue and dark blue respectively [8].

2.2.2 Collagen

Collagen is a protein, but it exhibits a much higher elastic modulus than elastin resulting in low elasticity [10]. Collagen accounts for about 20–30% of total body proteins of many vertebrates. Thus it could be considered as one of the proteins used most extensively by mammals [10]. It exists mainly in tissues that have a mechanical function. About one half of the total body collagen is in the skin. If skin was analysed further it could be shown that it posses 70% collagen, when water is excluded [10]. The molecular structure of collagen is based on evidences from other studies. These studies used different investigations techniques; such as amino acid composition analysis, X-ray diffraction analysis, electron microscopy and physicochemical examination of solutions[10].

The collagen molecule looks like a twisted thread as it consists of three polypeptide chains twined around each other. This triple helix shape is formed due to a high content of glycine and amino acid residues [10]. The strands are held together primarily by hydrogen bonds and covalent bonds. There are 19 different types of collagen. They differ in location and chemical structure and also in function. They could be divided into 6 subgroups [11] as summarised in table 2.3.

Table 2.3

Collagen types[11]

Collagen type	group
fibril forming collagens	types I, II, III, V
network forming collagens	types IV,VIII, and X
fibril-associated collagens	types IX,XI, XII, XIV,XVI, and XIX
beaded filaments forming collagens	type VI
anchoring fibrils forming collagens	type VII
transmembrane collagens	types XIII and XVII

Collagen different types and their characteristics could also be classified as follows: Collagen types I, II, III, V and XI are built up of three chains in a formation called continuous triple-helical structure. In the other hand, Fibril forming collagens: Collagen types I, II, III, and V; have large sections of homologous sequences. While In type IV collagen (basement membrane), the regions with the triple-helical conformation are interrupted with large non-helical domains as well as with the short non-helical peptide interruption. Also collagens Types IX, XII and XIV; they have small chains, which contain some non-helical domains, form a type called Fibril associated. This is in addition to Microfibrillar collagen which is mainly formed of Type VI. Type VII is known as anchoring fibril collagen as it wraps around type III that forms the reticular connective tissue , which exist around lymphoid organs[10].

It is also worth mentioning that, they differ in location for example type II exist mainly in cartilaginous tissues while type III generally exists in arteries walls and intestines. Collagen is far stiffer than elastic as shown by [12]. The stress-strain curve produced by [12] for collagen is shown in figure 2.3.

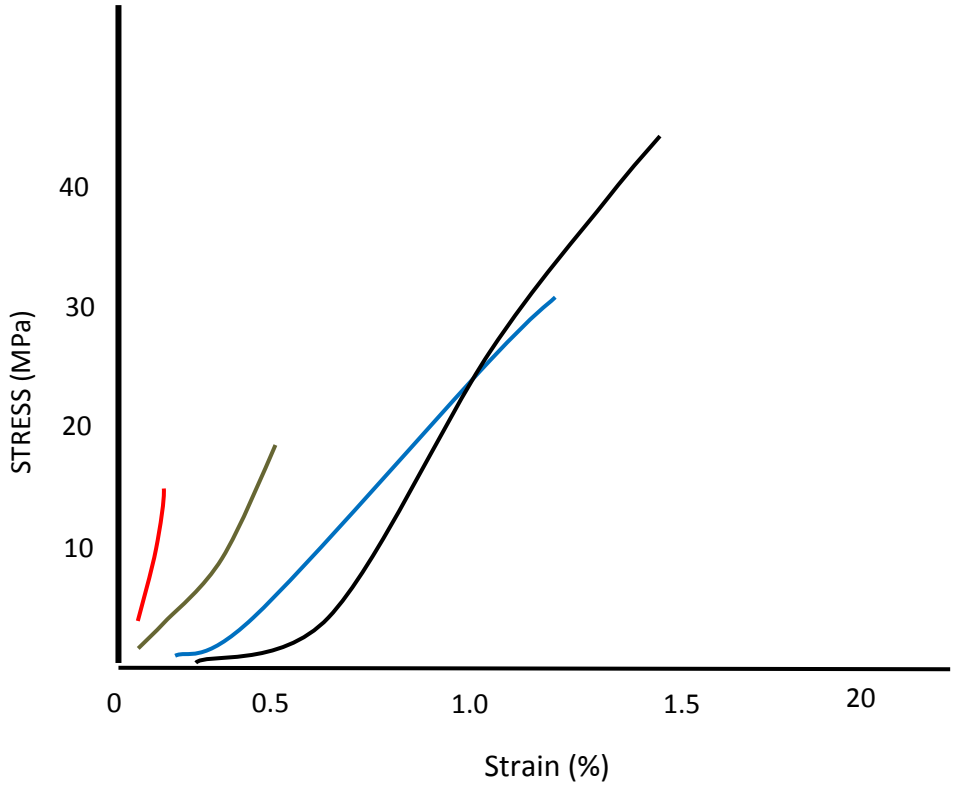

Figure 2.3: Stress-strain curve of collagen molecule for tendon specimen 1 (red) , tendon specimen 2 (green) , tendon specimen 3 (blue) and tendon specimen 4 (black)[12].

2.2.3 Smooth muscle

Smooth muscle cells are widely distributed in the body and their function varies with location. They are mainly located in hollow organs. These cells take the form of broad thin sheets, in arrays of bundles. They also exist in the ovaries, bladder and the iris[13]. It is thought that smooth muscle cells contribute up to 2% of the total human weight. Smooth muscle cells are made of small elongated, uninucleated cells, embedded in the extracellular matrix. A smooth muscle cell contains actin and myosin filament which gives the cell its contractile ability, although this contraction is much slower than other contracting muscular cells[13]. The smooth muscle cells also exist in arteries as shown in figure 2.4.

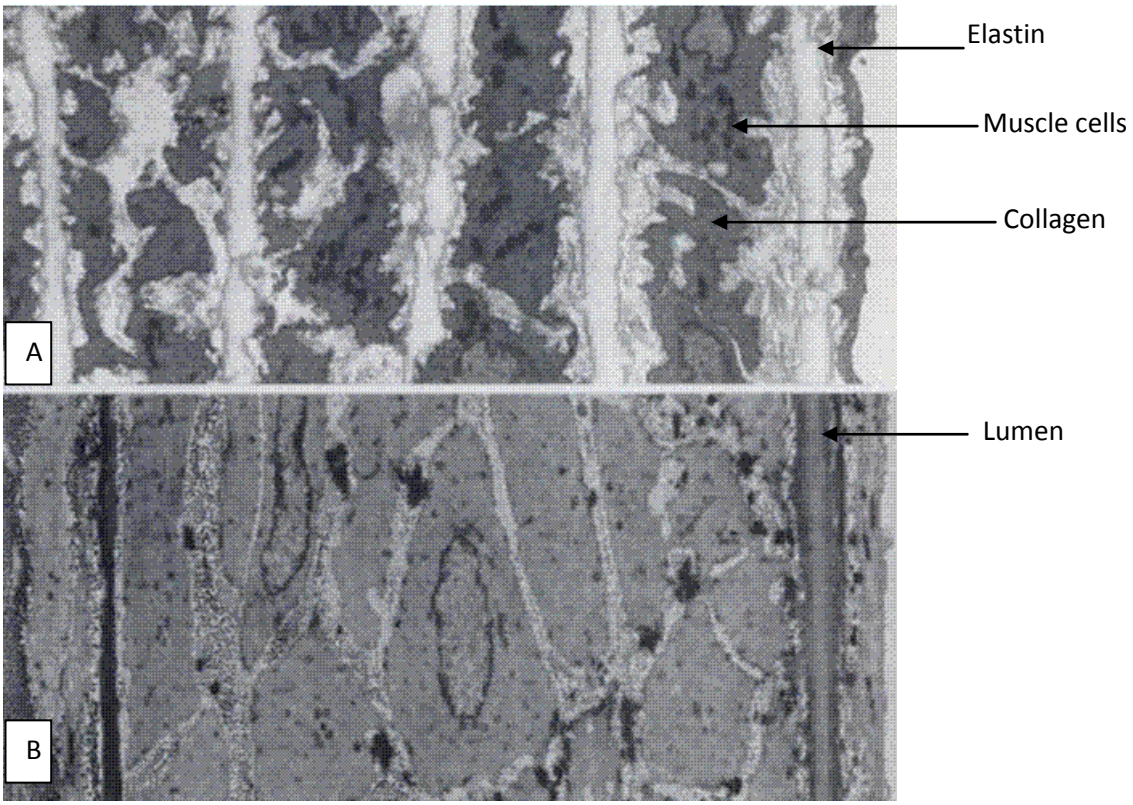

Figure 2.4: A. Longitudinal section of the pulmonary artery of a rat B. Longitudinal section of a rat mesenteric artery[13].

In figure 2.4A, bands of muscle cells alternating with elastic lamellae can be seen. To the right are the lumen, the endothelium and the inner elastic lamina. Between the muscle cells, there is collagen. In figure 2.4B, the full thickness of the wall is clear. To the right are the lumen, the endothelium and the inner elastic lamina. To the left the adventitia (with a visible nerve bundle) and the outer elastic lamina could be seen. The muscle cell profiles of the media are separated from each other by elastin fibres and collagen fibrils. It is worth noting that after the specimen was stained, it was magnified 600 times for the different components of the arterial wall to be clear[13]. The arterial wall extends passively, but the smooth muscle controls the active tension of the vessel [14] [15-16]. Evidence shows that smooth muscle cells do not have a role in the passive expansion of the arterial wall. i.e. it was found that digesting the smooth muscle cells of a wall had negligible impact on stress-strain relationship [1, 15-16]. The active tension is affected by intrinsic factors (bayliss myogenic response, endothelial secretion, vasoactive metabolites that causes acidosis) and extrinsic factors such as vasomotor function and hormones[1]. Smooth muscles cells, elastin and collagen are shown in the medial layer of the arterial wall in figure 2.5.

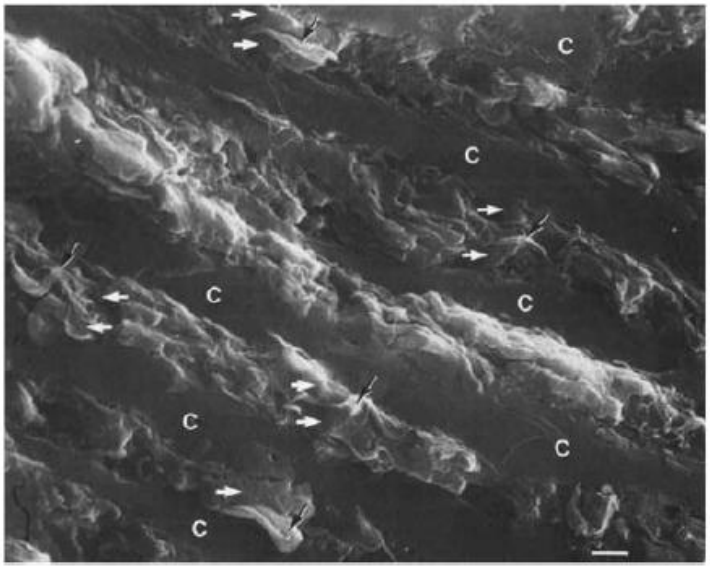

Figure 2.5: Electron microscope view of the transversal cross section of the media of 8-year-old rabbit descending thoracic aorta. C marks the SMCs, white arrows mark the fibres of elastin and black arrows mark the bundles of collagen fibres, redrawn from [6].

2.2.4 Comparison of tissues

This section explores the question, how do collagen, elastin and smooth muscle cells work together in the expansion and contraction of vascular walls?

This was investigated by Holzapfel in[17]. An interesting experiment was done to show the effect of elastin and collagen on the total response of the arterial wall. Uniaxial tension was measured in relation to the extension ratio of an arterial wall segment. This relationship was used as a form of control in comparison with collagen digestion ad then elastin digestion. Collagen was digested (removed) by applying a certain enzyme to the arterial segment. Thus the new response was named collagen digested and it shows the typical stress response of elastin. Elastin was digested and the relationship now was dominated by the collagen response [17]. It could be said that in the case of digested elastin the curve is collagen dominated and in the case of collagen digested it is the case of elastin domination [17]. This is shown in figure 2.6.

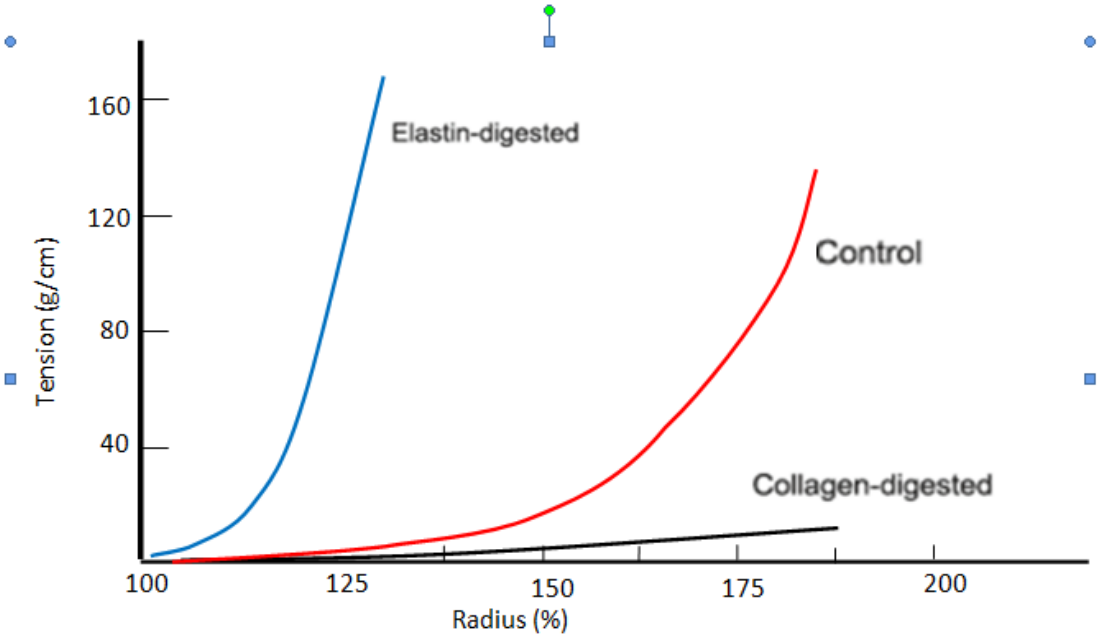

Figure 2.6: Collagen digested curve is elastin dominated, and vice versa, both compared with the control (elastin and collagen are not digested) [17].

These results can be used to explain vessel radius regulation, by considering the elastin and collagen as resistances, with the collagen having higher magnitude. The smooth muscle cells can be thought of as a motor that actively contracts the whole body of the wall.

When the central nervous system acts to constrict a vessel, it actively sends a signal to contract the smooth muscle cells. The dilation of vessels is passive. Thus, at low radii the elastin is dominant allowing easy expansion. At higher radii the effect of collagen response dominates to prevent over-expansion.

2.3 Vascular tissue

2.3.1 Whole wall investigations

2.3.1.1 Histological studies

On the macro scale the vascular walls are considered as three distinct histological layers as shown in figure 2.7. The image suggests that an abrupt interlayer connection is a reasonable assumption for producing a model, and any effects of the internal elastic lamina and external elastic lamina that separate the media from the intima and adventitia can be considered negligible [14, 18]. A more realistic assumption would be to assume a contribution from inter layer lamina effects [19].

The method used to produce the image in figure 2.7 is as follows. Specimens were fixed in 10% formalin. Samples were taken and were placed in cassettes. Then samples were dehydrated in

alcohol baths of concentration of 90% alcohol. The samples were then clarified in xylene and at the end they were embedded in paraffin. After being mounted on slides, Sections were stained using hematein-phloxin-saffron (HPS), Masson's trichrome stain and orcein [20].

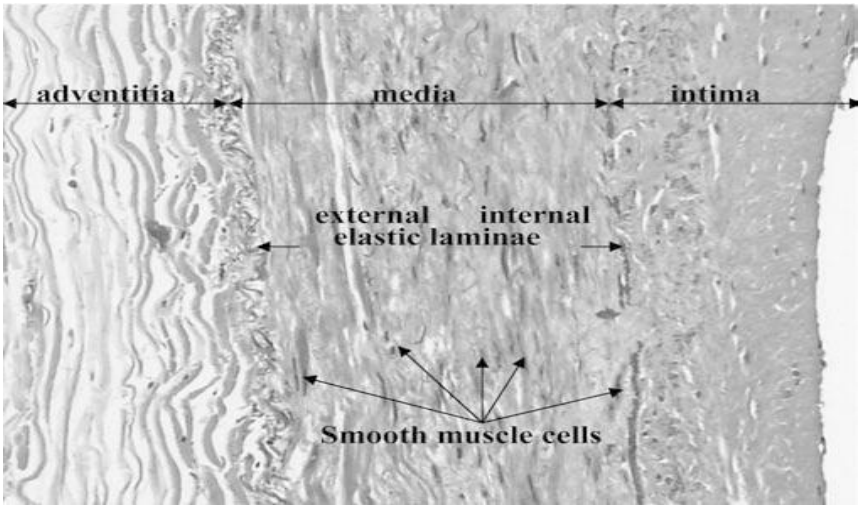

Figure 2.7: A cross section in the arterial wall, showing the three distinct layers; intima, media and adventitia, [20].

2.3.1.2 Mechanical studies

It is well documented that the composition of arterial walls varies along the arterial tree [14]. Thus, a systematic relationship between the shapes of the stress–strain curve for a blood vessel and its anatomical location has been suggested [14]. But it is also worth noting that although the mechanical properties of arterial walls vary along the arterial tree, the general mechanical characteristics exhibited by arterial walls are the same.

In this section, experiments that were performed on the whole vessel wall to calculate its stress-strain response will be discussed. Whether it is an artery or vein, an in vitro or in vivo test or a uniaxial or biaxial test, calculating the stress-strain response starts with measuring the relationship between luminal pressure and axial tension with vessel radius. Using cylindrical coordinates, there are 3 main axes, namely; longitudinal direction, radial direction and the circumferential direction as shown in figure 2.8.

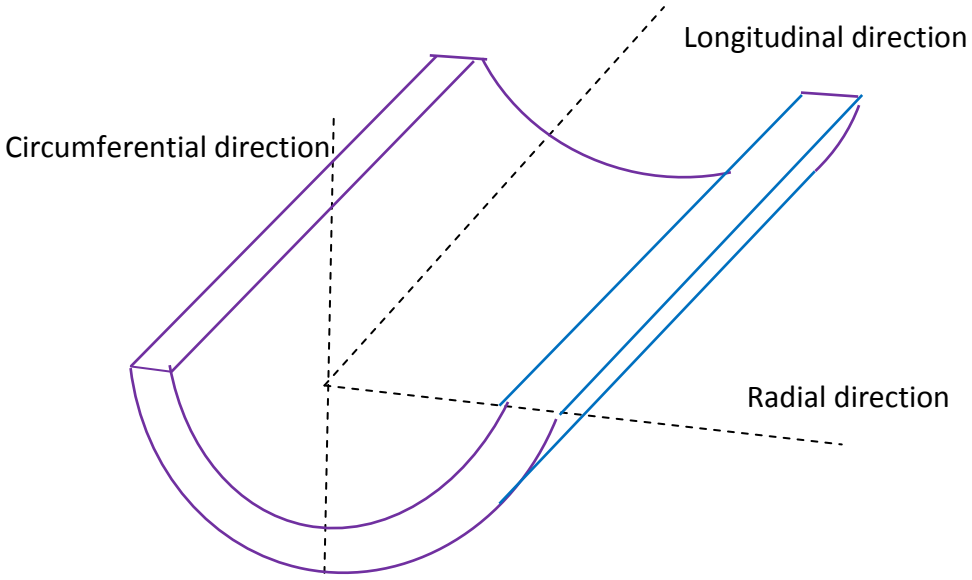

Figure 2.8: Schematic diagram of the arterial wall showing the three main reference coordinates [21].

There are two types of tests, in vivo and in vitro. One of the main advantages of using in vivo experiments is that the vessel is observed under real life conditions. However, in vivo tests have certain limitations because, in that case, the wall is subjected to other factors other than its material characteristics such as: hormones and nervous system reaction. Thus, in vitro experiments could give two main advantages, firstly it allows the partial characteristics of the arterial wall to be investigated in isolation of other external factors that may exist inside the body, and also it allows the pre-conditioning of the arterial wall through cyclic inflation before applying the required experiments. Pre-conditioning helps in showing repeatable stress-strain curves[22-23]. Also in vitro allows the application of more complex mechanical concepts like twists and bending. Thus, this research will only concentrate on in vitro experiments.

There are two types of in vitro experiments. The first type involves the application of a uniaxial luminal pressure in the radial direction. The second type involves the application of a biaxial luminal pressure in the radial direction and tension in the axial direction. As early as the sixties, uniaxial experimental investigations of vascular walls were produced. In [4] vascular segments were mounted at their in situ length in a plastic box. Typically, a syringe is connected at one end of the arterial segment while a strain gauge at the other. Blood is injected from the syringe and the radius calculated as from the measured pressure.

It is important to note that uniaxial extension tests on arterial walls provide basic information about the material[14], but are not sufficient to quantify completely the anisotropic behaviour of arterial walls. In general, a segment of vessel shortens on removal from the body [14]. The in vivo

pre-stretch in the longitudinal direction must therefore be reproduced within in vitro tests[24] [14].

Although other uniaxial extension tests performed on small arterial rings (so-called ring tests) can account for the in vivo length by longitudinal stretching, this technique also proved to be insufficient [14].

The most common biaxial tests use straight arterial tubes. Since arteries do not change their volume within the physiological range of deformation [14], they can be regarded as incompressible materials. Hence, using the incompressibility constraint the mechanical properties of three-dimensional specimens can be extracted from biaxial tests[14]. This will be further investigated in chapters 4 and 5.

Biaxial tests have been performed on different types of arteries thoracic, abdominal aorta, femoral and carotid arteries [15, 25]. A typical procedure for biaxial testing is as follows. After the specimen is prepared, the specimen is then stretched vertically to its *in vivo* length [14]or a bigger extension ratio[14-15]. Pressure is then applied circumferentially. A static pressure relationship is developed. Static means that the radius at each step of 20 mm Hg between 0 and 240 mm Hg was measured, with a pause of 2 min after each change. A schematic diagram of the procedure is shown in figure 2.9.

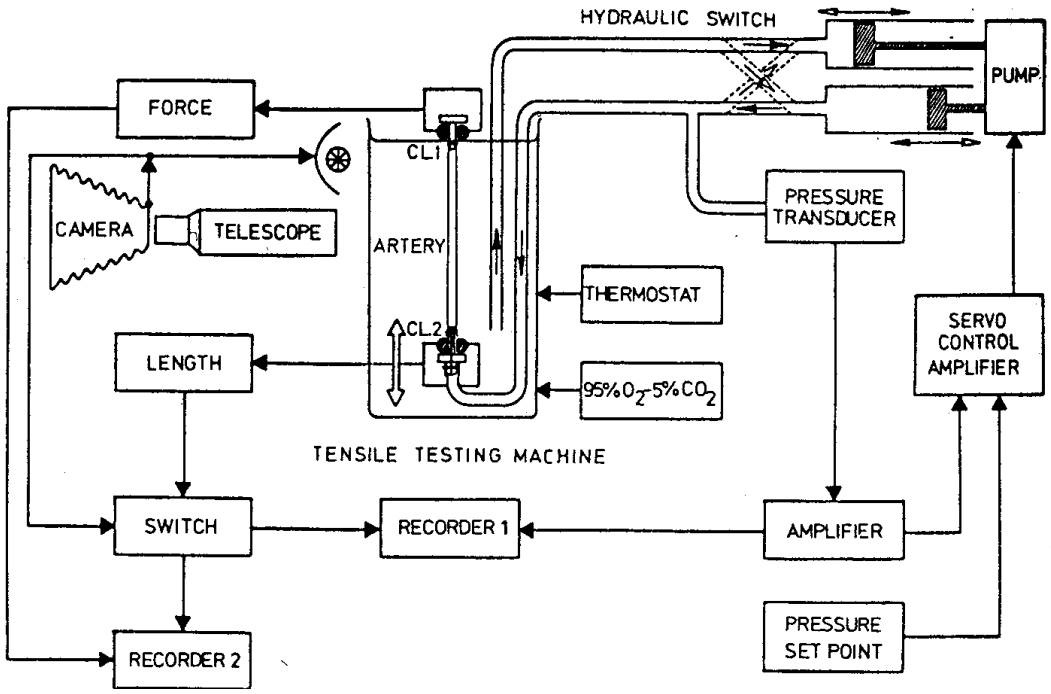

Figure 2.9: Biaxial test formation, the sample is stabilised from one side, pulled from the other and pressure applied from inside [26].

Because biaxial loading is symmetric, shear is absent [27]. The mechanical behaviour of arteries depends on physical and chemical environmental factors, such as temperature, osmotic pressure, pH, partial pressure of carbon dioxide and oxygen, ionic concentrations and monosaccharide concentration. In *ex vivo* conditions the mechanical properties are altered due to biological degradation. Therefore, arteries should be tested in appropriate oxygenated, temperature controlled salt solutions as fresh as possible[28].

Typically the results of the above biaxial experiments, whether it is on an artery or on a vein is in the form of pressure radius relationship and pressure axial force relationship as shown in figure 2.10.

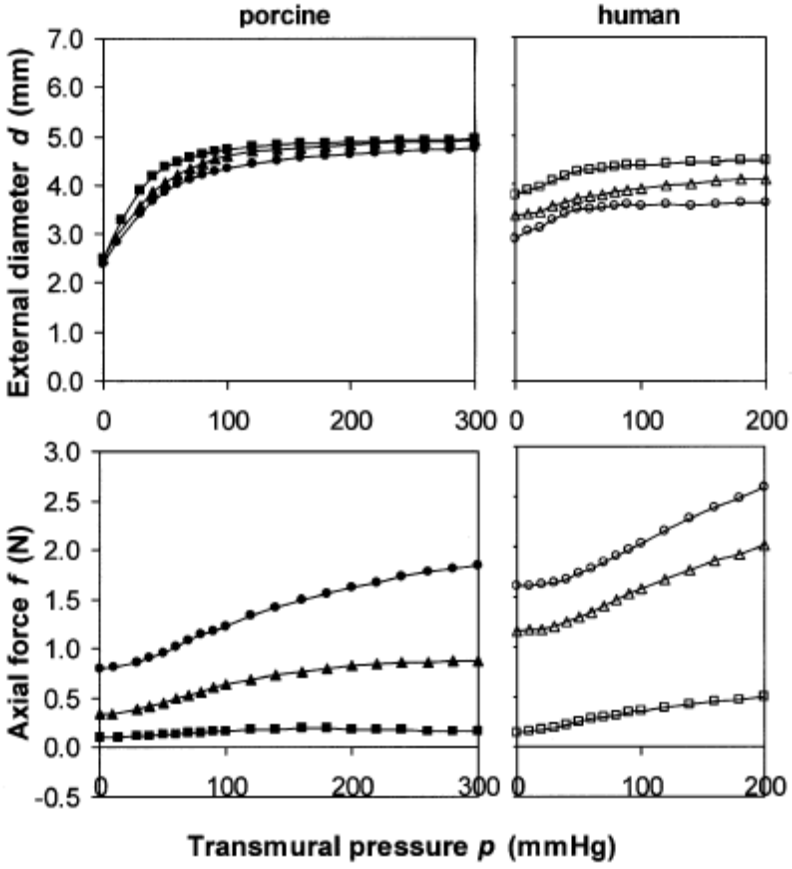

Figure 2.10: Relationship between transmural pressure and external diameter and with the axial force is shown the dark symbols are for porcine coronary artery tissue, while the light symbols are for humans[29].

In the last section the differences between *in vivo* and *in vitro* experiments were shown. Types of *in vitro* experiments were discussed together with the typical relationships resulting from biaxial experiments in figure 2.10. In the next section, mechanical results resulting from different experimental procedures for the whole wall will be covered, namely, Bergel static experiments [25], and experiments by Fung [23], and Holzapfel [30]. Also, Attinger's experiments on the vein will be covered[4]. Afterwards, the focus of the next section will be the layer oriented experiments performed by Demiray [31], von Maltzahn [32] and Holzapfel [22]. Using biaxial testing, with arterial extension within the *in vivo* range, Berge [25]calculated the static incremental elastic modulus versus the luminal pressure (figure 2.11). The incremental elastic

modulus gives a picture on the elastic response but it does not relate to the intrinsic properties of the wall. It is impractical to mimic the material elastic performance

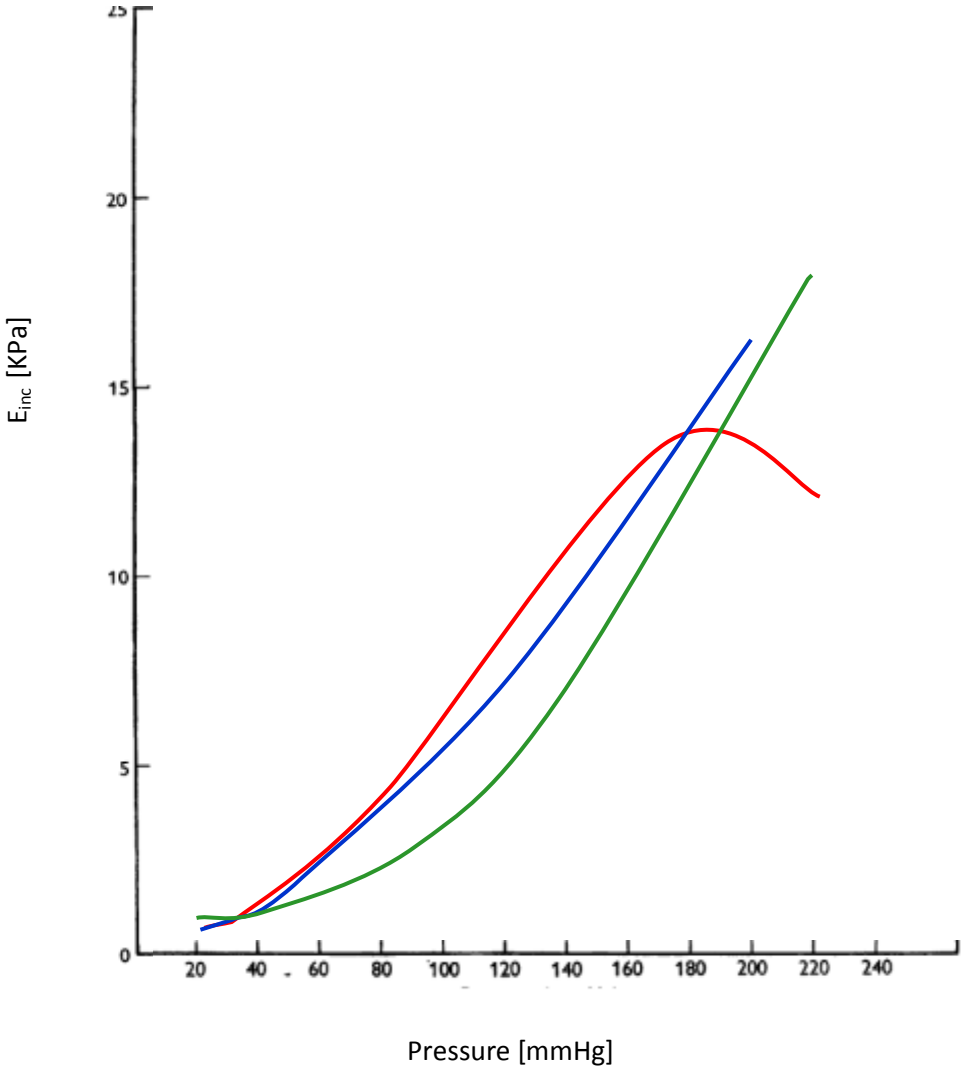

Figure 2.11: Mean values for the static incremental modulus (E_{inc}) of three types of artery. A blue line represents thoracic aorta; red is used for the abdominal aorta; x, femoral artery is drawn in green.

This was also repeated to cover different types of arteries by Cox [15]. Pressure–diameter was calculated as shown in figure 2.12.

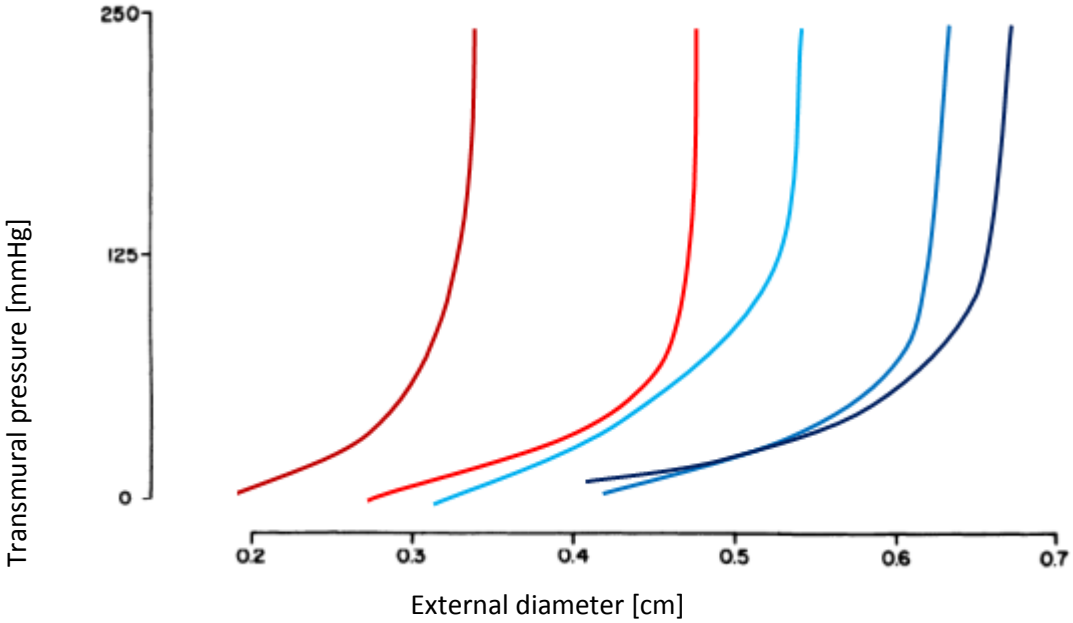

Figure 2.12: External diameter versus transmural pressure for different artery [15], Coronary (green), Renal (red), Carotid (navy blue), Mesenteric (blue) and Iliac (dark blue).

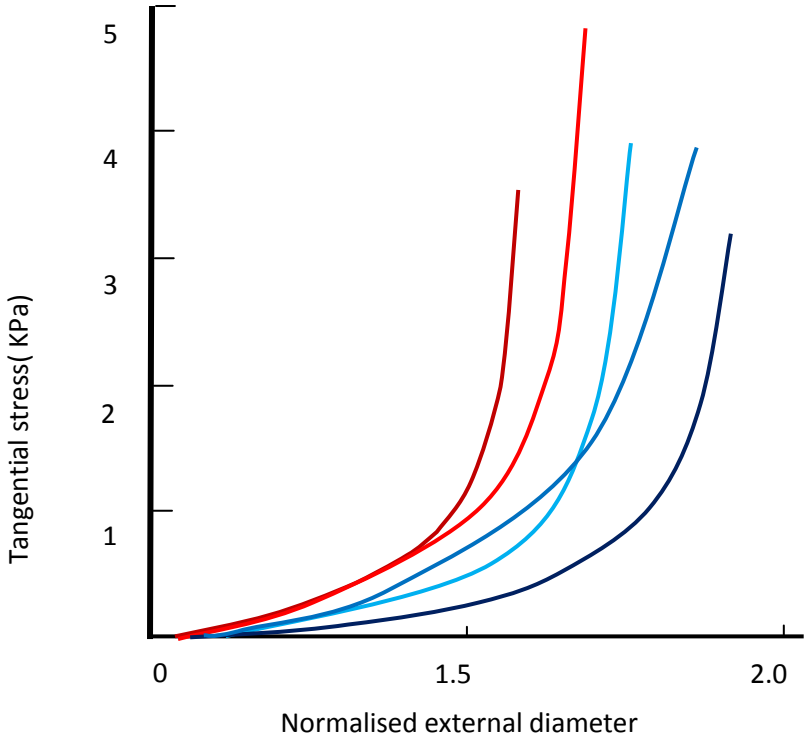

Figure 2.13: Normalised external diameter extension ratio was drawn versus the tangential stress[15], Mesenteric (green), renal (red), lilac (navy blue), carotid (blue) and coronary artery (dark blue).

In figure 2.13, Cox converted all the pressure–diameter relationships to diameter- tangential stress relationships. He then used a polynomial strain-energy function that was later proved to be inefficient in representing the collagen and elastin response by Fung [23].

Investigating the elastic properties continued through the work of Fung et al[23]. A pressure–radius relationship was produced as a result of a biaxial test (figure 2.14). This was further transferred (using thin wall theory) to a relation between stress and strain, figure 2.15, but no investigation has been done on the layers properties.

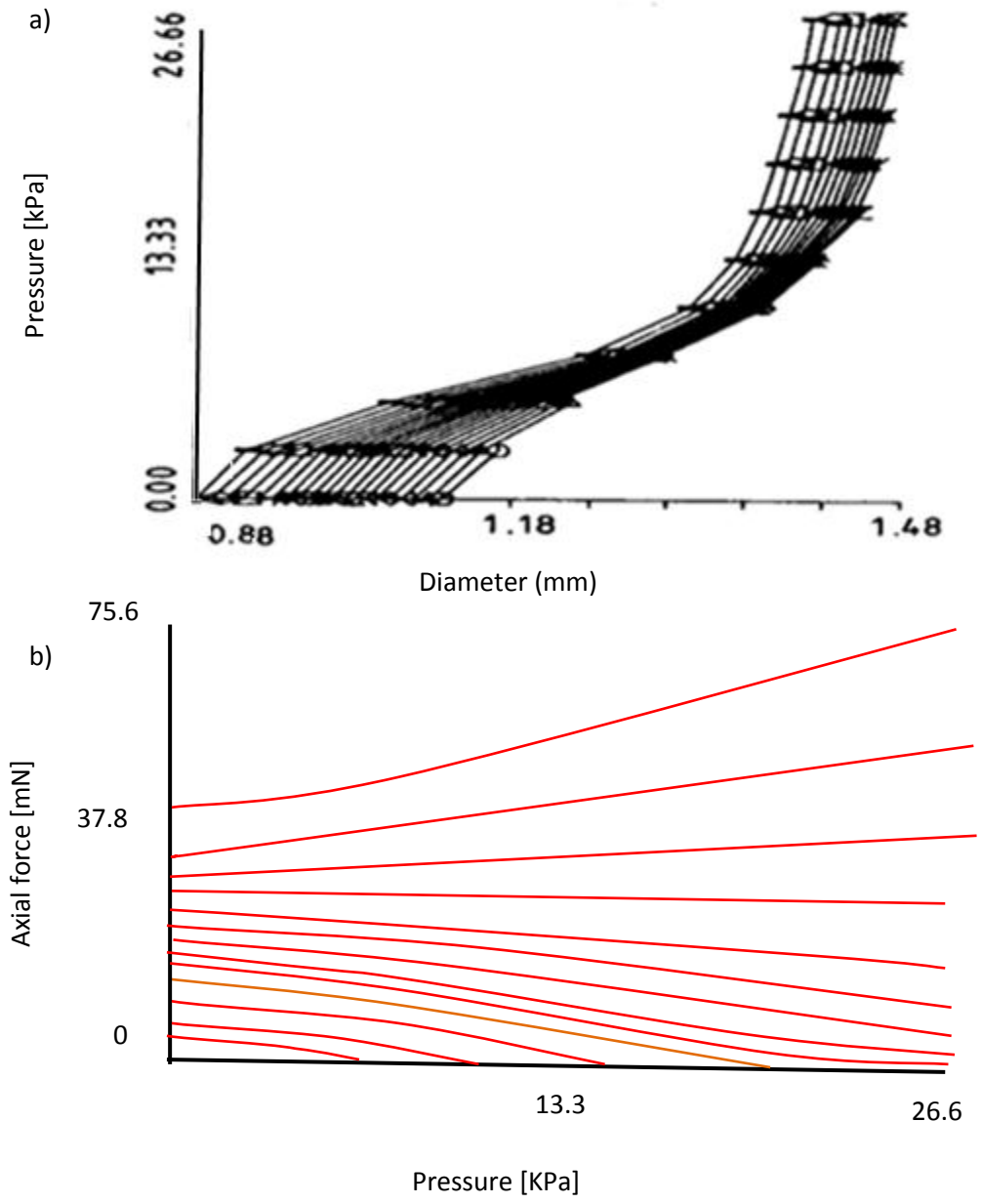

Figure 2.14: Pressure versus diameter in figure (a), axial force versus pressure in the figure (b) [23].

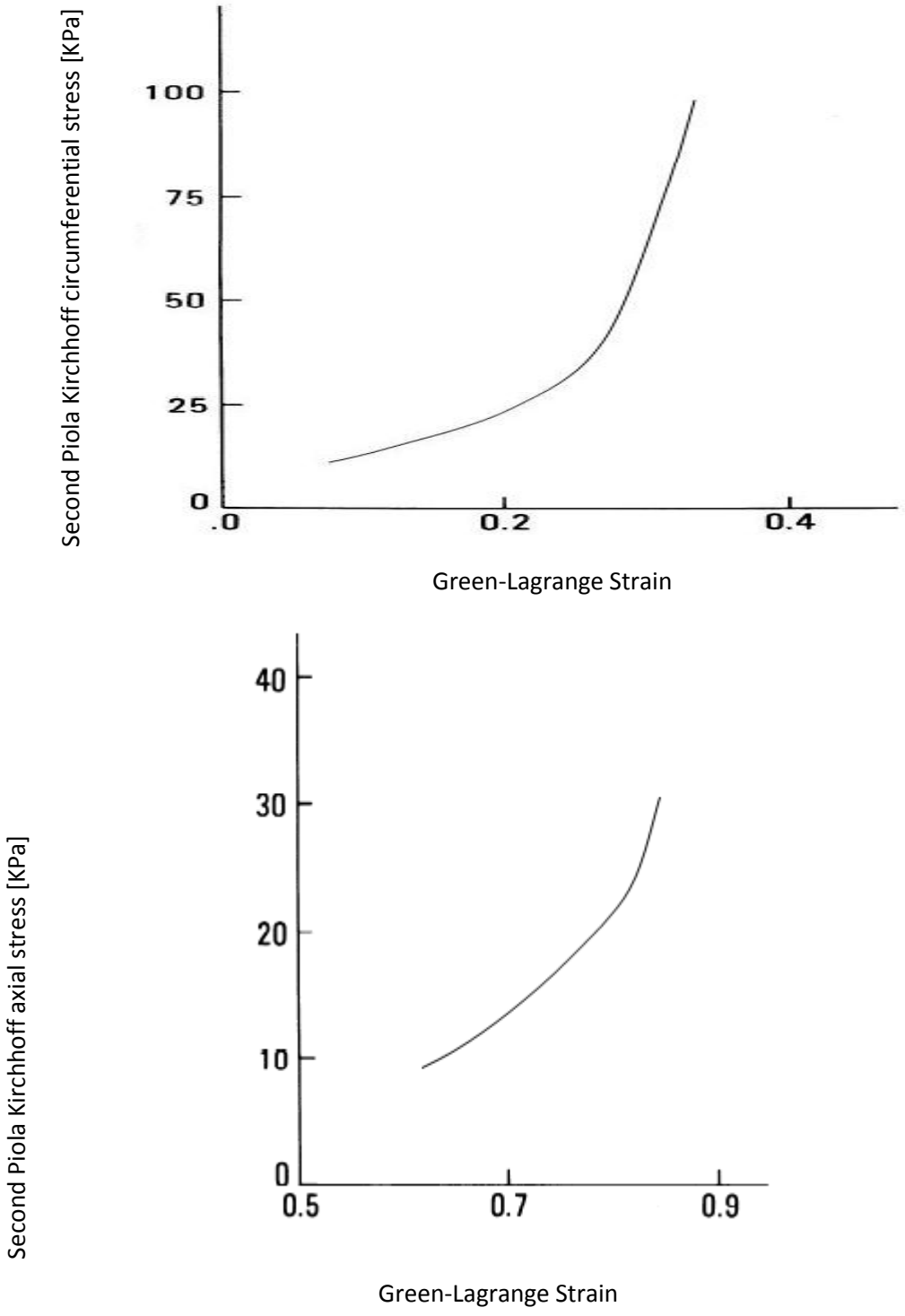

Figure 2.15: Fung relationship for the whole wall, in the circumferential and axial direction[23].

In [30], after performing experiments on the arterial wall , Holzapfel et al introduced a new strain energy function to represent the stress strain relationship for the arterial wall (figure 2.16) , but still no layer representation (experimental or analytical) was shown.

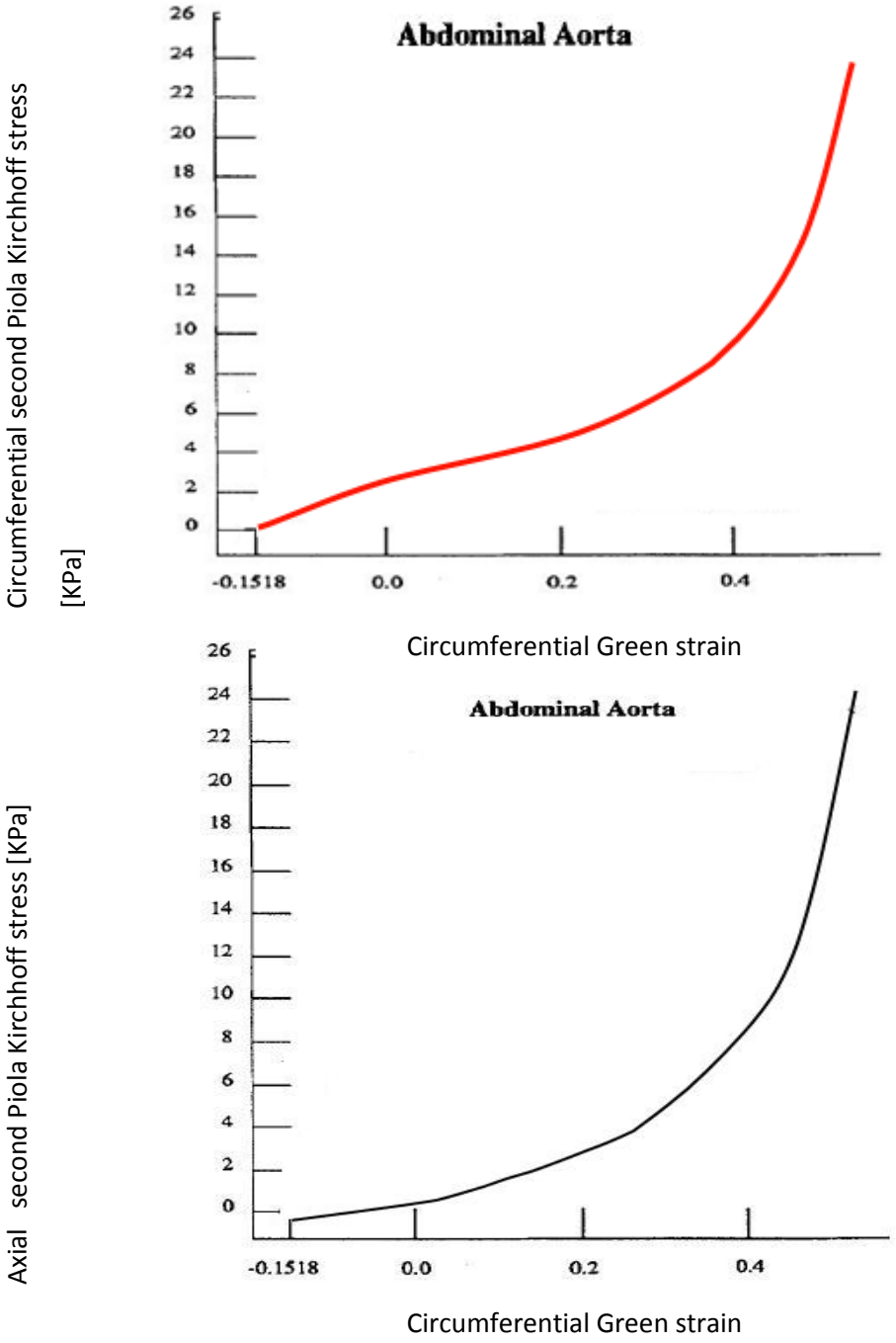

Figure 2.16: Holzapfel green strain relationship with the circumferential stress and axial stress [30].

In the last section, different experimental investigations of the arterial wall were described. The next section will describe investigations on veins. Finally, layers experimental investigations will be presented.

There are fewer studies of the mechanical properties of veins compared to arteries. This seems oblivious to the importance of veins as vessels that return blood to the heart, having passive and active features that affect returning blood to the heart and cardiac filling[2, 4, 33]. Typically most veins studies are focused on using veins as arterial grafts, but few papers have investigated the vein wall stress-strain relationship or layer characteristics [33]. More studies are needed to investigate vein mechanical characteristics, as veins have a high incidence of pathological conditions such as varicose veins, venous insufficiency, and blood occlusion to clot formation.

One of the first studies of veins was done by Attinger [4], where pressure-diameter relationships (figure 2.17) were presented, but no layer comparison was described.

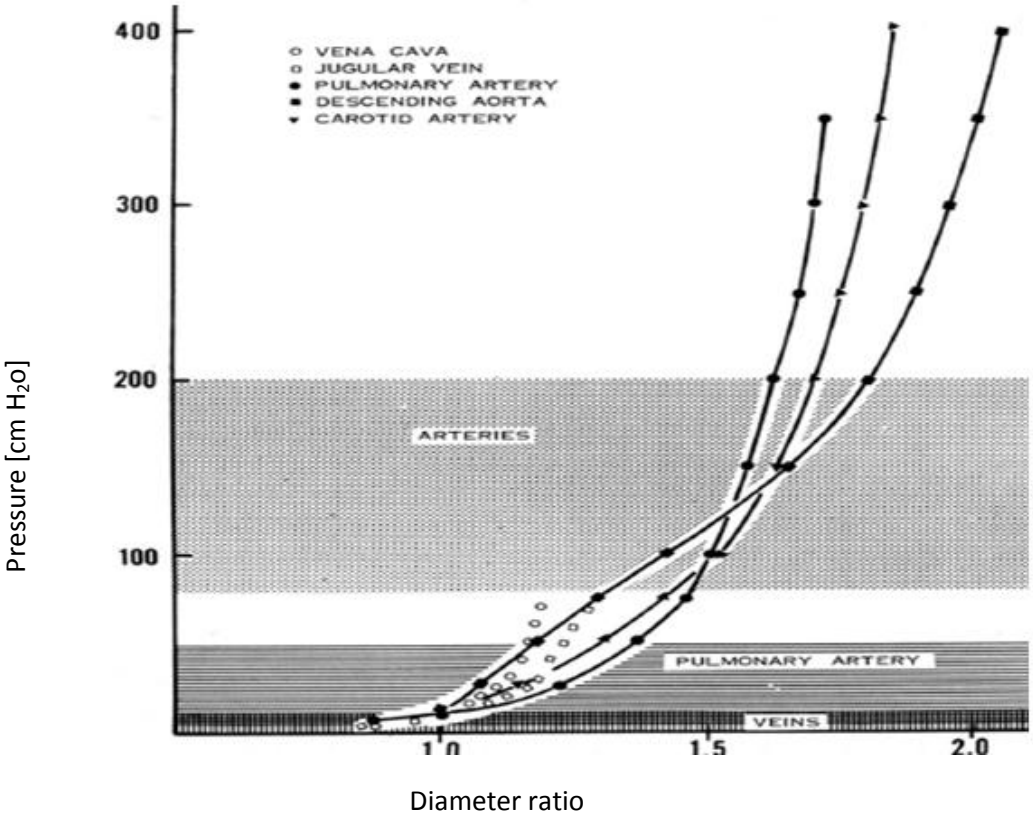

Figure 2.17: Comparison of the diameter radius relationship for different arteries, veins [4].

Recently, [2] calculations of stress as the force over area and the strain as the change in length over the original length were used to produce stress-strain curves for bovine vena cava as shown in figure 2.18. No layer features were investigated [2].

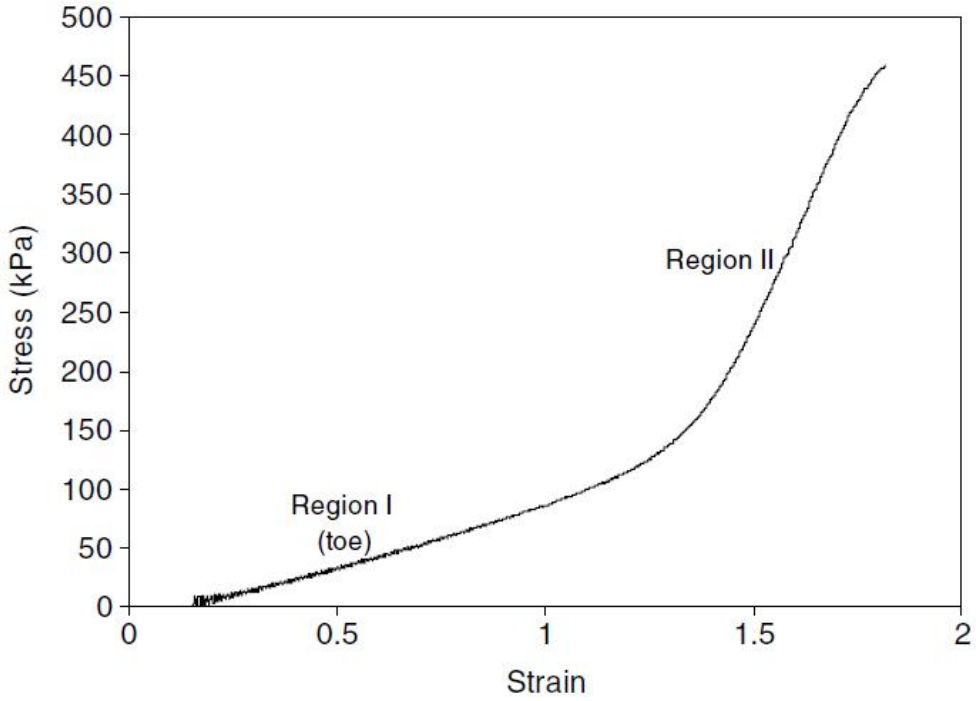

Figure 2.18: Pressure-radius relationship is transferred to stress-strain curves using simple assumptions [2].

2.3.2 Summary

In the past section, experimental techniques were introduced focusing on biaxial *in vitro* methods. Whole wall experiments were shown for both different types of arteries and veins. In the following sections, experimental data describing the histological and mechanical properties of these layers are presented. The three layers are referred to the intima, media and adventitia and exist as concentric cylindrical-like layers.

2.4 Layer investigations

Recent interest in studying vascular wall layer characteristics has gained a huge momentum. The goal behind that is a better understanding of pathological conditions such as arteriosclerosis and atherosclerosis**.** It is also a better way to understand the nature of any grafts that could be used e.g. vein grafts. Even more, it is a way of investigating (as the case in here) the function of elements embedded in the arterial wall such as baroreceptors and other cells. One may think that as the baroreceptors are embedded mainly in the media and adventitia[34-35], studying the intimal stress strain structure would be irrelevant. The answer for this debate would be that the pressure generated by the blood is converted to stress on the whole wall. Thus it is impossible to

understand the stress strain relationships acting on the actual baroreceptors without considering both the whole wall and the layers stress strain relationship.

Normally, as the scope of science is ever changing as explained above, scientists have used two main techniques in investigating the layers characteristics.

I. Technique 1: (No separate role for the intima) used by Demiray, Vito[31, 36] , von Maltzahn [32, 37-38] and others

   Although in the above technique, the intima role was acknowledged, it has been annexed to the media and both of them were treated as one layer. The reason behind that is that the intima was thought to be the thinner especially because all the sources of their experiments were young animal models)[14].

II. Technique 2: (separate Intima role) This has been proven not to be a general feature as Holzapfel et al have found that in older human subjects, the intimal thickness is universally 27% of the whole thickness and it is the stiffest layer from the mechanical point of view.

Thus in the following section each layer will be presented from two points of view, histological and mechanical using the experimental results discussed above.

2.4.1 Intima

2.4.1.1 Histological studies

The intima functions as an interface between thrombogenic media and the blood. It has been suggested to be the mechanically dominant layer [21-22]. The intima is the inner most layer and is composed of a layer of endothelium cells and a subendothelial layer which is formed of dispersed collagen fibres (Type I), dispersed smooth muscle cells [14, 21] and elastin. Unlike collagen and smooth muscle cells, elastin is arranged in a three-dimensional network of elastic fibres. This may be due to the existence of a high content of collagen (Type I)[21]. The histological features of the intima is summarised in table 2.4.

Table 2.4

Intima histological features

intima	Histological feature
Collagen distribution	Dispersed
Collagen content	Highest
Elastin distribution	Three-dimensional network of elastic fibres.

2.4.1.2 Mechanical studies

As mentioned above Holzapfel et al carried out the first experiments on the intima. The arteries were separated from the adipose and connective tissues, after that, a cut was made longitudinally, the results were in the form of rectangular pieces. Then Strips from adjacent parts were cut in the axial and circumferential orientations of the arterial wall, as shown in figure 2.19.

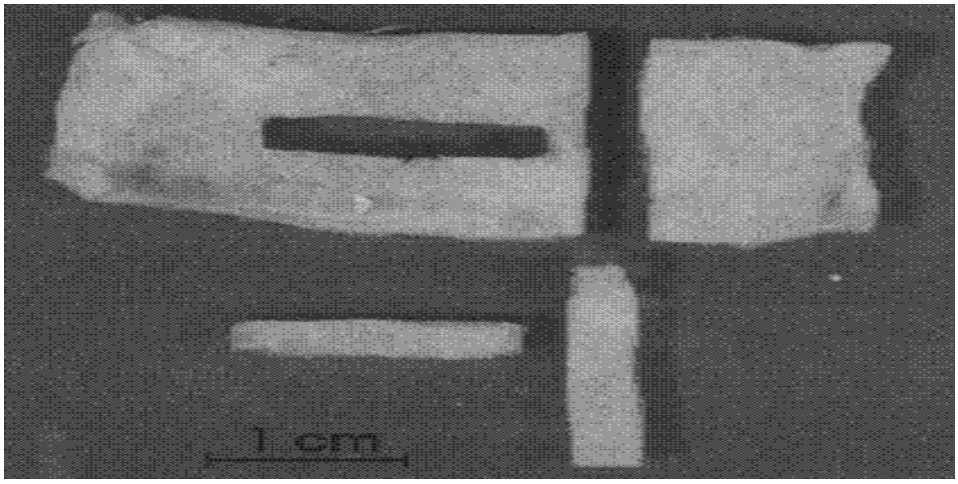

Figure 2.19: Representative axial and circumferential strips excised from a dissected adventitial layer[39].

A video extensometer was used to measure sample dimensions (length, width, and thickness). The layers were separated by disconnecting the interconnective tissue using a scalpel. After that uniaxial tests with biaxial measurements were done. The associated experimental Cauchy stresses, σ_θ and σ_z, were calculated directly from the original data as $\sigma_{tens} = f\lambda_{tens}/A$, where σ_{tens} represents the Cauchy stress in the circumferential or axial direction and $\lambda_{tens} = l/L$ for the associated stretch ratio, with gauge lengths l and L measured in the loaded and unloaded configurations, respectively. The experimental results are shown in figure 2.20.

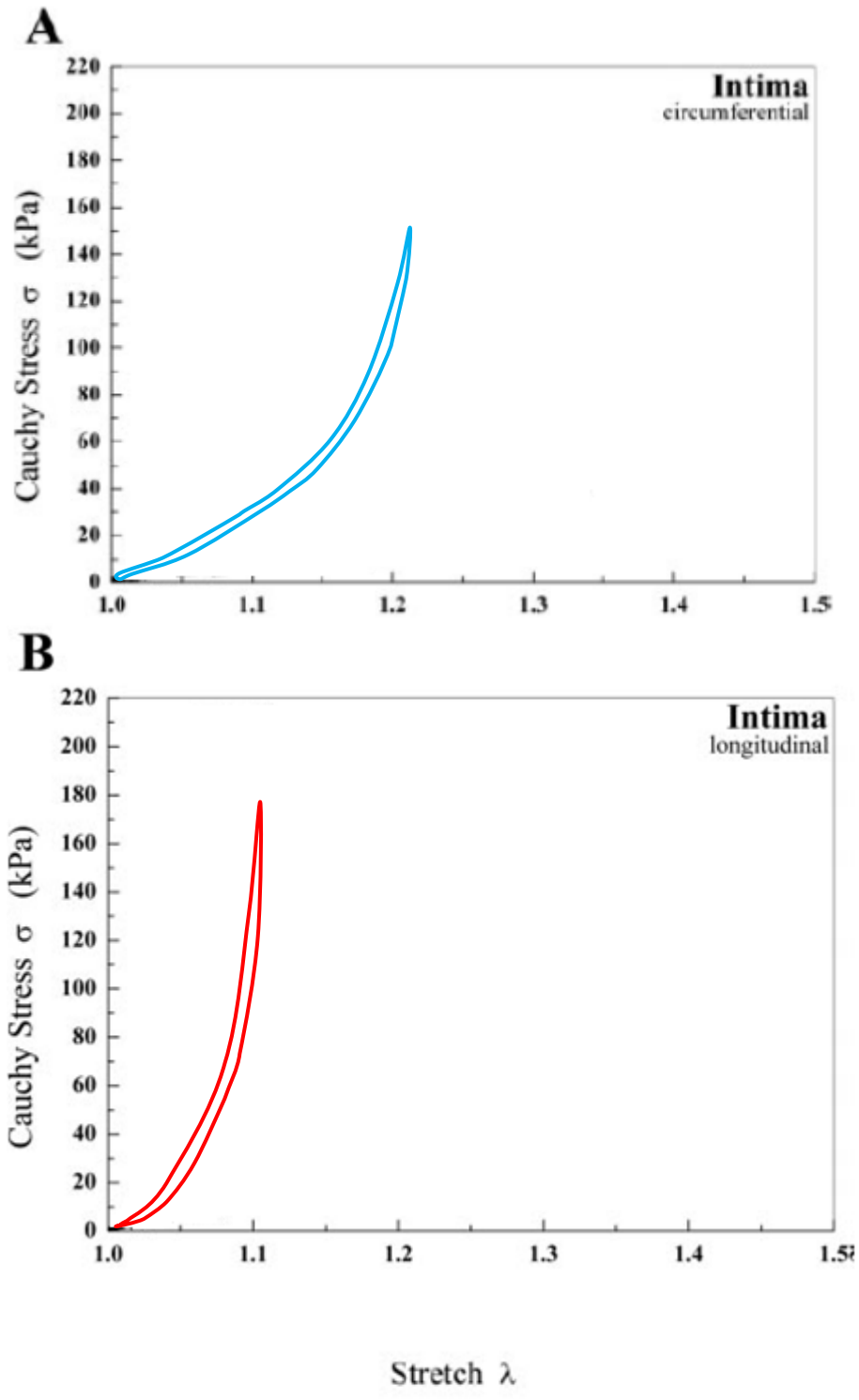

Figure 2.20: Circumferential(a) and longitudinal (b) experimental responses for the intima data take from [22],showing loading and unloading conditions for each curve.

It can be seen from these tests, that the intimal reaction was stiffer in the axial direction than the circumferential direction. The stress curve consists of two phases. The first one governed by the

elastin and it is almost a linear relationship between stretch and stress. After that the collagen effect starts. The mechanical properties of the intima is summarised in table 2.5.

Table 2.5

Mechanical properties of the intima

Mechanical feature	Description
Stiffer direction	Longitudinal
Stiffness	Stiffest
Effect at the start of the curve	Linear relationship at the start of response

2.4.2 Media

2.4.2.1 Histological studies

The media layer sits between the intima and adventitia. As a whole, the media is thought to be the softest layer [14, 22, 40]. It consists of a three-dimensional network of bundles of collagen fibrils, elastin and smooth muscle cells [14, 41]. Collagen (Type III), and smooth muscle cells, are located in the circumferential direction. This structured arrangement gives the media the ability to resist high loads in the circumferential direction[41]. When under stress, these fibres are reoriented to the circumferential direction. This is one of the reasons why the media is stiffer in the circumferential direction more than in the longitudinal direction [22]. The histological features of the intima is summarised in table 2.6.

Table 2.6

Media histological features

Media	Histological feature
Collagen distribution	Circumferentially
Collagen content	Lowest
Elastin distribution	Three-dimensional network of elastic fibres

2.4.2.2 Mechanical studies

von Maltzahn et al [32, 37-38] offered one of the most important contributions to the field. In [32], experimental measurements of the elastic properties of media and adventitia were presented but no measurements were done on the intima. In doing this, they first tested the whole arterial segment to obtain the inner pressure-radius relations, and then they removed the adventitial layer from the original segment and repeated the experiment for the remaining medial segment. The results are shown in figure 2.21.

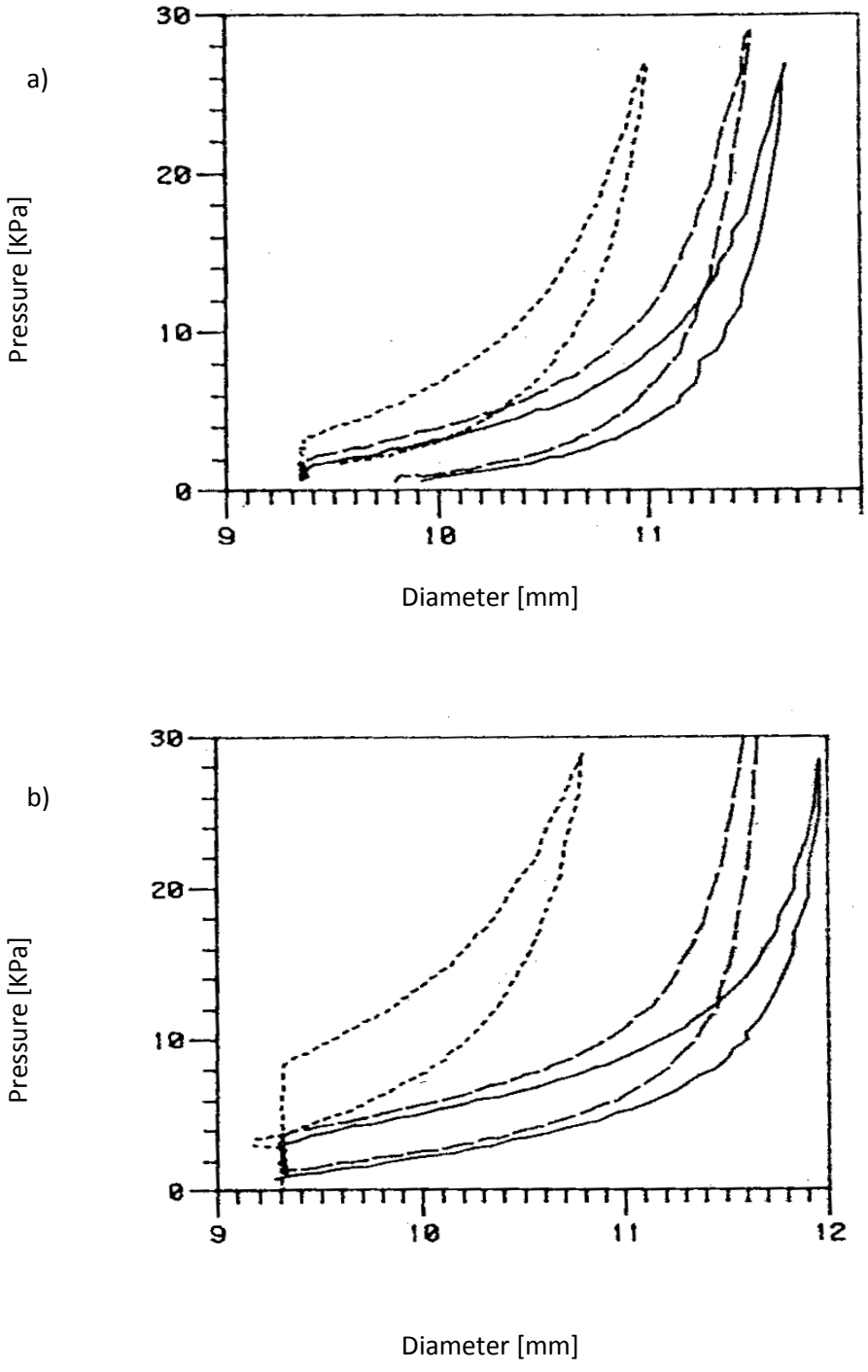

Figure 2.21: Media pressure [KPa] versus diameter in [mm] is shown in figure a, while the same is shown in figure b for the whole wall [32].

This was also the case with the research done by Demiray and Vito [31, 36]. Here experiments were carried out on the media and the adventitia only, approximating the media and the intima to be one layer. It was thought that the intimal thickness was not sufficient for it to contribute to the mechanical properties of the arterial wall as a whole. The properties of the media and, adventitia are shown in table 2.7. Circumferential strain is given by λ_1, axial strain is given by λ_2, σ_{11}, and σ_{22} are the Cauchy stresses in the circumferential and axial direction respectively.

Table 2.7

Strain is calculated against stress [31]

λ_1	λ_2	t_{11}(exp.)(dyne/cm^2)	t_{12}(exp.)(dyne/cm^2)
1.91	1.112	123,200	179,100
1.127	1.144	217,100	302,300
1.158	1.175	310,700	448,800
1.200	1.219	449,000	627,800
1.230	1.237	586,600	807,100

Using Holzapfel layer data for the media mentioned in section 4.23, the results are shown in figure 2.22.

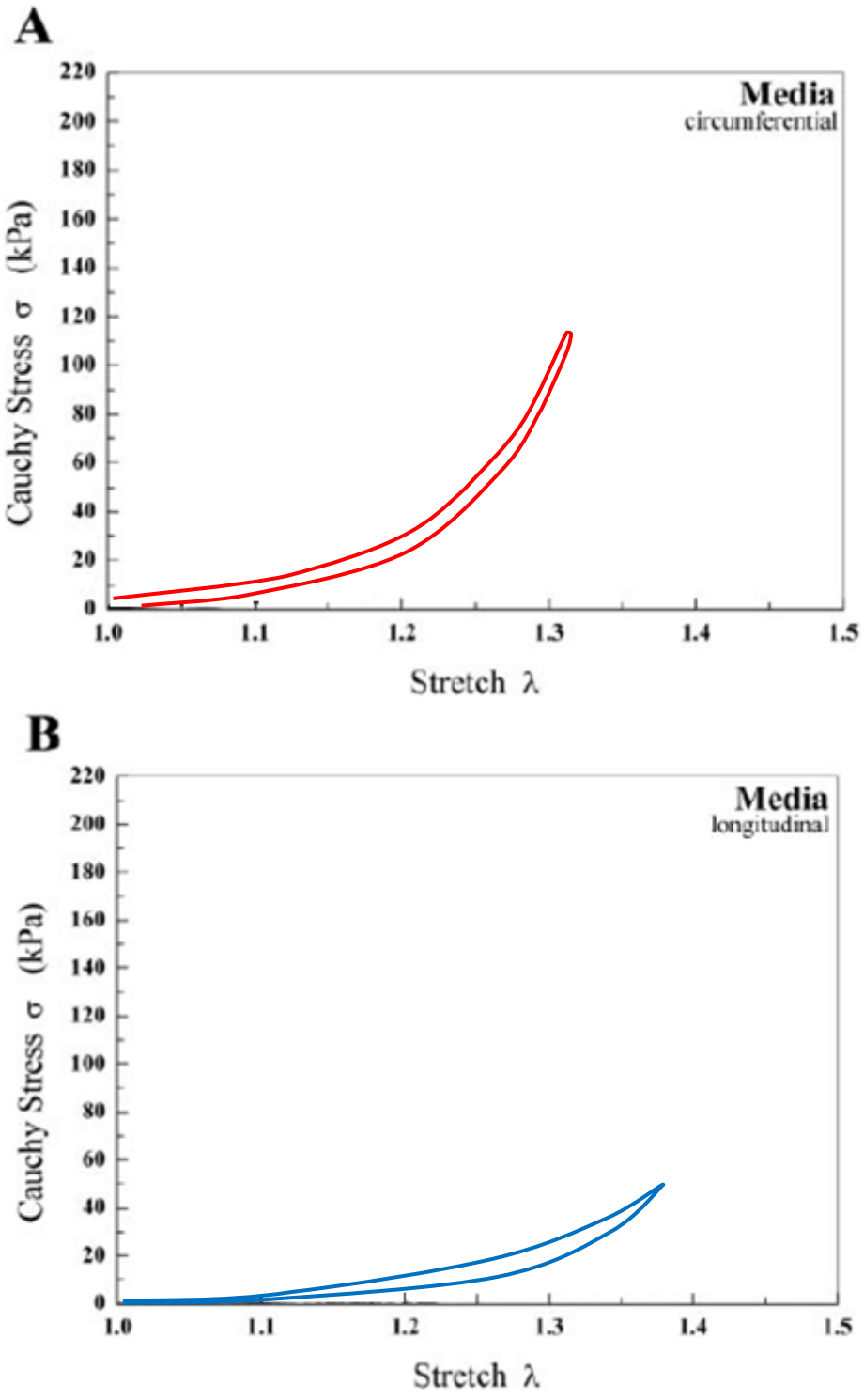

Figure 2.22: Circumferential(a) Longitudinal (b) experimental responses for the media [22].

These data suggest that the media is the softest layer. It is stiffer circumferentially than axially. Its mechanical feature are summarised in table3.8.

Table 2.8

Mechanical properties of the media

Mechanical feature	Description
Stiffer direction	Circumferential
Stiffness	Softest
Dominates at lower stresses	Linear relationship at lower stresses

2.4.3 Adventitia

2.4.3.1 Histological studies

The adventitia or outermost layer consists mainly of fibroblasts, fibrocytes, and collagen fibres organised in thick bundles. The collagen fibres (Type I) [42]are arranged within the ground-matrix and form a fibrous tissue. In the adventitial layer the orientation of the collagen fibres is dispersed[42]. The relationship between histological structure and the mechanical load bearing system is summarised in table 2.9.

Table 2.9

Histological properties of the adventitia

Adventitia	Histological feature
Collagen distribution	Dispersed
Collagen content	Medium stiffness
Elastin distribution	Three-dimensional network of elastic fibres.

2.4.3.2 Mechanical studies

In the same work by Demiray and Vito[36] , the stress and strain were calculated for the adventitia as shown in table 2.10.

Table 2.10

Stress and strain relationship for the adventitia [31]

λ_1	λ_2	t_{11}(exp.)(dyne/cm^2)	t_{12}(exp.)(dyne/cm^2)
1.094	1.120	201,990	232,170
1.129	1.156	284,570	318,450
1.59	1.186	378,760	426,190
1.206	1.222	502,620	543,590
1.235	1.258	626,580	680,070
1.271	1.287	811,430	843,330

The results calculated by Holzapfel for the adventitia are shown in figure 2.23.

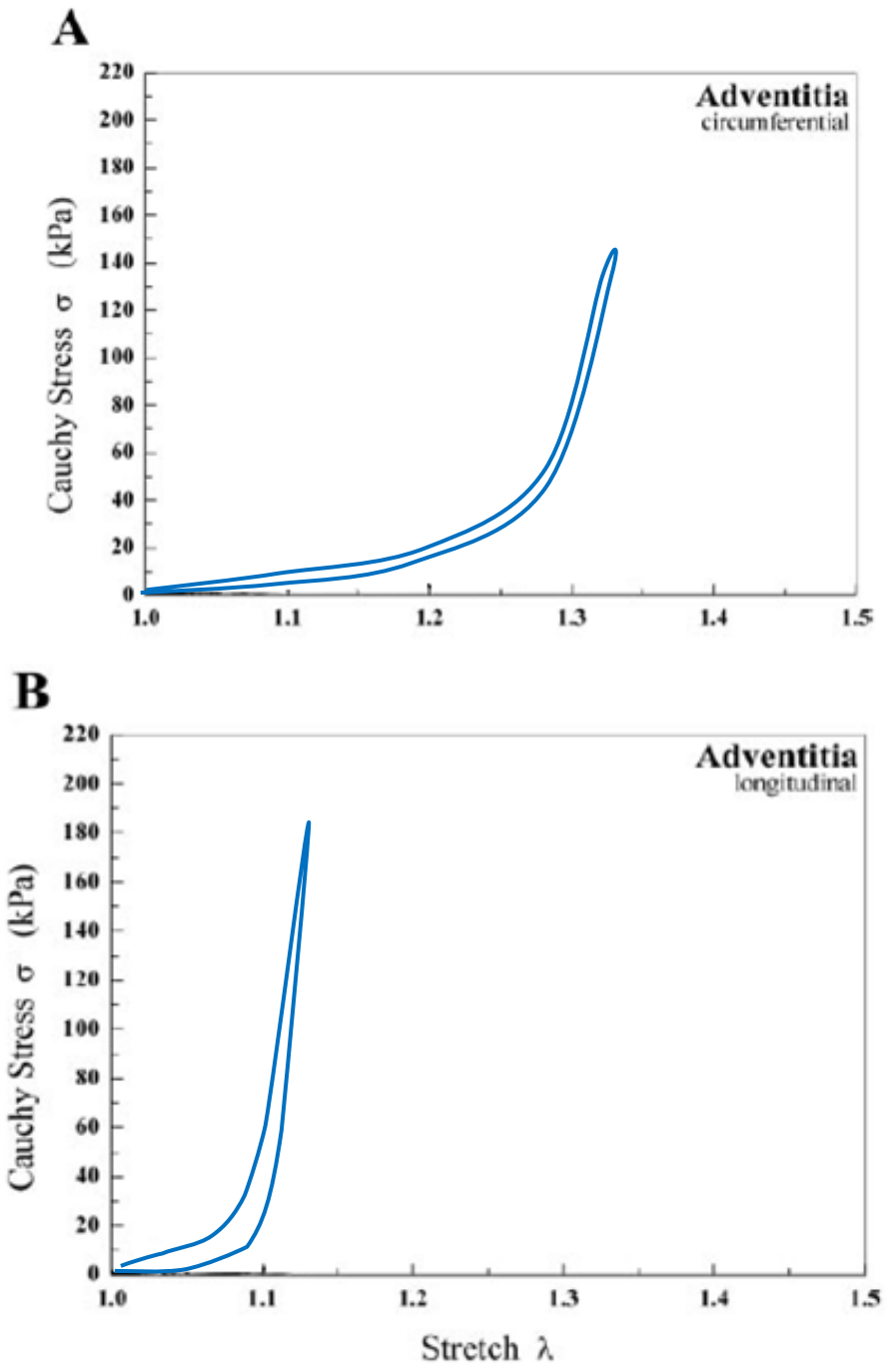

Figure 2.33: Stretch-stress relationship for the adventitia.

Table 2.11

Mechanical features of the adventitia

Mechanical feature	Description
Stiffer direction	Longitudinal
Stiffness	Medium stiffness
Dominant at low stresses	Linear relationship at low stresses

2.5 Layers constraints and inter-relations

These experiments revealed interesting results concerning the stress response of each layer. The typical non linear elasticity was shown by all layers, where a starting linear increase with strain followed by exponential increase at higher stretches.

Investigating the resulting curves revealed the following relationships

$k_{circumferential\ intima} > k_{circumferential\ adventitia} > k_{circumferential\ media}$

$k_{axial\ intima} > k_{circumferential\ intima}$

$k_{axial\ adventitia} > k_{circumferential\ adventitia}$

$k_{circumferential\ media} > k_{axial\ media}$

$k_{axial\ intima} > k_{axial\ adventitia} > k_{axial\ media}$

where k is the stiffness of each layer. It is clear that the media although it is known as the biggest layer it is also found to be the softest layer. The relationship between the layers stiffness are shown in figure 2.24.

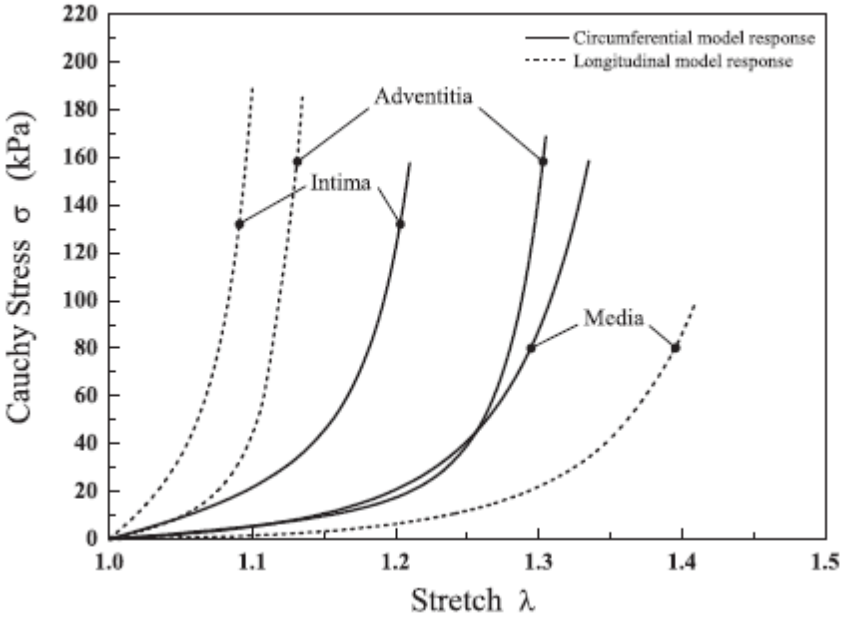

Figure 2.24: Stretch versus stress for different layers of the arterial wall[22].

However through all these experiments, there no clear relationship between the stress contribution of each layer and the whole wall stress response. These might be due to the difficulty of the experiments mentioned in [22] concerning separation of the layers from the whole wall. It also arises from the difficulty of getting hold of human specimens to perform the required experiments.

Thus the need arises for a numerical method to connect the relationship of the three layers with the total whole wall relationship. A numerical or analytical method could eliminate the need for such experiments and could open the door for further investigation of the mechanical properties of the layers without doing the actual experiments on them separately. In other words; having the data of the whole wall through basic bidirectional experiments and using a method to give insight into the properties of the layers. That is the purpose of the model proposed in this thesis.

The applications of such a model or method are huge it varies through investigating pathological conditions ,arterial connectors or even investigating the stress or strain which is a certain type of sensors already embedded inside the wall might be subjected to. This could help in designing biosensors that could work on molecular scale.

2.6 Conclusions

In the previous section experimental evidences for arteries and veins, First vascular vessels were classified according to their functions, into elastic, muscular, resistance, exchange and

capacitance vessels. After that arterial wall main components were identified to be elastin, collagen and smooth muscle cells. Elastin is an extracellular matrix protein which is responsible for the resilience (ability to recover to its original shape) of tissues found in the skin, arteries and lungs. Collagen accounts for about 20–30% of total body proteins of many vertebrates. Thus it could be considered as one of the proteins used most extensively by mammals. Stress strain relationship is linear in case of elastin and nonlinear in case of collagen. An interesting test was presented through which control, elastin digested and collagen digitised curves were shown. It was also shown that the collagen is far stiffer than elastin. Smooth muscle cells were shown not take part in the passive filling of vascular walls. After that, whole wall investigations were presented on two levels; histological and mechanical. Mechanical tests types were discussed including uniaxial and biaxial tests. After that histological and mechanical studies were introduced for separate layers, intima, media, and adventitia. Intima was shown to be the stiffest layer in both the axial and circumferential directions, followed by the adventitia then finally the media. The intima is stiffer axially that circumferentially, same as the adventitia. In contrast the media is stiffer circumferentially than axially. As a whole, arterial walls are stiffer axially than circumferentially. Also comparisons between arteries and veins responses showed that arteries are stiffer and thicker while veins are thinner and wider. What is yet to be explained through our modelling approach is how the stress strain profile for the whole wall is related to that of the three distinct mechanical layers.

2.7 References

1. Levick JR, *An Introduction to Cardiovascular Physiology*. 2003, London: Hodder. 384.
2. Rossmann JS, *Elastomechanical Properties of Bovine Veins.* J Mech. Behave. Biomed. Mat, 2010. **3**(2): p. 210-215.
3. Schneck DJ, *An Outline of Cardiovascular Structure and Function*, in *The Biomedical Engineering Handbook* Bronzino JD, Editor. 2000, Boca Raton: CRC Press LLC,.
4. Attinger E, *Wall Properties of Veins.* IEEE Trans on bio-med, 1969. **16**(4).
5. Pandit A, Lu X, Wang C, and Kassab G, *Biaxial Elastic Material Properties of Porcine Coronary Media and Adventitia.* Am J Physiol Heart Circ Physiol, 2005. **288**: p. H2581–H2587.
6. Kalita P and Schaefer R, *Mechanical Models of Artery Walls.* Arch Comput Methods Eng, 2008(15): p. 1–36.
7. Stein WH and Miller EG, *The Composition of Elastin*, in *Faculty of Pure Science* 1938, Columbia University.
8. Parsons JC, Hoffman Y, Potter KA, and Besser TE, *Normal Elastin Content of Aorta in Bovine Marfan Syndrome.* EXPERIMENTAL AND MOLECULAR PATHOLOGY, 1992. **57**: p. 145-152
9. Gundiaha N, Ratcliffea MB, and Pruittc LA, *Determination of Strain Energy Function for Arterial Elastin: Experiments Using Histology and Mechanical Tests.* J. Biomech., (2007)(40): p. 586–594.
10. Lee CH, Singla A, and Lee Y, *Review: Biomedical Applications of Collagen.* International Journal of Pharmaceutics, 2001(221): p. 1–22.
11. Nykvis Pt, Tu H, Ivaska J, Ka pyla J, Pihlajaniemi T, and Heino J, *Distinct Recognition of Collagen Subtypes by A1b1 and A2b1 Integrins.* Vol. 275, 2000. **275**(11): p. 255–8261.
12. Sasaki N and Odajimat S, *Stress-Strain Curve and Young's Modulus of a Collagen Molecule as Determined by the X-Ray Diffraction Technique.* J. Btomechics, 1996. **29**(5): p. 655-658.
13. Gabella G, *Morophology of Smooth Muscles*, in *Cellular Aspects of Smooth Muscle Function*, Kao CY and Carsten ME, Editors. 2005, Cambridge University Press.
14. Holzapfel GA, Gasser T, and Ogden R, *A New Constitutive Framework for Arterial Wall Mechanics and a Comparative Study of Material Models.* J. Elast., 2000. **61**(1): p. 1-48.
15. Cox RH, *Regional Variation of Series Elasticity in Canine Arterial Smooth Muscles.* Am. J. Physiol. Heart. Circ. Physiol., 1978. **234**(5): p. H542-551.
16. VanBavel E, Siersma P, and Spaan JAE, *Elasticity of Passive Blood Vessels: A New Concept.* Am J Physiol Heart Circ Physiol, 2003. **285**: p. H1986–H2000.
17. Holzapfel GA, *Collagen. Structure and Mechanics*, in *Collagen in Arterial Walls: Biomechanical Aspects*, P. Fratzl, Editor. 2008, Springer-Verlag, Heidelberg: New York. p. 285-324.
18. Fenner R, *Mechanics of Solids*. 1989, Oxford: Blackwell scientific publications. 615.
19. Kroon M and Holzapfel GA, *A New Constitutive Model for Multi-Layered Collagenous Tissues.* J. Biomech., 2008 **41**(12): p. 2766-2771.
20. Barry M, Foulon P, Touati G, Ledoux B, Sevestre H, Carmi D, and Laude M, *Comparative Histological and Biometric Study of the Coronary, Radial and Left Internal Thoracic Arteries.* Surg. Radiol. Anat., 2003. **25**(3): p. 284-289.

21. Canham PB, Finlay HM, Dixon JG, Boughner DR, and Chen A, *Measurements from Light and Polarised Light Microscopy of Human Coronary Arteries Fixed at Distending Pressure.* Cardiovasc. Res., 1989. **23**(11): p. 973-982.
22. Holzapfel GA, Sommer G, Gasser CT, and Regitnig P, *Determination of Layer-Specific Mechanical Properties of Human Coronary Arteries with Nonatherosclerotic Intimal Thickening and Related Constitutive Modeling.* Am. J. Physiol. Heart Circ. Physiol., 2005. **289**(5): p. H2048-2058.
23. Fung YC, Fronek K, and Patitucci P, *Pseudoelasticity of Arteries and the Choice of Its Mathematical Expression.* Am. J. Physiol. Heart Circ. Physiol., 1979. **237**(5): p. H620-631.
24. Cox RH, *Comparison of Arterial Wall Mechanics Using Ring and Cylindrical Segments.* Am J Physiol Heart Circ Physiol, 1983. **244** p. H298–H303.
25. BERGEL DH, *The Static Elastic Properties of the Arterial Wall.* J. Physiol. , 1961. **156**: p. 445-457.
26. Weizsacker HW, Lambert H, and Pascale K, *Analysis of the Passive Mechanical Properties of Rat.* J. Biomech., 1983. **16,**: p. 703-715.
27. Holzapfel GA, *Biomechanical Behavior of the Arterial Wall and Its Numerical Characterization.* Comp. Biol. Med., 1998. **28**: p. 377-392.
28. Humphrey JD, *Mechanics of Arterial Wall: Review and Directions.* Critical Reviews in Biomed.Engr., 1995. **23** p. 1–162.
29. van Andel CJ, Pistecky PV, and Borst C, *Mechanical Properties of Porcine and Human Arteries: Implications for Coronary Anastomotic Connectors.* Ann. Thorac. Surg., 2003. **76**(1): p. 58-64.
30. Holzapfel GA, Eberlein R, Wriggers P, and Weizsäcker HW, *A New Axisymmetrical Membrane Element for Anisotropic,Finite Strain Analysis of Arteries.* Commun. Num. Meth. Eng., 1996. **12**(8): p. 507-517.
31. Demiray H, *A Note on the Elasticity of Soft Biological Tissues.* J. Biomech., 1972. **5**(3): p. 309-311.
32. von Maltzahn WW, Besdo D, and Wiemer W, *Elastic Properties of Arteries: A Nonlinear Two-Layer Cylindrical Model.* J. Biomech., 1981. **14**(6): p. 389-397.
33. Desch GW, *A Model for Passive Elastic Properties of Rat Vena Cava.* J. Biomech., 2007. **40**: p. 3130-3145.
34. Wolfgang K, *Three Types of Neurochemically Defined Autonomic Fibres Innervate the Carotid Baroreceptor and Chemoreceptor Regions in the Guinea-Pig.* Anat Embryol, 1990. **181**: p. 477-489.
35. Chapleau MW, Li Z, Meyellers S, Ma X, and . Abboud F, *Mechanisms Determining Sensitivity of Baroreceptor Afferents in Health and Disease.* Ann N Y Acad Sci, 2001. **940**: p. 1-19.
36. Demiray H and Vito RP, *A Layered Cylindrical Shell Model for an Aorta.* Int. J. Engrng. Sci., 1991. **29**(1): p. 47-54.
37. von Maltzahn WW, *Stresses and Strains in the Cone-Shaped Carotid Sinus and Their Effects on Baroreceptor Functions.* J. Biomech., 1982. **15**(10): p. 757-765.
38. von Maltzahn WW, Warriyar RG, and Keitzer WF, *Experimental Measurements of Elastic Properties of Media and Adventitia of Bovine Carotid Arteries.* J. Biomech., 1984. **17**(11): p. 839-847.
39. Holzapfel GA, Sommer G, and Regting P, *Anisotropic Mechanical Properties of Tissue Components in Human Atherosclerotic Plaques.* J Biomech Eng., 2004. **126**.
40. Sokolis DP, Kefaloyannis EM, Kouloukoussa M, Marinos E, Boudoulas H, and Karayannacos PE, *A Structural Basis for the Aortic Stress-Strain Relation in Uniaxial Tension.* J. Biomech., 2006. **39**(9): p. 1651-1662.

41. Clark JM and Glagov S, *Structural Integration of the Arterial Wall. I. Relationships and Attachments of Medial Smooth Muscle Cells in Normally Distended and Hyperdistended Aortas.* Lab. Invest., 1979. **40**(5): p. 587-602.
42. von der Mark K and Ocalan M, *Immunofluorescent Localization of Type V Collagen in the Chick Embryo with Monoclonal Antibodies.* Coll. Relat. Res, 1982. **2**(6): p. 541-555.

CHAPTER 3

REVIEW OF MATHEMATICAL MODELS

---

3 Overview

This section describes the various types of models and assumptions used to predict the mechanical properties of arterial walls. Firstly, a comparison of one dimensional partial differential equation is given, together with, two reported model structures. Secondly, the assumptions used to simplify the models are discussed. The next sections in the chapter concentrate on non linear models with particular emphasis on phenomenologically derived strain-energy functions. These form the basis of the research presented in this thesis. For comparison, finite element non-linear models are discussed. The chapter concludes with a comparison of the models presented.

3.1 Analytical models

Modelling the elasticity of arteries has been an interesting topic for scientists over the last few centuries. Hales[1] was the first person to realise the effect of arterial elasticity on blood flow. Later, Otto Frank [1] presented the simple 'air kettle theory'. This theory assumes that energy is stored inside the arterial wall during systole and is transferred to blood during diastole. Nowadays, investigating the elasticity of the arterial wall is done through PDE (partial differential equations). PDE models range from simple 1-D (1-dimensional) models to more complicated 3-D ones. Fewer factors are considered in the 1-D models than the 3-D models. However, 1-D models serve as a simplistic approach for explaining the basics of nonlinear elastic phenomena of arterial walls.

For example complex 3-D models are sensitive to parameters such as geometry of the domain, initial and boundary conditions, physical parameters of the equations including those that are not directly measureable[2]. Furthermore, the development of models is bounded by complexity of underlying physiology[2]. New physiological phenomena are constantly being discovered, including sophisticated control and self regulation mechanisms, presence of stresses and strains in unloaded arteries (residual stresses) and structure and function of various components of the wall which determines its heterogeneous and anisotropic behaviour[2]. One example of simple models is given by equation 1. The systole is represented by a charging the capacitor, while the diastole is represented by the capacitance discharge.

$$\mathrm{I_{cur}} = \frac{\mathrm{U_{volt}}}{\mathrm{R_{res}}} + \mathrm{U'C_{cap}} \tag{1}$$

Current I_{cur} (current) represents the flow rate of blood; U_{volt} is the voltage (pressure) current, $\mathrm{R_{res}}$is the resistance and $\mathrm{C_{cap}}$ is the compliance (extendibility).

3.1.1 One-dimensional models

One-dimensional models take into the consideration the shape of the wall. The wall is either assumed to be an independent ring or a cylindrical membrane. Equations used in this framework can be derived from general 2-D membrane or shell equations if we assume the cylindrical symmetry of the geometry, load and boundary conditions [2]. In the next section the two basic families will be described.

3.1.2 Independent rings model

In this model, it is assumed that the radial displacement at a certain point only depends on the load at this point[3]; the equation governing this relation is given by equation 2.

$$\frac{\mathrm{d^2\eta_{rd}}}{\mathrm{dt^2}} + \frac{\mathrm{E_{ym}}}{\rho_W(1-\nu^2)\mathrm{R_{or}}} = \mathrm{H_{radf}} \tag{2}$$

In the above equation $\mathrm{E_{ym}}$ and ν represent the Young's modulus and Poisson's ratio, $\mathrm{R_{or}}$ is the original vessel radius and ρ_w is the density of the wall material. $\mathrm{H_{radf}}$ stands for the radial load on the wall, $\eta_{rd}$is the radius deformation. Sometimes another term is added to the equation to represent the viscoelasticity of the arterial wall.

3.1.3 Cylindrical Membrane Models

The same equation is used for the cylindrical membrane model, but with an added term to represent the effect of radial stress on deforming the wall [4]. In this case the equation is given by equation 3.

$$\frac{d^2\eta_{rd}}{dt^2} + \frac{E_{ym}}{\rho_W(1-\nu^2)R_O} + \frac{d^2\eta_{rd}KG_m}{dt^2\rho_W} = H_{radf} \tag{3}$$

Constants K and G_m are called the Timoshenko shear correction factor and shear modulus.

In the previous section, 0-D and 1- D models were considered. In the following section the main points controlling 3-D models of the arterial wall will be presented and state-of-the-art models will be introduced.

3.2 Review of model assumptions

The framework utilised aims to solve elastic nonlinear deformation using the theory of nonlinear elasticity. The aim of this theory is to find a relationship between stress and strain in 3-D for a nonlinear elastic material. Its main tools are: the deformation gradient tensor, right Cauchy Green deformation tensor, Green Lagrange strain tensor, principal stretches, first Piola Kirchhoff stress tensor and second Piola Kirchhoff stress tensor. Stress and strain are usually correlated using the strain-energy density function given by equation 4.

$$\mathbf{S} = \frac{\partial \bar{W}}{\partial \mathbf{E}} \tag{4}$$

Where **S**= second Piola Kirchhoff stress tensor, **E**= Green Lagrange strain tensor, $\bar{W}$= strain-energy density function. Table 3.1 summarises the key parameters considered in the models and the factors they affect.

Table 3.1

Summary of the properties

Parameter	Affecting factor
Reference state	Number of dimensions, geometrical shape.
Load	Axial loading, radial loading caused by: blood pressure, shear stress, torsion.
Control phenomena	Short term regulation, long term regulation.
Heterogeneity	Position along the arterial wall, Multilayer responses, multi-responses within each layer, wall structure changes with time.
Anisotropy	Layer mechanical response, fibre dispersion.
Incompressibility	% of Water content inside the wall.
Viscoelasticity	Viscous, elastic properties of the arterial wall material.
Pulse	Pressure , flow velocity , arterial displacement , shear stress
Residual stress and strains	Effect of stress that intrinsically exists inside the arterial wall after dissecting it.
Poroelasticity and random elasticity	Biphasic nature of the arterial wall (solid and fluid)
Polyconvexity	allows existence of solution for stationary boundary value problem

3.2.1 Reference state

The artery wall is composed of three main layers which are the intima, media and adventitia. Each layer has its own thickness and fibre orientation. Often the arterial wall is modelled using a cylindrical domain, which is not very accurate especially in pathological conditions as the cross section of the artery shown in figure 3.1 indicates. Simplifying the geometrical shape often simplifies the equations and simplifies the analytical assumptions. However, it may be insufficient for full meaningful physiological modelling.

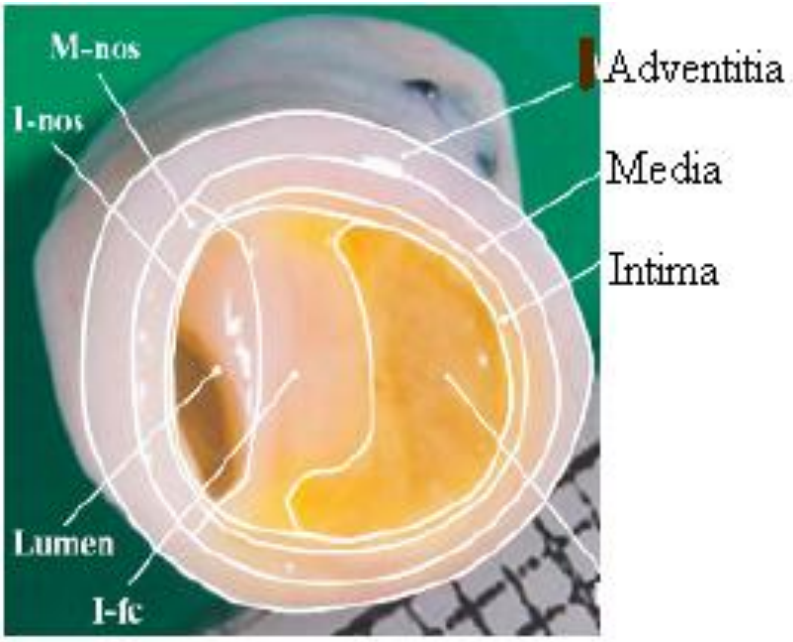

Figure 3.1 : Stenotic human external iliac artery [5].

3.2.2 Load

In normal physiological conditions arteries are constantly subjected to loading conditions in two main directions. Firstly, axial loading appears because of the forces caused by the surrounding tissues and the wave pulse of blood. It may change depending on the location of the artery. Usually the affect of axial displacement is overlooked during modelling the artery wall. Secondly, radial loading, caused by blood pressure and shear stress. Shear stress occurring at the wall is several orders of magnitude smaller than the pressure; its mechanical influence is usually neglected.

3.2.3 Control phenomena

Smooth muscles are constantly contracting and extending as a part of the short term control process and also as a result of spontaneous activities of these muscles. This type of activity is known as vasomotion. Measuring the affect of the vasomotion on the artery wall is difficult.

Also, there is another type of regulation (long term regulation) usually done through the effect of certain hormones which have a nonlocal control system. For example the kidney regulates the 'renin- angiotensin reflex'. This makes modelling the control loop very difficult. Furthermore the wall is affected by the shear stress; this effect is mediated by the reaction of the endothelium. However the mechanism is not yet completely understood [6].

3.2.4 Heterogeneity

Arteries walls are nonhomogenous [heterogeneous]. This statement can be validated in several ways: The proportion of elastin, collagen, and smooth muscles depends on the location of the artery with respect to the artery tree. In addition to that, the artery wall is layer structured, with each layer having different mechanical features. Also within each layer, the structure is nonhomogenous. Furthermore, the wall structure changes with time. The concept of heterogeneity was covered in different models, such as Maltzahn [7] , Holzapfel [8] and Demiray [9].

3.2.5 Anisotropy

Experimental evidence shows that the stress-strain response of the arterial wall depends on the material direction [8, 10-11]. Hence it is anisotropic. This is due to the presence of fibres in the wall. Since these fibres can have different orientations their stress-strain characteristics differ depending on the direction along which a stress is applied.

The classical method of solving this problem is by using the orthotropy assumption in which three mutual orthogonal directions are chosen such that the material response is the same for the planes perpendicular to these directions.

For example Maltzahn [7, 12-13],Fung[14], Holzapfel [8] assumed that the model is orthotropic with the three axes coinciding with the axial, circumferential and radial directions, while Ogden [15] and Holzapfel et al[11, 16] [17] assumed the wall is built of transversely isotropic materials. Furthermore, the concept of anisotropy was dealt with in the following models.

Holzapfel [18] assumed that the wall consists of three layers with the inner and the outer being isotropic while the middle is orthotropic reinforced with two families of fibres. In another

publication [19] Holzapfel assumed that the artery wall is a composite of six layers in which the inner and the outer ones are isotropic while the middle four layers are transversely isotropic materials in which fibres are arranged helically. In [16] Holzapfel assumed that the artery wall is composed of two orthotropic layers which are the media and adventitia, thus neglecting the intima. Each of the two layers is built of orthotropic material reinforced by two families of fibres.

Holzapfel [17] added the concept of fibres dispersion having a factor k which takes a value between 0 (completely isotropic) and k= 1/3, (For completely dispersed).

Zulliger [20] assumed that the wall consists of one family of circumferentially directed collagen fibres. The strain is determined by the mean response of these fibres. Bischoff [21] [22]as well as Zhang [23] assumed that the constitutive laws are based on the statistical mechanical properties of the chain molecules (elastin–collagen), where the strain-energy depends on the stretch in the directions of orthotropy and on the change in length of the molecular chain.

3.2.6 Incompressibility

The tissue forming the arterial wall has a water content of 70 % which means that it is almost incompressible. Most researchers assume it is incompressible, thus having a constant volume. This means that, a stretch in one direction is accompanied by shrinking in the two other directions. This idea was further developed by Fung in[24] and Usyk in [25] using a nearly incompressible model with the Total strain-energy used as the sum of isochoric strain-energy (due to constant volume) and volumetric strain-energy (due to the change in volume).

The same idea was adopted by Holzapfel assuming that the volumetric term is a convex function with zero as its minimum value. This was further developed by Simo-Taylor-Pister in [26].

3.2.7 Viscoelasticity

Normally the stress-strain relationship for a viscoelastic material shows a hysteresis loop as shown in Figure 3.2.

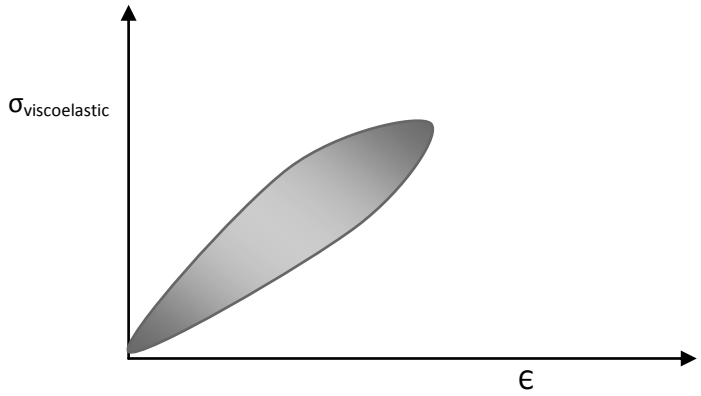

Figure 3.2: Stress- strain relationship for a viscoelastic material [27].

This also applies to the stress-strain relationship for the arterial wall. It is thought [28] that the hysteresis is due to the arterial wall material being viscoelastic. This can be confirmed validated by considering the following: Stress relaxation appears in the case of constant strain which is the case for viscoelastic materials. Furthermore a phase shift occurs between the displacement and load when the load oscillates around a fixed deformation state. There are various models for the wall viscoelasticity, Maxwell's equation for viscoelastic liquids is given by equation 5.

$$\frac{\mathrm{d}\epsilon_{\mathrm{total}}}{\mathrm{dt}} = \frac{\mathrm{d}\epsilon_1}{\mathrm{dt}} + \frac{\mathrm{d}\epsilon_2}{\mathrm{dt}} \tag{5}$$

Where $\epsilon_{\mathrm{total}}$ = the total strain, ϵ_1 is the elastic strain, and ϵ_2 is the viscoelastic strain. The stress is assumed to be the same in both cases. It is given by equation 6.

$$\sigma_{\mathrm{viscoelastic}} = \frac{\mathrm{d}\epsilon_2}{\mathrm{dt}} + \mathrm{G}\epsilon_1 \tag{6}$$

where $\sigma_{\mathrm{viscoelastic}}$ is the stress, η is the dynamic viscosity and G is the elasticity. However under constant load, the Maxwell model goes to infinity. The Kelvin Voigt equation for viscoelastic solids is given by equation 7.

$$\sigma_{\mathrm{viscoelastic}} = \mathrm{G}\epsilon = \eta\frac{\mathrm{d}\epsilon}{\mathrm{dt}} \tag{7}$$

No stress relaxation appears through this model. Holzapfel in [19] used the second Piola Kirchhoff stress tensor with the Kelvin Voigt equations. There were other models that used a combination of Maxwell elements or Kelvin Voigt elements or both, such as the standard linear solid model, 3-D standard nonlinear solid model, generalised Maxwell model and quasi linear viscoelastic model.

3.2.8 Pulse

The artery wall displacement changes with time within the pulse cycle. The wave causing the artery wall displacement is accompanied by a wave of increased pressure and flow of the blood. Thus the displacement of the artery wall depends on the pressure and the shear stress. The pressure and velocity of the blood depend on the boundary velocities which change as the wall moves. There are various approaches to reflect the pulse effect on the artery wall. 2-D or 3-D models exist. They assume the pulse wave is governed by a prescribed formula to define the changing domain [29]. Models of fluid structure interaction, use the Navier Stokes equations to describe the blood while the wall equation is governed by the strain-energy density function [SEDF] equation [30-31].

3.2.9 Residual stress and strains

After dissecting a certain artery segment from the body it is relieved from its physiological loads. This appears in the form of vessel retraction (draw back) which can reach up to 70 %. Stress still exists in these unloaded vessels [32]. Evidence of this could be seen when a fully retracted section of the vessel is cut longitudinally; it springs open to form a sector releasing bending stress. The quantity that describes this phenomenon is called the opening angle. This is shown in figure 3.3.

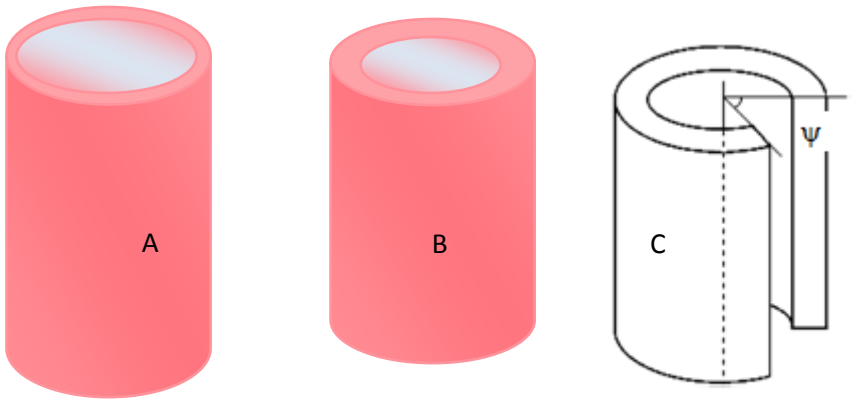

Figure 3.3: a) Loaded artery segment. b) Unloaded artery segment but residually stressed. c) Sector formed after a longitudinal cut of unloaded segment; ψ is the opening angle [2].

There are three main types of models that cover the residuals stress concept. Fung[24] assumes that the artery is a uniformly inflated cylindrical tube. The incompressibility condition is used to relate the radii of the stress free, unloaded configuration with the opening angle. Holzapfel and Gasser in [16] assumed that the open ring configuration is not stress free. Thus was due to the evidence that the opening angle is different for media and adventitia [16]. Holzapfel assumed the artery was a two layer fibre reinforced structure. In [33] Olsson assumes an initial distribution of the stress along with an unknown initial configuration. The unknown unstressed configuration is found using a nonlinear minimisation procedure. Residual stresses are claimed to be associated with the process of remodelling (which is permanent alteration of the geometry of the wall aimed to minimize the circumferential stress gradient in the radial direction) [34].

3.2.10 Poroelasticity and random elasticity

Poroelasticity models take into account that there are both solid and fluid components in the wall. It can be represented as a biphasic fluid saturated solid structure. The equations of the incompressible liquid are coupled with a nonlinear elastic solid as in [35].

3.2.11 Polyconvexity

This property means that strain-energy function as a function of its deformation gradient should be convex. Itskov et al [36] have found that Fung strain-energy function is not polyconvex and give its polyconvex alternative.

3.2.12 Summary

The key parameters for modelling the stress- strain relationship for the arterial wall have been presented and summarised in Table 3.1. However it could be noted that it is very difficult for a certain model to cover all the key parameters. Many modelling specialists normally choose certain parameters to concentrate on according to the degree of complexity and the relevance to their specific point of application or research. In the following section, different models for arterial wall elasticity will be covered.

3.3 Non linear 3D models

Experimental evidence suggests [8, 11]that the stress-strain relationships for both a whole arterial wall and its layers are nonlinear. The curve can be considered in two distinct regions [15]. At lower strains the relationship is approximately linear due to elastin dominating the behaviour whilst the collagen dominance at higher strains gives a more rapidly increasing nonlinear response. Several advances have been made in modelling this curve. The first one is the concept of an incremental modulus as will be discussed in section 3.4.1. After that the concept of hyperelasticity will be introduced

3.3.1 Incremental modulus

Many attempts to model the elasticity of the arterial wall were unsuccessful due to the nonlinearity of the stress-strain relationship. To address this problem, Bergel in [37] developed the incremental modulus method. Here, the elastic modulus could be derived from equation 8 given by

$$\mathrm{E_{inc}}p_2 = \frac{p_3 - p_1}{R_{03} - R_{O1}} \frac{2(1-\nu^2)}{(R_O^2 - R_i^2)} R_{i2}^2 R_{02} \tag{8}$$

The results can be seen in figure 3.4. The subscripts (1, 2, 3) represent successive measurements of pressure and radius. If no volume change occurs in the wall, then R_{o2}-R_{i2} is constant. p is the pressure, R radius, v is known as Poisson's ratio and R_o and R_i are the outer and inner radius respectively, $\mathrm{E_{inc}}$ is the incremental elasticity modulus.

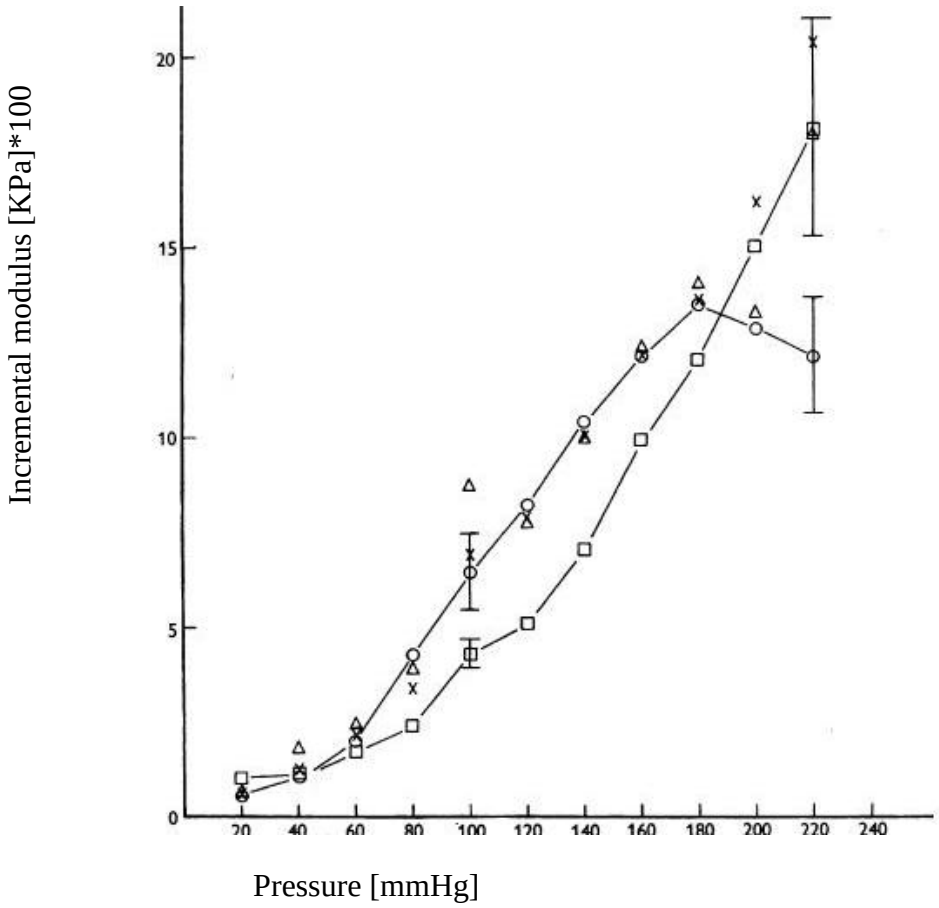

Figure 3.4: Calculated incremental elastic modulus versus pressure [37]for four arteries. A square for thoracic aorta; triangle abdominal aorta; x femoral artery; Circle for carotid artery.

One of the advantages of this model is its suitability for finite element analysis method; on the other hand, its disadvantages include lacking a relationship with the components forming the arterial wall. In addition to that, this mode was not successful in estimating the stress as function of strain.

3.3.2 Hyperelastic model

In this section, a continuum mechanics approach for creating constitutive models for arterial tissue is presented. Firstly, the concept of a constitutive equation will be discussed, before focusing on one particular one, based on a strain-energy function for hyperelastic materials. Finally, some forms for the strain-energy function, presented in the literature, will be presented and discussed.

A constitutive equation (or equation of state) is one which inter-relates the state variables for a system. For a thermo-elastic solid, there are seven states, six of which correspond to the strains and one to temperature [38]. Arterial walls are considered to consist of three layers of homogeneous hyperelastic materials. A hyperelastic material is one in which a Helmholtz free-energy function, W, exists. This free energy is defined per reference volume. If it is purely a function of deformation gradient, **F**, then it is referred to as the strain-energy function. Often the term strain-energy is commonly used [38]. Homogeneous materials are those in which the distributions of the state variables are uniform on a continuum scale. The strain-energy function, W, can be used to find the relationship between the second Piola- Kirchhoff stress tensor, **S**, and Green-Lagrange strain tensor, **E**, as was shown in equation (4). However, the second Piola-Kirchhoff stress tensor does not represent a physical interpretation, but can be used to calculate the Cauchy stress tensor $\boldsymbol{\sigma}$, which does, using the inverse Piola transformation, shown in equation 9.

$$\boldsymbol{\sigma} = \mathrm{J}^{-1}\mathbf{F}\mathbf{S}\mathbf{F}^{\mathrm{T}} \tag{9}$$

where J is the volume ratio (determinant of Jacobian). To find the strain-energy functions for homogeneous hyperelastic materials such as arterial tissue, a phenomenological approach is often used. To aid with the form of the equation to which the experimental data is fitted, the general characteristics of the strain-energy function need to be considered.

The strain-energy function, W,

- has a single minimum value of zero at the reference state, due to a deformation gradient of unity,
- has no residual stress in the reference state; it is the stress free state,
- requires an infinite amount of strain-energy to expand a continuum body to an infinite range or compress it until its volume vanishes,
- is independent of any translation or rotation,
- is polyconvex. This is an important property that guarantees the existence of a solution for a stationary boundary value problem of nonlinear elasticity. It means that the strain-energy function [SEF] must be convex.

In the following section, various forms of the strain-energy function presented in the literature will be reviewed.

3.4 Phenomenological strain-energy functions

The three main forms of phenomenological models used for the strain-energy function in the literature for arterial tissue are the

i) exponential model,
ii) polynomial model,
iii) logarithmic model.

This section reviews these models, together with the main developments and findings.

3.4.1 Exponential model

Fung [14] introduced an exponential model as shown in equation 10 for experimental data consisting of positive strains. The exponent q is given by

$$W = \frac{c_1}{2}(e^q - 3) \tag{10}$$

$$q = b_1 E_{\theta\theta}^2 + b_2 E_{zz}^2 + 2b_3 E_{\theta\theta} E_{zz} \tag{11}$$

where

c_1 is a material parameter in Nm^{-2}

b_1, b_2, b_3 are material constants,

$E_{\theta\theta}$, E_{zz} are the main Green-Lagrange strains in the circumferential and axial directions respectively.

Equation 10 was based on the assumptions that the arterial wall is a hyperelastic, incompressible, anisotropic and homogeneous material. The model did not take into account the residual stress, viscoelasticity or the active behaviour of the artery. From this, a relationship was introduced between the circumferential second Piola- Kirchhoff stress and the circumferential Green-Lagrange strain. This relation is shown in figure 3.5 for four different arteries; the carotid artery, left iliac, lower aorta and upper aorta.

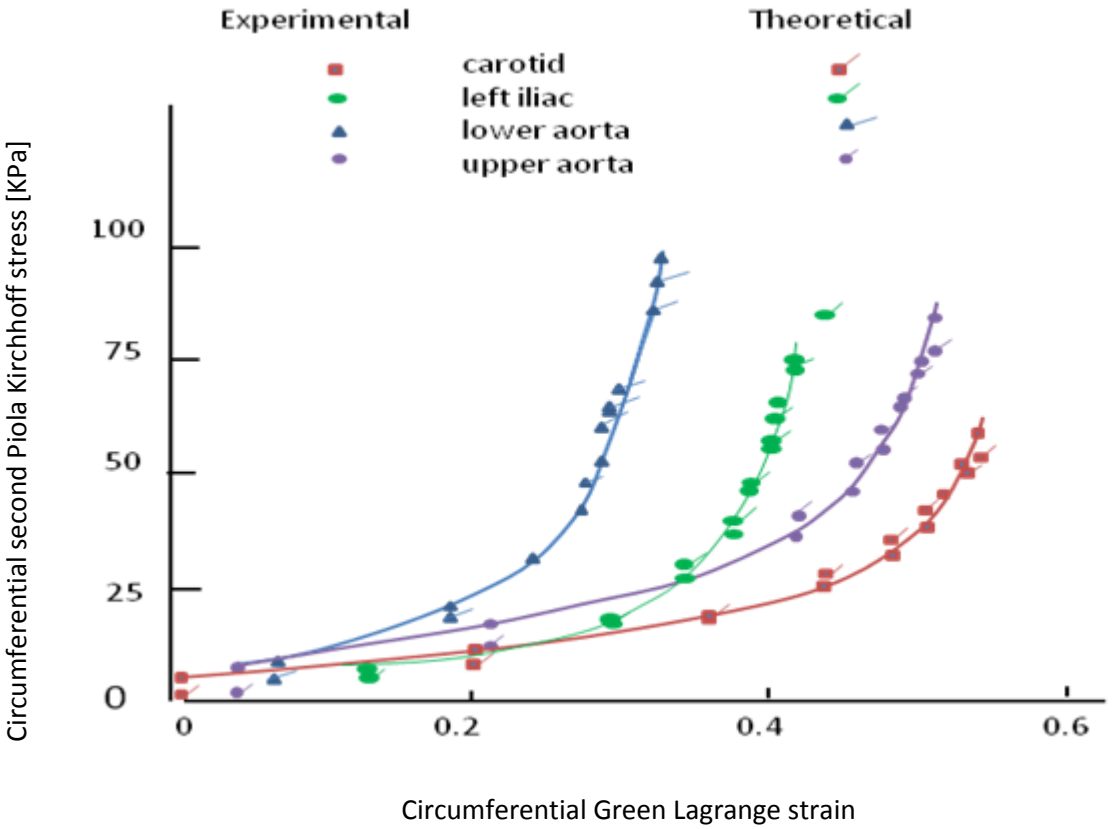

Figure 3.5: Circumferential second Piola -Kirchhoff stress against circumferential Green-Lagrange strain for four different arteries [14].

This form of strain-energy model has several advantages, for example, the model has a low number of material parameters, which means that the model has a high degree of repeatability. In addition, the model also obeys the convexity constraint that ensures the existence of a solution for the strain-energy function problem. On the other hand, one of the disadvantages of the model is the low accuracy of fitting, especially at low stresses. Delfino in [39] presented another model that also used an exponential form. In this case, the strain-energy function is as shown

$$W = \frac{a}{b}\left(e^{\frac{b(I_{1-3})}{2}} - 1\right) \tag{12}$$

$$I_1 = E_{\theta\theta} + E_{rr} + E_{zz} \tag{13}$$

I_1 is the first strain invariant and it is given by equation 13, a is a material parameter in Nm^{-2}, b is a dimensionless material parameter and E_{rr}, $E_{\theta\theta}$, E_{zz} are the main Green-Lagrange strains in the radial, circumferential and axial directions respectively. In addition to assuming the arteries are homogeneous hyperelastic materials, this model also assumes the arteries are incompressible, isotropic, and residual stresses can exist. Viscoelasticity, the active behaviour of the artery, and

anisotropy are not considered. There is also no verification of the simulated data using experimental data. Holzapfel [8] assumed the main building blocks of the arterial wall, that affect the stress-strain response, are collagen and elastin. Thus, it was also assumed that the total strain-energy of the arterial wall is the summation of the strain-energy of both the elastin and collagen. The collagen component was based on an anisotropic material model of the exponential type presented by Fung [14],as represented by equations 10,11 and The elastin component was based on an isotropic neo-Hookean as shown in equation 14.

$$W_{elastin} = c_1(I_1 - 3) \tag{14}$$

where c_1 is a material parameter in Nm^{-2}.

This combination resulted in an improvement in the accuracy of fit. However, no quantitative comparison of "goodness of fit" is given in the literature. A visual comparison between the Holzapfel and the Fung models is shown in figure 3.6.

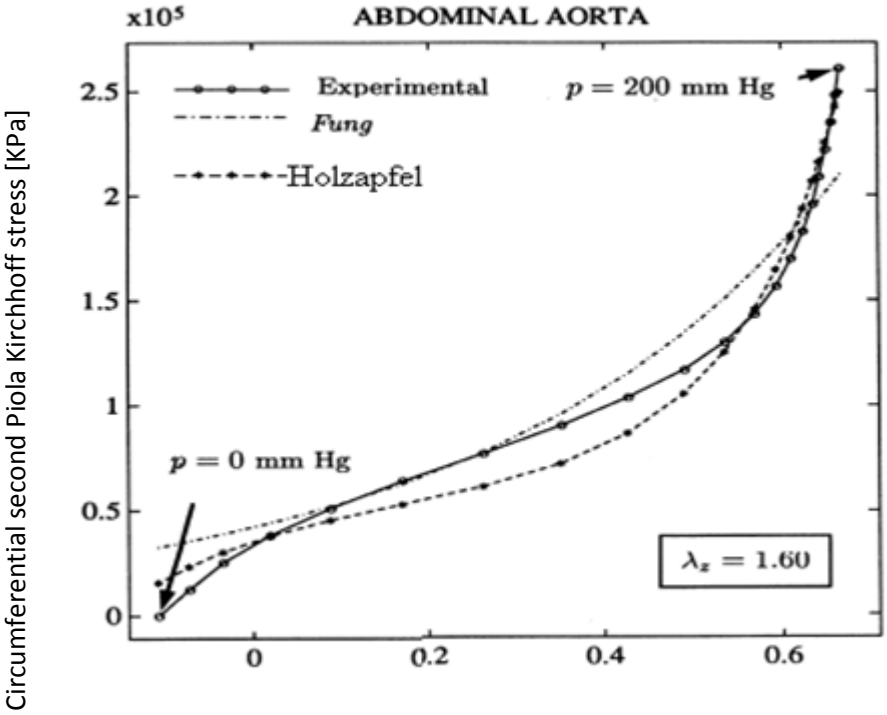

Figure 3.6: Circumferential second Piola-Kirchhoff stress against circumferential Green-Lagrange strain for Fung and Holzapfel models (reproduced from[8]).

However, the above model did not include any terms that indicate the variation of the collagen fibre orientation inside the arterial wall. The model was further developed in [10]. The equation used for elastin remained the same, but the collagen was assumed to be distributed in the form of two separate families with two different directions. Equation 15 shows only one direction as a simplification.

$$W_{icaniso} = \frac{k_1}{k_2}(e^q - 1) \tag{15}$$

$$q = k_2(I_4 - 1)^2 \tag{16}$$

$$I_4 = \lambda_{\theta\theta}^2 \cos^2\varphi + \lambda_{zz}^2 \sin^2\varphi \tag{17}$$

The exponent q is given by equation 16 and the fourth invariant by equation 17 where $\lambda_{\theta\theta}$ and λ_{zz} are the main stretches in the circumferential and axial directions respectively, φ is the angle between collagen fibres and the circumferential direction, k_1 is a material parameter in Nm^{-2}, and k_2 is a dimensionless material parameter.

3.4.2 Polynomial model

There are two main models using the polynomial form. The first was presented by Vaishnav in [40]. It took the form of equation 18.

$$W = a_1 E_{\theta\theta}^2 + a_2 E_{ZZ} E_{\theta\theta} + a_3 E_{ZZ}^2 + a_4 E_{\theta\theta}^3 + a_5 E_{ZZ} E_{\theta\theta}^2 + a_6 E_{ZZ}^2 E_{\theta\theta} + a_7 E_{ZZ}^3 \qquad (18)$$

where a_1 to a_7 are material parameters in Nm^{-2}. However, this model had several major drawbacks. Firstly, the model uses seven material constants; these material constants differ between experimental subjects and they even differ on repeating the experiment. Thus, the overall repeatability of the model was very low. In addition, the model had very low accuracy of fit at low stresses. The results are shown in figure 3.7 for four different arteries; carotid, left iliac, lower aorta and upper aorta.

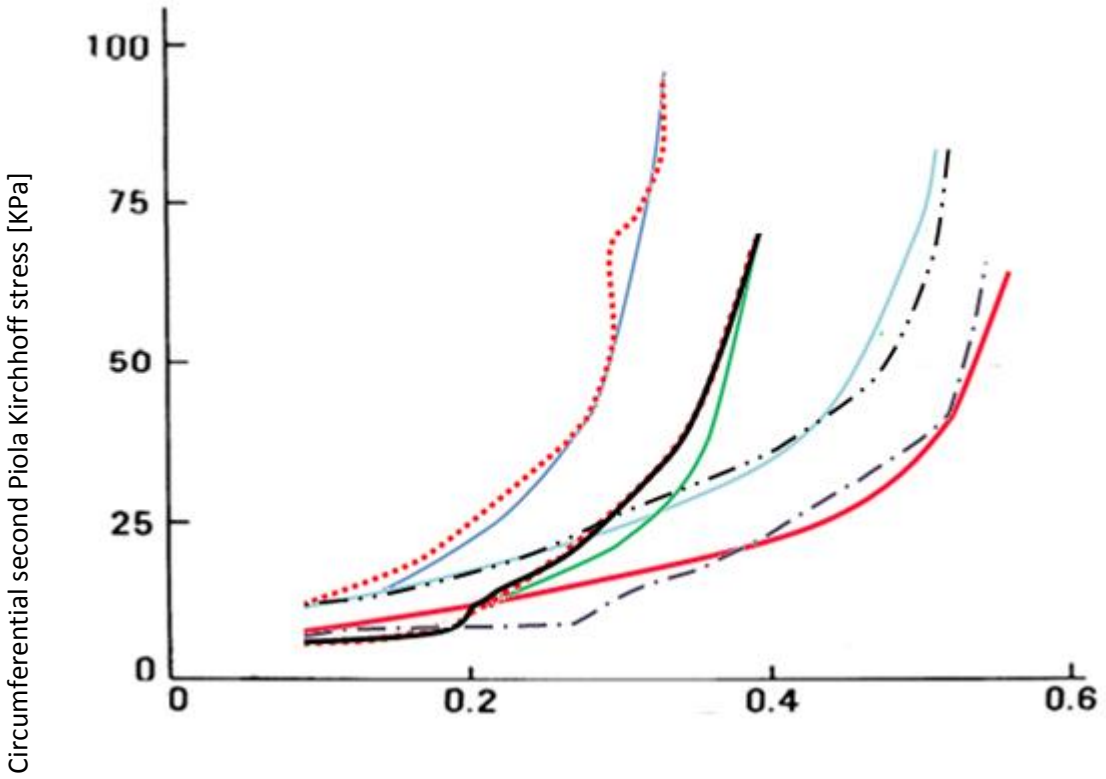

Figure 3.7: Green-Lagrange strain in the circumferential direction was plotted against circumferential second Piola Kirchhoff stress for four different arteries [14].

The second model, presented by Ogden[15], assumed the arterial walls behaved similar to rubber-like materials which share the strain stiffening effect within the material. It was assumed that the strain-energy function used is given as

$$W = \sum \frac{\mu_i}{\alpha_i}(\lambda_1^{\alpha_i} + \lambda_2^{\alpha_i} + \lambda_3^{\alpha_i}) \tag{19}$$

where μ_i is a parameter in Nm^{-2}, α_i is a dimensionless material parameter and λ_1, λ_2 and λ_3 denote the three principal stretches. It can be seen by considering figure 3.8, that the mechanism behind the strain stiffening effect in the arterial wall is different from that of the rubber-like material; this might be due to the existence of collagen fibres that do not act as rubber-like materials.

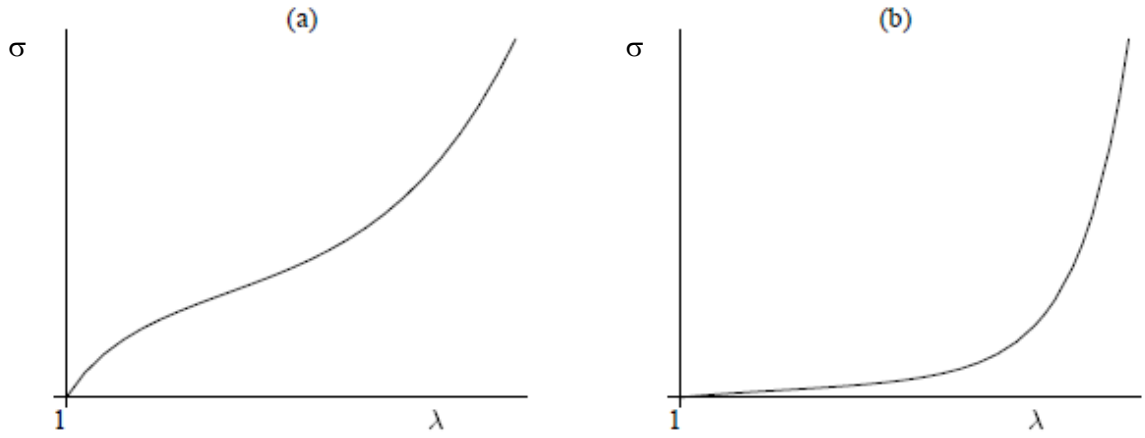

Figure 3.8: Typical simple tension response of (a) rubber and (b) soft tissue. Nominal stress (*σ)* was plotted against strain (λ)[15].

This section has considered two polynomial forms of the strain-energy function presented in the literature. The results indicate that they do not represent the experimental data as well as the exponential forms and will not be considered further.

3.4.3 Logarithmic model

The strain-energy function presented by Hayashi [27] assumed the arterial walls to be homogeneous, incompressible, hyperelastic materials. However, it used a logarithmic function, as shown in equation 20, to represent the relation between strain-energy and strain.

$$W = -c_1 \ln(1 - \frac{a_{\theta\theta} E_{\theta\theta}^2}{2} - \frac{a_{zz} E_{zz}^2}{2} - a_{\theta z} E_{\theta\theta} E_{zz}) \quad (20)$$

Here c_1 is a material parameter in Nm^{-2}, $a_{\theta\theta}$, a_{zz}, $a_{\theta z}$ are material constants. Typical results from this model are shown in figure 3.9. It was found that this model was not robust, in that it gave infinite stress values for finite strain values.

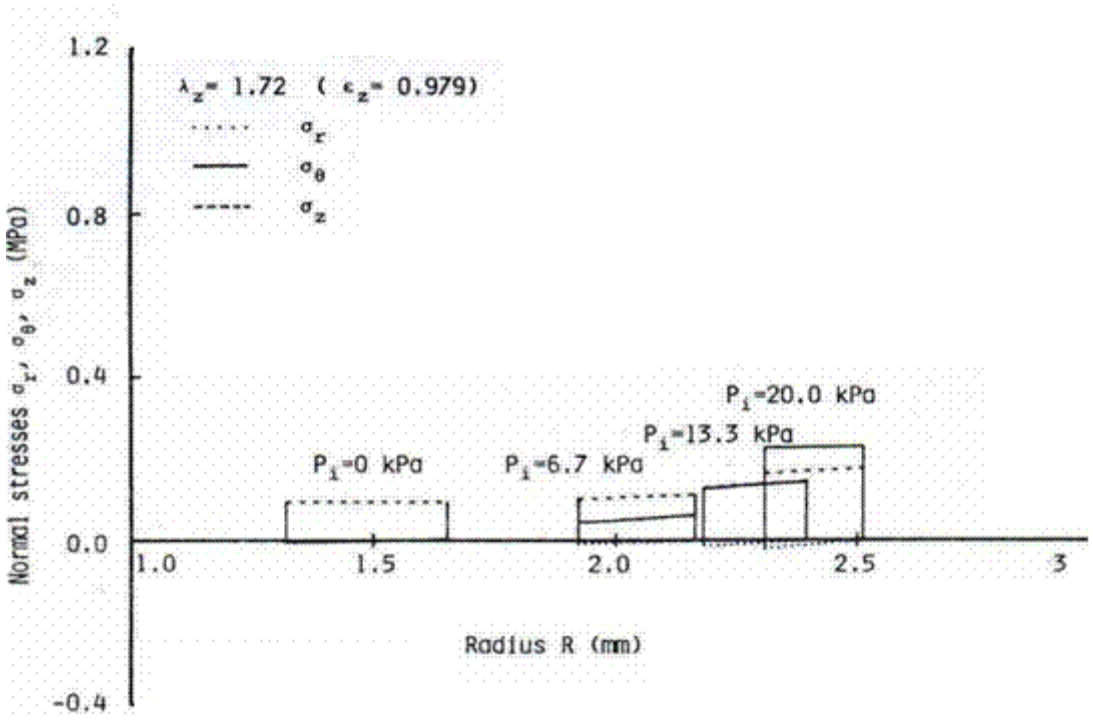

Figure 3.9: First Piola-Kirchhoff stresses are plotted against change in radius [27].

3.4.4 Comparison

In reviewing the different forms of the strain-energy function and their fit to experimental data, it was found that comparisons were mainly based on visual interpretations. Using this method it was found that the model presented by Holzapfel produced the closest fit as he considered more factors, such as directionality of the collagen fibres in addition to the difference in properties of the three layers within the arterial wall.

3.4.5 Summary

This section has presented the concept of the strain-energy function for hyperelastic materials and has reviewed three forms of the function. It was found that the exponential form developed by Holzapfel [8, 10-11] gave the best fit and will be used as a basis for the model developed in this thesis. In the next section the basis of a numerical method to calculate the stress-strain relationship for the arterial wall is presented.

3.5 Finite element non-linear models

Sometimes the addressed mechanical problem is too complicated to be solved analytically. The finite element method is a numerical approach by which general differential equations could be solved in an approximate manner.

One of the attempts to solve the stress-strain relationship for the arterial wall was done by Holzapfel et al [41]. The authors used the principle of virtual work which states that at equilibrium internal work done by a rigid body is equal to external work done on it [41] .Thus equation 21 could be derived.

$$\int \delta \mathbf{E}_{\mathrm{AB}} \mathbf{S}_{\mathrm{AB}} \, \mathrm{HdS}_{\mathrm{sa}} - \int \mathrm{Pn}.\, \delta \mathrm{uds}_{\mathrm{sa}} = 0 = \alpha(\mu, \eta) = \alpha_{\mathrm{int}} - \alpha_{\mathrm{ext}} \tag{21}$$

Where P= load pressure, n = outward unit vector, E_{AB}= Green Lagrange strain tensor, S_{AB}= second Piola Kirchhoff stress tensor, H= thickness, u = displacement, S_{sa}=area in the undeformed state, s_{sa}= area in the deformed state, α (u,η)=function of displacement and (η) virtual displacement' , $\alpha_{\mathrm{int}} = \text{internal work}$, α_{ext} =external work

To solve equation (21), α is linearised according to equation 22 which is given by

$$L\alpha(\mu,\eta,\Delta\alpha)=\alpha'+\Delta\alpha \tag{22}$$

Where α'= constant term, α= linear term

The elastic modulus is then calculated according to equation 23.

$$\mathbb{C}_{\mathrm{ABCD}} = \frac{\partial \mathbf{S}_{\mathrm{AB}}}{\partial \mathbf{C}_{\mathrm{CD}}} \tag{23}$$

Then the material matrix (components of the elastic modulus) could be derived to be as shown in equation 24.

$$\mathbf{D}=\begin{bmatrix} \left[\frac{1}{\lambda_1}\frac{\partial}{\partial\lambda_1}\left(\frac{1}{\lambda_1}\frac{\partial \mathrm{w}}{\partial\lambda_1}\right) - \frac{2\mathrm{P}}{\lambda_1^4} + \frac{1}{\lambda_1^3}\frac{\partial \mathrm{P}}{\partial\lambda_1}\right] & \left[\frac{1}{\lambda_2}\frac{\partial}{\partial\lambda_2}\left(\frac{1}{\lambda_1}\frac{\partial \mathrm{w}}{\partial\lambda_1}\right) + \frac{1}{\lambda_1^2\lambda_2}\frac{\partial \mathrm{P}}{\partial\lambda_2}\right] \\ \left[\frac{1}{\lambda_2}\frac{\partial}{\partial\lambda_2}\left(\frac{1}{\lambda_1}\frac{\partial \mathrm{w}}{\partial\lambda_1}\right) + \frac{1}{\lambda_1^2\lambda_2}\frac{\partial \mathrm{P}}{\partial\lambda_2}\right] & \left[\frac{1}{\lambda_2}\frac{\partial}{\partial\lambda_2}\left(\frac{1}{\lambda_2}\frac{\partial \mathrm{w}}{\partial\lambda_2}\right) - \frac{2\mathrm{P}}{\lambda_2^4} + \frac{1}{\lambda_2^3}\frac{\partial \mathrm{P}}{\partial\lambda_2}\right] \end{bmatrix} \tag{24}$$

Where **D**= material matrix containing elasticity tensor components, $\lambda_{1,2}$= eigenvalues which correspond to principal directions of strain.

After certain calculations

$$\Delta\alpha = \int (\Delta \boldsymbol{E} D \Delta \boldsymbol{E} + \Delta \boldsymbol{E} D \boldsymbol{S}) H d\mathrm{S}_{\mathrm{sa}} - \alpha_{ext} \tag{25}$$

After that the authors applied the spatial discretisation method before using a specific software program to compute the final finite element formulation. The results from the finite element (FE) method are then compared with the analytical method and are presented in figure 3.10

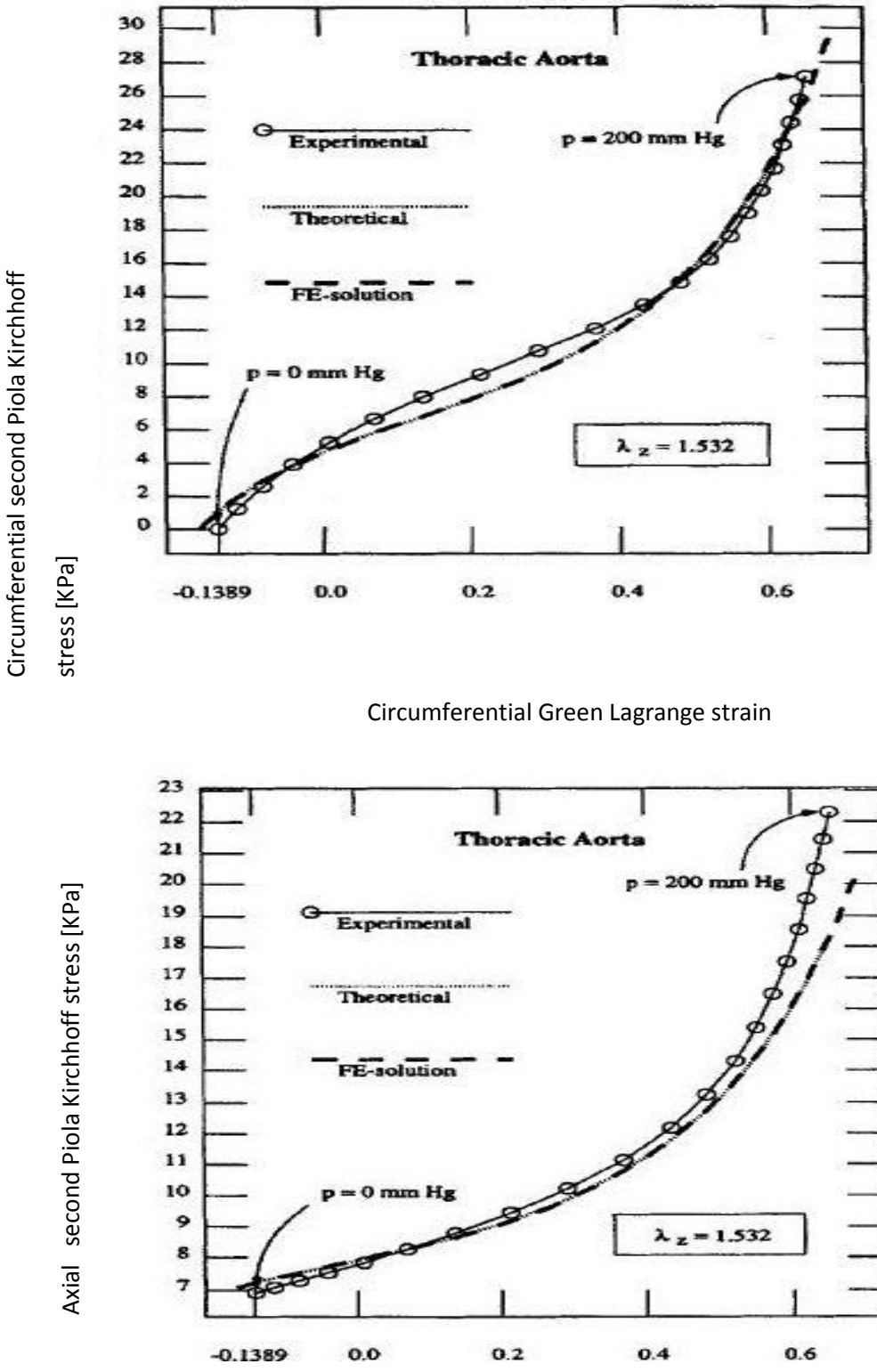

Figure 3.10: The relation between circumferential 2nd Piola Kirchhoff and circumferential green Lagrange strain [8, 41].

Both the finite element and the analytical techniques differ from the experimental results in certain areas of the graph with errors up to 20% at higher strains. This could be due to only using the elastin (rubber like material component) in the nonlinear displacement equation (equation 14). Thus neglecting the effect of other main components especially collagen that begin to show response at higher strain rates. This was solved in the subsequent models, where a term representing collagen energy response to stress was later added. This will be shown in more detail in section 3.7.It is worth noting that forming the proper constitutive equation will be the aim of this research and not forming an FE solution for it.

3.6 Model variations

3.6.1 Layered vessel

The research performed by Von Maltzahn et al [7, 12-13] offers one of the most important contributions to the field. In [7] experimental measurements of the elastic properties of the media and adventitia were presented. The arterial wall was considered to be orthotropic, but it did not include the role of the intima. The intima has been proven to be of significant importance, especially in older patients [11]. The strain-energy presented by Maltzahn et al in [12] lacked a coherent relationship with the materials constituting the arterial wall (e.g: elastin and collagen). Demiray et al introduced another strain-energy function in [9]. Their model lacked any comparison with experimental data and it also assumed the vascular wall to be completely isotropic, which did not take into the consideration the transverse isotropy. In [42] Demiray and Vito used a two layer model, neglecting the role of the intima. The media was considered orthotropic, while the adventitia was considered isotropic. No axial force–pressure relation was presented. Similarly the relation between the two layers and the whole structural stress was not presented. Results for the Von Maltzahn model are presented in figure 3.11. The results for Demiray and Vito models are summarized in table 3.2.

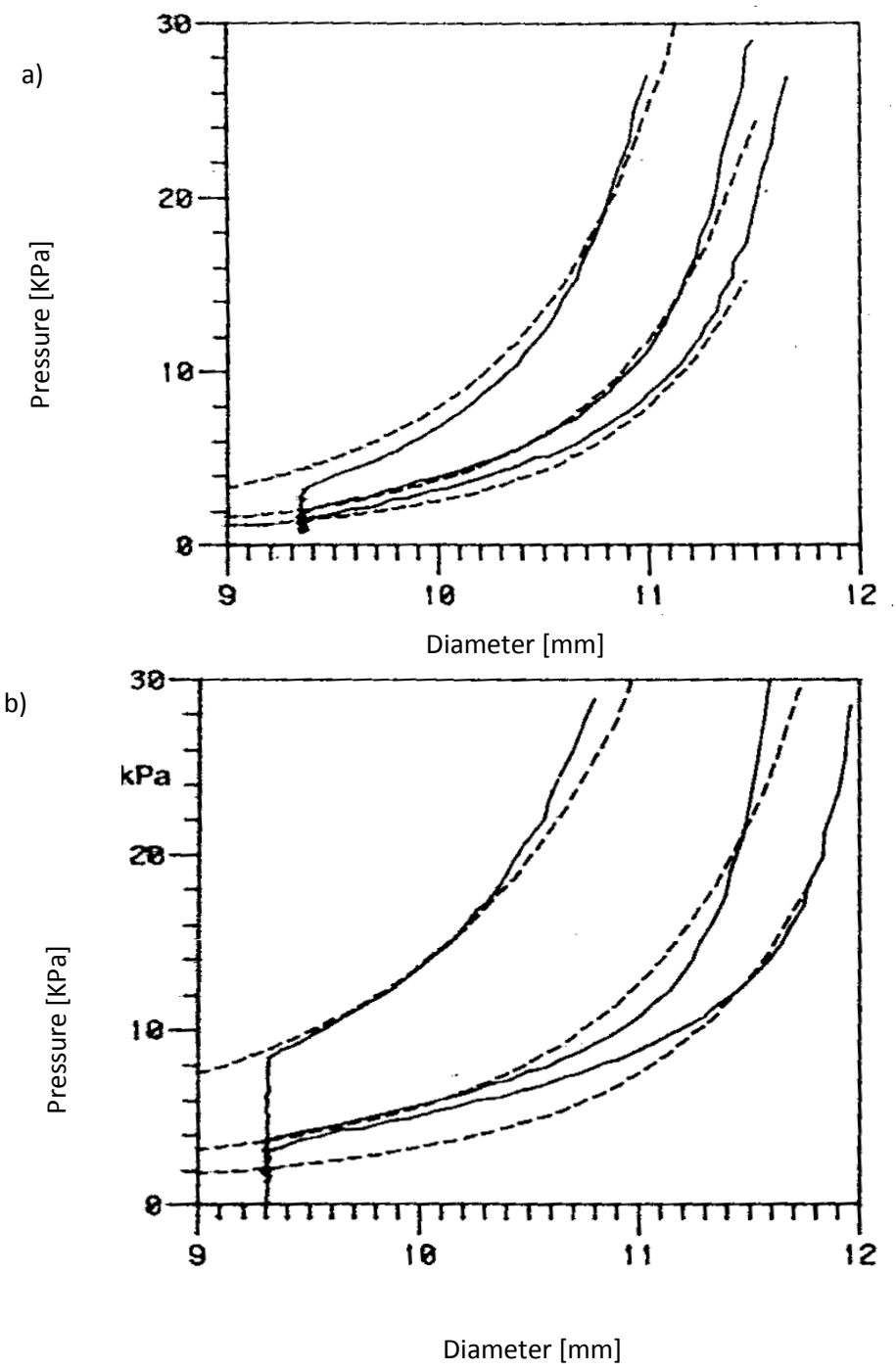

Figure 3.11 :a) the media model is compared with its data ,in figure (b) the data of the whole wall is compared with its model [13].

Table 3.2

Stress results are compared with the theoretical model for the media and then the whole wall [42]

λ_1	λ_2	t_{11} (exp.) (dyne/cm^2)	t_{11} (theor.) (dyne/cm^2)	Dev. (%)	t_{22} (exp.) (dyne/cm^2)	t_{22} (theor.) (dyne/cm^2)	Dev. (%)
1.091	1.112	123,200	118,431	−3.9	179,100	215,546	20.3
1.127	1.144	217,100	199,596	−8.1	303,300	310,563	2.4
1.158	1.175	310,700	290,843	−6.4	448,800	423,579	−5.6
1.200	1.219	449,000	462,768	3.1	627,800	641,819	2.2
1.230	1.237	586,600	599,349	2.2	807,100	791,169	−2.0

λ_1	λ_2	t_{11} (exp.) (dyne/cm^2)	t_{11} (theor.) (dyne/cm^2)	Dev. (%)	t_{22} (exp.) (dyne/cm^2)	t_{22} (theor.) (dyne/cm^2)	Dev. (%)
1.094	1.120	201,990	209,966	3.9	232,170	232,738	0.2
1.129	1.156	284,570	294,358	3.4	318,450	320,771	0.7
1.159	1.186	378,760	377,271	−0.4	426,190	406,615	−4.6
1.206	1.222	502,620	522,668	4.0	543,590	543,095	−0.1
1.235	1.258	626,580	653,035	4.2	680,070	686,741	1.0
1.271	1.287	811,430	823,625	1.5	843,330	850,772	0.9

In [11] Holzapfel et al presented layer specific strain-energy equations assuming arterial layers, but no mean (or total) relationship for the stress-strain response of the whole wall was given. The results from the literature indicate that the combined elastin and anisotropic collagen models developed by Holzapfel using three layers [11] gives the best fit to experimental data as shown in figure 3.12 .

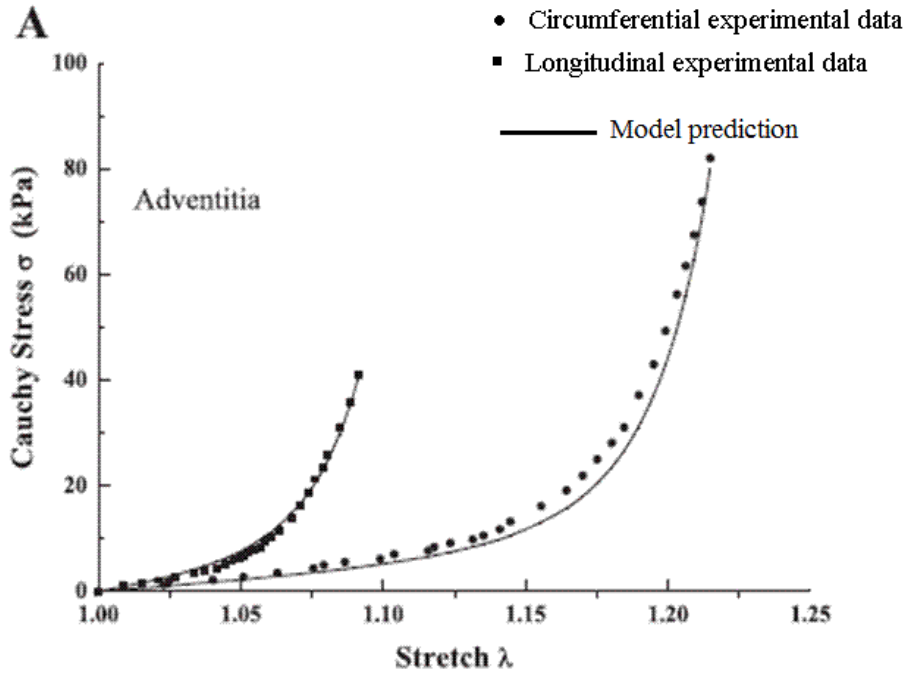
A
Circumferential experimental data
Longitudinal experimental data
Model prediction
Adventitia
Cauchy Stress σ (kPa)
Stretch λ
0
20
40
60
80
100
1.00
1.05
1.10
1.15
1.20
1.25

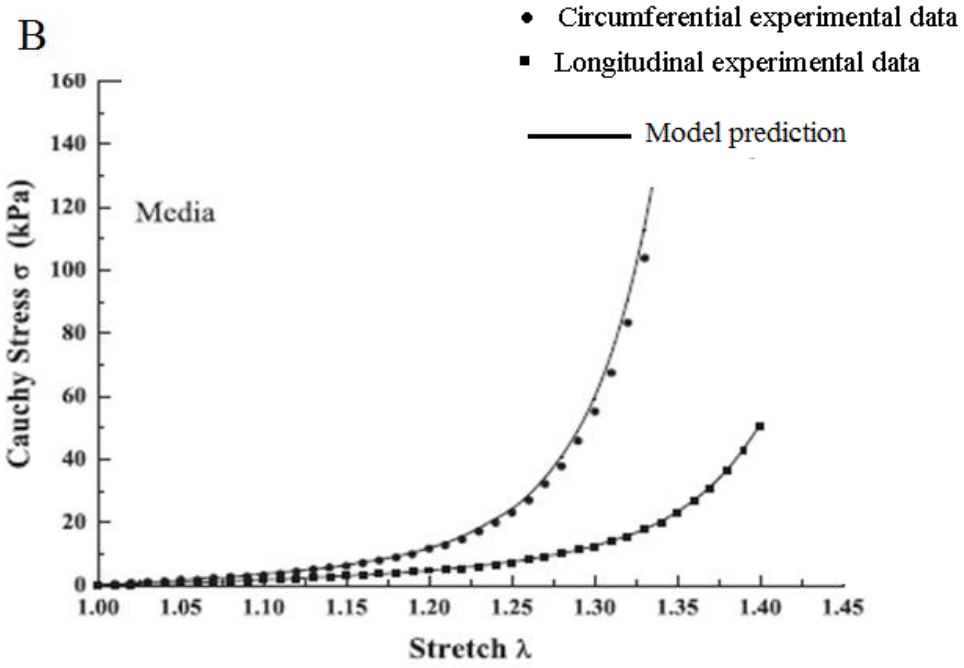
B
Circumferential experimental data
Longitudinal experimental data
Model prediction
Media
Cauchy Stress σ (kPa)
Stretch λ
0
20
40
60
80
100
120
140
160
1.00
1.05
1.10
1.15
1.20
1.25
1.30
1.35
1.40
1.45

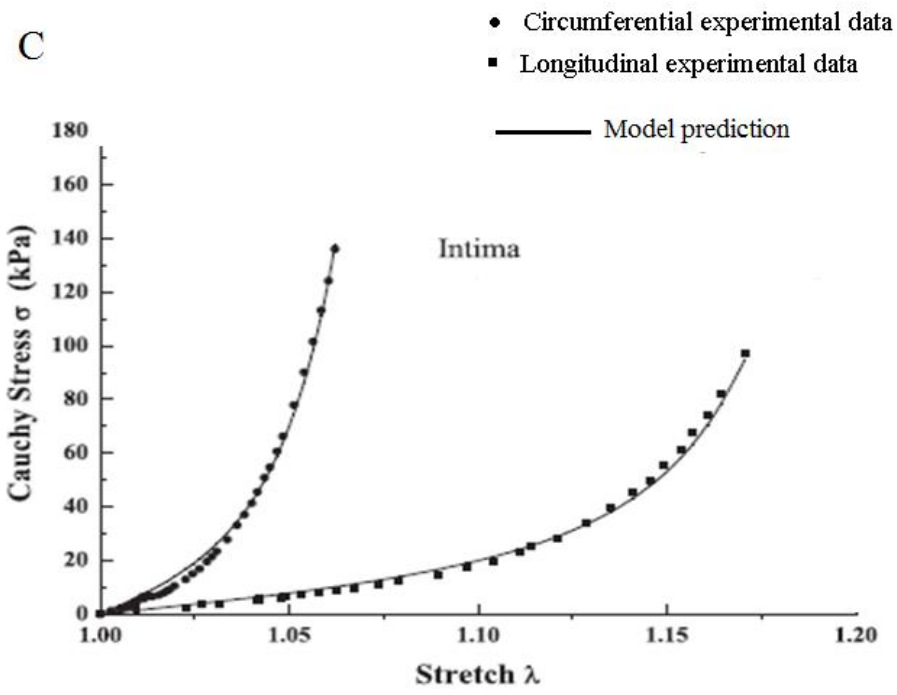

Figure 3.12 : A comparison between the layers responses in the circumferential and longitudinal direction, for A) Adventitia, B) Media C) Intima [11].

3.6.2 Fibre orientation

The arterial wall has been shown to be composed of a network of elastin and collagen fibres. At lower stresses elastin is easily strained because of its low elastic modulus. On the other hand collagen does not begin to be affected by stress until higher values. At these higher values, the collagen fibres are redirected circumferentially, to allow the arterial wall to withstand higher pressure. This is explained in figure 3.13.

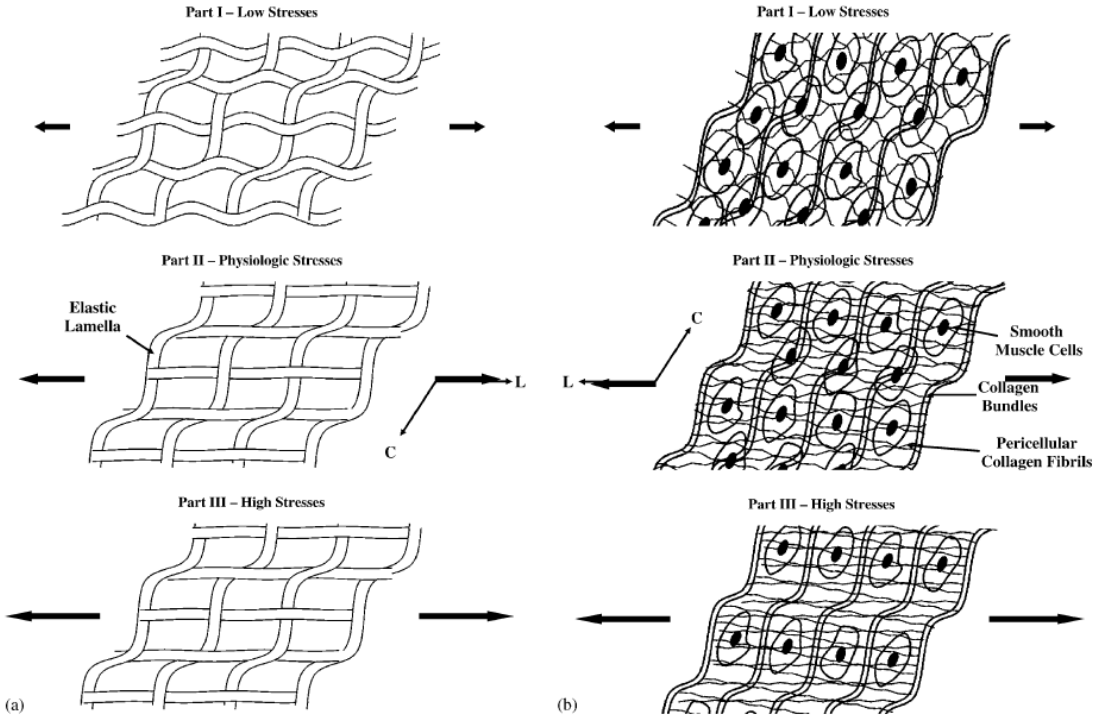

Figure 3.13: Collagen fibres are re-oriented at higher stress giving the chance for the artery to withstand higher pressure[43].

Thus, it is apparent that the fibre orientation controls the stress value. This was further investigated in [16]. Holzapfel assumed that the collagen fibres are grouped in two main groups with two preferred fibre orientations. These directions are represented by a second order tensor which is the dyadic product of two vectors. Each vector is given by three components covering the angular relation with the three main directions. Thus the direction of one family (A) would be given as by equation 26.

$$A = \begin{vmatrix} a_{11} & a_{12} & a_{13} \\ a_{21} & a_{22} & a_{23} \\ a_{31} & a_{32} & a_{33} \end{vmatrix} = \begin{vmatrix} 0 \\ \cos\varphi \\ \sin\varphi \end{vmatrix} \otimes \begin{vmatrix} 0 \\ \cos\varphi \\ \sin\varphi \end{vmatrix} = \begin{vmatrix} 0 & 0 & 0 \\ 0 & cos^2\varphi & \cos\varphi\, sin\varphi \\ 0 & \cos\varphi\, sin\varphi & sin^2\varphi \end{vmatrix} \quad (26)$$

3.6.3 Thin wall approximation

Fung et al in [14, 24, 44] noted that the arterial wall is not very thin, but it was considered to be thin enough to justify the use of thin wall theory. In [44] Fung et al observe that neglecting the variation of stress through the wall thickness will have an effect on the quality of a model prediction. However, no quantitative error estimation was given.

Holzapfel et al in [8] used thin wall theory to represent the circumferential and axial responses. In [11, 16, 38] when modelling the layer response, they discussed the use of different strain-energy forms for each layer. In order to formulate the analytical model, Holzapfel et al made certain assumptions. As all collagen fibres are embedded in the tangential surface of the tissue, it was assumed that there are no components in the radial direction [11]. This supported the use of the thin wall approximation [11]. In this case only circumferential and axial stresses become relevant.

Thin wall theory [45] offers a simple approximation for the relationship between mean circumferential and axial Cauchy stresses, σ_θ and σ_z respectively. A deformed thickness, h, deformed radius, r, luminal pressure, p, and axial force, f_a are assumed. These are shown in equations 27 and 28.

$$\sigma_\theta = p\left(\frac{r}{h} - \frac{1}{2}\right)\lambda_\theta \tag{27}$$

$$\sigma_z = \frac{\sigma_\theta}{2} + \frac{f_a}{2\pi h} \tag{28}$$

3.6.4 Comparison of models

In the last section, it was seen that there are many models that tackled the stress-strain relationship. These models vary in their complexity, covering 1-D and 3-D models. 3-D strain-energy based models were compared. Three main types were presented, exponential, logarithmic and polynomial. It was seen that the exponential form representing the roles of elastin and collagen gave better estimates of the stress-strain relationship in the circumferential and longitudinal directions. In the exponential modelling method, it was seen that model complexity increases side by side with its accuracy. It was found that the models that take the building blocks of the arterial wall into account perform better. Nevertheless, there is no reported relationship between the layered and whole wall models. That is the research gap which this thesis explores.

3.6.5 Conclusions

This chapter covered the model assumptions, including: cylindrical reference state, radial and axial loading. Two types of control loops were introduced (Long and short term regulation). Only short term loop was considered. The arterial wall was considered to be homogenous transversally isotropic incompressible. Viscoelasticity, residual stress, Poroelasticity were not considered by this model. Two nonlinear 3D models were discussed, namely incremental model and hyperelastic model. Incremental model was discarded based on the fact that no relation between the model parameters and the materials forming the arterial wall. Strain-energy function was defined as the potential energy stored in the arterial wall. Three forms of strain-energy function were investigated (i.e: Exponential, polynomial, logarithmic). Polynomial strain-energy functions suffer from very low accuracy as well as model parameters were patient specific. Logarithmic strain-energy functions gave infinite results for finite values of strain. Different model variations were considered including layered vessels, fibre orientation and thin wall approximations. This review has highlighted a research gap to find the relationship between layered models and the whole arterial wall. This relationship could provide opportunities to explore the function of baroreceptors and the study of arthrosclerosis.

3.7 References

1. Ganong MD and William F, *Review of Medical Physiology*. 22 ed. 2005: The MacGraw-Hill Companies.
2. Kalita P and Schaefer R, *Mechanical Models of Artery Walls.* Arch Comput Methods Eng, 2008(15): p. 1–36.
3. Canic S, Hartley CJ, Rosenstrauch D, Tambaca J, Guidoboni G, and Mikelic A *Blood Flow in Compliant Arteries: An Effective Viscoelastic Reduced Model, Numerics and Experimental Validation.* Ann Biomed Eng, 2006. **34**(4): p. 572-592.
4. Causin P, Gerbeau JF, and Nobile F, *Added-Mass Effect in the Design of Partitioned Algorithms for Fluid-Structure Problems.* Comput Methods Appl Mech Eng, 2005. **194**(42-44): p. 4506-4527.
5. Holzapfel GA, Sommer G, and Regting P, *Anisotropic Mechanical Properties of Tissue Components in Human Atherosclerotic Plaques.* J Biomech Eng., 2004. **126**.
6. Davies PF, Spaan JA, and Krams R, *Shear Stress Biology of the Endothelium.* Ann Biomed Eng, 2005. **33**(12): p. 1714–1718.
7. von Maltzahn WW, Besdo D, and Wiemer W, *Elastic Properties of Arteries: A Nonlinear Two-Layer Cylindrical Model.* J. Biomech., 1981. **14**(6): p. 389-397.
8. Holzapfel GA, Eberlein R, Wriggers P, and Weizsäcker HW, *A New Axisymmetrical Membrane Element for Anisotropic,Finite Strain Analysis of Arteries.* Commun. Num. Meth. Eng., 1996. **12**(8): p. 507-517.
9. Demiray H, *A Note on the Elasticity of Soft Biological Tissues.* J. Biomech., 1972. **5**(3): p. 309-311.
10. Holzapfel GA, Gasser T, and Ogden R, *A New Constitutive Framework for Arterial Wall Mechanics and a Comparative Study of Material Models.* J. Elast., 2000. **61**(1): p. 1-48.
11. Holzapfel GA, Sommer G, Gasser CT, and Regitnig P, *Determination of Layer-Specific Mechanical Properties of Human Coronary Arteries with Nonatherosclerotic Intimal Thickening and Related Constitutive Modeling.* Am. J. Physiol. Heart Circ. Physiol., 2005. **289**(5): p. H2048-2058.
12. von Maltzahn WW, *Stresses and Strains in the Cone-Shaped Carotid Sinus and Their Effects on Baroreceptor Functions.* J. Biomech., 1982. **15**(10): p. 757-765.
13. von Maltzahn WW, Warriyar RG, and Keitzer WF, *Experimental Measurements of Elastic Properties of Media and Adventitia of Bovine Carotid Arteries.* J. Biomech., 1984. **17**(11): p. 839-847.
14. Fung YC, Fronek K, and Patitucci P, *Pseudoelasticity of Arteries and the Choice of Its Mathematical Expression.* Am. J. Physiol. Heart Circ. Physiol., 1979. **237**(5): p. H620-631.
15. Ogden RW, *Nonlinear Elasticity,Anisotropy,Material Stability and Residual Stresses in Soft Tissue*, in *Biomechanics of Soft Tissue in Cardiovascular System*, Holzapfel GA and Ogden RW, Editors. 2003, Springer: New York. p. 65–108.
16. Holzapfel GA, *Collagen. Structure and Mechanics*, in *Collagen in Arterial Walls: Biomechanical Aspects*, P. Fratzl, Editor. 2008, Springer-Verlag, Heidelberg: New York. p. 285-324.
17. Ogden RW Gasser TC, Holzapfel GA *Hyperelastic Modelling of Arterial Layers with Distributed Collagen Fibre Orientations.* J R Soc Interface, 2006. **3**(6): p. 15-35.
18. Holzapfel GA, Gasser TC, and Stadler M, *A Structural Model for the Viscoelastic Behaviour of Arterial Walls:Continuum Formulation and Finite Element Analysis.* Eur. J. Mech. of solids, 2002. **21**(3): p. 441-463.

19. Holzapfel GA, *Structural and Numerical Models for the Viscoelastic Response of Arterial Walls with Residual Stresses*, in *Biomechanics of Soft Tissue in Cardiovascular System*, Holzapfel GA and Ogden RW, Editors. 2003, Springer: New York. p. 109-184.
20. Zulliger MA, Rachev A, and Stergioupulos N, *A Constituitive Formulation of Arterial Mechanics Including Vascular Smooth Muscle Tone.* Am J Physiol Heart Circ Physiol, 2004. **287**(3): p. H1335-H1343.
21. Bischoff JE, Arruda EA, and Grosh K, *Finite Element Simulations of Orthotropic Hyperelasticity.* Finite Elem Anal Des, 2002. **38**(10): p. 983-998.
22. Bischoff JE, Arruda EA, and Grosh K, *A Microstructurally Based Orthotropic Hyperelastic Constituitive Law.* J Appl Mech, 2002. **69**(5): p. 570-75.
23. Zhang Y, Dunn Ml, Drexler ES, McCowan CN, Slifa AJ, Ivy DD, and Shandas RA, *A Microstructural Hyperelastic Model of Pulmonary Arteries under Normo and Hypertensive Conditions.* Ann Biomed Eng, 2005. **33**(8): p. 1042-1052.
24. Chuong CJ and Fung YC, *Compressibility and Constitutive Equation of Arterial Wall in Radial Compression Experiments.* J. Biomech., 1984. **17**(1): p. 35-40.
25. Usyk TP and McCulloch AD, *Computational Methods for Soft Tissue Biomechanics*, in *Biomechanics of Soft Tissue in Cardiovascular System*, Holzapfel GA and Ogden RW, Editors. 2003, Springer: New York. p. 273–342.
26. Simo JC, Taylor RL, and Pister KS, *Variational and Projection Methods for the Volume Constraint in Finite Deformation Elastoplasticity.* Comput Methods Appl Mech Eng, 1985. **51**(1-3): p. 177–208.
27. Takamizawa K and Hayashi K *Strain Energy Density Function and Uniform Strain Hypothesis for Arterial Mechanics.* J. Biomech., 1987. **20**(1): p. 7-17.
28. Mohan D and Melvin JW, *Failure Properties of Passive Human Aortic Tissue. Ii—Biaxial Tension Tests* J Biomech Eng., 1983. **16**(1): p. 31-44.
29. Chakravarty S, Mandal PK, and Mandal A, *Numerical Simulation of Unsteady Two-Layered Pulsatile Blood Flow in a Stenosed Flexible Artery: Effect of Peripheral Layer Viscosity.* Math Model Anal, 2004. **9**(2): p. 99-114.
30. Bazilevs Y, Calo VM, Zhang Y, and Hughes TJR, *Isogeometric Fluid-Structure Interaction Analysis with Applications to Arterial Blood Flow.* Comput Mech, 2006. **38**(4-5): p. 310-322.
31. Bischoff JE, *Reduced Parameter Formulation for Incorporating Fiber Level Viscoelasticity into Tissue Level Biomechanical Models. .* Ann Biomed Eng, 2006. **34**(7): p. 1164-1172.
32. Vaishnav RN and Vassoughi J, *Estimation of Residual Stresses*
in Aortic Segments, in *Biomedical Engineering Ii, Recent Developments*, Hall CW, Editor. 1983, Pergamon: New York. p. 330-333.
33. Olsson T, Stålhand J, and Klarbring A, *Modeling Initial Strain Distribution in Soft Tissues with Application to Arteries.* Biomech Model Mechanobiol, 2006. **5**(1): p. 27-38.
34. Rachev A, *A Model of Arterial Adaptation to Alterations in Blood Flow.* J Elast, 2000. **61**(1-3): p. 83-111.
35. Simon BR, Kaufmann MV, McAfee MA, Baldwin AL, and Wilson LM, *Identification and Determination of Material Properties for Porohyperelastic Analysis of Large Arteries.* J Biomech Eng., 1998. **120**(2): p. 188-194.
36. Itskov M, Ehret AE, and Mavrilas D, *A Polyconvex Anisotropic Strain-Energy Function for Soft Collagenous Tissues.* Biomech Model Mechanobiol, 2006. **5**(1): p. 17-26.
37. BERGEL DH, *The Static Elastic Properties of the Arterial Wall.* J. Physiol. , 1961. **156**: p. 445-457.
38. Holzapfel GA, *Nonlinear Solid Mechanics*, ed. Wiley. 2006, Sussex. 455.
39. Delfino A, Stergiopulos N, Moore JE, and Meister JJ, *Residual Strain Effects on the Stress Field in a Thick Wall Finite Element Model of the Human Carotid Bifurcation.* J. Biomech., 1997. **30**(8): p. 777-786.

40. Vaishnav RN, *Distribution of Stresses and of Strain-Energy Density through the Wall Thickness,*. Circulation Research, 1973. **32**(5): p. 577-583.
41. Holzapfel GA, Eberlein R, and Wriggers P, *Large Strain Analysis of Soft Biological Membranes: Formulation and Finite Element Analysis.* comput. methods App, 1996. **132**(45-61).
42. Demiray H and Vito RP, *A Layered Cylindrical Shell Model for an Aorta.* Int. J. Engrng. Sci., 1991. **29**(1): p. 47-54.
43. Sokolis DP, Kefaloyannis EM, Kouloukoussa M, Marinos E, Boudoulas H, and Karayannacos PE, *A Structural Basis for the Aortic Stress-Strain Relation in Uniaxial Tension.* J. Biomech., 2006. **39**(9): p. 1651-1662.
44. Chuong CJ and Fung YC, *Three-Dimensional Stress Distribution in Arteries.* J. Biomech. Eng., 1983. **105**(3): p. 268-274.
45. Fenner R, *Mechanics of Solids*. 1989, Oxford: Blackwell scientific publications. 615.

Table of Contents

Chapter 4

HYPER ELASTIC MODEL OF ARTERIAL TISSUE

---

4 Overview

It is well known that all physical objects are composed of smaller units called molecules, which in turn are formed of atomic and subatomic particles. A microscopic system is concerned with molecules, particles, subparticles. On the other hand, a macroscopic system approximates a large number of particles into a few quantities, hence the term continuum mechanics. This type of mechanics is not concerned with the internal microstructures of materials, for example water from the continuum mechanics point of view is treated as a continuous medium, with certain quantities which are associated with internal structures, for example density, temperature and velocity.

Continuum mechanics could be divided into 3 main branches:

a) The configuration and motion of continuum bodies known as kinematics
b) The study of stress in a continuum (the concept of stress)
c) The mathematical descriptions of the laws that govern the motion of a continuum (Balance principles)

In the following chapter these three concepts will be covered. This will include the configuration concept, the continuum theory, the deformation gradient, and the strain tensors. After that, the concept of hyperelastic material is introduced and then the novelty in this research is introduced mainly using thin wall theory to derive a relationship between layer stresses and whole wall stress response.

It is worth noting that the convention of used characters is as follows:

- Lower case Greek letter for scalars
- Lowercase bold face Latin letters for vectors
- Uppercase bold face Latin letters for second order tensors
- Upper blackboard Latin letters for fourth order tensors
- To differentiate between reference and current configuration in denoting scalar, vector and tensor quantities, we use uppercase letters, in reference configuration, and lowercase letters for current configuration.

4.1 Configuration and motion of continuum bodies

The science of kinematics is based mainly on the continuum theory, which will be covered in this section. A body β may be viewed as having a continuous distribution of matter in space and time. The body is imagined to be composed of continuum particles as shown in figure 4.1. It is also assumed that the mass and the volume of such a body is a continuous function.

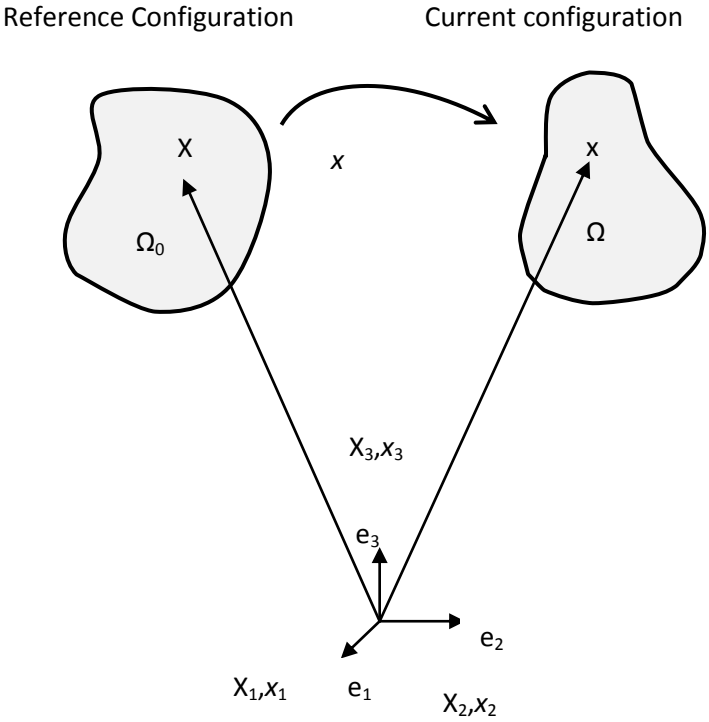

Figure 4.1: A certain motion transfers the deformable body from the reference configuration into the current configuration [1].

4.2 Configuration concept

The body β is embedded in 3-D Euclidean space at a given time *t.* The reference frame is related to rectangular coordinates with bases of 3 orthonormal vectors $\mathbf{e_1}$, $\mathbf{e_2}$, $\mathbf{e_3}$, with the following relationship between them

$$\boldsymbol{e_1}.\boldsymbol{e_2} = \boldsymbol{e_1}.\boldsymbol{e_3} = \boldsymbol{e_2}.\boldsymbol{e_3} = \mathbf{0} \tag{1}$$

$$\boldsymbol{e_1}.\boldsymbol{e_1} = \boldsymbol{e_2}.\boldsymbol{e_2} = \boldsymbol{e_3}.\boldsymbol{e_3} = \mathbf{1} \tag{2}$$

As the continuum body β moves from one state to the other, it occupies a sequence of geometrical regions denoted by Ω_o to Ω. The region occupied by the body at a certain time t is called the configuration. Thus for example at time t_o , the body β occupies the region Ω_o. This is referred to the undeformed configuration. If there exists a point X on the body β at the undeformed configuration Ω_o, then this point could be defined by the position vector relative to the point of origin 0. The deformed state is assumed to exist at time t, with a deformed configuration Ω. Now the point **x** is the mapping of the point **X** by a certain motion ***x***. This motion could be summarised as

$$\mathbf{x} = \boldsymbol{x}(\mathbf{X}, \mathrm{t}) \tag{3}$$

In that case the displacement field in the material description form (with respect to the undeformed state) is given by

$$\mathbf{U}(\mathbf{X}, \mathrm{t}) = \mathbf{x}(\mathbf{X}, \mathrm{t}) - \mathbf{X} \tag{4}$$

In that case the displacement field in the spatial description form (with respect to the deformed state) is

$$\mathbf{u}(\mathbf{x}, \mathrm{t}) = \mathbf{x} - \mathbf{X}(\mathbf{x}, \mathrm{t}) \tag{5}$$

It is worth noting that the two displacements **U** or u have the same values, the difference between them is the reference to the coordinates, i.e **U** is referred to the material (undeformed coordinate while, u is referred to the spatial, deformed coordinates.

In that case the velocity and acceleration are given by the first and second derivative as shown in equations 6 and 7

$$\mathbf{V_i}(\mathbf{X}, \mathrm{t}) = \frac{\partial \mathbf{x}(\mathbf{X}, \mathrm{t})}{\partial \mathrm{t}} \tag{6}$$

$$\mathbf{A_{acc}}(\mathbf{X}, \mathrm{t}) = \frac{\partial \mathbf{V_i}(\mathbf{X}, \mathrm{t})}{\partial \mathrm{t}} \tag{7}$$

4.3 Deformation gradient

If an assumed curve, Γ, exists on the body β , the curve is not function in time, and this body is subjected to a certain motion, then this curve is deformed with the respect to the deformed state. Thus

$$\mathrm{d}\mathbf{x} = \mathbf{F}(\mathbf{X}, \mathrm{t})\mathrm{d}\mathbf{X} \tag{8}$$

Where **F**(X,t) is the deformation gradient, **F** is nonsingular , i.e (det(**F**)≠0) and it is invertible. Applying the same concept from the volume respect, equation 9 could be derived

$$\mathrm{dv} = \mathrm{J}(\mathbf{X}, \mathrm{t})\mathrm{dV} \tag{9}$$

$$\mathrm{J}(\mathrm{X}, \mathrm{t}) = \mathrm{det}\mathbf{F}(\mathbf{X}, \mathrm{t}) > 0 \tag{10}$$

Where **J**(X,t) is known as the Jacobian determinant (Jacobian) If J=1, then the motion is called isochoric or volume preserving. In the previous section, the concepts of configuration, undeformed state, deformed state, deformation gradient and the Jacobian were introduced. In the following section strain tensors will be covered.

4.4 Strain concept

Strain tensors are concerned with determining the changes of material elements during motion. Unlike displacements which are measurable quantities, strains are based on a concept that was introduced to simplify analysis. Thus many definitions have been introduced. Only common definitions to nonlinear continuum mechanics will be covered. If point **X** and **Y** exist on a body β in the reference (undeformed) configuration, during a motion then according to figure 4.2, equation 8 applies.

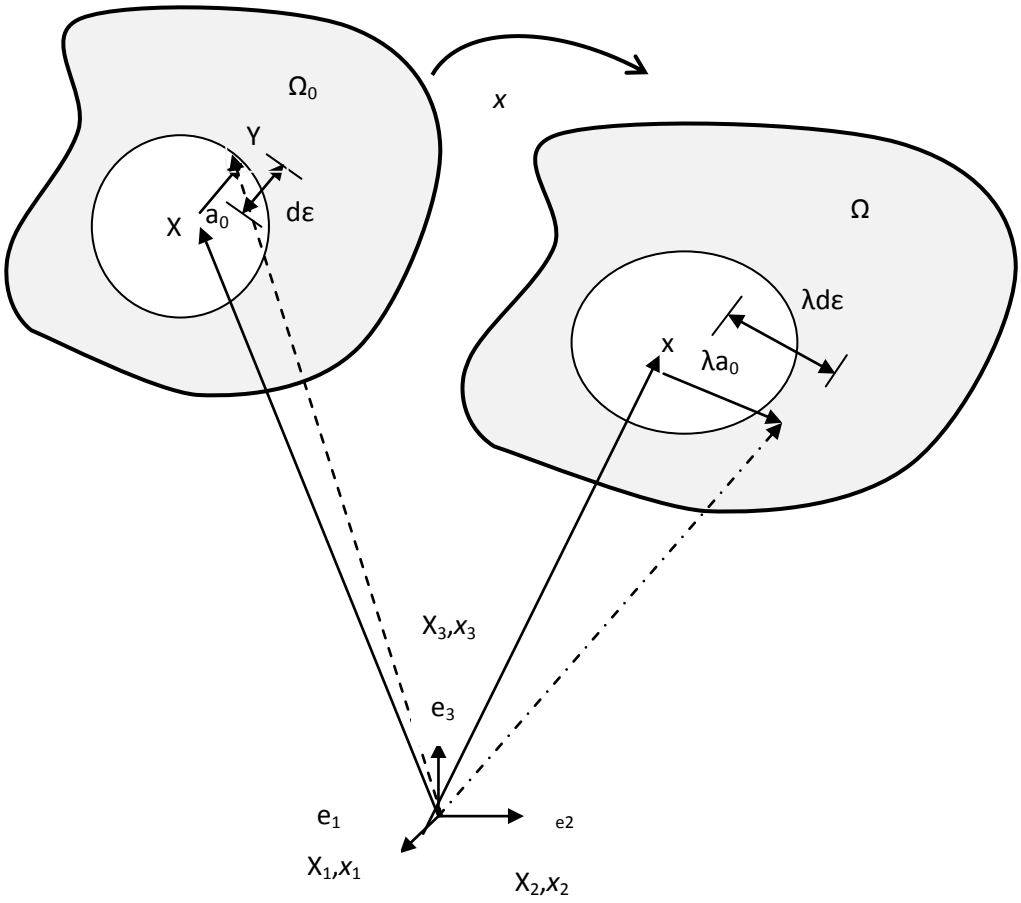

Figure 4.2: Strain concept[1].

$$\mathbf{Y} = \mathbf{Y} + (\mathbf{X} - \mathbf{X}) = \mathbf{X} + |\mathbf{Y} - \mathbf{X}| \frac{\mathbf{Y} - \mathbf{X}}{|\mathbf{Y} - \mathbf{X}|} = \mathbf{X} + \mathrm{d}\mathbf{X} \tag{11}$$

Let $$\mathrm{d}\varepsilon = |\mathbf{Y} - \mathbf{X}| \tag{12}$$

$$\mathbf{a}_0 = \frac{\mathbf{Y} - \mathbf{X}}{|\mathbf{Y} - \mathbf{X}|} \tag{13}$$

Where, the value a_0 is defined as the unit vector

substitute in11 to get $$\mathrm{d}\mathbf{X} = \mathrm{d}\varepsilon \mathbf{a}_0 \tag{14}$$

$$\mathrm{d}\mathbf{X}.\,\mathrm{d}\mathbf{X} = \mathrm{d}\varepsilon \mathbf{a}_0.\,\mathrm{d}\varepsilon \mathbf{a}_0 = \mathrm{d}\varepsilon^2 \tag{15}$$

Regarding the state of the spatial configuration, the points x and y could be defined through Taylor expansion to the following equations

$$\mathbf{y} - \mathbf{x} = \mathrm{d}\varepsilon \mathbf{F}(\mathrm{X}, \mathrm{t})\mathbf{a}_0 + \mathrm{o}(\mathbf{Y} - \mathbf{X}) \tag{16}$$

λ known as the stretch is taken to be the product of the deformation gradient and the unit vector according to equation 17.

$$\boldsymbol{\lambda} = \mathbf{F}(\mathbf{X}, \mathrm{t})\mathbf{a}_0 \tag{17}$$

Substituting in equation 17 gives

$$|\mathbf{y} - \mathbf{x}| = |(\mathbf{y} - \mathbf{x}).\,(\mathbf{y} - \mathbf{x})|^{\frac{\mathbf{1}}{\mathbf{2}}} = |(\mathrm{d}\varepsilon \mathbf{F}(\mathbf{X}, \mathrm{t})\mathbf{a}_0).\,(\mathrm{d}\varepsilon \mathbf{F}(\mathbf{X}, \mathrm{t})\mathbf{a}_0)|^{\frac{1}{2}} = \lambda \mathrm{d}\varepsilon \tag{18}$$

In summary, the distance between **X** and **Y** in the undeformed state was dε, after a certain motion for the body, these two points become **x** and **y** and the distance between them becomes λdε. It could be said that these distance is compressed, extended or unstretched depending on the value of λ , whether it is bigger, equal or smaller than 1.

Using the matrix identity given in equation 19

$$\mathbf{v}.\,\mathbf{A}^{\mathbf{T}}\mathbf{u} = \mathbf{u}.\,\mathbf{A}\mathbf{v} = \mathbf{A}\mathbf{v}.\,\mathbf{u} \tag{19}$$

For all vectors **v** and **u** And applying to equation 17 gives

$$\lambda^2 = \boldsymbol{\lambda}.\,\boldsymbol{\lambda} = \mathbf{F}\mathbf{a}_{\mathrm{o}}.\,\mathbf{F}\mathbf{a}_{\mathrm{o}} = \mathbf{a}_{\mathrm{o}}\mathbf{F}^{\mathrm{T}}\mathbf{F}\mathbf{a}_{\mathrm{o}} = \mathbf{a}_{\mathrm{o}}.\,\mathbf{C}\mathbf{a}_0 \tag{20}$$

$$\mathbf{C} = \mathbf{F}^{\mathrm{T}}\mathbf{F} \text{ or } \mathbf{C}_{\mathrm{AB}} = \mathbf{F}_{\mathrm{aA}}\mathbf{F}_{\mathrm{aB}} \tag{21}$$

C is known as the right Cauchy-Green tensor or the Green deformation tensor. It is worth noting that **C** is symmetric and positive definite.

An n × n real symmetric matrix **C**is positive definite if $\mathbf{z}^{\mathrm{T}}\mathbf{C}\mathbf{z} > 0$ for all non-zero vectors **z** with real entries

$$\mathbf{C} = \mathbf{F}^{\mathrm{T}}\mathbf{F} = (\mathbf{F}^{\mathrm{T}}\mathbf{F})^{\mathrm{T}} = \mathbf{C}^{\mathrm{T}} \tag{22}$$

$$\det\mathbf{C} = (\det\mathbf{F})^2 = \mathrm{J}^2 > 0 \tag{23}$$

$$\mathbf{E} = \frac{1}{2}(\mathbf{F}^{\mathrm{T}}\mathbf{F} - \mathbf{I}) \tag{24}$$

E is known as Green-Lagrange strain tensor.

4.5 Stress concept

Strain types that are linked to spatial deformation are not the scope of this research. In the last section material (undeformed/reference) strain concepts were covered along with deformation gradient and displacement. These concepts cover the interaction between the material and its neighbours in the interior part of a certain body. One consequence of these interactions is stress, which has a physical dimension of force per unit area. For example, if there is a deformable body and it is subjected to finite motion, several stress tensor types and vectors could be defined. Also, in this section only stresses referred to the undeformed configuration will be discussed as they are more relevant to the scope of the research more than those of the spatial deformation.

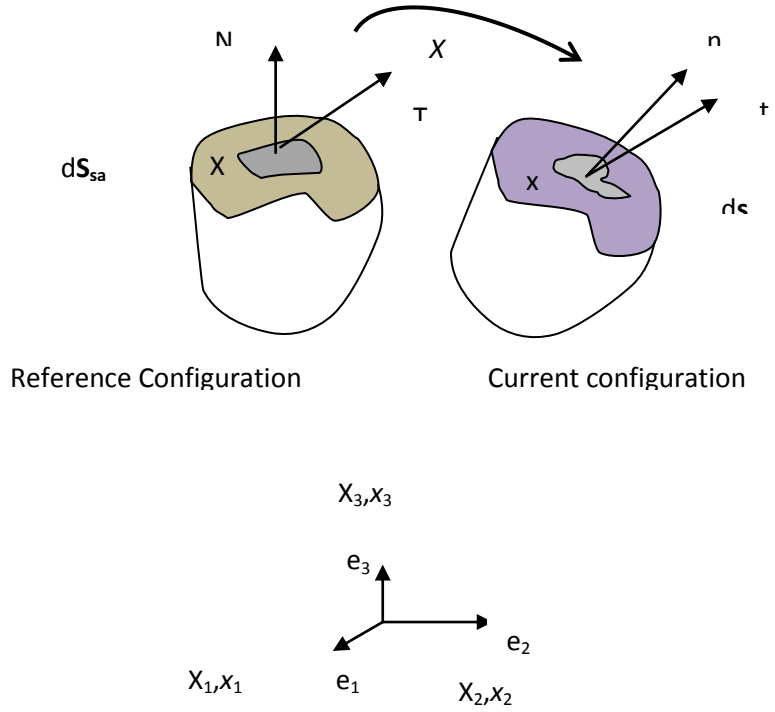

Figure 4.3: A cross section in a body β shows an area S_{sa} with a normal vector N and traction vector T[1].

If a certain body β (figure 4.3) is cut, by a plane surface which passes through a point **X** in the reference state with spatial coordinates $\mathbf{x}_o$, then the infinitesimal resulting force is denoted df. It can also be concluded that for every surface element d**s**, equations 25 and 26 apply:

$$\mathrm{d}\mathbf{f} = \mathbf{t}\mathrm{d}\mathbf{s}_{\mathbf{sa}} = \mathbf{T}\mathrm{d}\mathbf{S}_{\mathbf{sa}} \tag{25}$$

$$\mathbf{t} = \mathbf{t}(\mathbf{x}, \mathrm{t}, \mathbf{n}) \text{ and } \mathbf{T} = \mathbf{T}(\mathbf{X}, \mathrm{t}, \mathbf{N}) \tag{26}$$

t represents the Cauchy or true traction vector and **T** represents the first Piola-Kirchhoff (nominal) traction vector. The two vectors **t** and **T** are known as the surface tractions. They are surface or friction forces, while t is the time.

Having introduced the surface traction vectors, the Piola-Kirchhoff **P** and Cauchy stress **σ** tensors can be derived to be in the form given by equation 27.

$$\mathbf{t}(\mathbf{x}, \mathrm{t}, \mathbf{n}) = \boldsymbol{\sigma}(\mathbf{x}, \mathrm{t})\mathbf{n} \tag{27}$$

$$\mathbf{T}(\mathbf{X}, \mathrm{t}, \mathbf{N}) = \mathbf{P}(\mathbf{X}, \mathrm{t})\mathbf{N} \tag{28}$$

Where, n and N are the normals to the surface. This could be written in matrix notation according to equation 29 and shown in figure 4.4.

$$[\mathbf{t}] = [\boldsymbol{\sigma}][\mathbf{n}] \tag{29}$$

$$[\mathbf{t}] = \begin{bmatrix} \mathrm{t}_1 \\ \mathrm{t}_2 \\ \mathrm{t}_3 \end{bmatrix} = \begin{bmatrix} \sigma_{11}\sigma_{12}\sigma_{13} \\ \sigma_{21}\sigma_{22}\sigma_{23} \\ \sigma_{31}\sigma_{32}\sigma_{33} \end{bmatrix} \begin{bmatrix} \mathrm{n}_1 \\ \mathrm{n}_2 \\ \mathrm{n}_3 \end{bmatrix}$$

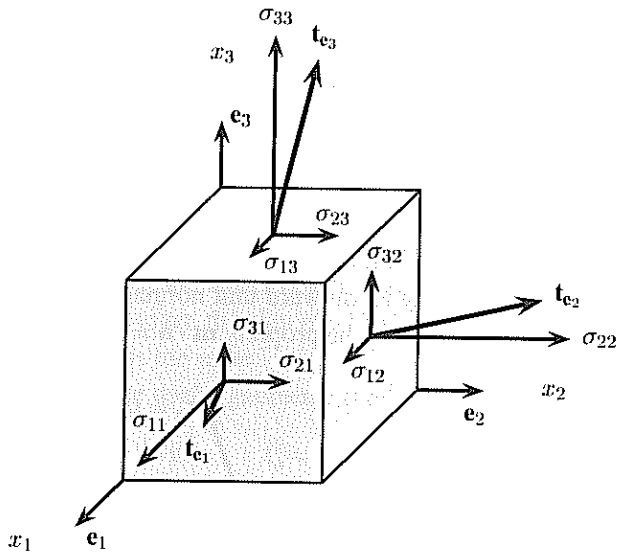

Figure 4.4: Stress components and their respective traction vector [1].

The Piola-Kirchhoff transformation could be applied as shown in equation 30.

$$\mathbf{P} = \mathrm{J}\boldsymbol{\sigma}\mathbf{F}^{-\mathbf{T}} \tag{30}$$

Second Piola Kirchoff stress tensor

This tensor does not admit a physical interpretation in terms of surface traction. Nevertheless it is a symmetrical matrix and parameterised by material coordinates. Thus it is often used to represent stress measure in computational mechanics. It is given by equation 31.

$$\mathbf{S} = \mathrm{J}\mathbf{F}^{-1}\boldsymbol{\sigma}\mathbf{F}^{-\mathrm{T}} \tag{31}$$

The transfer from second Piola Kirchhoff to Cauchy stress is given by equation 32

$$\boldsymbol{\sigma} = \mathrm{J}^{-1}\mathbf{F}\mathbf{S}\mathbf{F}^{\mathrm{T}} \tag{32}$$

4.6 Balance principles

In the last section deformation gradient, strain and stress tensor types and concepts were introduced. In the following section gives a brief discussion of the mechanical laws governing the branches of continuum mechanics and its fundamental principles. For example, conservation of mass, momentum balance principles and balance of energy must be satisfied in all times.

4.6.1 Conservation of mass

Every continuum body β possesses mass, denoted by m, it is assumed that mass is continuously distributed on the arbitrary region Ω and bounded by a surface $\partial\Omega$ at a time t. The mass is a scalar positive number, which is invariant during motion.

Closed and open systems

A closed system consists of a fixed amount of mass, no mass can cross its boundary, but energy can. The volume in a closed system does not have to be fixed. On the other hand in an open system mass and energy can cross the boundary as shown in figure 4.5.

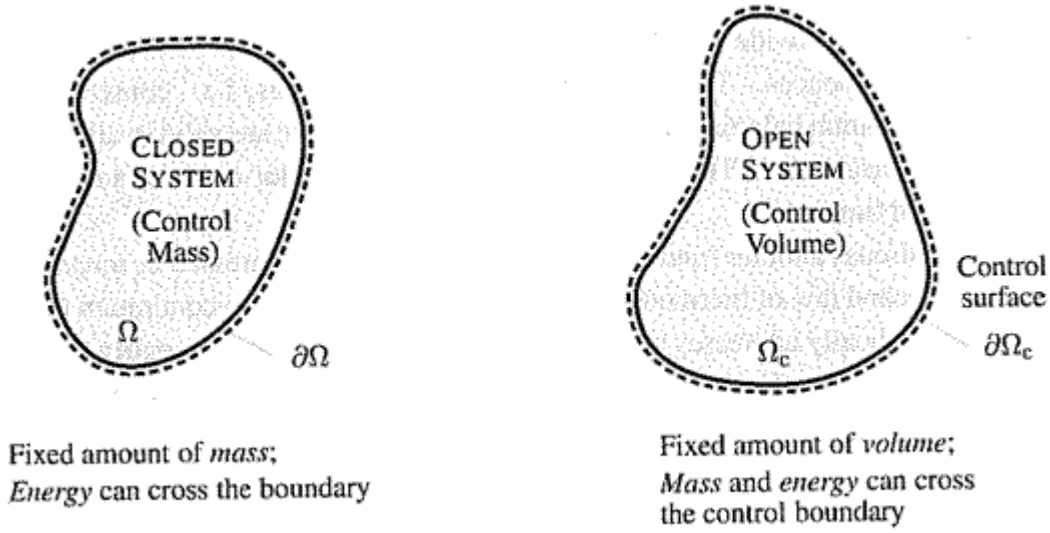

Figure 4.5: Closed and opened systems[1].

In non-relativistic physics, mass cannot be produced or destroyed. It is assumed that during a motion there are not any mass sources or mass sinks, so that a body mass is conserved. Considering a closed system this holds for the total mass thus

$$\mathrm{m}(\Omega_0) = \mathrm{m}(\Omega) > 0 \tag{33}$$

$$\mathrm{dm}(\mathbf{X}) = \mathrm{dm}(\mathbf{x}, \mathrm{t}) > 0 \tag{34}$$

$$\mathrm{m} = \int \rho_{\mathrm{O}}(\mathbf{X})\mathrm{dV} = \int \rho(\mathbf{x}, \mathrm{t})\mathrm{dv} = \mathrm{const} > 0 \tag{35}$$

Where ρ is the density deformed state, while, V is the volume in the undeformed state and v is the volume in the deformed state. From the mass continuity equation it can be deduced that

$$\rho_{\mathrm{o}}(\mathbf{X}) = \rho\big((\mathbf{X}, \mathrm{t}), \mathrm{t}\big)\mathrm{J}(\mathbf{X}, \mathrm{t}) \tag{36}$$

4.6.2 Balance of linear momentum

Linear momentum equation is given by equation 37:

$$\mathbf{L}(\mathrm{t}) = \int \rho(\mathbf{x},\mathrm{t})\mathbf{v_i}(\mathbf{x},\mathrm{t})\mathrm{dv} = \int \rho_{\mathrm{o}}\,(\mathrm{X})\mathbf{V_i}(\mathbf{X},\mathrm{t})\mathrm{dV} \tag{37}$$

Where v_i is the velocity, From equation 37, linear balance of momentum is given by equation 38

$$\frac{\mathrm{D}}{\mathrm{Dt}}\int \rho(\mathbf{x},\mathrm{t})\mathbf{v_i}(\mathbf{x},\mathrm{t})\mathrm{dv} = \frac{\mathrm{D}}{\mathrm{Dt}}\int \rho_{\mathrm{o}}\,(\mathbf{X})\mathbf{V_i}(\mathbf{X},\mathrm{t})\mathrm{dV} = \mathbf{F_{res}}(\mathrm{t}) \tag{38}$$

But the resultant force $\mathbf{F}_{res}(t)$ could be defined by equation 39.

$$\mathbf{F_{res}}(\mathrm{t}) = \int \mathbf{t}\mathrm{ds} + \int \mathbf{b}\mathrm{dv} \tag{39}$$

Where b_f is body force, s_{sa} is the area, v is the volume

Hence equation 39 becomes

$$\int \mathbf{t}\mathrm{ds_{sa}} + \int \mathbf{b_f}\mathrm{dv} = \frac{\mathrm{D}}{\mathrm{Dt}}\int \rho(\mathbf{x},\mathrm{t})\mathbf{v_i}(\mathbf{x},\mathrm{t})\mathrm{dv} \tag{40}$$

But knowing that

$$\int \mathbf{t}\mathrm{ds_{sa}} = \int \mathrm{div}\,\boldsymbol{\sigma}\,\mathrm{dv} \tag{41}$$

By substituting in equation 40 to get

$$\int (\mathrm{div}\,\boldsymbol{\sigma} + \mathbf{b_f} - \rho\mathbf{v_i}')\mathrm{dv} = 0 \tag{42}$$

If there is n acceleration then Cauchy equation of equilibrium is achieved

$$\int (\mathrm{div}\,\boldsymbol{\sigma} + \mathbf{b_f})\mathrm{dv} = 0 \tag{43}$$

If there is no external force

$$\int (\mathrm{div}\,\boldsymbol{\sigma})\mathrm{dv} = 0 \tag{44}$$

This is known as self equilibrated stress field.

From that and applying thin wall theory it could be proved that Cauchy stresses can be related back to luminal blood pressure and axial stress using thin wall theory [2-3]. Assuming a deformed thickness, h, deformed radius, r, a luminal pressure, p, and an axial force, f_a, we have

$$\sigma_{t\theta} = p\left(\frac{r}{h} - \frac{1}{2}\right) \tag{45}$$

$$\sigma_{tz} = \frac{\sigma_\theta}{2} + \frac{f_a}{2\pi\, rh} \tag{46}$$

4.6.3 Constitutive equation

The fundamental equations in the last section are essential to understand kinematics, stress and balance principles, and hold any continuum body for all times. However they do not distinguish between materials, and they remain valid for all branches of continuum mechanics. For the case of deformable bodes like the arterial wall, the equations mentioned are not sufficient on their own to determine the material response. Hence the need rise for appropriate constitutive equations that are furnished to specify the nature of the materials building the arterial wall.

Generally, constitutive equations aim is to specify the stress components in terms of other field functions such as strain. The constitutive equation role is to determine the state of stress at any point x of a continuum body at time t and it is unique for different types of continuous bodies. Also, it is worth noting that in general continuum mechanics deals with different media like liquids hence the name fluid mechanics and also solid hence solid mechanics.

The main goal of the next section is to describe the constitutive equations for the arterial layers from that the whole wall will be derived. These constitutive equations are still applicable for use of approximation methods like finite element analysis. The path flowed in this research is the phenomenological approach describing the nature of the material as continua. The phenomenological approach is mainly concerned with fitting mathematical equations to experimental data.

The aim of constitutive theories is to develop mathematical models for representing the real behaviour of the matter. The focus of this research is the finite hyperelastic models. These cover the materials with large strain (finite) response like the arterial walls. Such constitutive theory postulates the existence of a Helmholtz free energy function (W), which is defined per unit volume. In that case equation 47applies

$$W = W(\mathbf{F}) \tag{47}$$

This means that this free energy function is only a function of deformation gradient. In this case this Helmholtz free-energy function is referred to as the strain energy function. Strain energy function is defined as the stored energy inside a unit volume of a material; it is a scalar value continuous function.

The scope of this research is to concentrate on homogenous materials, in which the distribution of the internal constituents is assumed to be uniform. For this material the strain energy function only depends on the deformation gradient. Of course for the so called heterogeneous materials, the strain energy function will also depend on the position of a certain point inside the material or the medium which is subject of interest.

A hyperelastic material is defined as a subclass of an elastic material; it has a physical expression in the form of the equation 48.

$$\mathbf{P} = \frac{\partial \mathrm{W}(\mathbf{F})}{\partial \mathbf{F}} \tag{48}$$

After some transformation, the relation between second Piola Kirchoff and strain energy function could be given by equation 49.

$$\mathbf{S} = \frac{\partial \mathrm{W}(\mathbf{E})}{\partial \mathbf{E}} \tag{49}$$

These types of equation, is knows as purely mechanical constitutive equation or equations of state. They form an empirical model as the basis of approximating the behaviour of real material, hence the name material model or constitutive model. Such material could also be known as perfectly elastic material which means it does not produce any entropy i.e the internal dissipation is zero. It is worth noting that the strain energy function vanishes in the reference configuration, thus the normalisation condition given by equation 50 holds.

$$\text{at } \mathbf{F} = \mathrm{I} \tag{50}$$

Then

$$\mathrm{W} = \mathrm{W}(\mathbf{I}) = 0$$

Also, it is known from physical observation that the strain energy increases with increasing the deformation, therefore equation 51 applies:

$$\mathrm{W} = \mathrm{W}(\mathbf{F}) \geq 0 \tag{51}$$

The strain energy function has a global minimum at F=I and its equal to zero. It is assumed that the strain energy does not have any stationary points in the strain space. It is also assumed that

that residual stress in the reference configuration is zero; in this case the reference configuration is stress free.

For the behaviour of finite strains, the strain energy function satisfies the growth conditions, which means that equation 52 applies

$$\mathrm{W}(\mathbf{F}) \to +\infty \text{ as } \det \mathbf{F} \to +\infty \qquad (52)$$
$$\mathrm{W}(\mathbf{F}) \to +\infty \text{ as } \det \mathbf{F} \to 0^{+}$$

Physically, this means that, an infinite amount of energy would be required to expand a continuum body to an infinite range or to compress it to a point with vanishing volume.

4.6.4 Incompressible hyperelastic materials

Using the Lagrangian multiplier, a relationship is derived between the total strain-energy and the volumetric, W_{ic} (**E**, $\mathbf{A_1}$). Assuming the arterial walls to be incompressible, and that the total strain-energy is a function of the Green-Lagrange strain tensor representing one family of collagen fibres, we have

$$\mathrm{W}\,(\mathbf{E}, \mathbf{A}_1\,) = \mathrm{W}_{\mathrm{ic}}\,(\mathbf{E_{ic}}\,, \mathbf{A}_1) \qquad (53)$$

where

$$\mathbf{A}_1 = a_1 \otimes a_1 \qquad (54)$$

and

$$a_1 = \begin{pmatrix} 0 \\ \cos\varphi \\ \sin\varphi \end{pmatrix} \qquad (55)$$

given that, φ, is the angle between collagen fibre orientation and the circumferential direction, using cylindrical coordinates.

Assuming no change in volume, and using equation 49 and applying Lagrangian multiplier P

$$\mathbf{S} = \frac{\partial \mathrm{W}_{\mathrm{ic}}}{\partial \mathbf{E}} + \mathrm{P}\frac{\partial \mathrm{J}}{\partial \mathbf{E}} \qquad (56)$$

where P has the units of hydrostatic pressure. The isochoric Green-Lagrange strain-stretch relationship is given by

$$\mathbf{E}_i = \frac{1}{2}(\lambda_i^2 - 1) \qquad (57)$$

where λ_i is the isochoric principal stretch.

The circumferential and axial second Piola Kirchhoff stress components, s_θ, and, s_z, respectively, are given by

$$s_\theta = \frac{1}{\lambda_\theta}\frac{\partial W_{ic}}{\partial \lambda_\theta} - \frac{1}{\lambda_\theta^3}\frac{1}{\lambda_z}\frac{\partial W_{ic}}{\partial \lambda_r} \tag{58}$$

where λ_θ, λ_z, λ_r are the principal stretches in the circumferential, axial and radial directions

$$s_z = \frac{1}{\lambda_z}\frac{\partial W_{ic}}{\partial \lambda_z} - \frac{1}{\lambda_z^3}\frac{1}{\lambda_\theta}\frac{\partial W_{ic}}{\partial \lambda_r} \tag{59}$$

respectively.

4.6.5 Collagen and elastin strain-energy functions

For each layer, the strain-energy, W_{ic}, is considered to be the linear combination of elastin and collagen contributions.

$$W_{ic}(\mathbf{E}, \mathbf{A}_1) = W_{iciso}(\mathbf{E_{ic}}) + W_{icaniso}(\mathbf{E_{ic}}, \mathbf{A}_1) \tag{60}$$

The form of the elastin strain-energy component $W_{iciso}(\mathbf{E_{ic}})$, is approximated to be

$$W_{iciso}(\mathbf{E_{ic}}) = \frac{c_1}{2}(I_1 - 3) \tag{61}$$

The first invariant of stretch , I_1, is defined as

$$I_1 = {\lambda_\theta}^2 + {\lambda_z}^2 + {\lambda_r}^2 \tag{62}$$

and c_1, is a material constant related to the elastin stress response.

The form of the collagen contribution can be described by

$$W_{icaniso}(\mathbf{E_{ic}}, A_1) = \frac{k_1}{k_2}(e^q - 1) \tag{63}$$

where k_1, and k_2 are material constants related to the collagen stress response and q is calculated to be

$$q = \rho_{disp} k_2 (I_4 - 1)^2 + (1 - \rho_{disp})(I_1 - 3)^2 \quad (64)$$

where ρ_{disp} is the dispersion factor. I_4 is the fourth stretch invariant given by

$$I_4 = \lambda_\theta^2 \cos(\phi)^2 + \lambda_z^2 \sin(\phi)^2 \quad (65)$$

The dispersion factor value represents the amount of dispersion from the ideal alignment of the fibres [4]. A value of unity assumes that all the fibres are oriented in the ϕ direction. For a value of zero the fibres are assumed to be randomly isotropically oriented, as presented by Demiray et al [5].

4.7 Thin wall approximation

To estimate the mean stress-strain relationships in each layer and the whole arterial wall, it is assumed that thin wall theory can be applied. Fung et al [6] noted that the arterial wall is not so thin, but it was considered to be thin enough to justify the use of thin wall theory. Fung et al observed that neglecting the variation of stress through the wall thickness will have an effect on the quality of a model prediction [7]. However, no quantitative error estimation was given. Holzapfel et al used thin wall theory to represent the circumferential and axial responses [2]. When modelling the layer response, he discussed the usage of different strain-energy forms for each layer. In order to formulate the analytical model, Holzapfel et al made certain assumptions. As all collagen fibres are embedded in the tangential surface of the tissue, it was assumed that there are no components in the radial direction [2, 8-9]. This supported the use of the thin wall approximation [10]. On comparing circumferential and radial stresses, circumferential stresses appear to be far bigger. Thus this justifies only considering circumferential and axial stresses in this investigation [2]. Although bending and residual stresses are important in some arterial regions, it is not taken into consideration in this study due to lack of experimental data that fits within the scope of this research.

4.8 Layer stress response

Equations (32), (58) and (59) can now be used to describe each of the three arterial layers, *l* to calculate the Cauchy stress components, $\sigma_{\vartheta l}$ and σ_{zl}, in the circumferential and axial directions respectively. Thus for the intima (*l* = n),and applying in equations 60-65 gives

$$\sigma_{\theta n} = [c_{1n}\left(1 - \frac{1}{\lambda_\theta^4 \lambda_z^2}\right) + k_{1n} e^{qn}(\left(1 - \rho_{dispn}\right)(I_{1n} - 3)\left(1 - \frac{1}{\lambda_\theta^2}\right)\rho_{dispn}(I_{4n} - 1)\cos(\phi_n)^2)]\,\lambda_\theta^2 \tag{66}$$

$$\sigma_{zn} = [c_{1n}\left(1 - \frac{1}{\lambda_\theta^2 \lambda_z^4}\right) + k_{1n} e^{qn}(\left(1 - \rho_{dispn}\right)(I_{1n} - 3)\left(1 - \frac{1}{\lambda_z^2}\right) + \rho_{dispn}(I_{4n} - 1)\sin(\phi_n)^2)]\lambda_z^2 \tag{67}$$

Similar expressions can be obtained the media layer (*l*=m) and the adventitia (*l*=a).

4.9 Whole-wall stress response

This research presented here proposes using stress equilibrium [11-12] in the wall to calculate the mean wall Cauchy stress components, $\sigma_{t\theta}$ and σ_{tz} in the circumferential and axial directions as shown in equations (68) and (69) where h is the wall thickness after deformation.

$$\sigma_{t\theta} = \frac{(\sigma_{\theta n} h_n + \sigma_{\theta m} h_m + \sigma_{\theta a} h_a)}{h} \tag{68}$$

$$\sigma_{tz} = \frac{(\sigma_{zn} h_n + \sigma_{zm} h_m + \sigma_{za} h_a)}{h} \tag{69}$$

4.10 Conclusion

In this chapter, the concept of continuum mechanics was introduced. Three main branches were discussed: configuration of continuum bodies, study of stress and study of motion. Deformation gradient were also studied, conservation of mass was also presented. Then the stress energy of each of the materials building the arterial wall were also introduced, such that the total stress energy of the arterial wall is equal to the summation of the stress energies of elastin and collagen, as they are the materials that take part in the passive filling of the arterial wall. Through the use of thin wall theory as well as stress equilibrium; a new method was proposed that show a relationship between phenomenological derived layer response and the total stress response. This method still needs parameters estimation which will be presented in the next chapter. In chapters 6 and 7 Experimental examples will be shown to prove the efficiency of the proposed model.

4.11 References

1. Holzapfel GA, *Nonlinear Solid Mechanics*, ed. Wiley. 2006, Sussex. 455.
2. Holzapfel GA, Eberlein R, Wriggers P, and Weizsäcker HW, *A New Axisymmetrical Membrane Element for Anisotropic,Finite Strain Analysis of Arteries.* Commun. Num. Meth. Eng., 1996. **12**(8): p. 507-517.
3. Fenner R, *Mechanics of Solids*. 1989, Oxford: Blackwell scientific publications. 615.
4. Holzapfel GA, *Collagen. Structure and Mechanics*, in *Collagen in Arterial Walls: Biomechanical Aspects*, P. Fratzl, Editor. 2008, Springer-Verlag, Heidelberg: New York. p. 285-324.
5. Demiray H, *A Note on the Elasticity of Soft Biological Tissues.* J. Biomech., 1972. **5**(3): p. 309-311.
6. Fung YC, Fronek K, and Patitucci P, *Pseudoelasticity of Arteries and the Choice of Its Mathematical Expression.* Am. J. Physiol. Heart Circ. Physiol., 1979. **237**(5): p. H620-631.
7. Chuong CJ and Fung YC, *Three-Dimensional Stress Distribution in Arteries.* J. Biomech. Eng., 1983. **105**(3): p. 268-274.
8. Holzapfel GA, Sommer G, Gasser CT, and Regitnig P, *Determination of Layer-Specific Mechanical Properties of Human Coronary Arteries with Nonatherosclerotic Intimal Thickening and Related Constitutive Modeling.* Am. J. Physiol. Heart Circ. Physiol., 2005. **289**(5): p. H2048-2058.
9. Holzapfel GA, *Biomechanical Behavior of the Arterial Wall and Its Numerical Characterization.* Comp. Biol. Med., 1998. **28**: p. 377-392.
10. Holzapfel GA and Gasser TC, *A Viscoelastic Model for Fiber-Reinforced Composites at Finite Strains Continuum Basis, Computational Aspects and Applications.* Comput. Methods Appl. Mech. Engr., 2001. **190**(34): p. 4379-4403.
11. Mickael M, Heydari A, Crouch R, and Johnstone S, *Estimation of Stress-Strain Relationship in Vascular Walls Using a Multi-Layer Hyperelastic Modeling Approach*, in *Cinc2010*: Belfast.
12. Mickael M, Heydari A, Crouch R, and Johnstone S. *Mechanical Properties of Arterial Walls: Do They Play a Role in Determining Stretch Receptor Firing Rates?* in *ICABB-2010*. Venice.

CHAPTER 5

OPTIMISATION AND PARAMETER ESTIMATION

---

5 Overview

In this thesis an analytical model is produced to relate the material constants of arterial layers to both individual layer and whole wall experimentally derived stress-strain characteristics. To achieve this, the set of resulting equations require optimizing to find an optimum solution within the physiological range. This section looks at the process of selecting data and two optimization methods, steepest descent and nonlinear least square. To address the question of uniqueness of solution parameters sensitivity analysis will be also discussed. It is worth noting that bold letters are used to represent vectors in this chapter.

5.1 Selection of data

Experimental data was taken from [1]. This data consists of whole wall relationship for change in diameter and axial force as a function of transmural pressure as shown in figure 5.1. The experimental setup reported was as follows [1]. Cadvers with arteriosclerosis were selected, and then arteries were dissected from them. After that arteries were preconditioned to make sure that the mechanical response is stable. Then a pre pre-stretch was applied using a static experimental technique. i.e the generated relationship is not a function in time. Finally, the external diameter and corresponding axial force were measured and graphically presented in [1].

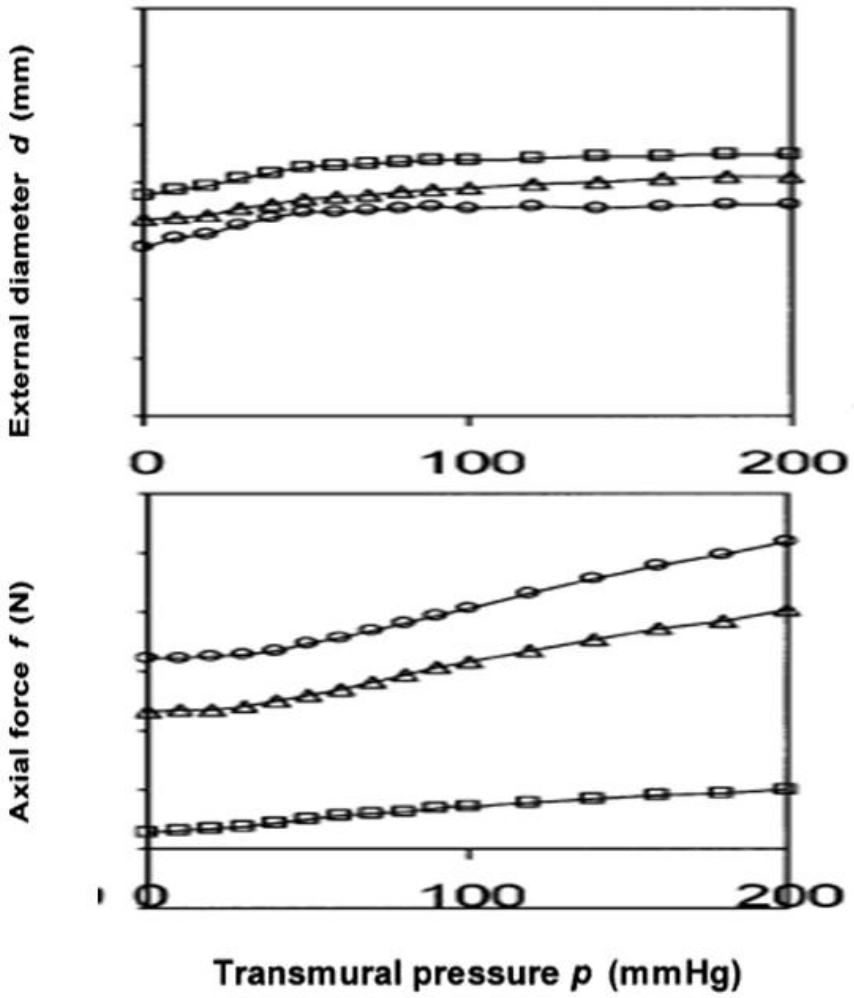

Figure 5.1: Transmural pressure versus external diameter and axial force [1]. The square, triangle and circle represent axial stretch of 1.1, 1.2 and 1.25 respectively.

5.2 Optimisation method

Optimisation is generally defined as choosing the most suitable set of parameters from a set of alternatives [2]. Optimisation could be classified into linear programming, nonlinear programming and multi-objective optimisation. All these three groups share the basic idea which is described below:

If there exists a certain experimental curve, given by a set of points represented by (y_i, t_i), and if there exists an analytical model equation, which results in values M(x,t),then the least square value method optimisation could be used to minimize the residual value i.e. the difference between the values of y_i and M(x,t) given by $f_{iop}(x)$ according to equation 1:

$$F_{op}(x) = \frac{1}{2}\sum_{i=1}^{m}(f_{iop}(x))^2 \quad (1)$$

An example (y_i,t_i), as well as M(x,t) is given in figure 5.2.

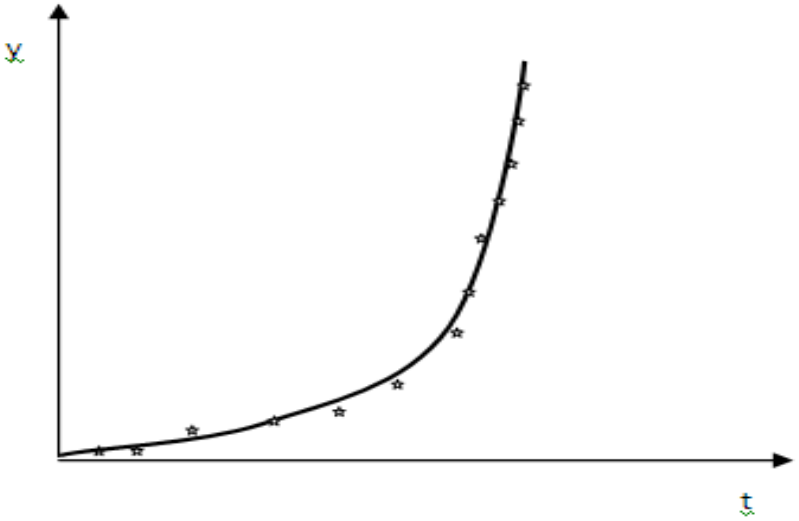

Figure 5.2 : Data points (y_i, t_i) marked by a star and M (x,t) marked by a full line, in this case M(x,t) was be given by $x_1 + e^{x_2 t}$[2].

F(x) in that case is known as the objective function, or cost function. It could be subjected to linear or nonlinear set of constraints. If the objective function and the constraints are linear then linear programming optimisation is used. If the objective function or any constraint is nonlinear then nonlinear programming is applied[2]. Multi-objective optimization is concerned with the minimization of multiple objective functions. The main method for solving linear programming problems is known as the simplex method, which is applied after replacing constrained inequalities with equalities. Also the interior point and the active set algorithms could be used to solve linear programming problems. However, nonlinear problems are the main concern of this section. These types of problems aim at finding the local minima, this will be explained in details in the following section, and also different methods will be shown.

An extremum point can be either local or global, the term 'local' means that the (maximum or minimum point) is the extrermum over a certain region, where 'global' means that this extremum point is the one and truly max/min point over the whole real numbers range. Finding the global point is done in two ways; the first is achieved through finding the local maxima/minima by using widely varying values and then choosing the most extreme point among them, the second method uses a different starting point and then checks if the routine used would give the same solution over time. Solving global minimiser value problems is not the focus of this research. The main aim of this investigation is to examine different local minimiser routines and compare between them. The goal of the local minimiser is to find the parameters values that would

minimize the value of x* (defined as the minimum value of (x) [2]. To find the local minimiser values, a certain value δ is chosen to represent the size of the region. The relation between x* and δ is given by equation 2.

$$\mathrm{F_{op}}(\mathrm{x}*) \leq \mathrm{F_{op}}(\mathrm{x}) \text{ for } \|\mathrm{x} - \mathrm{x}*\| < \delta \tag{2}$$

This is shown in figure 5.3.

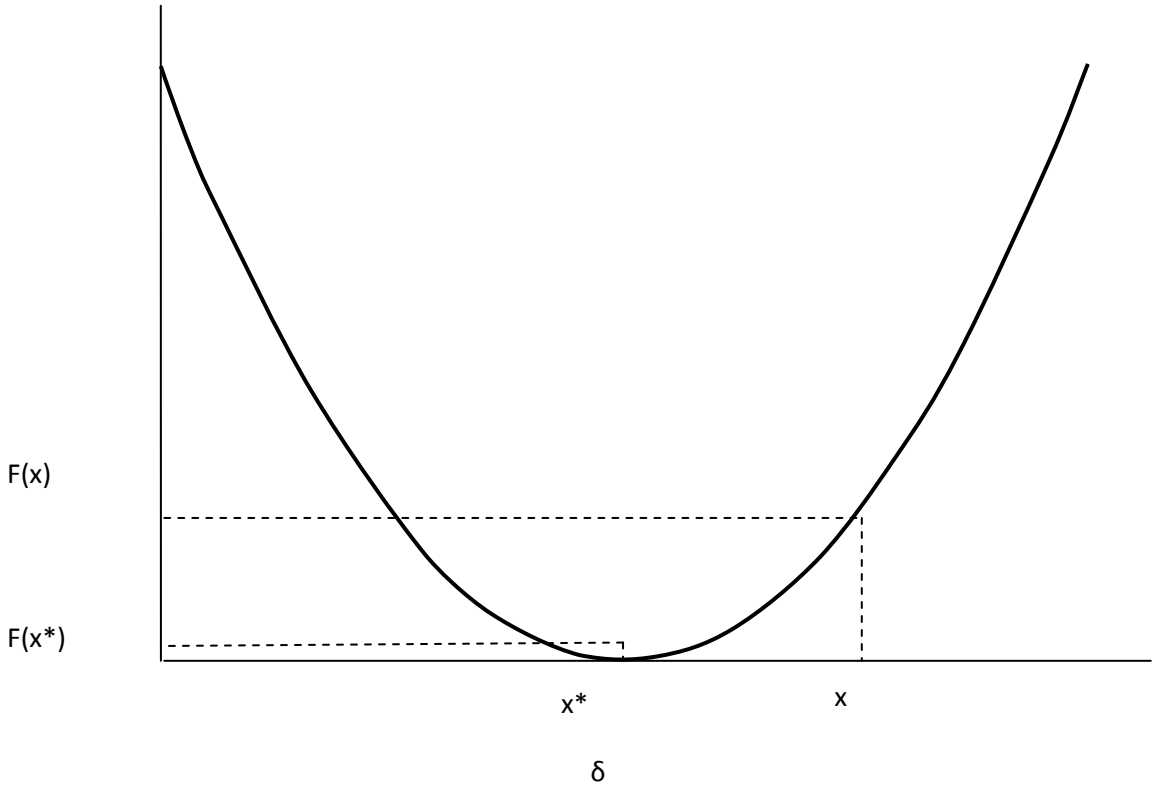

Figure 5.3: While the value of x-x*<δ, $f_{op}(x*) < f_{op}(x)$, this ensures the convergence to a minimum*.

There are three types of local stationary point, namely known as local maximiser, local minimiser and a saddle point. These types are shown in figure 5.4.

a)

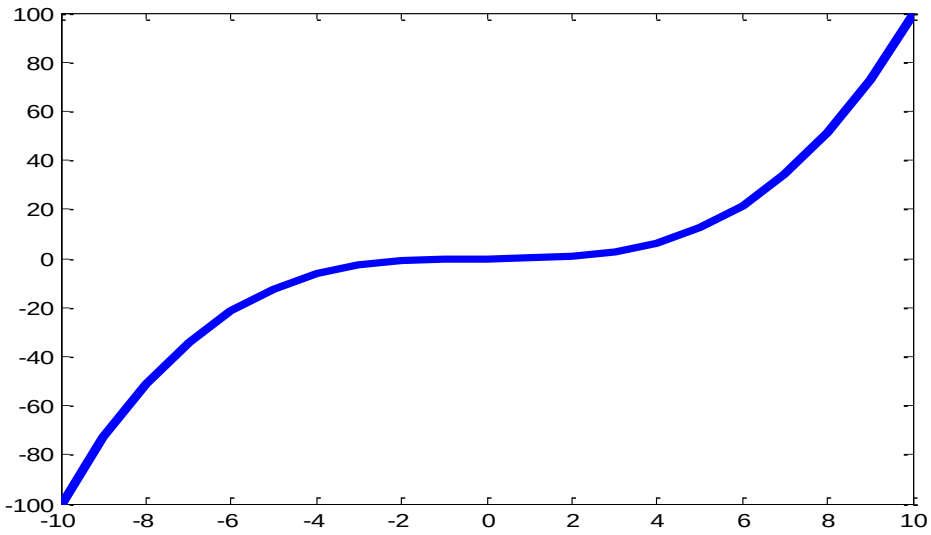

b)

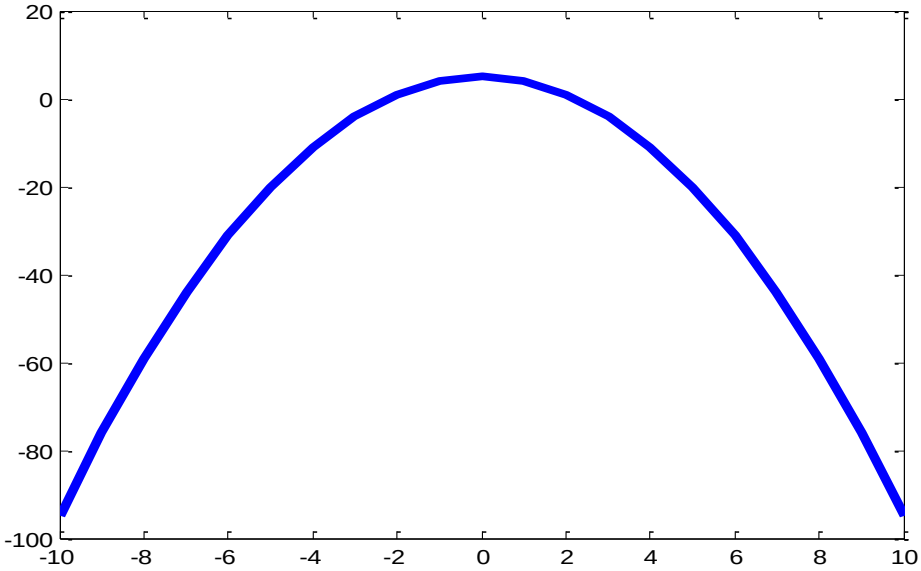

c)

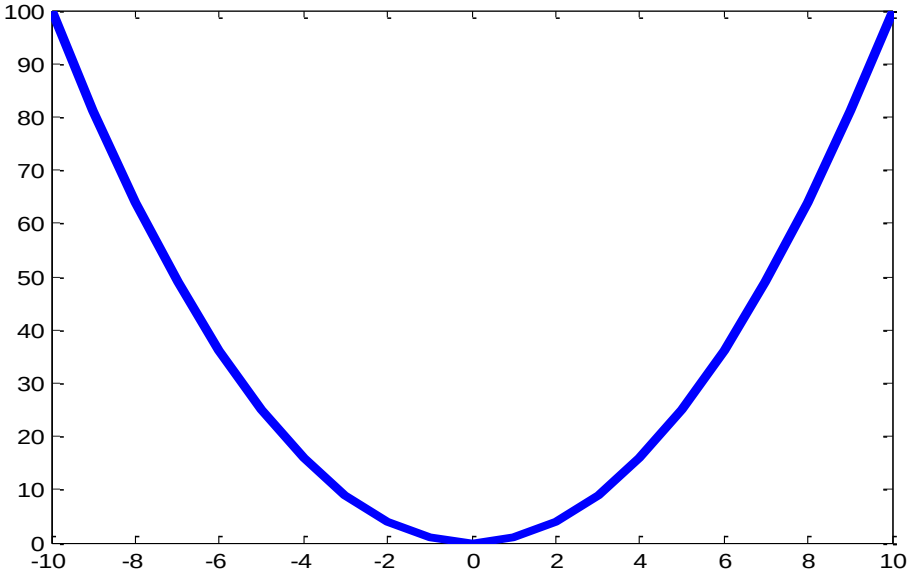

Figure 5. 4: a) Saddle point b) Local maximum c) Local minimum.

It is assumed that the function F (also known as the cost function) is smooth such that the following Taylor expansion applies

$$\mathrm{F_{op}}(x + \boldsymbol{h_{op}}) = \mathrm{F_{op}}(\mathrm{x}) + \mathbf{h_{op}}^{\mathrm{T}}\mathbf{g} + \frac{1}{2}\mathbf{h_{op}}^{\mathrm{T}}\mathbf{H}\mathbf{h} + \mathrm{O}\left\|\mathbf{h_{op}}\right\|^{3} \quad (3)$$

Here $\mathbf{h_{op}}$, is known as the $\mathbf{h_{op}}$ is a descent direction as will be explained later.

Where **g** is the gradient and it is given by

$$\mathbf{g} = \mathbf{F_{op}}'(\mathrm{x}) \quad (4)$$

$\mathbf{H_{op}}$ is the Hessian and it is given by

$$\mathbf{H_{op}}=\mathbf{F}''_{\mathrm{op}}(\mathrm{x}) \quad (5)$$

There are two known conditions to make sure the computed value is the local minimum, the first is that the gradient is equal to zero, this insures that the value of x is a stationary point and the second condition is that the Hessian is a positive definite value this insures that this point is a local minima.

It is worth noting that the matrices could be categorized as follows:

- A matrix M is positive Definite if the determinants of all of its principal submatrices are all positive. Another test for positive definiteness is that the eigen values of M are all positive real numbers.
- Negative Definite , is the case if the determinants of all the matrix principal submatrices are nonzero and alternate in sign with the first being negative. Another test for negative definiteness is that the eigen values of M are all negative real numbers.
- If we happen to have a few zero determinants (which will imply a zero eigen value) then M is: Positive Semi-definite, the same applies if the determinants of all of its principal sub matrices are all non-negative, or if all of its eigenvalues are non-negative real numbers. Note that any positive definite matrix also satisfies the definition of positive semi-definite.
- Negative Semi-definite if the determinants of all of its principal submatrices alternate in sign, starting with a negative (with the allowance here of 0 determinants replacing one or more of the positive or negative values). A better test is to check if all of its eigenvalues are non-positive real numbers. Note that any negative definite matrix also satisfies the definition of negative semi-definite.

There are different methods that could be used to solve the local minimiser least square problem. Most of these methods are iterative, from a starting point x_0, producing a series of vectors x_1,x_2 till they converge at a certain local minimum value x*. The method covered in this section is called the descent method which depends on ensuring that each given iteration function value is less than the value of the function value before it. This is normally done through an algorithm. The objective of the algorithm is to find the minimum value of a certain function. Starting with the first iteration at $x= x_0$ and with number of iteration k= 0, two steps are performed[2]:

a) Finding a decreasing (descent) direction ($\mathbf{h}_{dop}$)
b) Finding the step length (α_{op})

After finding them, the new iterated value of x is calculated and the process is repeated until convergence. The details of the algorithm [2] are as follows:

Algorithm 5.1

Begin

Start with k=0 and $x= x_o$ and found = False

While (found = false) and ($k< k_{max}$)

Calculate the search direction ($\mathbf{h_{op}}$)

If the search direction does not exist then

Found = True

Else

Calculate

Step length α_{op}

Update $x = x+ \alpha_{op}\mathbf{h_{op}}$

In the next section, these two major steps are covered, for two different descent methods; namely; steepest descent and Newton method, after that another method that use these steps simultaneously will be covered, the method is known as the trust region. After that, specialised nonlinear method known as Levenberg-Marquardt method will be covered.

5.3 Finding a decreasing (descent) direction (h_d)

The decreasing direction is governed by Taylor expansion (equation 3). It can be seen that the following condition needs to be satisfied for a value of h_d to exit:

$$\mathbf{h}_{\mathrm{dop}}{}^{\mathrm{T}}\mathbf{F}_{\mathrm{op}}{}'(\mathrm{x}) < 0 \tag{6}$$

There are two main methods that calculate the value of $\mathbf{h}_d$ namely the steepest descent method and Newton method.

5.3.1 Steepest descent method

In the steepest descent method, taking the limit to the difference between the value of the current value of f(x) and a future value gives the following equation

$$\lim_{\alpha\to\infty 0}\frac{\mathrm{F_{op}(x)}-\mathrm{F_{op}(x}+\alpha\mathbf{h_{op}})}{\alpha_{\mathrm{op}}\mathbf{h_{op}}}=-\frac{1}{\mathbf{h_{op}}}\mathbf{h_{op}}{}^{\mathrm{T}}\mathbf{F}_{\mathrm{op}}{}'(\mathrm{X})\cos\phi=-\left\|\mathbf{F}_{\mathrm{op}}{}'(\mathrm{x})\right\|\cos\phi \tag{7}$$

This means that steepest descent would be 180^{O} between the steepest direction and the current gradient. This could be interpreted by the following set of equations

$$\mathbf{h}_{\mathrm{sdop}}=-\left\|\mathbf{F}'_{\mathrm{op}}(\mathrm{x})\right\| \tag{8}$$

$$\mathbf{F}'_{\mathrm{op}}(\mathrm{x})=\mathbf{c} \tag{9}$$

$$\mathbf{c}=\begin{bmatrix}\mathrm{c}_1\\ \vdots\\ \mathrm{c_n}\end{bmatrix} \tag{10}$$

$$\left\|\mathbf{F}'_{\mathrm{op}}(\mathrm{x})\right\|=\frac{1}{\sqrt{\mathrm{c}_1^2+\cdots\mathrm{c_n^2}}}\begin{bmatrix}\mathrm{c}_1\\ \vdots\\ \mathrm{c_n}\end{bmatrix} \tag{11}$$

After calculating the normalised gradient$\|\mathbf{F}'(\mathrm{x})\|$, its value in the following equation

$$\mathrm{x_{new}}=\mathrm{x_{old}}-\alpha\left\|\mathbf{F}'_{\mathrm{op}}(\mathrm{x})\right\| \tag{12}$$

After that f'(α)=0 is imposed to calculate the value of α and the process is repeated till convergence, where the Stopping criteria is given by equation 13.

$$\alpha_{\mathrm{op}}\left\|\mathbf{F}_{\mathrm{op}}{}'(\mathrm{x})\right\|<\varepsilon \tag{13}$$

Where the value of ε is arbitrary.

5.3.2 Newton method

Newton method uses the Taylor expansion for the first derivative as given below. Thus the basic idea, that if x* is a stationary idea, this would imply that the first derivative of the function at this value would be zero. From Taylor expansion:

$$\mathrm{F}(\mathrm{x}*) = \mathbf{F}_{\mathrm{op}}{}'\left(\mathrm{x} + \mathbf{h}_{\mathbf{op}}\right) = \mathbf{F}_{\mathrm{op}}{}'(\mathrm{x}) + \mathbf{F}_{\mathrm{op}}{}''(\mathrm{x})\mathbf{h}_{\mathbf{op}} + \mathbf{O}\left\|\mathbf{h}_{\mathbf{op}}\right\|$$

But

$$\mathrm{F}(\mathrm{x}*) = 0$$

And If $\mathbf{h}_{\mathbf{op}}$is sufficiently small then,

$$\mathbf{F}_{\mathrm{op}}{}'\left(\mathrm{x} + \mathbf{h}_{\mathbf{op}}\right) = \mathbf{F}_{\mathrm{op}}{}'(\mathrm{x}) + \mathbf{F}_{\mathrm{op}}{}''(\mathrm{x})\mathbf{h}_{\mathbf{op}} \tag{14}$$

Then it could be possible to calculate $\mathbf{h}_{\mathrm{nop}}$ according to the following equation:

$$\mathbf{H}_{\mathbf{op}}\mathbf{h}_{\mathrm{nop}} = -\mathbf{F}_{\mathrm{op}}{}'(\mathrm{x}) \tag{15}$$

$$\mathbf{h}_{\mathrm{nop}} = -\mathbf{H}_{\mathbf{op}}{}^{-1}\mathbf{F}_{\mathrm{op}}{}'(\mathrm{x}) \tag{16}$$

$$\mathrm{x}_{\mathrm{new}} = \mathrm{x}_{\mathrm{old}} + \mathbf{h}_{\mathrm{nop}} \tag{17}$$

$$\mathrm{x}_{\mathrm{new}} = \mathrm{x}_{\mathrm{old}} - \mathbf{H}_{\mathbf{op}}{}^{-1}\mathbf{F}_{\mathrm{op}}{}'(\mathrm{x}) \tag{18}$$

If x is in a position inside the region around x* where $\mathbf{F}_{\mathrm{op}}{}''(\mathrm{x})$ is positive definite, then we get quadratic convergence. On the other hand, if x is in a region where $\mathbf{F}_{\mathrm{op}}{}''(\mathrm{x})$ is negative definite everywhere, and where there is a stationary point, the Newton method would converge towards this stationary point. This is avoided by requiring that all steps are in the descent direction.

To decide the step size, steepest descent and Newton method use line search techniques. The line search is basically a one-dimensional minimisation problem (minimize a function of one variable). The value of α is calculated by setting $f_{op}'(\alpha)=0$.

5.4 Trust region and damped methods

Equation 20 can be derived from Taylor expansion to be

$$F_{op}(\mathrm{x}+\mathbf{h_{op}}) \simeq \mathrm{L_{op}}(\mathbf{h_{op}}) = \mathrm{F_{op}}(\mathrm{x}) + \mathbf{h_{op}}^{\mathrm{T}}\mathbf{c} + \frac{1}{2}\mathbf{h_{op}}^{\mathrm{T}}\mathbf{B_{op}}\mathbf{h_{op}} \tag{20}$$

It is worth noting that this model is only true, if the value of **h** is sufficiently small[2]. The main idea behind the trust region is the assumption that the model estimation is sufficiently accurate inside a sphere of radius Δ. Now **h** is determined according to the following equation

For the trust region method

$$\mathbf{h_{op}} = \mathbf{h}_{\mathrm{trop}} = \mathrm{argmin}_{\|\mathrm{h}\|\leq\Delta}[\mathrm{L_{op}}(\mathbf{h_{op}})] \tag{21}$$

And for the damped method

$$\mathbf{h_{op}} = \mathbf{h}_{\mathrm{dmop}} = \mathrm{argmin}[\mathrm{L_{op}}(\mathbf{h_{op}}) + \frac{1}{2}]\mu\mathbf{h_{op}}^{\mathrm{T}}\mathbf{h_{op}} \tag{22}$$

where the damping parameter μ≥0. The term $\frac{1}{2}\mu\mathbf{h}^{\mathrm{T}}\mathbf{h}$ is used to penalise large steps. Returning to [2] algorithm 5.1, the update for both methods would be as shown in algorithm 5.2,adopted from [2].

Algorithm 5.2

If $\mathrm{F_{op}}(\mathrm{x}+\mathbf{h_{op}}) < \mathrm{F_{op}}(\mathrm{x})$

$\mathrm{x_{new}}=\mathrm{x_{old}} + \mathbf{h_{op}}$

Update Δ for trust region or μ for damped method

The quality of the model with the computed step is evaluated with the gain ratio equation:

$$\rho = \frac{F_{op}(x) - F_{op}(x+\boldsymbol{h_{op}})}{L(0) - L(\mathbf{h})} \tag{23}$$

This represents the ratio between the actual and predicted decrease in function value. The denominator (lower part) is positive, thus the numerator (upper part) would be negative, if the step was not downhill, and the solution in that case would to reduce to the value of h. Now, the

trust region differs again from the damping method in the update technique used by each, the trust method uses the following technique [2]:

Algorithm 5.2 continued

If ρ<0.25

$$\Delta_{new} = \frac{\Delta_{old}}{2}$$

Else if ρ >0.75

$$\Delta_{new} = \max[3 * \mathrm{h_{op}}, \Delta_{old}]$$

Thus, if ρ < 0.25, a smaller step is used by the contracting the field the optimiser is working on. On the other hand, if ρ > 0.75, then it might be possible to expand the field the optimiser is working on. A trust region algorithm is not sensitive to minor changes in the thresholds 0.25 and 0.75.

In a damped method a small value of ρ indicates that the damping factor should be increased, but in that case the penalty on large steps given by $\frac{1}{2}\mu h^T h$ also increases. A large value of ρ indicates that L (h) is a good approximation to F (x+h) for the computed h, and the damping may be reduced[2]. The update technique [2] is shown in algorithm 5.3.

Algorithm 5.3

If ρ<0.25

$$\mu_{new} = \frac{\mu_{old}}{2}$$

Else if ρ >0.75

$$\mu_{new} = \frac{\mu_{old}}{3}$$

Again, the method is not sensitive to minor changes in the thresholds 0.25 and 0.75. One of the draw backs of the above two techniques is that they can give rise to a flutter. This slows down convergence as shown in the figure 5.5.

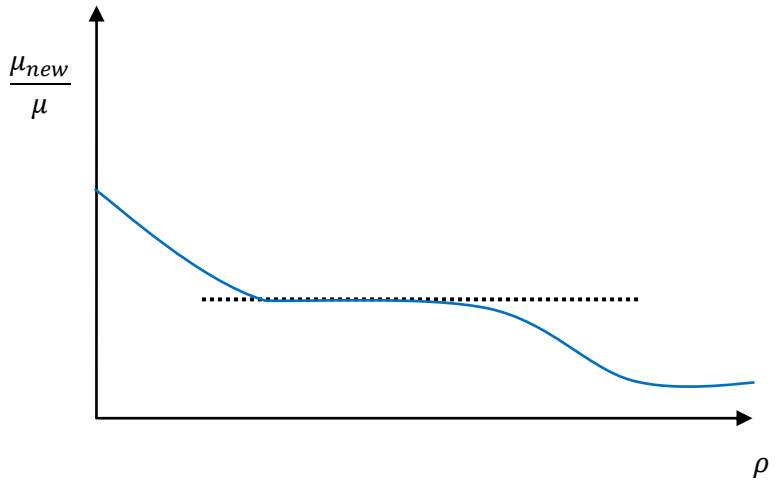

Figure 5.5: The optimiser is stuck with the flutter part of the curve; this slows up conversion to the local minimiser point [2].

This is also could be solved by using the Marquardt update given in [2] algorithm 5.4.

Algorithm 5.4

If ρ>0

$\mu_{new} = \mu_{old} * max[\frac{1}{3}, 1-(2\rho-1)^3]$ and $\nu = 2$

Else

$\mu_{new} = \mu_{old} * \nu$

$\nu = 2 * \nu$

Computation of the step

In a damped method the step is computed as a stationary point for the function

$$\psi(\mathbf{h_{op}}) = \mathrm{L}(\mathbf{h_{op}}) + \mu \mathbf{h_{op}}^{\mathrm{T}} \mathbf{h_{op}} \tag{24}$$

This means that $\mathbf{h}_{\mathrm{dmop}}$ is a solution to

$$\psi(\mathbf{h_{op}}) = \mathbf{L}'(\mathbf{h_{op}}) + \mu \mathbf{h_{op}} = 0 \tag{25}$$

from the definition of L($\mathbf{h_{op}}$) in (20)

$$(\mathbf{B_{op}} + \mu \mathbf{I})\mathbf{h}_{\mathrm{dmop}} = -\mathrm{c} \tag{26}$$

where **I** is the identity matrix. , the symmetric matrix $\mathbf{B_{op}}+\mu\mathbf{I}$ represent the Hessian, thus the symmetric matrix B+μI is positive definite , ad If μ is sufficiently large, and then h_{dm} is a minimiser for L.

5.5 Non-linear least square problems

There are other methods that could be used to solve nonlinear least square problems; in the following section two of these methods will be discussed, namely: Newton-Raphson, and Levenberg- Marquardt. The main aim of these methods is to find the value of x that minimises the least square function of the difference between the experimental values and the model one. In that sense, F(x) could be defined by equation27.

$$\mathrm{F_{op}}(\mathrm{x}) = \frac{1}{2}\sum_{1}^{\mathrm{m}} \mathrm{f_{op}}(\mathrm{x})^2 = \frac{1}{2}\mathbf{f}_{\mathrm{op}}(\mathrm{x})^{\mathrm{T}}\mathbf{f}_{\mathrm{op}}(\mathrm{x}) \tag{27}$$

Advantages of the above equation include that they achieve quadratic convergence without the need to implement the second derivatives. Using the Taylor expansion in equation 28, the gradient and the second derivative could be calculated as shown in equations 29 to 31.

$$\mathrm{f_{op}}(x + \boldsymbol{h_{op}}) = \mathrm{f_{op}}(\mathrm{x}) + \mathbf{J}(\mathrm{x})\boldsymbol{h_{op}} + \mathrm{o}\left\|\boldsymbol{h_{op}}^{\mathbf{2}}\right\| \tag{28}$$

J is the Jacobian given by equation 29.

$$(\mathbf{J}(x))_{ij}=\frac{\partial f_i op}{\partial x_j}(x) \tag{29}$$

It follows from the first formulation in (27)

$$\frac{\partial F_{op}}{\partial x_J}(x)=\sum_{i=1}^{m} f_{iop}(x)\frac{\partial f_{iop}}{\partial x_j}(x) \tag{30}$$

Thus, the gradient can be given by equation 31.

$$\mathbf{F_{op}}'(x)=\mathbf{J}(x)^T\mathbf{f_{op}}(x) \tag{31}$$

The Hessian can be calculated from (30)

$$\frac{\partial^2 F_{op}}{\partial x_j x_k}(x)=\sum_{i=1}^{m}(\frac{\partial f_{iop}}{\partial x_j}(x)\frac{\partial f_{iop}}{\partial x_k}(x)+f_i(x)\frac{\partial^2 f_{iop}}{\partial x_j x_k}(x) \tag{32}$$

Showing that

$$\mathbf{F_{op}}''(x)=\mathbf{J}(x)^T\mathbf{J}(x)+\sum_{iop=1}^{m} f_{iop}(x)\mathbf{f''_{iop}}(x) \tag{33}$$

Having covered the basic principles for nonlinear least square problems, the next section will cover the following method, Newton Raphson, and Levenberg-Marquardt techniques.

5.5.1 Newton Raphson

From an initial guess x_0 we compute x_1, x_2 by the following algorithm, which is based on finding the solution of nonlinear systems of equations.

$$f_{op}(x^*)=0 \tag{34}$$

This algorithm is based on ensuring that

$$f_{op}(x+h)=0 \tag{35}$$

Ignoring the term $O\|h_{op}{}^2\|$ in equation 28, gives equation 36.

$$\mathbf{J}(x)_k\mathbf{h}_{kop}=-f_{op}(x)_k \tag{36}$$

The new x is updated according to equation 37.

$$x_{k+1}=x_k+\mathbf{h}_{kop} \tag{37}$$

It can be noticed that the Newton-Raphson converges in few steps than descent methods. This method is the basis of a very efficient method we will describe in the next sections. It is based on implemented first derivatives of the components of the vector function.

5.5.2 The Levenberg–Marquardt Method

The Levenberg–Marquardt method is based on a linear approximation to the components of **F.** For small $\|\mathbf{h}_{\mathrm{lmop}}\|$we see from the Taylor expansion (28) that

$$\mathrm{f}(\mathbf{x}+\mathbf{h}_{\mathrm{lmop}}) = l(\mathbf{h}_{\mathrm{lmop}}) = \mathrm{f}(\mathrm{x}) + \mathbf{J}(\mathbf{x})\mathbf{h}_{\mathrm{lmop}} \tag{38}$$

And inserting in equation 27

$$\mathrm{F}(\mathbf{x}+\mathbf{h}_{\mathrm{lmop}}) = \mathrm{L}(\mathbf{h}_{\mathrm{lmop}}) = \frac{1}{2} l(\mathbf{h}_{\mathrm{lmop}}{}^{\mathrm{T}}) l(\mathbf{h}_{\mathrm{lmop}}) \tag{39}$$

$$\frac{1}{2} l(\mathbf{h}_{\mathrm{lmop}}{}^{\mathrm{T}}) l(\mathbf{h}_{\mathrm{lmop}}) = \frac{1}{2}\mathrm{f_{op}}{}^{\mathrm{T}}\mathrm{f_{op}} + \mathbf{h}_{\mathrm{lmop}}{}^{\mathrm{T}}\mathbf{J}^{\mathrm{T}}\mathbf{f} + \frac{1}{2}\mathbf{h}_{\mathrm{lmop}}{}^{\mathrm{T}}\mathbf{J}^{\mathrm{T}}\mathbf{J}\mathbf{h}_{\mathrm{lmop}} \tag{40}$$

$$\mathrm{L}'(\mathbf{h}_{\mathrm{lmop}}) = \mathbf{J}^{\mathrm{T}}\mathbf{f} + \mathbf{J}^{\mathrm{T}}\mathrm{J}\mathbf{h}_{\mathrm{lmop}} \tag{41}$$

Where **L**'(0)=**F**(x) (42)

In Levenberg -Marquardt, step h_{lm} is defined by the following equation:

$$(\mathbf{J}^{\mathbf{T}}\mathbf{J}+)\mathbf{h}_{\mathrm{lmop}} = -\mathrm{g_{lm}} \tag{43}$$

$$\mathrm{g_{lm}} = \mathrm{J}^{\mathrm{T}}\mathrm{f_{op}} \tag{44}$$

It could be proven that, for or all $\mu_{lm}>0$, where μ_{lm} is the damping parameter, h_{lm} is a descent direction. For large values of μ_{lm} we get

$$\mathrm{h_{lm}} = \frac{-1}{\mu_{\mathrm{lm}}}\mathrm{g_{lm}} = \frac{1}{\mu_{\mathrm{lm}}}\mathbf{F}'_{\mathrm{op}}(\mathrm{x}) \tag{45}$$

ie a short step in the steepest descent direction. This is good if the current iterate is far from the solution. It could be seen that Levenberg-Marquardt damping parameter influences both the direction and the size of the step. This is te reason this particular method is used without a search line method for the steepest direction.

It is worth noting that during iteration, the size of μ_{lm} can be updated as shown before in the trust region method. The updating is controlled by the gain ratio ρ_{lm}.

$$\rho_{\mathrm{lm}} = \frac{\mathrm{F_{op}}(\mathrm{x}) - \mathrm{F_{op}}(\mathrm{x}+\mathbf{h}_{\mathrm{lmop}})}{\mathrm{L}(0) - \mathrm{L}(\mathbf{h}_{\mathrm{lmop}})} \tag{46}$$

The denominator is given by the following equation

$$L(0) - L(\mathbf{h}_{lmop}) = \frac{1}{2}\mathbf{h}_{lmop}^{T}(\mu\mathbf{h}_{lmop} - g_{lm}) \quad (47)$$

For example, a large value of ρ_{lm} indicates that $L(h_{lm})$ is a good approximation to $F(x+h_{lmop})$. On the other hand ,If ρ_{lm} is small then $L(h_{lmop})$ is a poor approximation [2]. In that case an increase μ_{lm} is required to get closer to the steepest descent direction and to reduce the step length.

The stopping criteria for the algorithm should reflect that at a global minimiser we have

$$\mathbf{F_{op}}'(x^*)=g(x^*)=0$$

$$\|g\| < \varepsilon_1$$

where ε_1 is a small, positive number, chosen by the user. Another relevant criterion is to stop if the change in x is small.

In the last section, non linear least square problems were covered. Newton Raphson and Levenberg-Marquardt method were discussed. In the next section, the concept of sensitivity analysis will be covered. Different methods that measure, rank or produce intervals of parameters will also be discussed.

5.6 Sensitivity analysis

Any model has a set of variables called state variables. And if this particular model is deterministic then, these variable states could be determined by model parameters and previous states of these state variables

In that case a set of input parameters are applied in a certain number of equations to give outputs (or response variables)[3]. This also means that on each time of applying the input parameters, the results will be the same. However, in other cases, the problem would not be as simple as there might be some parameters values that could not be told with high accuracy, thus no unique values, as in the case of having complex, nonlinear equations. There is a highly developing mathematical branch which is concerned with finding this kind of techniques that ensure having a satisfying solution. These techniques will be addressed in the next section.

Sensitivity analysis is a broad concept that has been used across various disciplines. It can be used to identify a risk assessment of a certain procedure (model). Here risk assessment is defined in a general sense to mean the probability of a certain output of an equation. From a broad point of view, risk assessment can be used to determine which parameters are essential to control, to reduce, or to eliminate from the original model. Therefore, risk assessment can help in developing more effective control plans [3].

The objective of the sensitivity analysis is to answer the following question [3]:

- What happened?
- How did it happen?

Risk assessment of a certain process or a model based could be briefed in the following four steps:

Firstly, Parameter Identification: if we apply that to the proposed model, then this will mean identifying the parameters that control the stress strain relationship for the whole wall and as well as the layers relationship. Secondly; Parameter Characterization and this could be defined as the evaluation of the nature of the effects caused by changing these identified parameters. Thirdly; Exposure Assessment and It is the evaluation of the likely existence of such biological parameter and lastly, Risk Characterization and this involves estimation, of the probability of occurrence and severity of a certain output.

Sensitivity analysis methods can be classified as:

(1) mathematical sensitivity analysis methods

They assess sensitivity of a model output to the range of variation of an input. These methods typically involve calculating the output for a few values of an input that represent the possible range of the input. These methods also can be used for verification and validation.

(2) statistical methods

They are done through running simulations in which inputs are assigned probability distributions and assessing the effect of variance in inputs on the output distribution where one or more inputs are varied at a time. Statistical methods identify the effect of interactions among multiple inputs. The range and relative likelihood of inputs can be propagated using a number of methods such as Monte Carlo simulation, Latin hypercube sampling, variance, response surface methods, Fourier amplitude sensitivity test, and mutual information index.

(3) Graphical methods

It is concerned with representation of sensitivity in the form of graphs, charts, or surfaces. Generally, graphical methods are used to give visual indication of how an output is affected by variation in inputs. Graphical methods can be used as a screening method before further analysis of a model or to represent complex.

In the following section different mathematical and statistical methods will be discussed.

5.6.1 Nominal Range Sensitivity

This method is applicable to deterministic models. One use of nominal sensitivity analysis is as a screening analysis to identify the most important inputs to propagate through a model in a

probabilistic framework. It is carried out through evaluating the effect on model outputs by varying only one of the model inputs across its entire range of plausible values, while holding all other inputs at their nominal or base-case values [4].

The difference in the model output due to the change in the input variable is referred to as the sensitivity or swing weight of the model to that particular input variable.

In such cases, it would be possible to rank order the relative importance of each input based upon the magnitude of the calculated sensitivity measure as long as the ranges assigned to each sensitive input are accurate. However Nominal sensitivity analysis addresses only a potentially small portion of the possible space of input values, because interactions among inputs are difficult to capture. Conditional sensitivity analysis may be used to account for correlation between inputs or nonlinear interactions in model response, but it has limitations because of the combinational explosion of possible cases. Potentially important combined effects on the output due to small changes in a few or all inputs together are not shown by nominal sensitivity analysis.

5.6.2 Difference in Log-Odds Ratio (DLOR)

This is a specific application of nominal range sensitivity methodology. The DLOR is used when the output is a probability[5]. It is used to examine the change in the output as:

$$\Delta LOR = \log\left[\frac{\Pr(event \mid with\ changes\ in\ input)}{\Pr(No\ event \mid with\ changes\ in\ input)}\right] - \log\left[\frac{\Pr(event \mid without\ changes)}{\Pr(No\ event \mid without\ changes)}\right]$$

If D*LOR* is positive, changes in one or more inputs enhance the probability of the specified event. If D*LOR* is negative, then the changes in the inputs cause a reduction in the probability of the event occurring or increase the probability of the event not occurring. The greater the magnitude of D*LOR*, the greater is the influence of the input. However it has the drawbacks of the nominal range sensitivity.

5.6.3 Break-Even Analysis

Its purpose of break-even analysis is to evaluate the robustness of a decision to changes in inputs. It involves finding values of inputs that provide a model output for which a decision maker would be indifferent among the two or more risk management options. The combinations of values of inputs for which a decision maker is indifferent to the decision options are known as switchover or break-even values[6]. Then, in order to assess the robustness of a choice between the options, one can evaluate whether the possible range of values of the model inputs corresponds with only

one of the two choices. Indifference of a decision maker to the two choices is often represented by a break-even line or indifference curve such as an iso-risk curve. Ambiguity regarding selecting a particular choice exists if the uncertainty range associated with an output may correspond to either of the two or more possible choices. Different options that result in equivalent levels of risk reduction also can be identified so that a decision maker can evaluate these options. If there are more than two decision options, the analysis can get complex. (Edwards 1986). This method could be used to guide further modelling and elicitation. If the range of uncertainty regarding an input encloses the break-even point, then that input will be important in making a decision; that is, there will be uncertainty regarding which decision to take. In such a situation, further research can be directed so as to help the decision maker to narrow the range of uncertainty and make a decision with more confidence. On the other hand, if the uncertainty regarding an input does not enclose the break-even point then there will be high confidence regarding the decision. However one of the drawback of this method, that There also is not a clear ranking method to distinguish the relative importance of the sensitive inputs.

5.6.4 Automatic Differentiation Technique

This is an automated procedure for calculating local sensitivities for large models. In AD, a computer code automatically evaluates first-order partial derivatives of outputs with respect to small changes in the input[7]. The values of partial derivatives are a measure of local sensitivity. In AD the local sensitivity is calculated at one or more points in the parameter space of the model. At each point, the partial derivatives of the model output with respect to a selected number of inputs are evaluated. However, for nonlinear models, the significance of differences in sensitivity between inputs is difficult to determine, making the rank ordering of key inputs potentially difficult. This method cannot be used if partial derivatives cannot be evaluated locally.

5.6.5 Monte Carlo simulation

Monte Carlo simulation is categorised as a sampling method because the inputs are randomly generated from probability distributions to simulate the process of sampling from an actual population[8]. So, we try to choose a distribution for the inputs that most closely matches data we already have, or best represents our current state of knowledge. The data generated from the simulation can be represented as probability distributions (or histograms) or converted to error bars, reliability predictions, tolerance zones, and confidence intervals.

5.6.6 Latin hypercube sampling

This is a development of Monte Carlo method. The reasoning behind it is to ensure that all portions of the parameter space were sampled [9].

This is done by dividing the range of each parameter x_k into n strata of equal marginal probability 1/n, and sample once from each stratum. let this sample be x_{kj} where j = 1, ..., n. These form the x_k component, k = 1,...k, in x_i, i = 1,..., n. the components of the various x_k are matched at random.

One advantage of the Latin hypercube sample appears when the output y(t) is dominated by only a few of the components of x. this method ensures that each of those components is represented in a fully stratified manner, no matter which components might turn out to be important. It is worth mentioning here that the n intervals on the range of each component of x combine to form nk cells which cover the sample space of x. these cells, which are labelled by coordinates corresponding to the inter values, are used when finding the properties of the sampling plan.

5.6.7 Mutual Information Index

The objective of the Mutual Information Index (MII) sensitivity analysis method is to produce a measure of the information about the output that is provided by a particular input. The magnitude of the measure can be compared for different inputs to determine which inputs provide useful information about the output. MII is a computationally intensive method that takes into account the joint effects of variation in all inputs with respect to the output.

The MII method typically involves three general steps:

- generating an overall confidence measure of the output value;
- obtaining a conditional confidence measure for a given value of an input;
- calculating sensitivity indices

The overall confidence in the output is estimated from the CDF of the output. Confidence is the probability for the outcome of interest. For example, if the dichotomous output is whether risk is acceptable, the confidence is the probability that the risk is less than or equal to an acceptable level. Conditional confidence is estimated by holding an input constant at some value and varying all other inputs. The resulting CDF of the output indicates the confidence in the output conditioned on a particular value of the input. The mutual information between two random variables is the amount of information about a variable that is provided by the other variable. The MII for each input is calculated based on the distribution of the input and on both the overall and conditional confidence in the output. The average mutual information index for an input is given by:

$$I^{a}XY = \sum x \sum y P_X \, P_{Y|X} \log_n(P_{Y|X}/P_Y)$$

Where

$P_{Y|X}$ = Conditional confidence

P_Y = Overall confidence

P_X =Probability distribution for the input

n=2, to indicate binary output

The amount of information about a variable that is provided by the variable itself is measured in terms of the "average self information" (IYY) of that variable, also known as the entropy of that variable [10]. The calculation of MII may requires simplifying approximations regarding the use of a limited number of input values to represent the variation in an input and estimation of probabilities of the input values.

No analytical statistical measure is available to determine the significance of the sensitivity indices. However the robustness of rank ordering of key inputs can be difficult to evaluate. MII includes the joint effects of all the inputs when evaluating sensitivities of an input. The mutual information is a more direct measure of the probabilistic relatedness of two random variables than other measures such as correlation coefficients. For example, the correlation coefficient of two random variables examines the degree of linear relatedness of the variables. Although two uncorrelated variables may not be independent, two variables with zero mutual information are statistically independent. Therefore, the MII is a more informative method. Calculation of the MII by Monte Carlo techniques suffers from computational complexity, making practical application difficult.

5.6.8 Response Surface Method (RSM)

The Response Surface Method (RSM) can be used to represent the relation between a response variable (output) and one or more explanatory inputs[10]. The RSM is generally complex and therefore, used in later stages of an investigation when a limited number of factors are under investigation after using model reduction techniques.

The model must be exercised for various desired combinations of the selected input values in order to generate a data set that can be used to fit or calibrate a response surface. Monte Carlo

simulation methods are typically used to generate multiple values of each model input and to calculate corresponding values of the model output.

To develop a response surface, the sensitivity of the model output to one or more of the selected inputs can be determined by:

- inspection of the functional form of the response surface
- statistical analysis
- Application of other sensitivity analysis methods to the response surface.

The response surface can be thought of as a "model of a model" with the advantage of being simpler and faster to execute than the original model. Therefore computationally intensive sensitivity analysis methods, such as Mutual Information Index or others may be more readily applicable to the response surface than to the original model.

5.6.9 Fourier Amplitude Sensitivity Test

The FAST method is used to estimate the expected value and variance of the output, and the contribution of individual inputs to the variance of the output. The FAST method is independent of any assumptions about the model structure. It allows the study of the impact of more than one parameter [11].

The main feature of the FAST method is a pattern search method that selects points in the input parameter space. A transformation function is used to convert values of each model input to values along a search curve. As part of the transformation, a frequency must be specified for each input. By using Fourier coefficients, the variance of the output is evaluated. The contribution of parameter to the total variance is calculated based on the Fourier coefficients, fundamental frequency and higher harmonics of the frequency. The ratio of the contribution of each input to the output variance and the total variance of the output is referred to as the first order sensitivity index and can be used to rank the inputs. The first order indices correspond to the contribution of individual inputs.

The model needs to be evaluated at sufficient number of points in the input parameter space such that numerical integration can be used to determine the Fourier coefficients. The minimum sample size required to implement FAST is approximately eight to ten times the maximum frequency used. In the case of discrete inputs, if a sufficiently large sample size is not available, then the output can have frequent discontinuities. In such a case, the Fourier coefficients may not be estimated properly and hence, the reliability of the results can be adversely affected. Sobol's method is capable of handling discrete inputs. The FAST method suffers from computational complexity for a large number of inputs. In past section the concept of parameter sensitivity was

introduced, its main steps, were discussed. After that, 3 main types of sensitivity analysis were shown and finally, different relevant methods were summarised. The next section will cover the application of two of the above methods through the model parameter sensitivity process.

5.6.10 Application to the model

As discussed in the previous section, the solution here would be to use probability distribution to try and define such parameters. Thus the need for a certain scientific branch emerges. It is called sensitivity analysis and it has the following functions[12]. First to determine the importance of each parameter, so which parameter is more effective than the others? Also if one parameter value is changed how would it affect the result?

The process of sensitivity analysis for the proposed model in chapter 4 , was done in the following manner[12]:

(a) The models, its variables (dependent, independent) are defined.
(b) Each input parameter is assigned a probability density function.
(c) process called propagation of error :An input matrix is generated through a random sampling method
(d) The output is calculated
(e) The influence of each parameter is investigated

Using the process known as Propagation of error (uncertainty) is helpful in studying the effect of uncertainty on variables. In this research a well known sampling method is used. This sampling method is called the Monte Carlo. Through this iterative method a deterministic model can be evaluated using sets of random numbers as inputs. A simulation can typically involve over 10,000 evaluations of the model. In this way by using random inputs, the deterministic model is converted to a stochastic one.

The data generated from the simulation can be represented as probability distributions (or histograms) or converted to error bars, reliability predictions, tolerance zones, and confidence intervals as shown in figure 5.6.

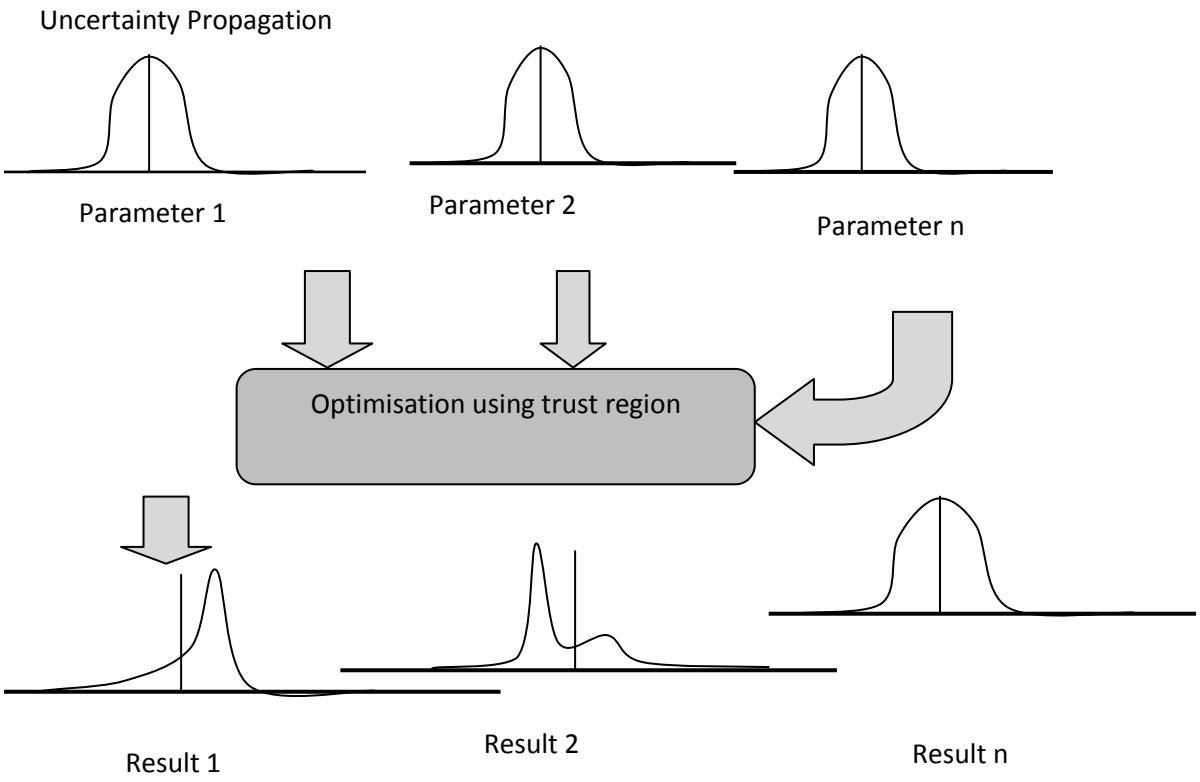

Figure 5.6**:** Schematic showing the principle of stochastic uncertainty propagation [3].

The steps in Monte Carlo simulation corresponding to the uncertainty propagation are listed below:

Step 1: Create a parametric model, $y_{model} = f(x_{1model}, x_{2model}, ..., x_{nmodel})$, in our case

Step 2: Generate a set of random inputs parameters, $x_{i1model}, x_{i2model}, ..., x_{imodelq}$.

Step 3: Evaluate the model and store the results as y_{imodel}

Step 4: Repeat steps 2 and 3 for i = 1 to n.

Step 5: Analyse the results using histograms, summary statistics, confidence intervals, etc.

Step 6: Use single sided sensitivity analysis to tell which parameter is more important than the other by changing one parameter at a time.

After getting the mean and the stranded deviation for each parameter of the proposed model, using Monte Carlo Simulation, Nominal range sensitivity method was used to assess the

importance of each of these parameters. The significance of each parameter was scaled by the margin of error it would result in if the average values for other parameters were used. Each time one parameter was used. The most important parameter resulted in the biggest error and vice versa.

5.7 Conclusion

This section has given the background theory to optimisation techniques from linear to non-linear problems. Finding a decreasing direction was covered. This included discussing steepest descent method and Newton method. After that trust region and damped method were also investigated. The second section of the chapter covered nonlinear square problems. Two methods were introduced, namely Newton-Raphson and Levenberg-Marquardt. In our model analysis we used trust region method, the next section covered different methods of parameter sensitivity analysis, Mont Carlo was used for propagation of uncertainty and parameter estimation while nominal range sensitivity method was used for parameter ranking.

5.8 References

1. van Andel CJ, Pistecky PV, and Borst C, *Mechanical Properties of Porcine and Human Arteries: Implications for Coronary Anastomotic Connectors.* Ann. Thorac. Surg.
, 2003Jul. **76**((1)): p. 58-64.
2. Madsen K, Nielsen HB, and Tingleff O, *Methods for Non-Linear Least Squares Problems*. 2 ed. 2004, Lyngby Informatics and Mathematical Modelling Technical University of Denmark.
3. Kaplan S and Garrick BJ, *On the Quantitative Definition of Risk.* Risk Analysis, 1981. **1**(1): p. 11-27.
4. Cullen AC and Frey HC, *Probabilistic Techniques in Exposure Assessment.* , ed. PlenumPress. 1999, New York.
5. Song FJ, Glenny AM, and Altman DG, *Indirect Comparison in Evaluating Relative Efficacy Illustrated by Antimicrobial Prophylaxis in Colorectal Surgery.* ControlledClinical Trials, 2000. **21**(5): p. 488-497.
6. Kottas JF and Lau HS, *Stochastic Break-Even Analysis.* Journal of the Operational Research Society, 1978. **29**(3): p. 251-257.
7. Hwang D, Byun DW, and Odman MT, *An Automatic Differentiation Technique Forsensitivity Analysis of Numerical Advection Schemes in Air Quality Models.* Atmospheric Environment,, 1997. **31**(6): p. 879-888.
8. McKay MD, Beckman RJ, and Conover WJ, *A Comparison of Three Methods for Selecting Values of Input Variables in the Analysis of Output from a Computer Code.* Technometrics, 1979. **21**(2): p. 239-245.
9. Critchfield GC and Willard KE, *Probabilistic Analysis of Decision Trees Using Mote Carlo Simulation.* Medical Decision Making, 1986. **6**(1): p. 85-92.
10. Myers RH and Montgomery DC, *Response Surface Methodology: Process Andproduct Optimization Using Designed Experiments*. 1995, New York: Wiley and Sons Ltd.
11. Cukier RI , Fortuin CM, Shuler KE, Petschek AG, and Schailby JH, *Study of the Sensitivity of the Coupled Reaction Systems to Uncertainties in Rate Coefficients: I. Theory.* Journal of Chemical Physics,, 1973. **59**(8): p. 3873-3878.
12. HAMBY DM, *A Review of Techniques for Parameter Sensitivity Analysis of Environmental Models.* Environmental Monitoring and Assessment, 1994. **32**: p. 135-154.

CHAPTER 6

MODEL ANALYSIS

---

6 Overview

In chapter 4 the model used in this thesis to relate material parameters in arterial walls using both layer and whole wall data was presented. In chapter 5 methods to optimise the parameters and assess their sensitivity were discussed. This chapter presents the results from implementing these techniques. The model assumptions are then revisited with particular emphasis on the roles played by the elastin and collagen.

6.1 How the model was built up

The system was built in the following manner: step (1), the experimental data for the whole wall (pressure versus diameter and pressure versus axial force) was converted into stress using thin wall theory as shown in figure 6.1.

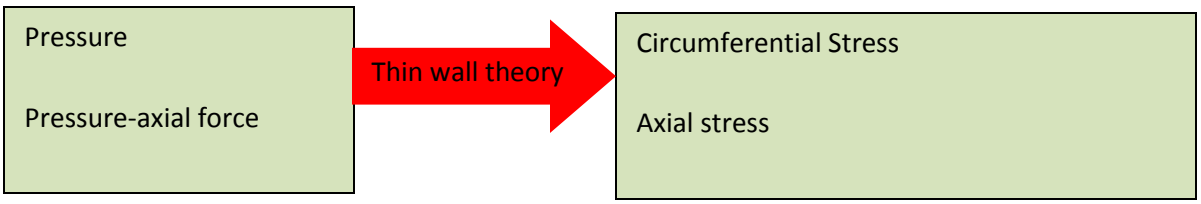

Figure 6.1: The experimental model was generated using thin wall theory.

The equations for step (1) are given by:

Assuming a deformed thickness, h, deformed radius, r, a luminal pressure, p, and an axial force, f_a, we have

$$\sigma_{t\theta} = p\left(\frac{r}{h} - \frac{1}{2}\right) \quad (1)$$

$$\sigma_{tz} = \frac{\sigma_\theta}{2} + \frac{f_a}{2\pi\, rh} \quad (2)$$

$\sigma_{t\theta}$ is the circumferential stress , $\sigma_{t\theta}$ is the axial stress.

Step (2): stretch was calculated using the formula

$$\lambda = \frac{r}{R} \quad (3)$$

r is the deformed radius to half the arterial segment , R is the original the radius of the arterial segment to half its thickness . λ is the ratio of the new radius to the old radius. This is shown in figure 6.2 and figure 6.3.

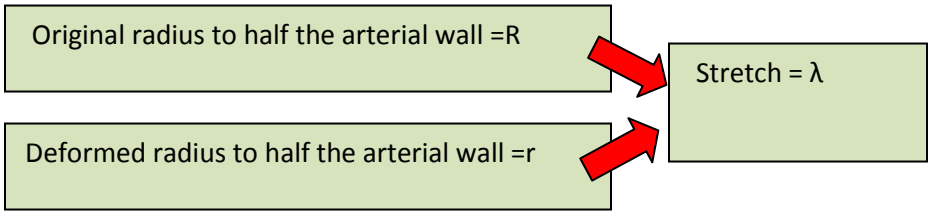

Figure 6.2: Stretch is calculated from radius ratio.

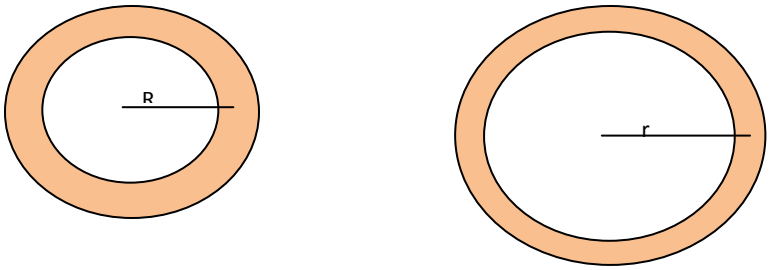

Figure 6.3: Stretch is the ratio of change in radius after and before deformation.

An important model assumption was made, regarding layer thickness, in the work by Hozapfel et al [1]. The thicknesses for the three layers were given by: 27±0.02, 0.36±0.03 and 0.40±0.03, but it could be noticed that these values when added exceeds unity as each thickness was measured separately after separating the three layers. It is also worth noting that the thickness of the artery increases after being taken out of the body. Thus the value of unity was assumed and the values of the intact thickness were calculated according to the above ratio to be for nominal layer thicknesses of 26.2%, 34.9% and 38.8% for the intima, media and adventitia respectively. Another important assumption, is that all layers will be compressed by the same ratio as no data is available on layer thickness after deformation

Step (3): The actual model was calculated in the following manner. Stretch calculated from step (2), was applied into different layer equations to get circumferential stress, axial stress for each layer, as shown in figure 6.4.

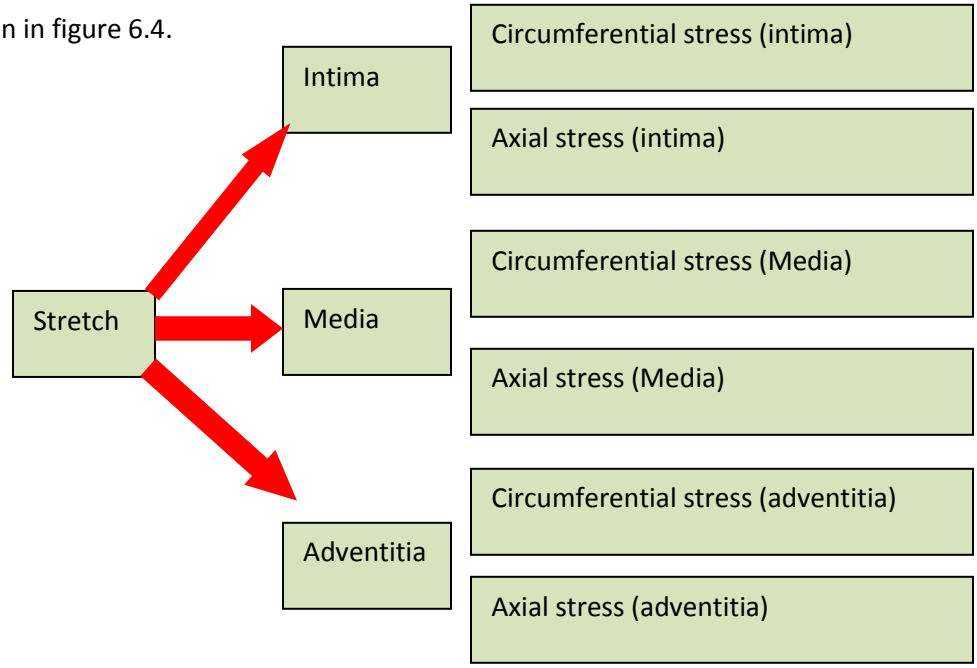

Figure 6.4: Layers circumferential and axial stresses are calculated.

Layers equations are represented by equation 4 and equation 5, to describe each of the three arterial layers, *I* to calculate the Cauchy stress components, $\sigma_{\vartheta I}$ and σ_{zI}, in the circumferential and axial directions respectively. Thus for the intima (*I* = n)

$$\sigma_{\theta n} = [c_{1n}\left(1 - \frac{1}{\lambda_\theta^4 \lambda_z^2}\right) + k_{1n} e^{qn}(\left(1 - \rho_{dispn}\right)(I_{1n} - 3)\left(1 - \frac{1}{\lambda_\theta^2}\right)\rho_{dispn}(I_{4n} - 1)\cos(\phi_n)^2)]\,\lambda_\theta^2 \quad (4)$$

$$\sigma_{zn} = \qquad (5)$$
$$[c_{1n}\left(1-\frac{1}{\lambda_\theta^2\lambda_z^4}\right)+k_{1n}e^{qn}(\left(1-\rho_{dispn}\right)\ (I_{1n}-3)\left(1-\frac{1}{\lambda_z^2}\right)+\rho_{dispn}(I_{4n}-1)\sin(\phi_n)^2)]\lambda_z^2$$

Similar expressions can be obtained the media layer (*l*=m) and the adventitia (*l*=a). Equations are explained in detail in chapter 4, sections 4.6.4 and 4.6.5.

Step (4): The layers were combined using the thin wall theory, such that the total circumferential stress was calculated from circumferential stress of the intima, media and adventitia. This was repeated with the axial direction as shown in figure 6.5.

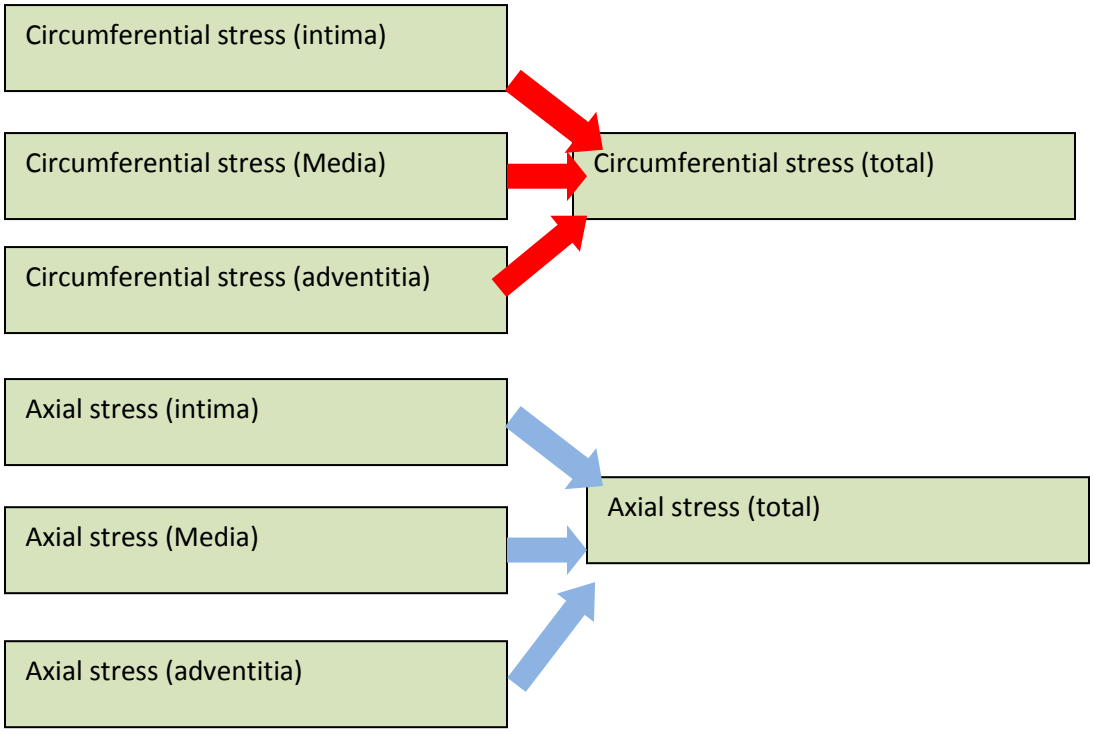

Figure 6.5: Total circumferential and axial stresses were calculated from layer stresses.

This was done through the use of stress equilibrium as described by equations 6 and 7.

$$\sigma_{t\theta} = \frac{(\sigma_{\theta n}h_n + \sigma_{\theta m}h_m + \sigma_{\theta a}h_a)}{h} \qquad (6)$$

$$\sigma_{tz} = \frac{(\sigma_{zn}h_n + \sigma_{zm}h_m + \sigma_{za}h_a)}{h} \quad (7)$$

Step (5): Error equation defined in chapter 4, was used.

The error range was calculated according to the following equation

$$\varepsilon = \frac{\sqrt{\frac{x^2}{n-q}}}{\sigma_{ref}} \quad (8)$$

where *n* is the number of data points and *q* is the number of parameters of the strain-energy function, which in our case is five; The value σ_{ref} is the sum of all Cauchy stresses for each data point divided by the number of all data points. The value of x^2 is given by the following equation:

$$x^2 = \sum_{i=1}^{n} (\sigma_{\theta mod} - \sigma_{\theta exp})^2 + (\sigma_{zmod} - \sigma_{zexp})^2 \quad (9)$$

Where, $\sigma_{\theta mod}$ and σ_{zmod} are Cauchy stresses in the circumferential and axial directions respectively of the model and $\sigma_{\theta exp}$ and σ_{zexp} are those of the experimental technique.

And then the optimisation function was called using Matlab optimisation tool box. If the error value was less than 0.005 the values of the optimised parameters were accepted. The optimisation technique used is called trust region and it is shown in chapter 5. This operation was repeated 50,000 times. Mean and standard deviation were calculated. This is called Monte Carlo simulation process and it is explained in details in chapter 5.

Step (6) step 5 was repeated 10 using different starting points. Mean and standard deviation were calculated. In the last section different segments of the system of the models was presented. In the next section whole wall estimation will be discussed then layer stresses will be investigated, parameters estimation and sensitivity will also be presented. To summarise the previous section a flow chart of the process is presented in figure 6.6.

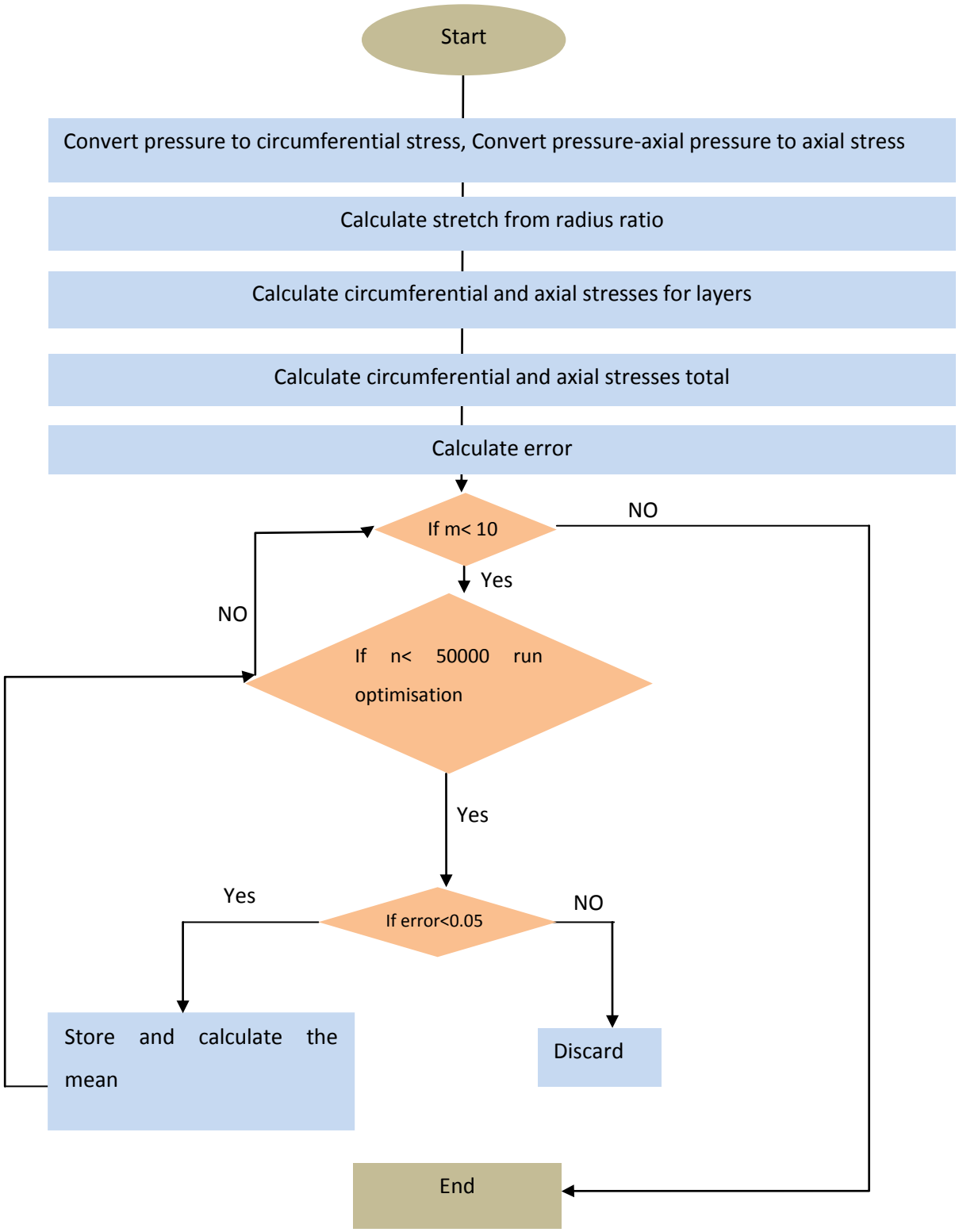

Figure 6.6: Flow chart of the modelling process, see text for description, where m is the number of new trials with new starting points and n is the number of trials within each run.

It is worth noting that to validate the code; it was divided into smaller units which were then tested for repeatability, accuracy and reliability. The whole code is presented in the appendix.

6.2 Whole wall estimations

Experimental data was imported from[2] as shown in section 5.1. Static pressure versus extension of diameter and axial force were used as a source to calculate stress–strain relationship for the whole wall (circumferential and axial). In that case, the whole wall was considered to be of one layer nature of single strain energy function.

Figure 6.7 shows a graph of the estimated axial and circumferential Cauchy stresses versus luminal pressure for the coronary artery data extracted from [2] as discussed in the previous section. The root mean square error (rms) values were found to be 0.060 and 0.096 respectively indicating a good fit in both cases. This results in a total rms error of 0.050, which compares favourably to the averaged layer rms error of 0.080 in [1].

It is also worth noting that the model results are consistent with the experimental data in that it estimates that the static axial stress response is higher than the circumferential static stress response. However, a possible method to decrease the error at low pressure is to take into consideration the assumption that at lower pressures only the elastin is under tension and stretches, whilst at higher pressures both the elastin and collagen are under tension and thus both fibre types stretch. Based on this it is suggested that improving the form of the elastin strain-energy function could increase the quality of the overall fit [3] . Further work would be needed to investigate this assumption.

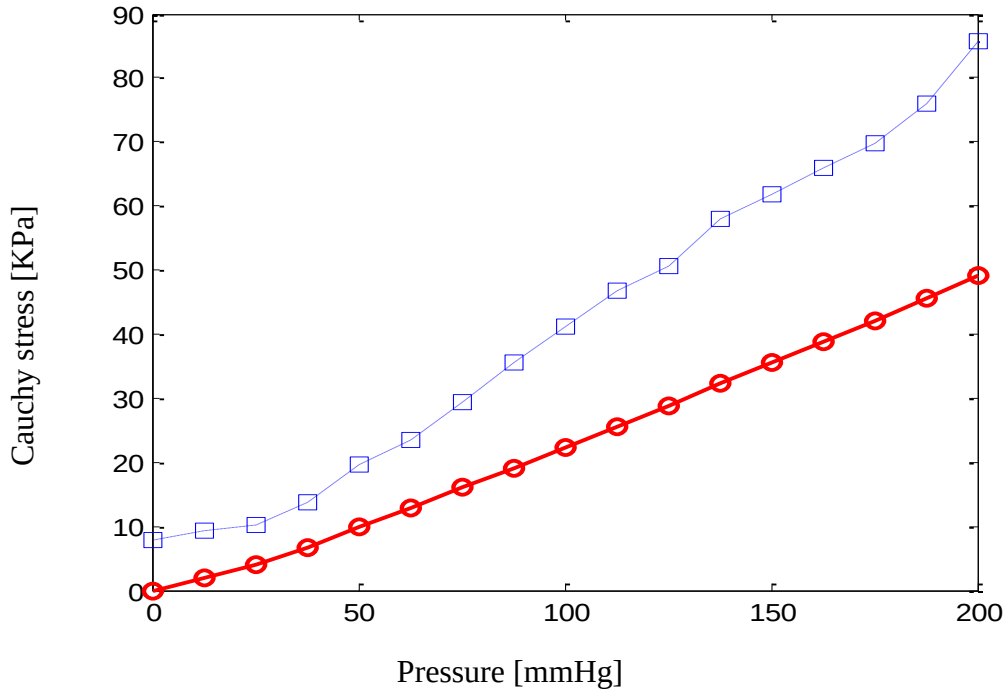

Figure 6.7: Estimated axial (square) and circumferential stresses (circle) using the hyperelastic layer model proposed in this paper for the coronary artery data extracted from [1] and the corresponding experimental axial (dashed line) and circumferential (continuous line) stresses.

It could be seen from the figure that the arterial wall is stiffer in the axial direction as for example if, we take the pressure value of 100 mmHg, it could be found that the axial stress is about 40 KPa, where the circumferential stress is about 20 KPa. This can suggest that baroreceptors may be more subjected to axial stress. The relation between the directions of stimulation of the baroreceptors has not been fully investigated, and this is a possible future development as will be discussed more in chapter 10. The role of collagen and elastin in forming both curves is evident, as at lower pressure values, elastin is the controlling element, so the relation is almost linear. At higher values of pressure however, collagen starts to be stiffer so the shape of the curves tends to be more exponential.

6.3 Wall layer estimations

Forces equilibrium principles, together with optimisation using trust region and Levenberg Marquardt algorithm, along with Monte Carlo simulation were used to calculate stress and strain for each layer as was shown in section 6.1. Each layer was assumed to have a different strain energy function.

Figure 6.8 shows estimated stress-strain data for the three layers, (intima, media and adventitia) in the same coronary artery. For comparison a shaded region, showing the range of the experimental data from [1], has been added. A set of experimental curves with similar material constants for a single coronary artery from [1] is also shown for comparison purposes. Figure 6.9 shows the effect of increasing axial pre-stretch on the maximum strain achieved by the artery. Figure 6.10 discusses the observed results that of interrelation between layers.

Figure 6.11 shows the whole-wall experimental, estimated results and the estimated layer stress-strain profiles for the same artery. The inferred layer stress-strain profiles produced in the process of estimating the whole-wall stress-strain profile, as shown in figure 6.8 and figure 6.11, are consistent with the experimental layer data in [1] and [4-7], as will be shown later in details.

Figure 6.8 is a very interesting graph as every plot holds three different curves. The shaded area is the area found to be physiologically correct by Holzapfel et al[1]. This was based on experimental uniaxial physiological tests, with biaxial measurement were performed. This shaded area consists of different lines; the nearest line (of them) to our produced results is shown in each plot, adjacent to our obtained curve which is plot in squares. The aim of these graphs is to show that our produced curves belong to the physiological area indicated by these experimental results.

The layer material parameters optimised to produce the stress-strain profiles have also been compared to those estimated by Holzapfel et al using layer experimental data [1] (Tables 6.1 and 6.2). It can be seen that the values estimated by the layer model in this research for the single coronary artery in [1] are within the range of values for the range of coronary arteries studied by Holzapfel et al [1].

Table 6.1

Optimised material parameters for the combined layer model and Holzapfel et al's individual layer experiments [1]

Estimated parameter	Model parameter Mean±std (to 2 d.p.)	Holzapfel's parameters Mean±std (to 2 d.p) [1]
k_{2n}	45.41 ± 0.00	170.88 ± 125.4
k_{2m}	9.14 ± 0.08	8.21 ± 3.27
k_{2a}	35.95 ± 0.09	85.03 ±58.94
c_{1n}, [kPa]	8.96 ± 0.47	13.95 ± 5.30
c_{1m} [kPa]	0.33 ± 0.04	0.63 ± 0.36
c_{1a} [kPa]	1.58 ± 0.27	3.78 ± 2.33
k_{1n} [kPa]	7.03 ± 0.52	65.91 ± 122.73
k_{1m} [kPa]	6.28 ± 0.24	5.40 ± 1.78
k_{1a} [kPa]	5.68 ± 0.36	9.64 ± 8.13
ρn	0.64 ± 0.00	0.51 ± 0.14
ρm	0.14 ± 0.01	0.25 ± 0.09
ρa	0.72 ± 0.00	0.55 ± 0.18

Table 6.2

Estimated collagen fibre angles (from the circumferential direction) for each layer for two vessels

Layer	Model angle Mean ± std (to 2 d.p.)	Holzapfel Model [1] Mean ± std (to 2 d.p.)
Intima	72.49±0.41	60.30 ± 18.20
Media	16.37±1.15	20.61 ± 5.50
Adventitia	62.87±0.42	67.00 ±8.50

From these it was estimated that the stress-strain profiles are similar to those in [1] for all layers and the adventitia and media in the axial direction. However it is important to note that there is a difference in the experimental techniques in producing the experimental data set for our results (biaxial test, with biaxial measurement) and the technique used to produce the shaded physiological area.

A possible explanation for this is due to the differences in applying the stresses. In the whole wall artery experiments, biaxial stresses were applied using an axial pre-stretch, whereas in the layered wall experiments, uniaxial stresses were applied. The effect of axial pre-stretch on maximum circumferential stress of a whole arterial wall was further investigated using the three layer model. The results are presented in Figure 6.9. It can be seen that increasing the axial pre-stretch increases the range of the circumferential strain. This could possibly explain why the intimal response falls outside the experimental range in [1].

a)

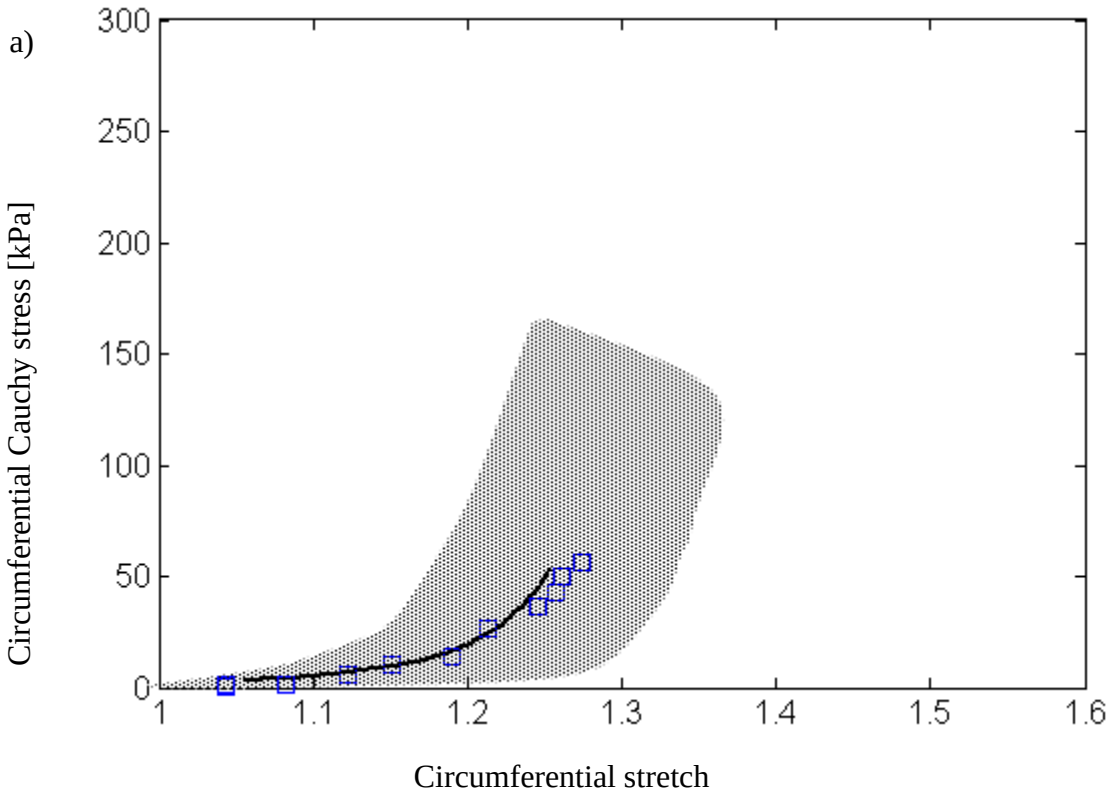
Circumferential Cauchy stress [kPa]
300
250
200
150
100
50
0
1
1.1
1.2
1.3
1.4
1.5
1.6
Circumferential stretch

b)

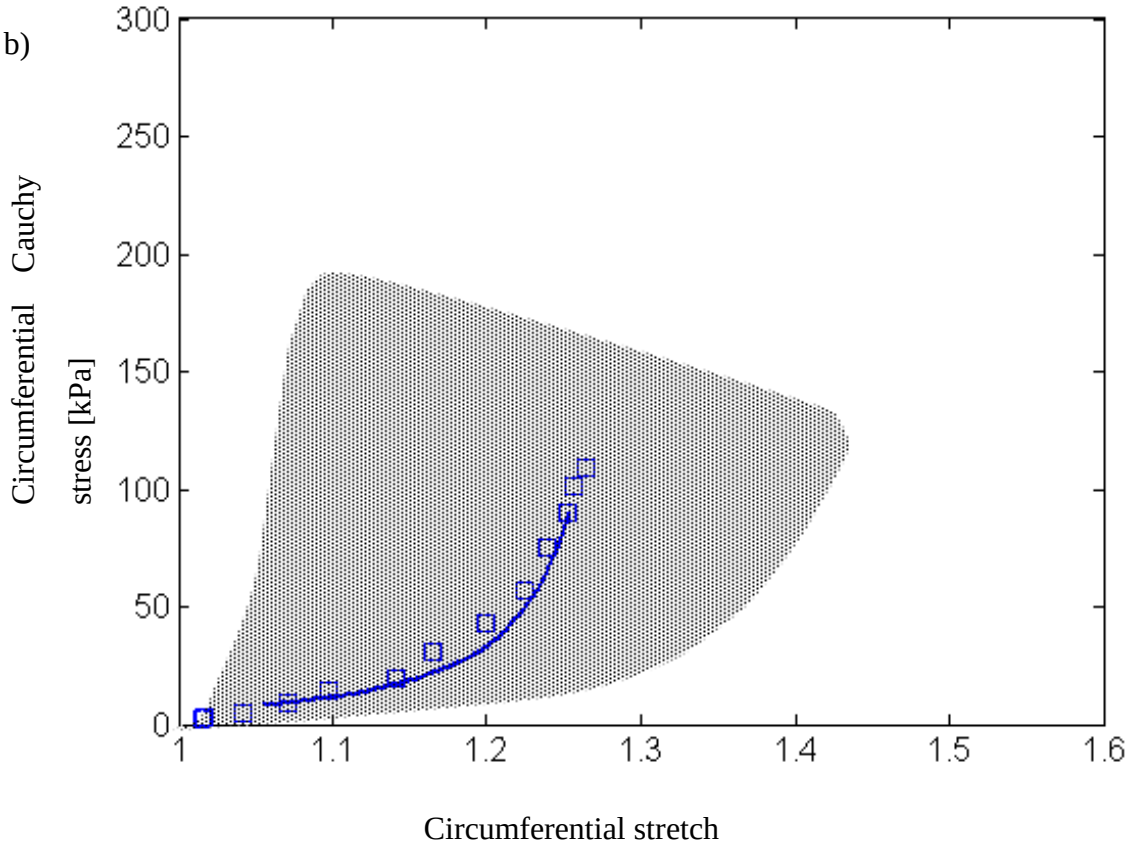
Circumferential Cauchy stress [kPa]
300
250
200
150
100
50
0
1
1.1
1.2
1.3
1.4
1.5
1.6
Circumferential stretch

c)

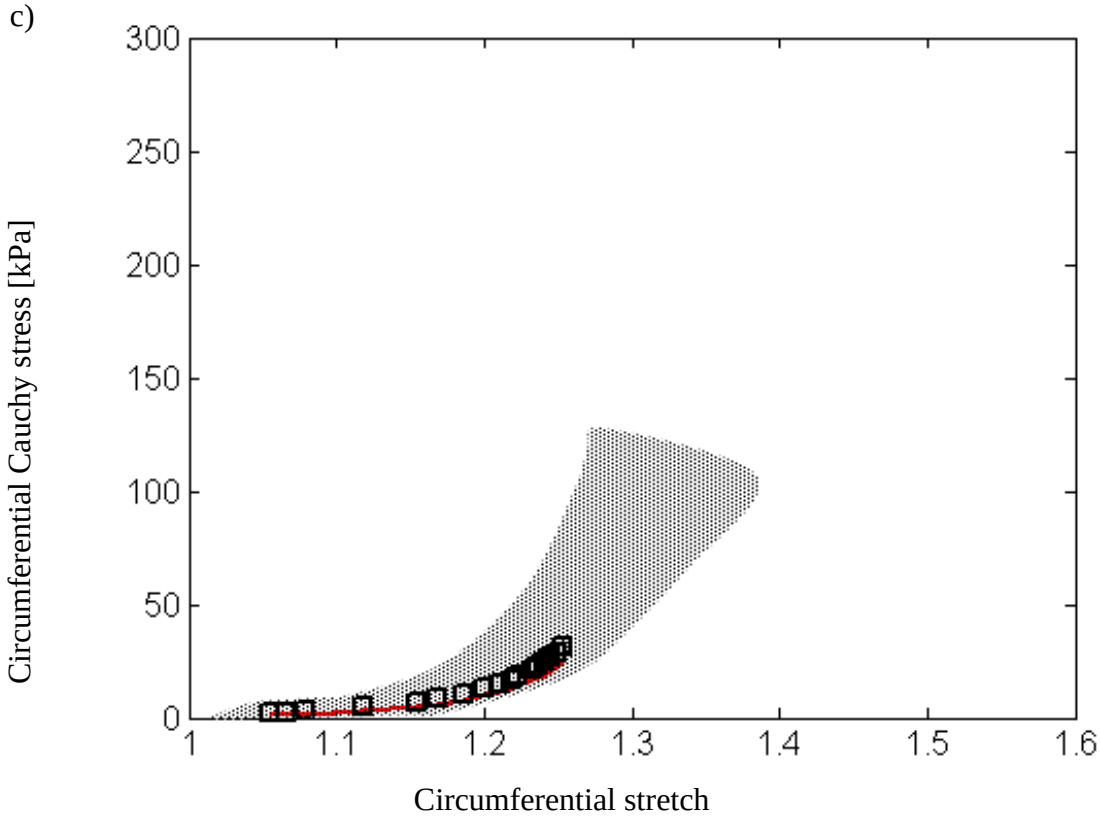
Circumferential Cauchy stress [kPa]
300
250
200
150
100
50
0
1
1.1
1.2
1.3
1.4
1.5
1.6
Circumferential stretch

d)

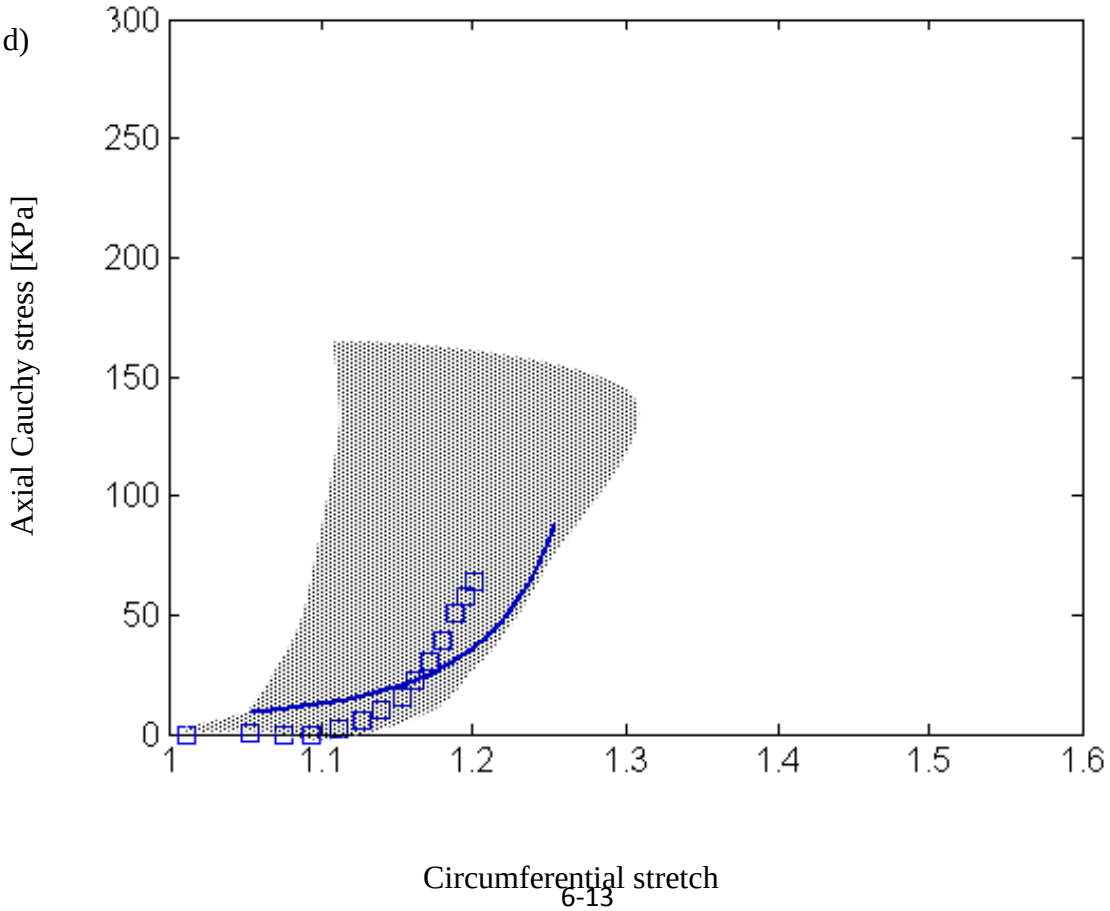
Axial Cauchy stress [KPa]
300
250
200
150
100
50
0
1
1.1
1.2
1.3
1.4
1.5
1.6
Circumferential stretch

e)

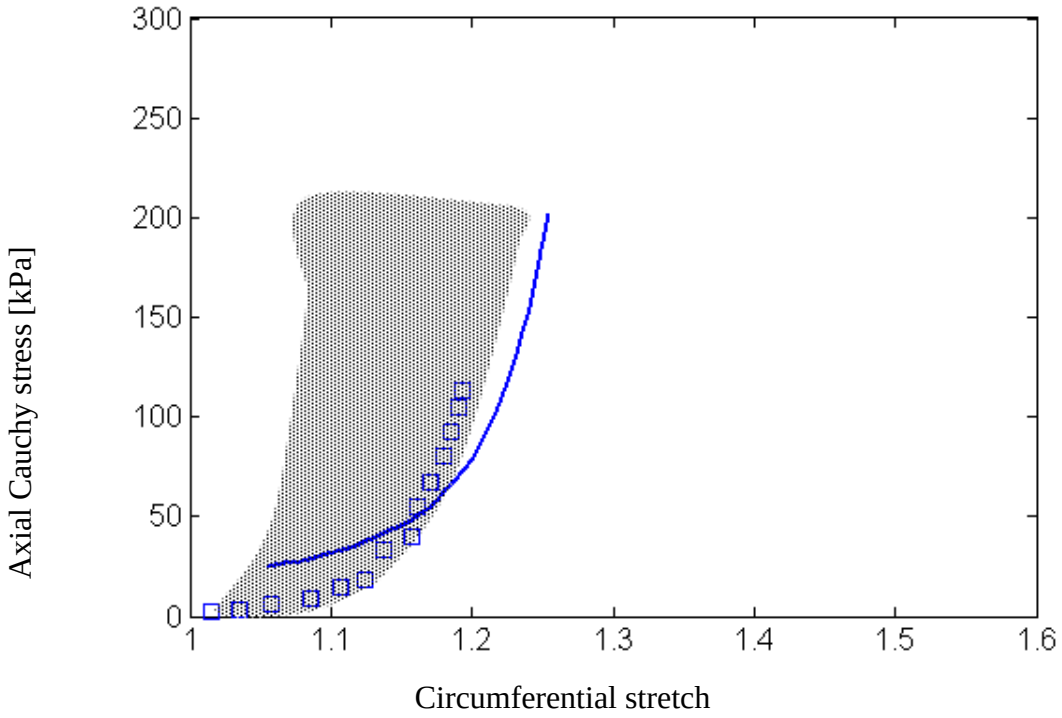

f)

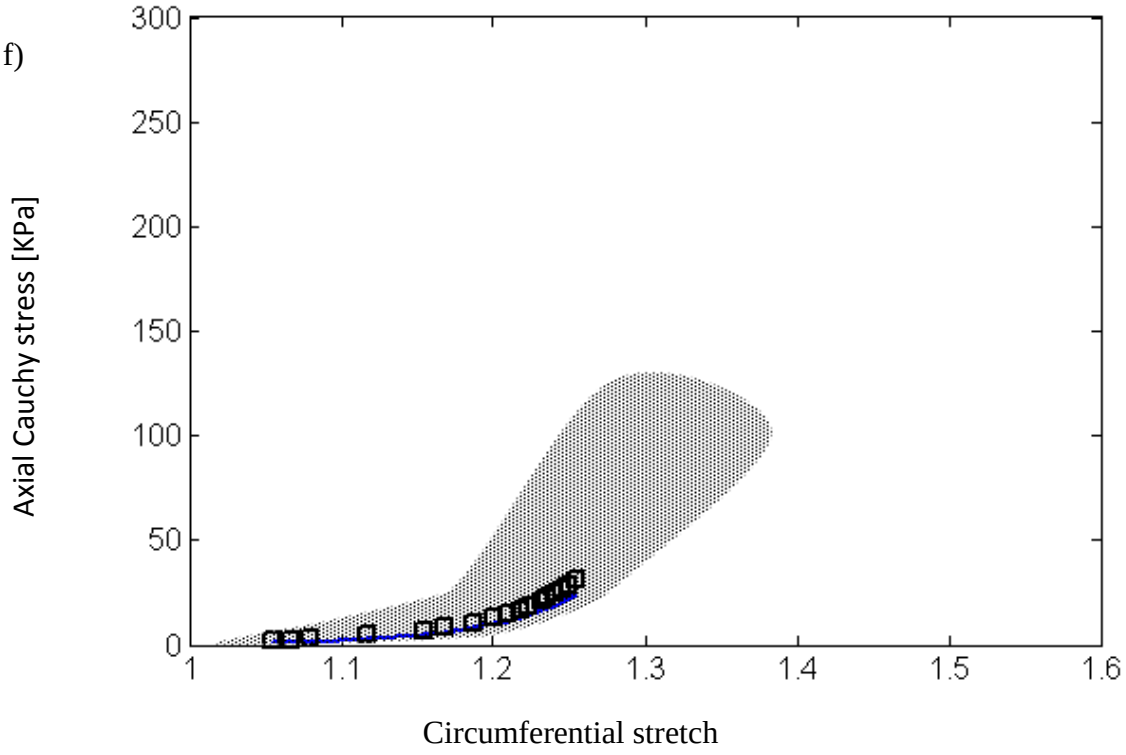

Figure 6.8: Layer stress (continuous line) for circumferential direction for a) adventitia, b) intima and c) media then in axial direction in d) adventitia e) intima f) media, compared with the experimental range (shaded area) presented in [1] with one data set (square) from the same reference.

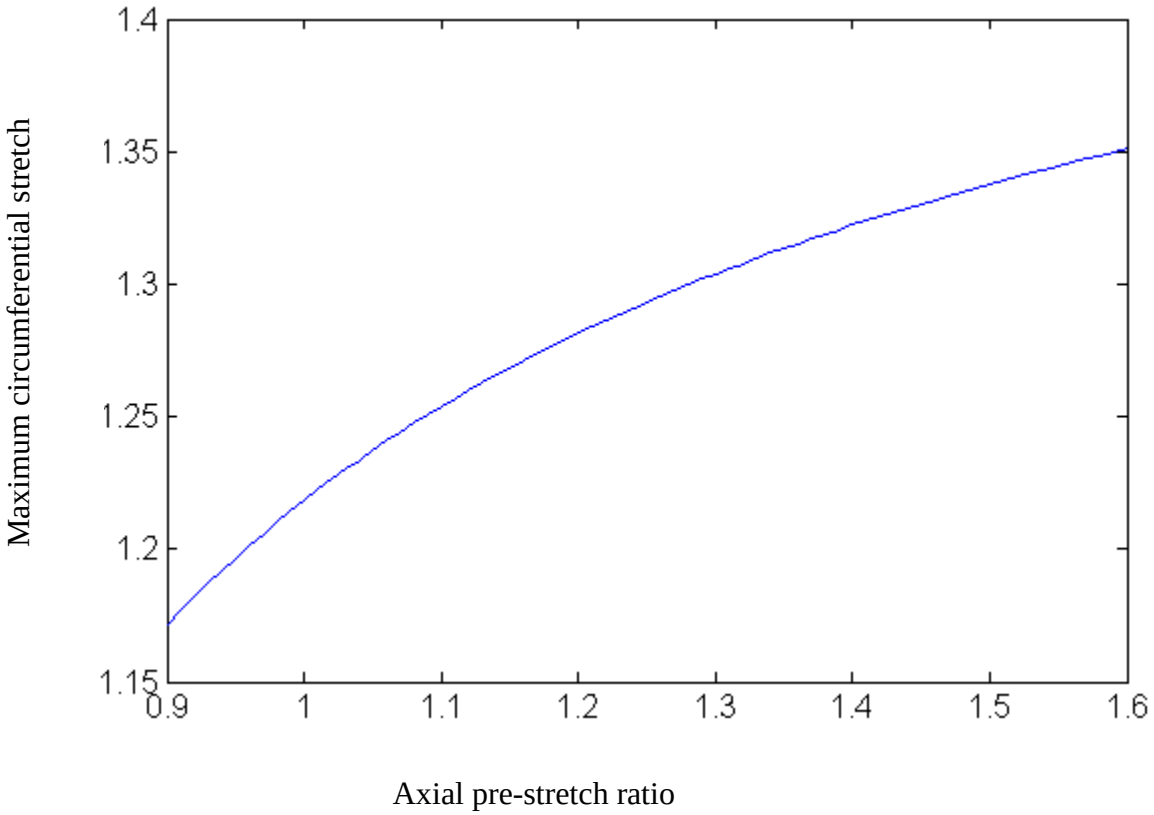

Figure 6.9: Axial pre-stretch ratio versus maximum stretch.

It is worth noting that relationship between stiffness of the layers is in line with the constraint proposed in chapter 2. So for example adventitia stiffness given by figure 6.8a and 6.8d shows that adventitia is stiffer axially more than circumferentially. The same applies to the intima; shown in figure 6.8b and 6.8e. However the contrary is true for the media, which is stiffer circumferentially than axially as shown in figure 6.8c and 6.8f. On comparison between layers stiffness, it could be seen that the intima in general is stiffer than the adventitia which in turn is stiffer than the media. The role of the intima in older subjects is still under investigation as the reason behind the increasing of thickness of the intima is not yet known. Studying the increase in the intimal thickness in healthy older subjects would be of huge importance, especially to link it with pathological conditions like atherosclerosis. On another note, the significance of such structure of the arterial wall is still an open

question. It seems that the arterial wall is composed of three layers with different stiffness in different directions as shown in figure 6.10.

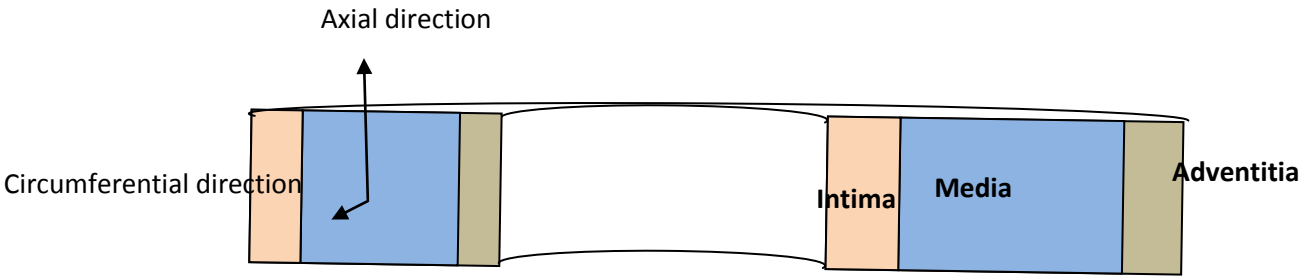

Figure 6.10: The internal structure of the whole arterial wall resists axially stress more than circumferential stress. The intima and the adventitia agree with this assumption in contrast to the media.

The reason for such structure might be as follows: Adventitia and intima in healthy older patients protect the media from excessive stress, and hence control the medial baroreceptors response. This might also have other implications in lowering the risk of damage to the arterial wall in general and the media in particular through preventing extensive stretching in the axial direction. In the same time the media is circumferentially stiffer than its axial direction and this might protect the media from over extension in that direction. In addition the media is stiffer in the circumferential direction; this might control the probability of medial baroreceptors being stimulated by any increase in blood pressure. This is further emphasised in figure 6.11, where the whole wall is nearer to the adventitial response in both direction. Thus it could be assumed that the whole wall as well as the intima and adventitia main role would be to protect the media from excessive extension or possible rupture. The role of the media on the other side would be to control extensive circumferential stimulation of medial baroreceptors, in the same time read any very high axial stimulation. This also suggests that baroreceptors might be more stimulated axially than circumferentially. Interestingly enough, the intima does not seem to play a crucial role in stimulating the baroreceptors, as most of the baroreceptors nerve ending either exist in the media and the adventitia[8]. Thus the role of the

intima is sharing to equilibrate the applied stress. Hence acting as a sort of stress constrain for medial and adventitia baroreceptors

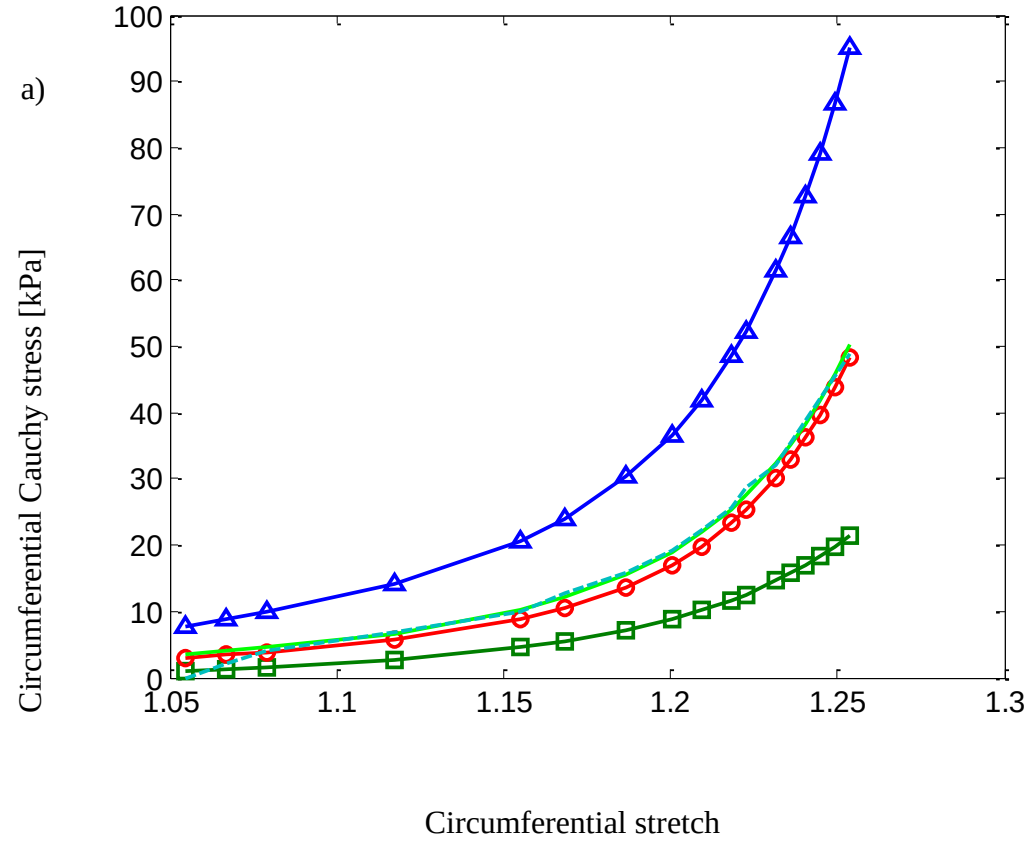

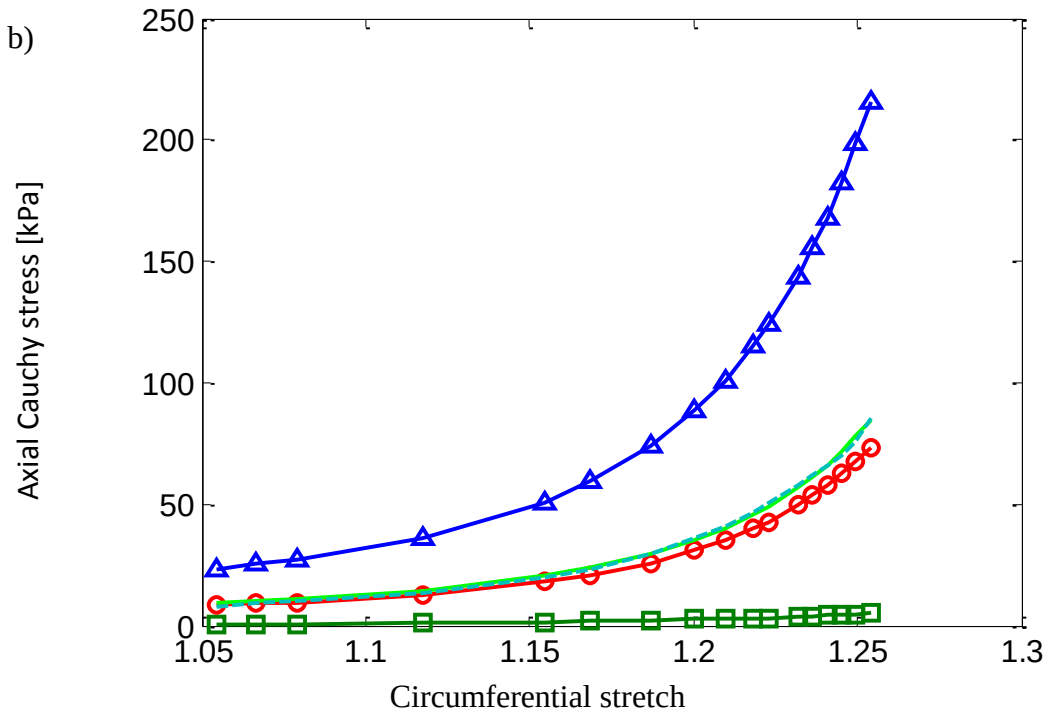

Figure 6.11: The layer response is compared with the total response in two directions. a) Circumferential b) axial, triangle is used for intima, circle for adventitia. The model results are shown in a dashed line and the experimental results are shown in continuous line.

Figure 6.11 shows that the arterial wall as a whole is nearest to the adventitia in its behaviour. Thus it is stiffer axially than circumferentially. This might be explained by the fact that the arterial wall axial extension should be as lower as possible. In the same time, it allows a bigger range of extension in the circumferential direction, which is the normal extension direction because of blood flow.

6.4 Uniqueness of solution

The optimisation procedure was repeated ten times from random starting points [9] within the physiological range defined by experimental data in [1]. For each optimisation run, 500 solutions with a mean square error less than 0.050 were accepted from 50000 simulations. From the total data set the probability density functions of all parameter were examined. They were all found to be unimodal, implying a unique set of parameters. Thus, the mean and standard deviation of each parameter were calculated according to the standard Monte Carlo procedure, results are shown in table 6.1. It is worth mentioning that, there was an agreement between the model results and that of Holzapfel. However it is important to note that at a certain values of Holzapfel model, the range with big for example k1n. The collagen fibre angles from the circumferential direction are assumed to be different for each of the three layers in the hyperelastic model [1] as shown in table 6.2..

Parameter sensitivity analysis was used to assess whether variations of the parameter values have a noticeable impact on the quality of simulation. Parameter sensitivity was carried out according to the following procedure [10-12] . Each parameter was varied ± 50 % across its mean, while the other parameters were kept constant at their optimised values. The error was plotted across the range of normalised parameter values. The parameters intersected at their lowest error point. This procedure is known as one way parameter sensitivity analysis[12] , it is also known as nominal range sensitivity analysis. To ensure the validity of the results a Kolmogorov–Smirnov test was used to compare the statistical distribution of the accepted and the unaccepted ranges. If the statistical distributions were identical, the parameter was deemed to be insensitive.

6.5 Parameter sensitivity estimation

Figure 6.12 shows graphs of the parameter sensitivity for the coronary artery data. Figure 6.13 concentrates on comparing the effect of the collagen fibre angle for each layer. To investigate the validity of the layer model parameters further, a sensitivity analysis was carried out. The Kolmogorov–Smirnov test indicated that the model was sensitive to all the material parameters within the physiological range.

Figure 6.12 shows that the minimum error occurs when all the parameters are at the optimised values and there are no other error minima observed within the physiological range. It also suggests that the solution is most sensitive to the predominant angle ϕ of the dispersed collagen fibres. It is also worth noting that the error range was included for 50% above and below the optimised value. This can be seen in more detail in Figure 6.13 which shows that the solution is most sensitive to ϕ in the layers with the highest collagen content and hence the greatest stiffness. This suggests that collagen fibre direction is a major factor in determining the arterial wall stiffness and thus dominates the response in the intima and adventitia, and a less significant effect in the media.

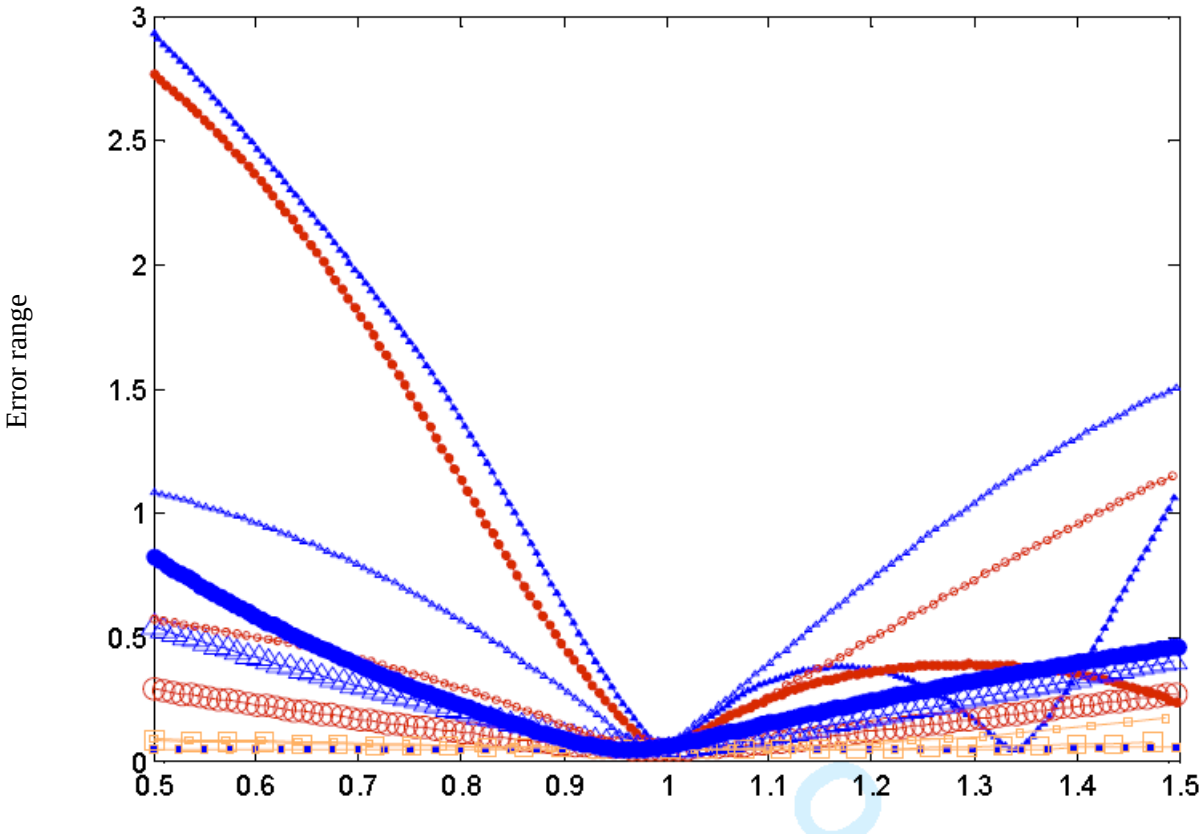

Figure 6.12: Parameter sensitivity for the fifteen parameters in the model of the coronary artery. A small full symbol is used for φ, k_2 is represented by a small empty symbol, k_1 is represented by a large closed symbol and finally the dispersion is represented by large empty symbol. The intimal layer is represented by a triangle, the adventitial layer by a circle and medial layer by a square. Elastin constants, c_1 are the least significant and are not shown.

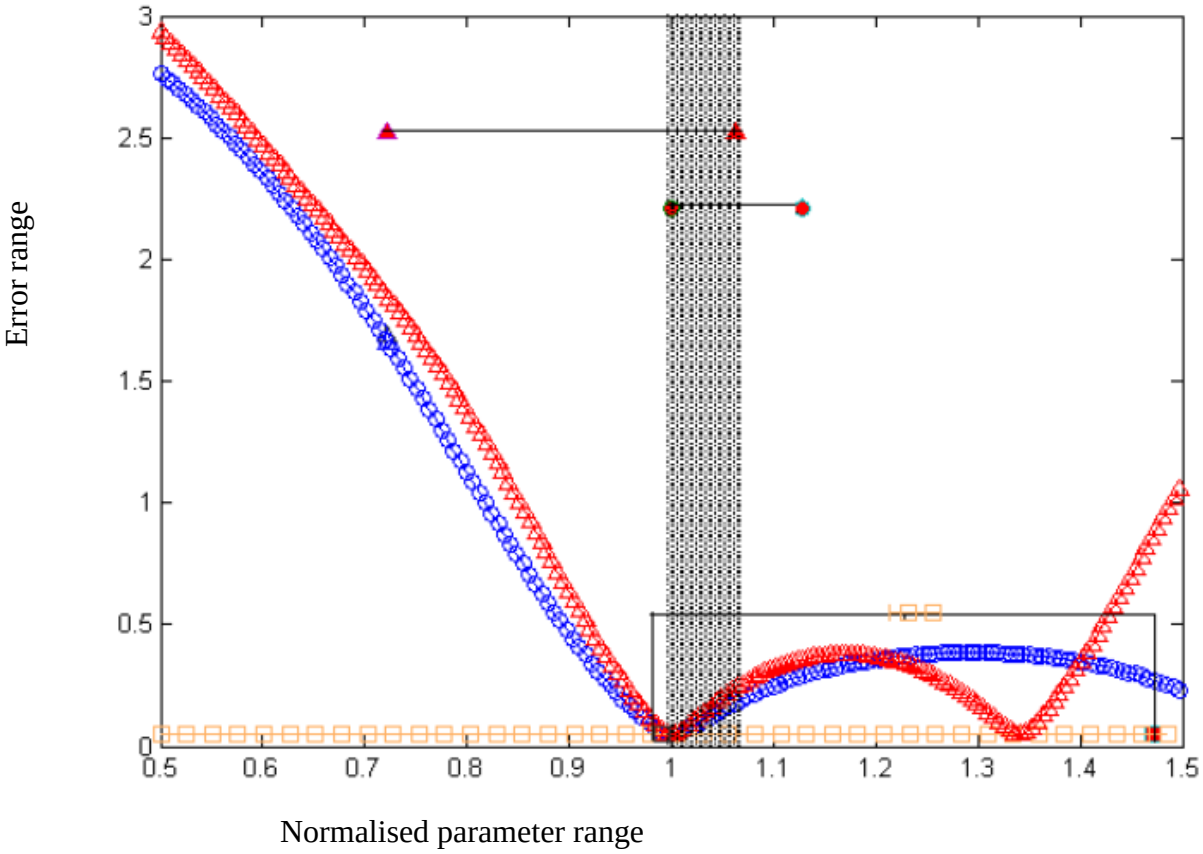

Figure 6.13: Parameter sensitivity for collagen fibre angles of the coronary artery. The intimal layer is represented by a triangle, the adventitial layer by a circle and medial layer by a square. Each respective physiological range is marked with its symbol and the common physiological range is shaded. The shading part is the intersection of the three physiological ranges presented by Holzapfel in [1].

6.6 Effects of assumptions

In this section the major assumptions used in producing the model are discussed. Factors considered include a thin wall cylinder approximation, abrupt junctions between the layers, a constant strain profile, and a constant ratio of layer thicknesses.

The aim of this study is to produce an analytically derived model such that the effect of material parameters can be studied. In chapter 3 a review of studies using cylindrical thin wall models

suggested that analytical solutions for thick wall vessels is far from a trivial task and finite element analysis is a more suitable method [13]. However, the results in this research based on [14] (as covered in chapters 3 and 4) suggest that a thin wall model does produce results that are consistent with experimental findings. The model is also based on assuming the layers have abrupt junctions. The results of the histological study show that the thickness of the junction regions is relatively small compared with the layer thicknesses and hence this is a reasonable assumption. However, this ignores any effects of the internal elastic lamina and external elastic lamina that separate the media from the intima and adventitia respectively [15] [16]. A model that takes into account inter layer lamina effects may act to improve the goodness of fit of the whole model [17]. The assumption of a constant strain across the three layers is used as this is one of the constraints required for the application of thin wall theory. Finally, the assumption of using fixed layer ratios is addressed [1], initially the separate thickness are given by [1]as follows: 27±0.02, 0.36±0.03 and 0.40±0.03, but it could be noticed that these values when added exceeds unity as each thickness was measured separately after separating the three layers. It is also worth noting that the thickness of the artery increases after being taken out of the body. Thus the value of unity was assumed and the values of the intact thickness were calculated according to the above ratio to be for nominal layer thicknesses of 26.2%, 34.9% and 38.8% for the intima, media and adventitia respectively [1].

6.7 Conclusions

This research has presented a mathematical model based on a hyperelastic formulation using the condition of stress equilibrium to estimate the stress-strain profiles in both whole and layered arterial walls. The material parameters in the model have been optimised using whole-wall experimental data from studies carried by Holzapfel [1] and van Andel [2]. For the whole-wall estimations of a single coronary artery, the total root mean square error was found to be 0.050 which compares well with previous studies. This suggests the proposed method provides a simple approach to estimating the layer material parameters. A comparison with experimental data from a study on layered data [1] suggested the solutions to the model were physiologically feasible; however, differences in experimental setup prevent this judgement from being completely conclusive.

In optimising the material parameters, it was revealing to find that the errors in the estimated stresses were particularly sensitive to the dominant collagen angle in the stiffest layer, the intima. This suggests the role of collagen content and possibly fibre orientation should be investigated further for conditions such as arteriosclerosis.

6.8 References

1. Holzapfel GA, Sommer G, Gasser CT, and Regitnig P, *Determination of Layer-Specific Mechanical Properties of Human Coronary Arteries with Nonatherosclerotic Intimal Thickening and Related Constitutive Modeling.* Am. J. Physiol. Heart Circ. Physiol., 2005. **289**(5): p. H2048-2058.
2. van Andel CJ, Pistecky PV, and Borst C, *Mechanical Properties of Porcine and Human Arteries: Implications for Coronary Anastomotic Connectors.* Ann. Thorac. Surg., 2003. **76**(1): p. 58-64.
3. Watton PN, Ventikos Y, and Holzapfel GA, *Modelling the Mechanical Response of Elastin for Arterial Tissue.* J. Biomech., 2009. **42**(9): p. 1320-1325.
4. von Maltzahn WW, *Stresses and Strains in the Cone-Shaped Carotid Sinus and Their Effects on Baroreceptor Functions.* J. Biomech., 1982. **15**(10): p. 757-765.
5. von Maltzahn WW, Besdo D, and Wiemer W, *Elastic Properties of Arteries: A Nonlinear Two-Layer Cylindrical Model.* J. Biomech., 1981. **14**(6): p. 389-397.
6. von Maltzahn WW, Warriyar RG, and Keitzer WF, *Experimental Measurements of Elastic Properties of Media and Adventitia of Bovine Carotid Arteries.* J. Biomech., 1984. **17**(11): p. 839-847.
7. Demiray H and Vito RP, *A Layered Cylindrical Shell Model for an Aorta.* Int. J. Engrng. Sci., 1991. **29**(1): p. 47-54.
8. Wolfgang K, *Three Types of Neurochemically Defined Autonomic Fibres Innervate the Carotid Baroreceptor and Chemoreceptor Regions in the Guinea-Pig.* Anat Embryol, 1990. **181**: p. 477-489.
9. Dahl S, Vaughn M, Hu J, Driessen F, Baaijens F, Humphery J, and Niklason L, *A Micostructurally Motivated Model of the Mechanical Behavior of Tissue Engineered Blood Vessels.* Ann. Biomed Eng., 2008. **36**(11): p. 1782-1792.
10. Chang F and Delleur JW, *Systematic Parameter Estimation of Watershed Acidification Model.* Hydrol. Process., 1992. **6**(1): p. 29-44.
11. Jeremy E and O'Hagan OA, *Probabilistic Sensitivity Analysis of Complex Models: A Bayesian Approach.* J. R. Statist. Soc. B, 2004. **66**(3): p. 751-769.
12. Petitti D, *Meta-Analysis,Decision Analysis, and Cost-Effectiveness Analysis*. 2,illustrated ed. 2000: Oxford University Press. 306.
13. Holzapfel GA and Gasser TC, *A Viscoelastic Model for Fiber-Reinforced Composites at Finite Strains Continuum Basis, Computational Aspects and Applications.* Comput. Methods Appl. Mech. Engr., 2001. **190**(34): p. 4379-4403.
14. Holzapfel GA, Eberlein R, Wriggers P, and Weizsäcker HW, *A New Axisymmetrical Membrane Element for Anisotropic,Finite Strain Analysis of Arteries.* Commun. Num. Meth. Eng., 1996. **12**(8): p. 507-517.
15. Holzapfel GA, Gasser T, and Ogden R, *A New Constitutive Framework for Arterial Wall Mechanics and a Comparative Study of Material Models.* J. Elast., 2000. **61**(1): p. 1-48.

16. Fenner R, *Mechanics of Solids*. 1989, Oxford: Blackwell scientific publications. 615.
17. Kroon M and Holzapfel GA, *A New Constitutive Model for Multi-Layered Collagenous Tissues.* J. Biomech., 2008 **41**(12): p. 2766-2771.

CHAPTER 7

OTHER VASCULAR VESSELS

---

7 Overview

This chapter describes investigations on different vessels using the techniques used for coronary arteries. The experimental data used is shown in figure 7.1 and is taken from [1] [2]. It is used to produce a model of the whole wall and wall layer responses for a mammary artery and a vena cava. Briefly, the method comprises (i) digitising the experimental data using Matlab® (ii) optimising the parameters in the strain energy functions using the methods described in chapters 4 and 5 and (iii) analysing and comparing the results for the mammary artery and vena cava. This will be shown in more details in the next section and then a comparison of different vascular vessels responses will be shown.

7.1 Mammary artery

Parameters for whole wall and layer wall models were optimized using the mammary artery data in figure 7.1 and table 7.1 (using the same principles discussed in chapters 4 and 5 and as shown in details in chapter 6). The steps of generating these relationships are as follows:

Step 1: transfer pressure to circumferential stress

Step 2: transfer pressure and axial force into axial stress

Step 3: calculate stretch as the ratio of the radius of the mammary artery after and before deformation

Step 4: apply stretch in the layers stress equations 4-5 equations in chapter 6

Step 5: apply thin wall theory to calculate total stress circumferentially and axially

Step 6: use the error equation given by equation 8 in chapter 6 to accept or reject solutions

Step 7: use Matlab generated code to generate the previous steps 3-6, 50000 times (presented in the appendix) to evaluate generate other set of accepted values

Step 8: calculate the mean for step 7

Step 9: choose another starting point and repeat step 8

Step 10: repeat step 9, 10 times and calculate the mean and plot curves

The layers response is shown in figure 7.2. The results show a response similar to that predicted by Holzapfel et al [2]. For example on comparison of curves in figure 7.2a, it could be clear that intima is constrained to be stiffer than adventitia which is constrained to be stiffer than the media in the circumferential direction. This is also true for the axial direction in figure 7.2b. Constraints for each layer could also be seen, for instance, the axial direction of the intima is constrained to be stiffer than the circumferential direction, for example at 1.25 stretch ratio, the axial intimal response is 150 KPa, where the circumferential stress for the intima is only 80 KPA. This is also true for the adventitia. On the contrary the media is constrained to stiffer axially than circumferentially than axially. This agrees with what has been discussed in chapter 2 and is in line with histological data presented in [2].

The two stress profiles shown in figure 7.3 demonstrate that collagen is the main load bearing component for the complete pressure range. As already mentioned in chapter 2 and shown in figure 2.6. Elastin is a highly elastic protein with a linear stress strain relationship. On the other hand Collagen is stiffer showing an exponential increase of stiffness at higher pressure[3-4]. Thus it could be evident that collagen controls the curve at higher pressure, while elastin only controls lower pressure regions as shown in figure 7.3. The whole wall results shown in figure 7.3 indicate a higher stress response and stiffness axially than circumferentially at this particular axial stretch, which is equal to 1.12, as indicated in the experimental technique for this artery [1].

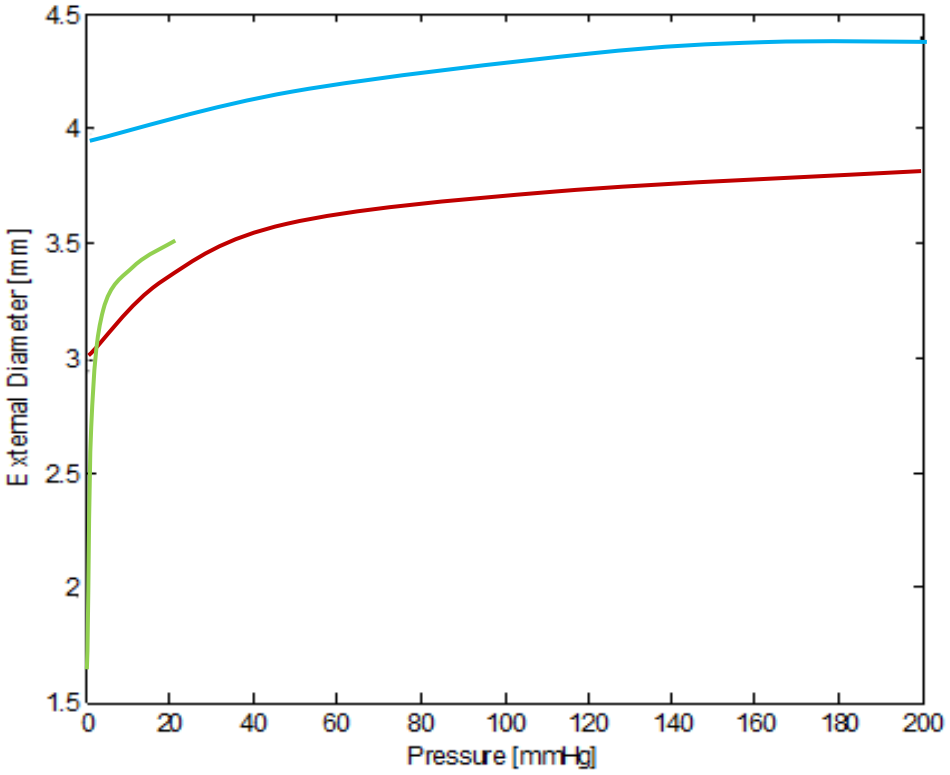

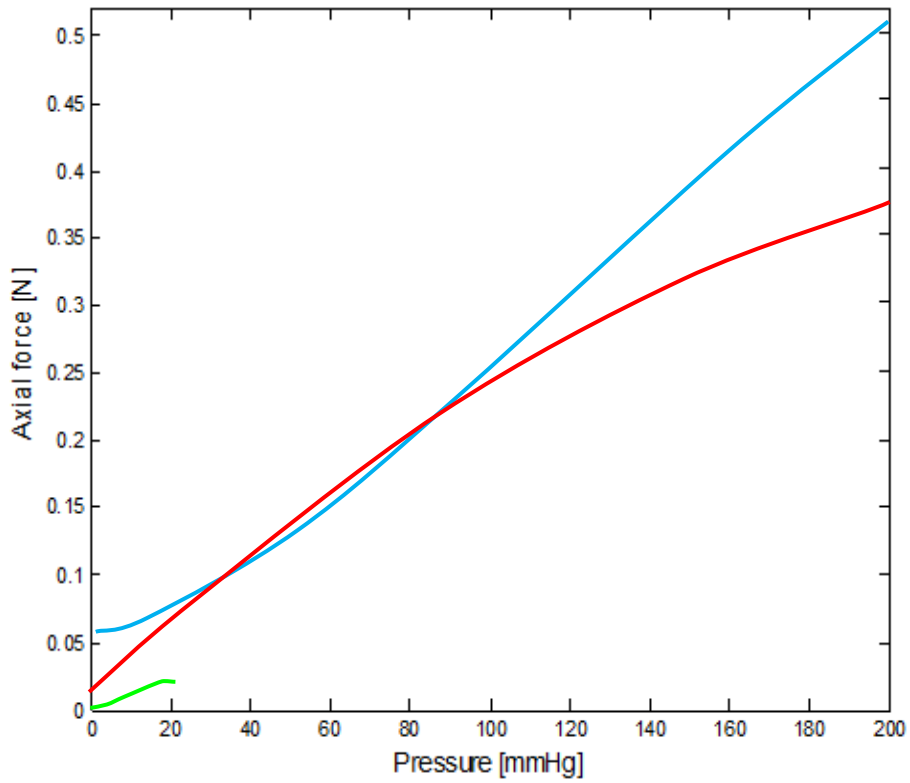

Figure 7.1: Pressure relationship with external diameter and axial force for coronary artery (blue), mammary artery (red) and vena cava (green) [1] [2].

Table 7.1

Experimental data for the mammary artery and vena cava

Characteristic	Mammary artery [1]	Vena cava [5]
External diameter	3.32 mm	2.28 mm
Thickness	0.69 mm	0.20 mm
Axial pre-stretch	20 %	91%

a)

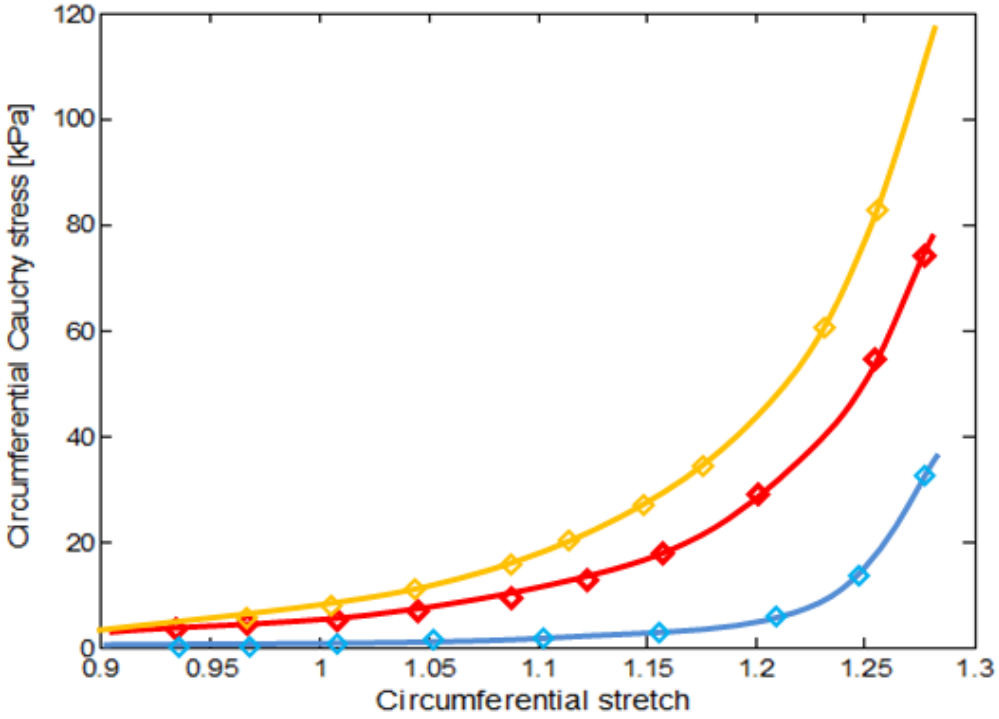

b)

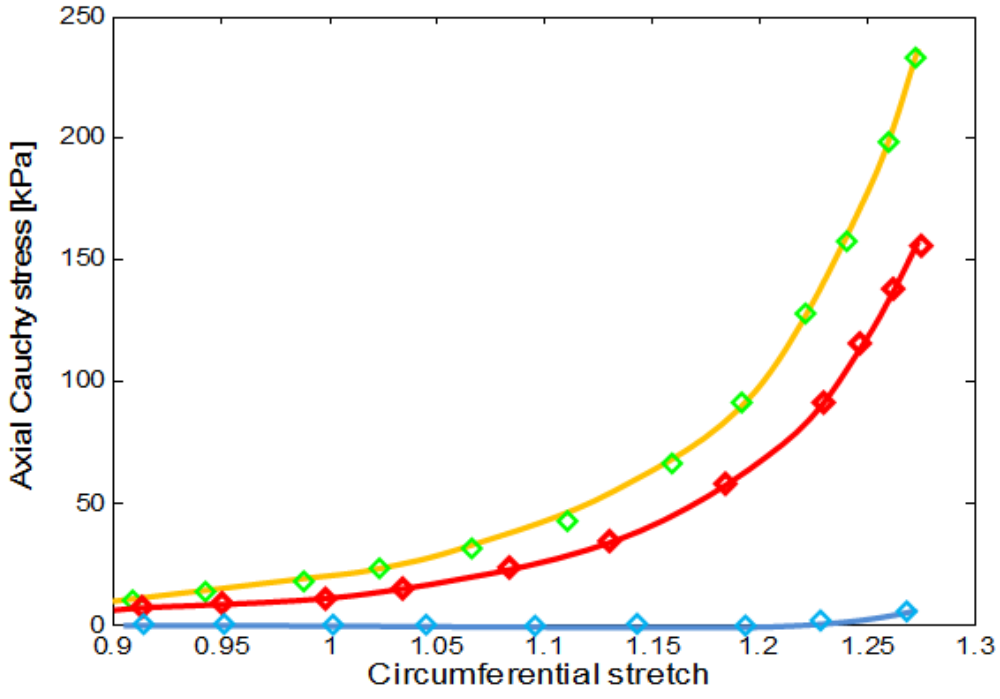

Figure 7.2: Hyperelastic model estimations of a) circumferential stress-stretch b) axial stress-circumferential stretch for a mammary artery for the intima (green), adventitia (red) and media (blue).

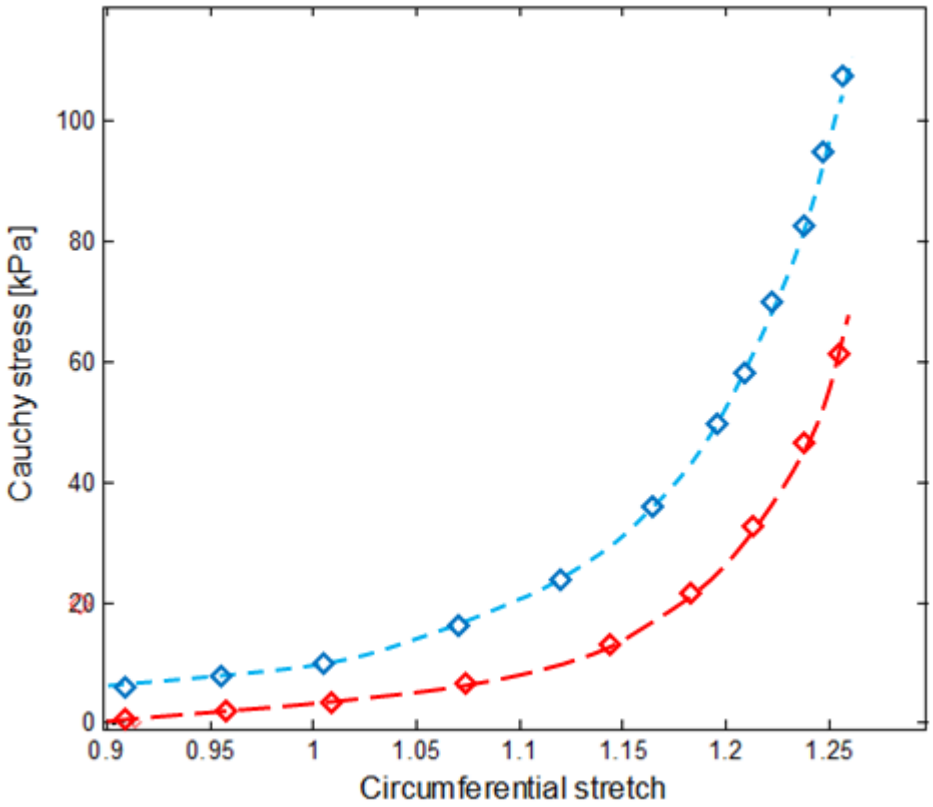

Figure 7.3: Comparison of the mean stress strain relationships of the mammary for the axial (blue) experimental model [1] (dotted) and hyperelastic model (blue squares), the circumferential (red) experimental model [1], (dotted) and circumferential hyperelastic model (red squares).

7.2 Vena Cava

The venous wall is also believed to be composed of three different layers, as the arterial wall, although vein walls are thinner and more distensible[6]. Vein experimental data was digitised and optimised to calculate layer (figure 7.4a & 7.4b) and whole wall response (figure 7.5). Our presented vena cava hyperelastic model has a good fit with the experimental model, at higher pressures, but at lower pressure there could be difference between the calculated and the experimental models. The reason behind that might returns to the elastin equation that controls the curve at lower pressure, future work may include enhancing the fit at lower ranges by modifying the elastin part in the strain energy function. Also it could be observed that the vena cava is stiffer axially (figure 7.5) as discussed in details in chapter 6.The main histological reason for that would be the same as the arterial wall, as the vein also consists of an inner intima which is the stiffest layer in both directions, followed by the adventitia and then the media,. Intima and adventitia are stiffer axially while the media is stiffer circumferentially. Thus it seems that the intima and the adventitia play a more protective role, where the media main role would be extending circumferentially to compensate for increase of blood pressure in this direction, in the same time t is able to simulate low threshold baroreceptors. Interestingly the adventitia would stimulate higher threshold baroreceptors as will be shown in detail in chapter 8.Also , the observation that the adventitia is axially stiffer, indicates that the baroreceptors that exist in this layer may be axially stimulated.

a)

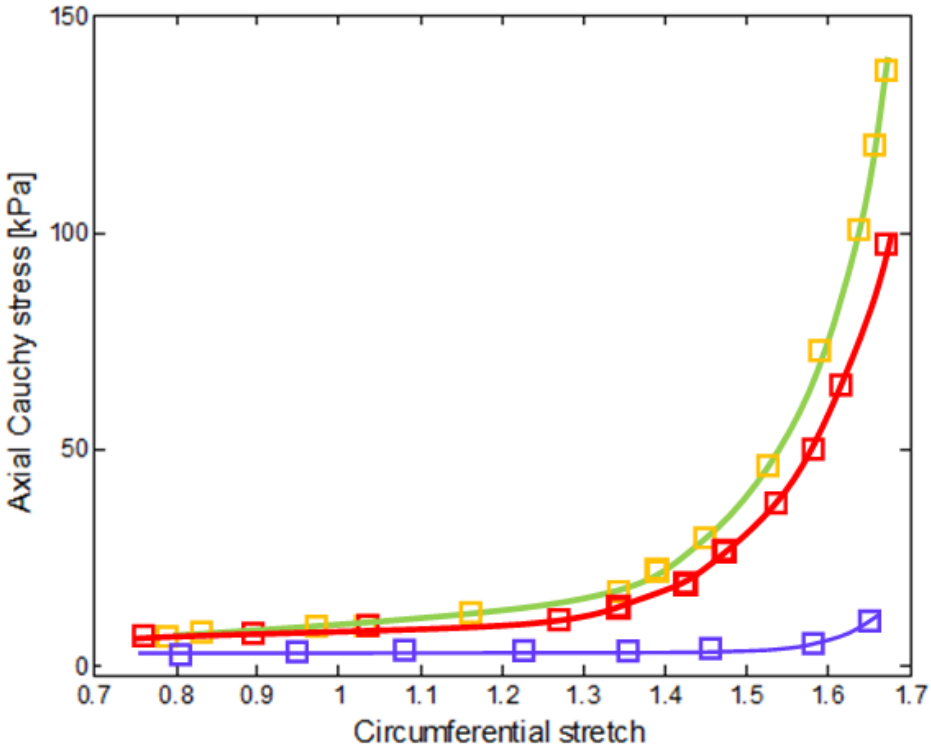

b)

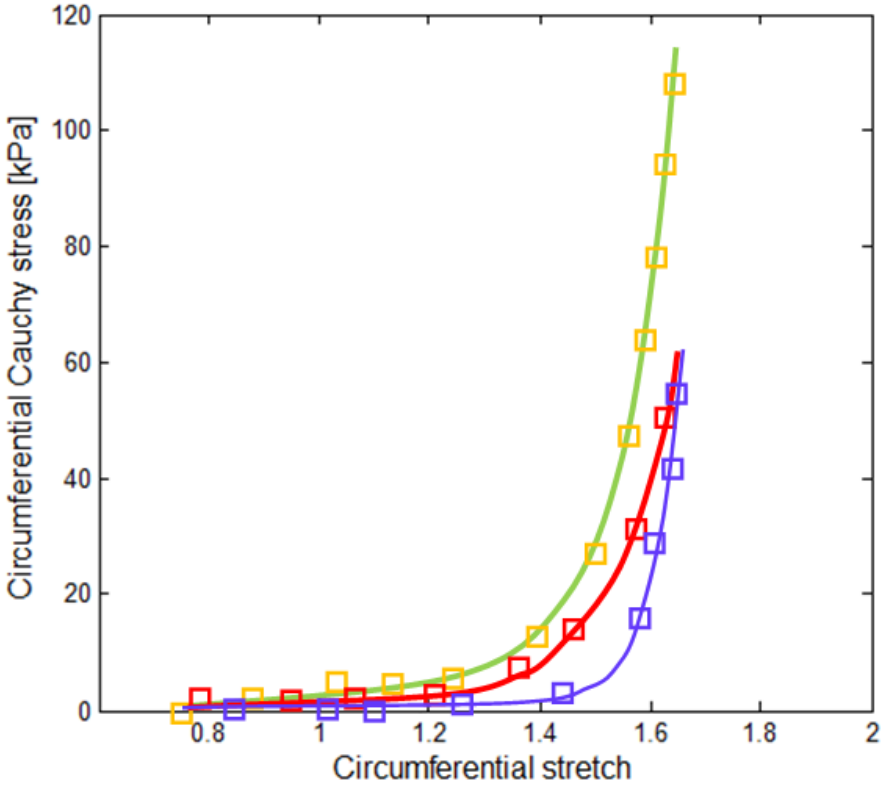

Figure 7.4: Hyperelastic model estimations of a) circumferential stress-stretch b) axial stress-circumferential stretch for vena cava for the intima (green), adventitia (red) and media (blue).

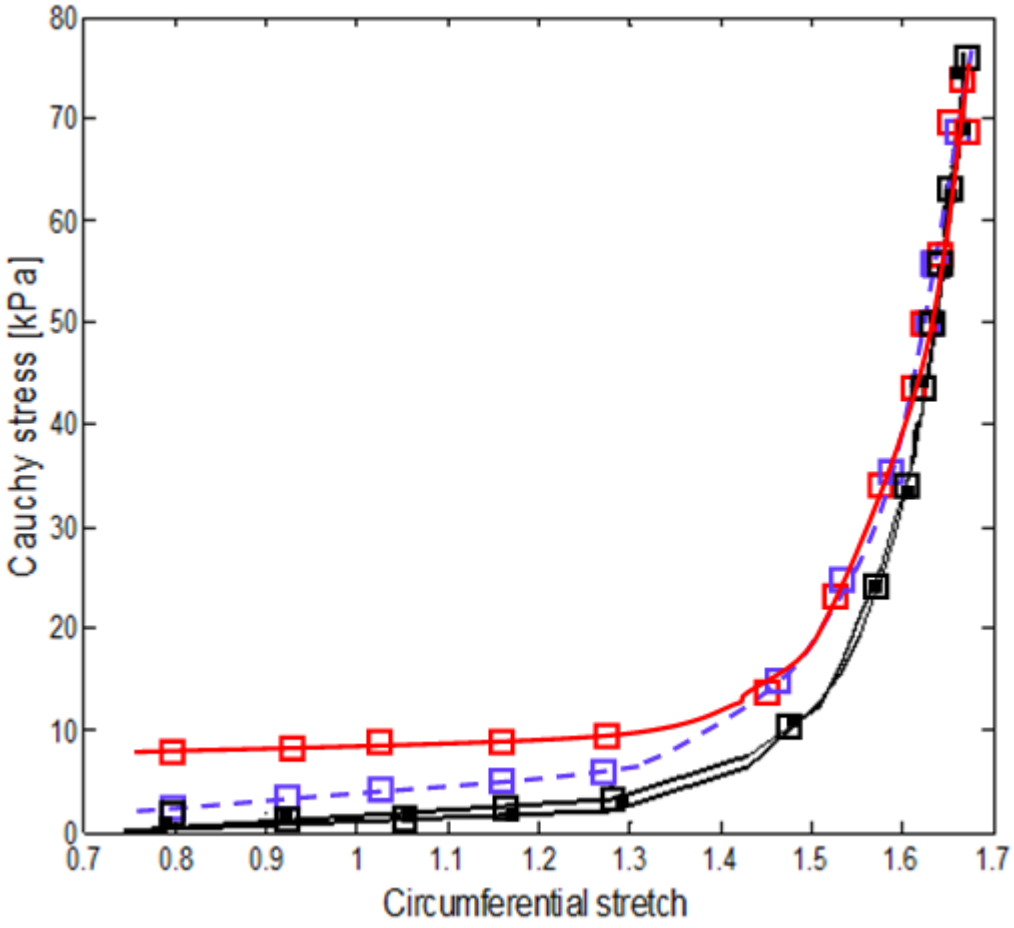

Figure 7.5: Comparison of the mean stress strain relationships of the vena cava for the axial experimental model (red) and hyperelastic model (blue), the circumferential (big sized symbol black) experimental model and circumferential hyperelastic model (line) for the vena cava (small sized symbol black).

In the last two sections results for both the mammary artery and the vena cava were shown for both the layer response and the whole wall response. In the following section a comparison of the responses of the three vessels represented in this research will be discussed here.

7.3 Comparison of vessels

Although the vein plays an important role in the cardiovascular system, there have not been many studies that have estimated the stresses within the vein [6]. Both the experimental and hyperelastic models indicate that the maximum extension ratio for the vena cava is much bigger than that of the arteries as shown in figure 7.6.

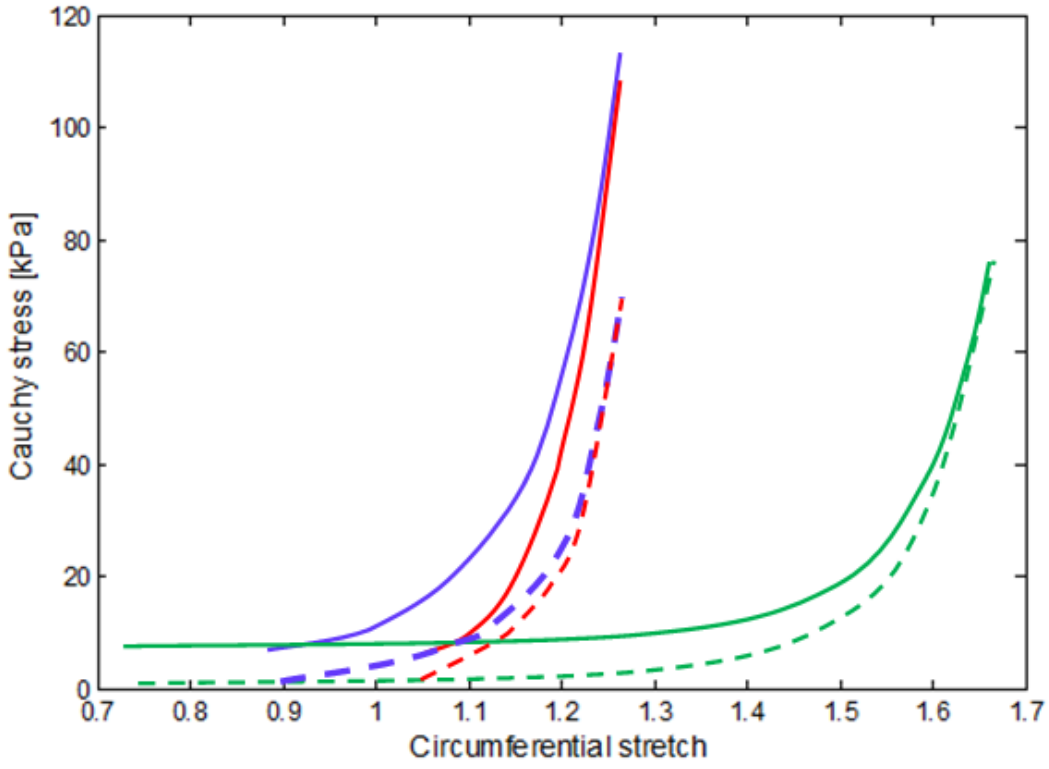

Figure 7.6: Comparison of mean stresses for the mammary (red), coronary (blue) vena cava (green), in both axial (continuous line) and circumferential (dashed line) directions.

The venous parameters are lower than the arterial ones table 7.2 and table 7.3, this could be expected as the pressure range for the vein is about one quarter of the artery and the axial force is about one tenth (figure 7.1). It is worth noting that the arterial and the venous values were generated through the standard biaxial test, hence our ability to compare results.

Table 7.2

Parameters of mammary artery and vena cava

	Parameter	Mammary artery	Vena Cava
Elastin	c_{1n}, [kPa]	7.07	1.6
	c_{1m} [kPa]	1	0.4
	c_{1a} [kPa]	3	0.48
Collagen	k_{1n} [kPa]	10	0.124
	k_{1m} [kPa]	1	0.03
	k_{1a} [kPa]	8	0.07
	k_{2n}	15.1	1.16
	k_{2m}	9.7	1.7
	k_{2a}	14.8	1.12

Table 7.3

Collagen fibre angles (from the circumferential direction) for each layer for two vessels

Layer	Mammary artery	Vena cava
Intima	57.2°	44.1°
Media	19.4°	20.1°
Adventitia	57.2.°	47.8 °

7.4 Elastin and collagen contribution in all investigated vessels

Figure 7.7 represents a quantitative comparison of elastin and collagen contribution for the coronary artery. Each value was calculated through the equations presented earlier in chapter 4. The figure shows that the collagen contribution to the mean stress is far greater than the elastin for all the three layers. This indicates that in terms of load-carrying capacity, vascular vessels are collagen dominated. Our study supports the theory which assumes that elastin is responsible for the linear start of the stress-strain curve, while collagen contributes more to the load bearing process at higher stresses.

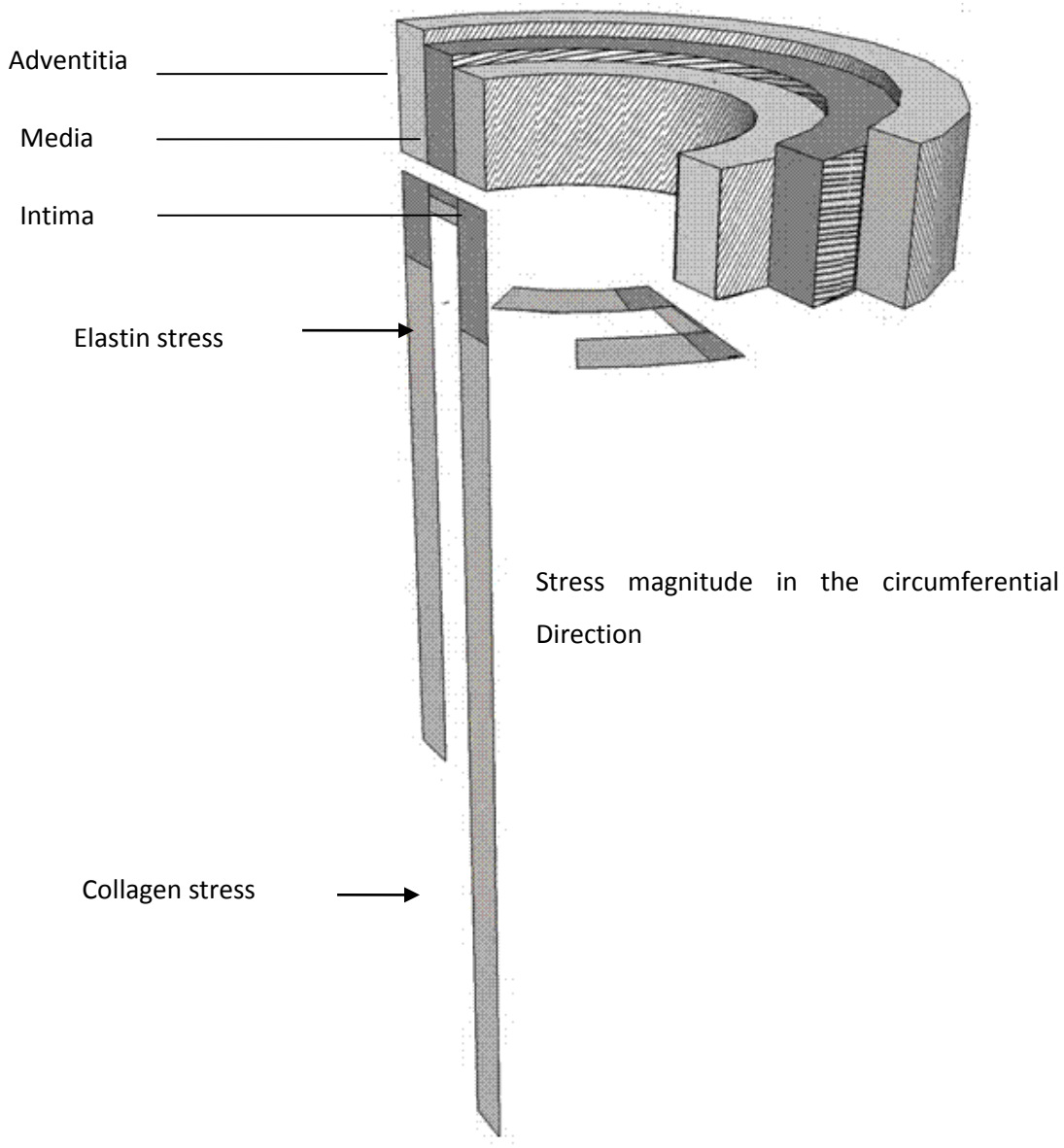

Figure 7. 7: Comparison of axial and circumferential stress profiles within the mammary artery at a stretch of 1.2. The length of stress blocks indicates the stress magnitudes. Collagen and elastin stress contributions are shown for each layer. The optimised collagen fibres angles are also shown. This is a" to scale "representation of the components forming the coronary artery represented in chapter 6.

The contribution of elastin and collagen for the stress components is shown in table 7.4 for the circumferential response and table 7.5 for the axial response.

Table 7.4

Comparison of circumferential stress values for elastin and collagen in Pascal

Si1e [10^3]	Si1c [10^5]	Sm1e [10^3]	Sm1c [10^4]	Sa1e [10^3]	Sa1c [10^4]	St1e [10^3]	St1c [10^4]
0.4423	0.0385	0.3685	0.1127	0.4054	0.2785	0.3995	0.2361
0.4942	0.0457	0.4118	0.1395	0.4530	0.3144	0.4464	0.2776
0.5452	0.0543	0.4544	0.1693	0.4998	0.3552	0.4925	0.3259
0.7039	0.0961	0.5866	0.2919	0.6452	0.5285	0.6359	0.5436
0.8566	0.1760	0.7138	0.4781	0.7852	0.7967	0.7738	0.9198
0.9126	0.2230	0.7605	0.5729	0.8366	0.9328	0.8244	1.1282
0.9864	0.3084	0.8220	0.7289	0.9042	1.1554	0.8911	1.4927
1.0412	0.3960	0.8677	0.8743	0.9544	1.3604	0.9405	1.8532
1.0774	0.4694	0.8979	0.9880	0.9876	1.5190	0.9733	2.1480
1.1135	0.5580	0.9279	1.1176	1.0207	1.6981	1.0058	2.4967
1.1314	0.6091	0.9429	1.1892	1.0372	1.7963	1.0221	2.6948
1.1672	0.7272	0.9727	1.3478	1.0700	2.0117	1.0544	3.1465
1.1851	0.7954	0.9876	1.4356	1.0863	2.1299	1.0705	3.4040
1.2029	0.8707	1.0024	1.5297	1.1026	2.2558	1.0866	3.6855
1.2206	0.9539	1.0172	1.6306	1.1189	2.3899	1.1026	3.9936
1.2383	1.0458	1.0320	1.7389	1.1351	2.5327	1.1186	4.3311
1.2560	1.1474	1.0467	1.8552	1.1514	2.6850	1.1346	4.7012

Table 7.5

Comparison of collagen and elastin stress contribution in the axial direction in Pascal

Si2e	Si2c [10^5]	Sm2e [10^3]	Sm2c [10^3]	Sa2e	Sa2c [10^4]	St2e	St2c [10^4]
560.0333	0.1017	0.3685	0.1965	424.2676	1.1701	479.1679	0.6341
580.5420	0.1178	0.4118	0.2376	439.8045	1.2903	496.7152	0.7154
600.1643	0.1368	0.4544	0.2819	454.6699	1.4249	513.5042	0.8091
657.6730	0.2259	0.5866	0.4533	498.2371	1.9771	562.7090	1.2226
708.3264	0.3874	0.7138	0.6952	536.6109	2.7903	606.0484	1.9128
725.8134	0.4792	0.7605	0.8133	549.8587	3.1904	621.0104	2.2859
747.9917	0.6425	0.8220	1.0033	566.6604	3.8310	639.9862	2.9271
763.8331	0.8064	0.8677	1.1763	578.6615	4.4092	653.5403	3.5507
774.0407	0.9418	0.8979	1.3095	586.3945	4.8503	662.2739	4.0543
783.9791	1.1032	0.9279	1.4596	593.9236	5.3428	670.7773	4.6442
788.8508	1.1953	0.9429	1.5418	597.6143	5.6103	674.9456	4.9768
798.4059	1.4065	0.9727	1.7221	604.8529	6.1927	683.1209	5.7295
803.0917	1.5275	0.9876	1.8212	608.4028	6.5096	687.1301	6.1555
807.7180	1.6602	1.0024	1.9267	611.9075	6.8451	691.0884	6.6189
812.2859	1.8058	1.0172	2.0393	615.3681	7.2005	694.9967	7.1236
816.7965	1.9658	1.0320	2.1594	618.7852	7.5771	698.8561	7.6737
821.2511	2.1417	1.0467	2.2877	622.1599	7.9763	702.6674	8.2738

7.5 Validation of the optimisation Matlab code

This was done by repeating other published data. This was done in the following manner: First data [7] was chosen to agree with experiential technique used in the previous chapter, in particular in the form of biaxial testing of human coronary artery. This resulted in circumferential Cauchy stress relation with circumferential strain as well as axial Cauchy stress versus circumferential strain [7]. After that using a digitizing code by Matlab, the graphs with axial extension of 1.1 were imported into Matlab this was named the experimental data. Then the same code was applied to the experiential technique resulting in total error range of 0.08. This will be discuss in detail in the next section

7.5.1 Experimental technique

Human arteries were harvested from cadavers [7]. Segments of 2 cm length were harvested from the left anterior descending and circumflex coronary arteries. Arteries were tested in a medium containing Hank buffered saline. Then biaxial testing was applied by applying axial extension increments, then rapid inflation followed by preconditioning and then this was repeated for different extension ratios. Pressure versus diameter and pressure versus axial force were transferred to circumferential stress relationship with circumferential strain as well as axial stress versus circumferential strain using thin wall theory as presented earlier in chapter 5 and in[2, 8-11]]. The resulting curves are shown in figure 7.8.

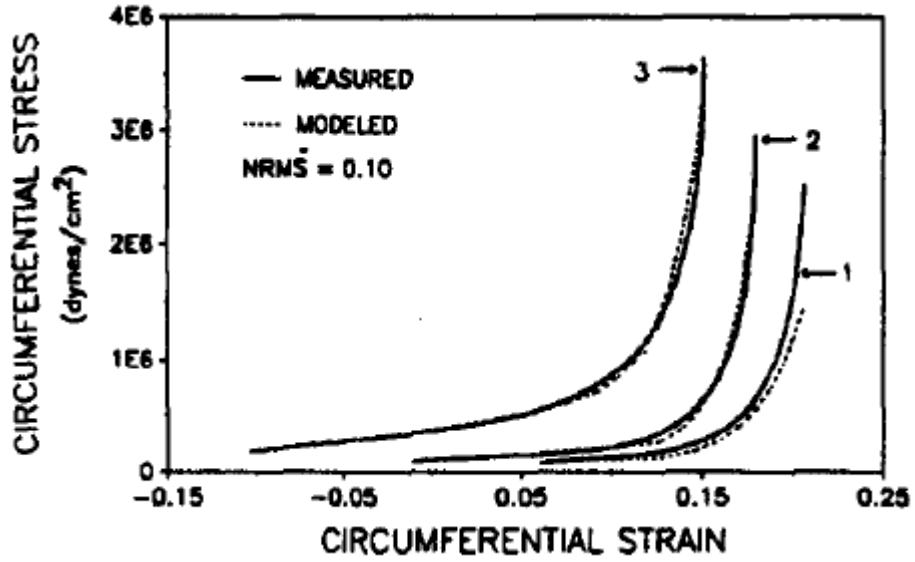

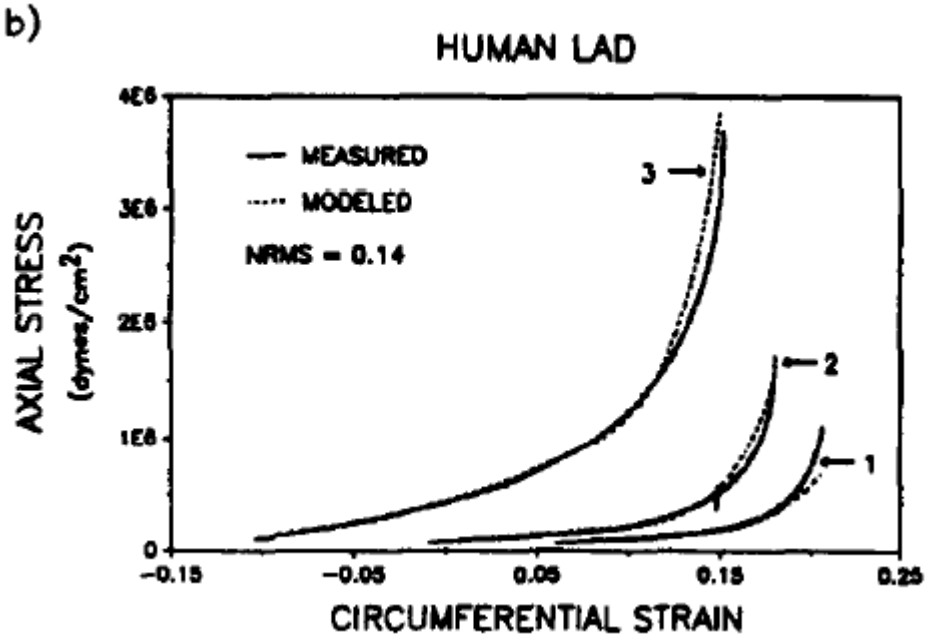

Figure 7.8: Experimental relationship for human coronary artery.

7.5.2 Optimisation

After that, optimisation was done in the same manner as presented in the previous chapter. The results are presented in figure 7.9. Error ranges were computed according to equations 6-8 and 6-9. This resulted in a total error range of 0.07 and the computed parameters are shown in table 7.6 and 7.7. The optimisation code is presented at the appendix.

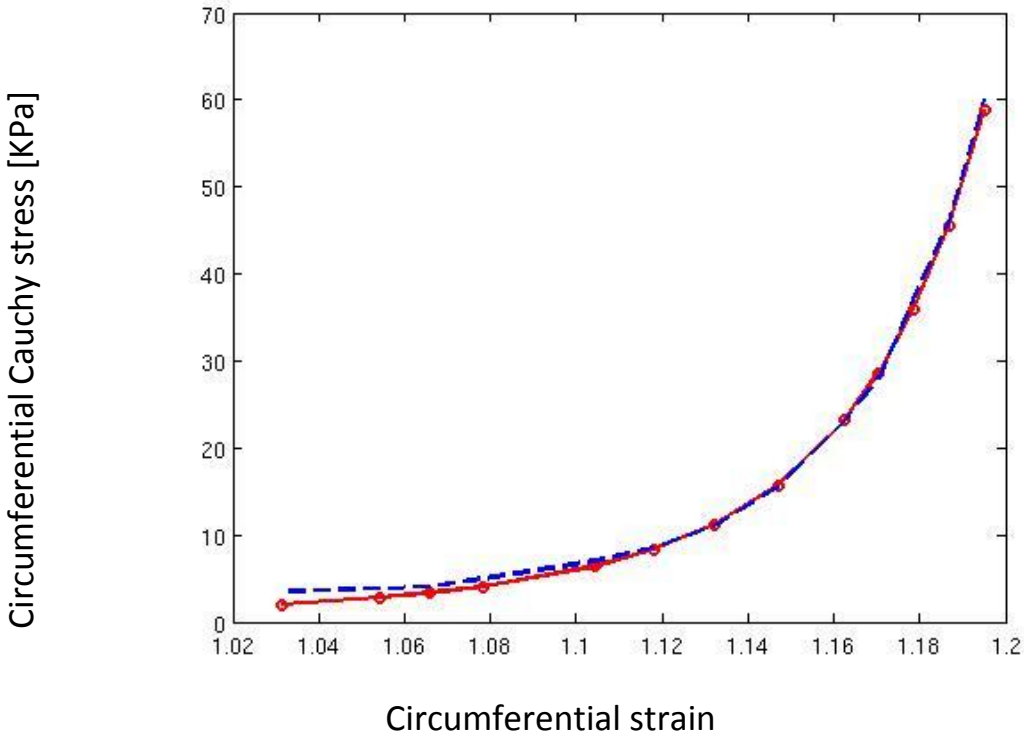

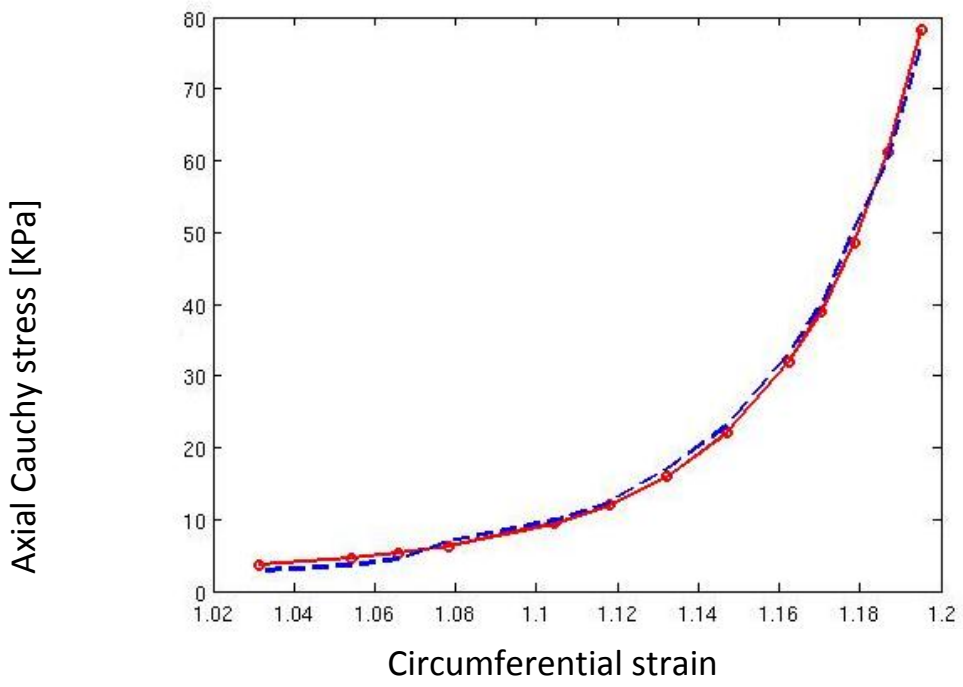

Figure 7.9 a) Circumferential stress is drawn versus circumferential strain b) Axial stress is shown. In both figures blue is used to represent the experimental technique while red id the model results

Table 7.6

Parameters of the coronary artery

Parameter	value
K2i	55.22
K2m	11.08
K2a	30.01
C1i [KPa]	4000
C1m [KPa]	400
C1a [KPa]	5500
K1i [KPa]	11817
K1m [KPa]	3700
K1a [KPa]	4305
rowi	0.58
rowm	0.15
rowa	0.55

Table 7.7

Collagen fibre angles (from the circumferential direction) for each layer for two vessels

Layer	coronary artery
Intima	52.62°
Media	16.81°
Adventitia	62.87°

7.6 Conclusions

In this chapter, models estimating the mammary artery and the vena cava responses were produced. It can be concluded that the model estimations of the whole wall and layer responses were consistent with both experimental data and current theories based on coronary artery

studies. Thus this provides some evidence that the model framework can be extended to estimate the layer response of vascular tissues with the similar material component responses i.e. elastin and collagen. Also, it could be applied to other organs such as the ventricle, but in that case different strain energy equations could be produced for each layer. It was also found that veins as arteries are stiffer axially than circumferentially. This might have an impact on the baroreceptors embedded in the walls of these vessels, as they could be more stimulated axially themselves.

7.7 References

1. van Andel CJ, Pistecky PV, and Borst C, *Mechanical Properties of Porcine and Human Arteries: Implications for Coronary Anastomotic Connectors.* Ann. Thorac. Surg., 2003. **76**(1): p. 58-64.
2. Holzapfel GA, Sommer G, Gasser CT, and Regitnig P, *Determination of Layer-Specific Mechanical Properties of Human Coronary Arteries with Nonatherosclerotic Intimal Thickening and Related Constitutive Modeling.* Am. J. Physiol. Heart Circ. Physiol., 2005. **289**(5): p. H2048-2058.
3. Holzapfel GA, Gasser T, and Ogden R, *A New Constitutive Framework for Arterial Wall Mechanics and a Comparative Study of Material Models.* J. Elast., 2000. **61**(1): p. 1-48.
4. Holzapfel GA, *Collagen. Structure and Mechanics*, in *Collagen in Arterial Walls: Biomechanical Aspects*, P. Fratzl, Editor. 2008, Springer-Verlag, Heidelberg: New York. p. 285-324.
5. Desch GW, *A Model for Passive Elastic Properties of Rat Vena Cava.* J. Biomech., 2007. **40**: p. 3130-3145.
6. Rossmann JS, *Elastomechanical Properties of Bovine Veins.* J Mech. Behave. Biomed. Mat, 2010. **3**(2): p. 210-215.
7. Carmines DV, McElhaney JH, and Stack R, *A Piece-Wise Non-Linear Elastic Stress Expression of Human and Pig Coronary Arteries Tested in Vitro* Journal of Biomechanics, 1991. **24**(10): p. 899-996.
8. Chuong CJ and Fung YC, *Three-Dimensional Stress Distribution in Arteries.* J. Biomech. Eng., 1983. **105**(3): p. 268-274.
9. Chuong CJ and Fung YC, *Compressibility and Constitutive Equation of Arterial Wall in Radial Compression Experiments.* J. Biomech., 1984. **17**(1): p. 35-40.
10. Fung YC, Fronek K, and Patitucci P, *Pseudoelasticity of Arteries and the Choice of Its Mathematical Expression.* Am. J. Physiol. Heart Circ. Physiol., 1979. **237**(5): p. H620-631.
11. Holzapfel GA, Eberlein R, Wriggers P, and Weizsäcker HW, *A New Axisymmetrical Membrane Element for Anisotropic,Finite Strain Analysis of Arteries.* Commun. Num. Meth. Eng., 1996. **12**(8): p. 507-517.

CHAPTER 8

A AND C TYPE RECEPTORS

---

8 Overview

The aim of this chapter is to investigate the relationship between the position of each nerve receptor and its stress response based on the baroreceptor type.

8.1 Stretch receptors

Research shows that there are two types of arterial baroreceptors, namely type A and type C. It was found that these two types have the same anatomical structure. These two types of baroreceptors fibres can be classified according to their threshold range (the lowest pressure that triggers an action potential) [1], a comparison between them is shown in table 8.1.

Table 8.1

A comparison between A-fibre and C –fibre [1]

Description	A-fibre	C- fibre
Diameter	Large	Narrow
Myelination	Myelinated	Non- myelinated
Threshold	Low 30 mmHg	High 70 mmHg
Number	Low	High
Conduction	Fast	Low
Activity at normal	All fibres are active	1/4 of the fibres are active
Sensitivity *	High	Low
Saturation**	Low	High
Sensitivity*: the mean discharge frequency of a baroreceptors increase with the mean blood pressure. Steepness (biggest slope of this response is called Sensitivity) Saturation ** : response to pressure		
Importance	High at low pressure	High at high pressure

A comparison between the curves of two fibres is shown in figure 8.1.

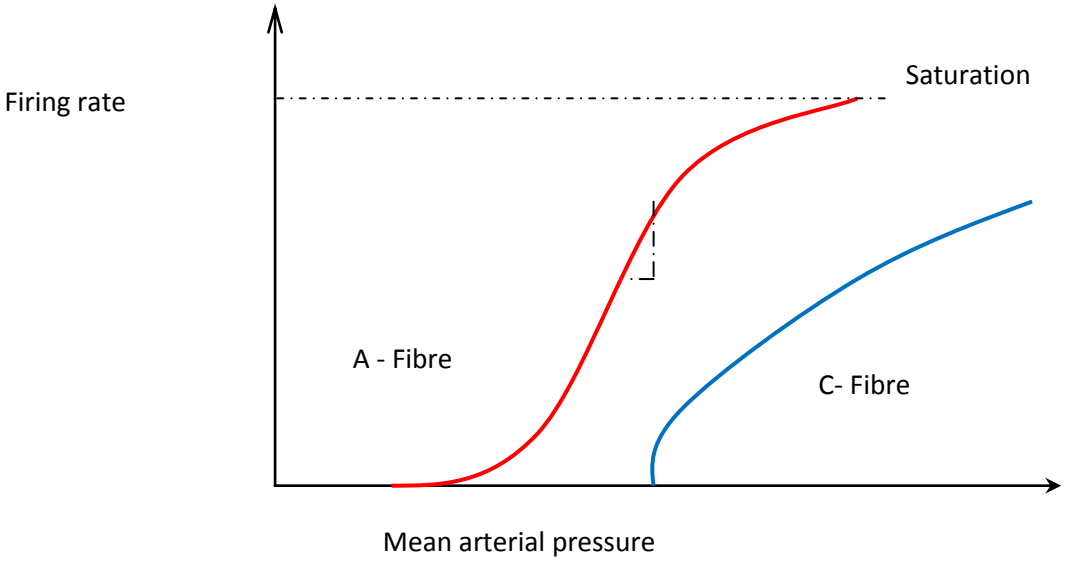

Figure 8.1: Response of single A- fibre and C-fibre to increasing pressure [1].

The question addressed in this chapter is: how can two fibres with the same anatomical structure have different firing pressure thresholds and thus operate in different pressure ranges?

The answer was hypothesised to be based on the location. The hypothesis was that there is a link between the position of the nerve receptor and its firing threshold and pressure range. This hypothesis was based on observations that baroreceptors location was layer specific, as this is stated in experimental observation shown in [2] [3].

To investigate this assumption, the strain-energy was calculated according to the following set of equations.

For each layer, the strain-energy, W_{ic}, is considered to be the linear combination of elastin and collagen contributions.

$$W_{ic}(\mathbf{E}, \mathbf{A}_1) = W_{iciso}(\mathbf{E_{ic}}) + W_{icaniso}(\mathbf{E_{ic}}, \mathbf{A}_1) \quad (1)$$

The form of the elastin strain-energy component $W_{iciso}(\mathbf{E_{ic}})$, is approximated to be

$$W_{iciso}(\mathbf{E_{ic}}) = \frac{c_1}{2}(I_1 - 3) \quad (2)$$

The first invariant of stretch , I_1, is defined as

$$I_1 = {\lambda_\theta}^2 + {\lambda_z}^2 + {\lambda_r}^2 \tag{3}$$

and c_1, is a material constant related to the elastin stress response.

The form of the collagen contribution can be described by

$$W_{icaniso}(\mathbf{E_{ic}}, A_1) = \frac{k_1}{k_2}(e^q - 1) \tag{4}$$

where k_1, and k_2 are material constants related to the collagen stress response and q is calculated to be

$$q = \rho_{disp} k_2 (I_4 - 1)^2 + (1 - \rho_{disp})(I_1 - 3)^2 \tag{5}$$

where ρ_{disp} is the dispersion factor. I_4 is the fourth stretch invariant given by

$$I_4 = \lambda_\theta^2 \cos(\phi)^2 + \lambda_z^2 \sin(\phi)^2 \tag{6}$$

The dispersion factor value represents the amount of dispersion from the ideal alignment of the fibres

Thus using, the above equations, the strain energy relation to circumferential stretch was calculated for each layer and compared with the energy needed for each type to operate. The result is shown in figure 8.2.

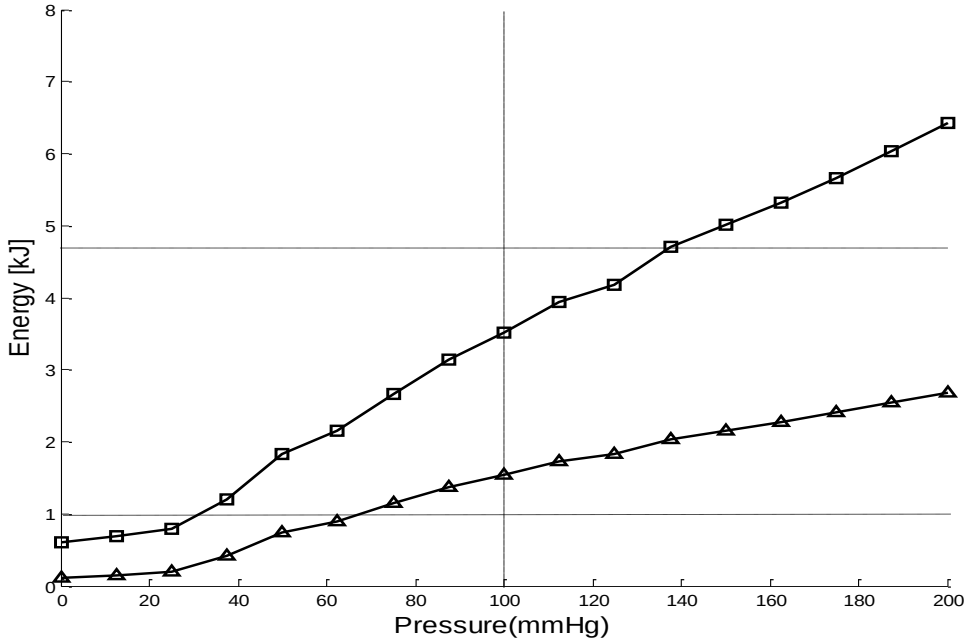

Figure 8.2: Estimated strain-energy for the adventitia (squares) and media (triangle) as a function of luminal blood pressure for the coronary artery.

Figure 8.2 suggests that at a given blood pressure, for example 100 mmHg, the strain-energy in the intima is highest (not shown) followed by adventitia and media [4-5] .To investigate the effect of firing rate from mechanoreceptors in each layer, all the receptors were considered to have the same arbitrary threshold strain-energy of around 1 kJ, with saturation occurring around 4.5 kJ. With these limits, the data suggests that mechanoreceptors in the adventitia would have a threshold blood pressure of around 30 mmHg and would saturate at around 140 mmHg. For the media, this scenario suggests receptors here would start firing at around 70 mmHg and do not saturate. Only the media and the adventitia are considered because histological studies [6] [7] suggest that mechanoreceptors do not exist in the intima. This data is an estimate with root mean square error for the three layers being shown to be as great as 0.05 for the media and the adventitia. However, this study does present some evidence that suggests C-fibres could be predominantly located in the more elastic regions such as the media with A-fibres predominantly in the stiffer regions such as the adventitia [4]. Further experimental studies would be needed to investigate this further.

8.2 Conclusions

A relationship between the location of each nerve receptor fibre and its nerve ending was suggested , such that, type A fibres were suggested to be located in the stiffer layer the adventitia, also type C fibres were suggested to operate in the medial layer. Further histological investigations are required. However this is a significant finding, as it solves the dilemma, of having two types of basically identically fibres but with different thresholds. The finding here suggest that the threshold is location controlled.

8.3 References

1. Levick JR, *An Introduction to Cardiovascular Physiology*. 2003, London: Hodder. 384.
2. LANDGREN S, *On the Excitation Mechanism of the Carotid Baroceptors.* Acta Physiol. Scand., 1952. **26**: p. 1-34.
3. KIRCHHEIM HR, *Systemic Arterial Baroreceptor Reflexes.* Physiol. Rev., 1976. **56**: p. 100-176.
4. Mickael M, Heydari A, Crouch R, and Johnstone S, *Estimation of Stress-Strain Relationship in Vascular Walls Using a Multi-Layer Hyperelastic Modeling Approach*, in *Cinc2010*: Belfast.
5. Mickael M, Heydari A, Crouch R, and Johnstone S. *Mechanical Properties of Arterial Walls: Do They Play a Role in Determining Stretch Receptor Firing Rates?* in *ICABB-2010*. Venice.
6. Wolfgang K, *Three Types of Neurochemically Defined Autonomic Fibres Innervate the Carotid Baroreceptor and Chemoreceptor Regions in the Guinea-Pig.* Anat Embryol, 1990. **181**: p. 477-489.
7. Chapleau MW, Li Z, Meyellers S, Ma X, and . Abboud F, *Mechanisms Determining Sensitivity of Baroreceptor Afferents in Health and Disease.* Ann N Y Acad Sci, 2001. **940**: p. 1-19.

CHAPTER 9

CONCLUSIONS

---

9 Overview

This chapter will focus on the conclusions of the research presented in the thesis. The main aims of this research were to understand various types of experimental data applied to the arterial wall, also to calculate the whole wall stress response using nonlinear solid mechanics as well as calculating layer arterial wall stress response. This was done using a simple model that connects the whole wall and the layer response using thin wall theory. The knowledge that has been gained through the previous process was used to differentiate various baroreceptors types based on their location. The finding of this research will be presented in the following section.

9.1 Main conclusions

Through this research it became clear that the structure, where the baroreceptors are embedded in have a high degree of effectiveness on its function. Thus, the role of elastin and collagen was investigated and it became evident that collagen dominates the stress response especially at high pressures. This was true for both the layers (intima, media and adventitia) as well as the whole wall response. In order to mathematically evaluate the role played by each constituent of the wall a hyperplastic exponential model was chosen. This model was in particular chosen because of the low error range it provides, in addition to the intrinsic relationship between the model components strain energy and the model parameters. The model was built up of layers equations this enabled taking into consideration the different mechanical properties forming the wall in order to get the best results. These layers equations were connected together using thin wall

theory that was proven to be sufficiently accurate to represent the stress strain relationship. The model was also shown to be valid based on mechanical concepts as conservation of mass, balance of linear momentum, the assumption of incompressibility of hyperelastic materials. To solve the problem of uncertainty of parameters Levenberg-Marquardt method was used in conjunction with Mont Carlo method. A one way sensitivity analysis (nominal range sensitivity method) was also performed. Analysis of the model results estimations were made, an error of 0.05 was achieved between the calculated analytical model using the constitutive equation and the experimental results. The sensitivity analysis confirmed that the highest effecting parameter is the collagen fibre angle and the least effecting parameter is the elastin. It was evident that collagen controls stresses at higher pressure and is the material responsible for the exponential shape of the stress strain relationship both for the layer and the whole wall curves. The same concept was applied with the mammary artery and the vena cava. It can be concluded that the model estimations of the whole wall and layer responses were consistent with both experimental data and current theories based on coronary artery studies. Thus this provides some evidence that the model framework can be extended to estimate the layer response of vascular tissues with the similar material component responses i.e. elastin and collagen. Also, it could be applied to other organs such as the ventricle, but in that case different strain energy equations could be produced for each layer. It was also evident that the structure of the blood vessel wall has an important functional role, as the intima is the stiffest layer axially and circumferentially, followed by the adventitia then the media. Both the intima and adventitia are stiffer axially than circumferentially, this protects the elastic media from rupture. Based on these findings a relationship between the location of each nerve receptor fibre and its nerve ending was suggested. Type A fibres were suggested to be located in the stiffer layer the adventitia, also type C fibres were suggested to operate in the medial layer. Further histological investigations are required. However the finding here is rather significant, as it solves an old research question about the reason the threshold and the saturation ranges of the A and C fibres differ although they are identical from a histological point of view. It was also found that the adventitial baroreceptors may be more axially stimulated than circumferentially as this is the direction of maximum stress.

CHAPTER 10

FUTURE WORK

---

10 Overview

This section will focus on future work that could be done to extend the work done presented by this research, through using other modelling techniques as well as on finding experimental links between the location of the baroreceptors, its strain energy and the rate of fibre firing.

10.1 Improvements in the modelling techniques

Levenberg Marquardt, optimisation was used in this research in conjunction with Monte Carlo technique. However, in order to account for uncertainty that exists in the model structure. Other techniques could be used such as Latin hypercube method. This will be discussed in the following section.

10.2 Latin hypercube sampling (LHS)

Latin hypercube sampling (LHS) is a form of stratified sampling that can be applied to multiple variables. Stratified sampling is a method of sampling from a population[1]. The idea behind stratified sampling is dividing a population into subgroups and then samples them independently. It is done in a way that every element is assigned to only one stratum. A stratum is a homogenous group. The advantage of using such a method is reducing sampling error and increasing representativeness. This happens in a way such that weighted mean has less variability than the arithmetic mean of a simple random sample.

The concept behind Latin hypercube is that variables are sampled using an even sampling method and the random set of variables are combined then they are used in one calculation for the target function. The sampling algorithm ensures that the distribution function is sampled evenly, but still

with the same probability trend. Figure 10 shows the difference between a pure random sampling method (Monte Carlo) and a stratified sampling of a log-normal distribution.

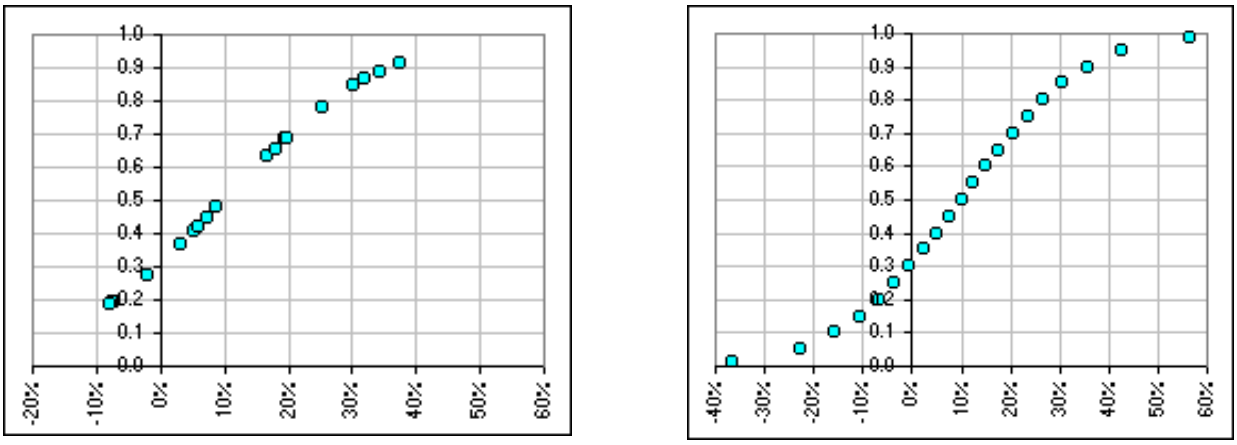

Figure 10.1: Mont Carlo method compared with the Latin hypercube method

It could be observed that When Monte Carlo method suffers from missing outliers which exist on the tails of the distribution; the Latin hypercube covers this range. The process of performing Latin hyper cube is involves 2 stages, sampling and then grouping. The next section will cover these two steps in detail.

10.2.1 Sampling

For each iteration, the cumulative probability is divided into segments, and then a probability is randomly chosen within each segment using a uniform distribution[2]. Thus for example, a simulation with 500 iterations will be divided to 500 segments each representing 0.2% of the total distribution. Then for the first segment a number would be chosen between 0 % and 0.2% and the second segment will be between 0.2 and 0.4%. This number will be used to calculate the parameter.

10.2.2 Grouping

Once each variable has been sampled using this method, a random grouping of variables is selected for each iteration [3]. Independent uniform selection is done on each of the variable's generated values. Each value must only be used once.

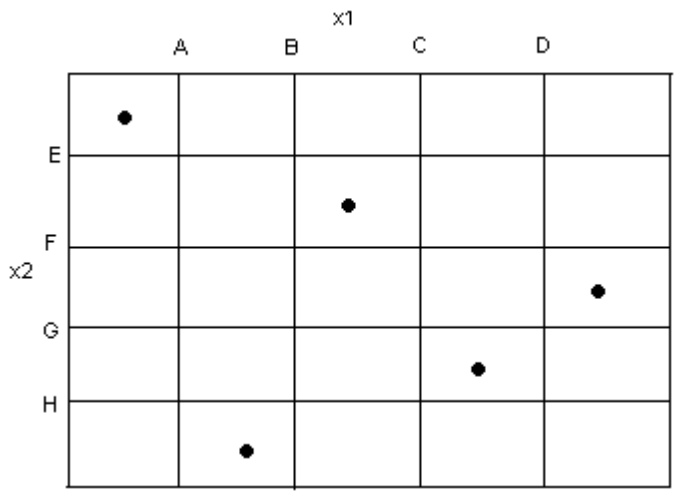

Figure 10.2: Grouping when n =5 , it could be noted that one element is chosen from each segment and from each iteration (column and row respectively)

10.2.3 Syntax

Latin hypercube could be generated in Matlab using:

lhsdesign - Latin hypercube sample

X = lhsdesign(n,p)

`X = lhsdesign(n,p)` generates a latin hypercube sample `X` containing `n` values on each of `p` variables. For each column, the `n` values are randomly distributed with one from each interval `(0,1/n)`, `(1/n,2/n)`, ..., `(1-1/n,1)`, and they are randomly permuted.

10.3 Link between firing rate and location in the arterial wall

It was suggested in chapter 8, that there is a link between the position of the baroreceptors and its strain energy. However it is not yet clear, if there is a relation between the location of the baroreceptors and its firing rate. Thus a need for an experimental protocol to determine the degree of confidence in this hypothesis is needed. This experimental protocol could be as follows:

10.4 Components of the Experimental Protocol

In the following section the main constituents of the experimental protocol will be shown, namely; the purpose, the materials used the methods and the data interpretation methods.

10.4.1 Purpose

The purpose of this experimental protocol is to determine if the hypothesis that there is a link between strain energy and firing rate in different arterial walls layers is true or false.

10.4.2 Materials

Sections of carotid arteries, stress applying apparatus, nerve signal measuring apparatus are to be used as shown in figure 10.1 and figure 10.2.

10.4.3 Methods

In vitro stress-strain relationship will be generated. Sections of carotid arteries containing baroreceptors could be dissected from swine. After removing connective tissue; intima, media and adventitia should be separated. Then these separate segments could be mounted in the biaxial apparatus shown in figure 10.1. This apparatus is a biaxial loading (radial pressure and axial force), biaxial measuring (diameter, axial extension) device [4]. It is also connected to means of measuring and recording the nerve signal. This could be another apparatus that has on chip electrodes as shown in the schematic figure 10.2 [5]. The experiment is set in the following way: pressure and axial force will be applied to the arterial segment in a manner that enables controlling the strain energy gradient. Nerve signal generated from these separate arterial wall segments wall would be recorded through the electrode on chip apparatus.

10.4.4 Data Interpretation

After that data will be plotted, fitted and related to the strain energy. In this way, the hypothesis that there is a relation between location and firing rate could be proven. Statistic analyses could also be made to compare experimental results. In this way complete assessment of the two phases of the baroreceptors function could be made [6].

In the last section an experimental protocol for linking strain energy and action potential was presented. In the following section, the functions of the two main devices will be summarised.

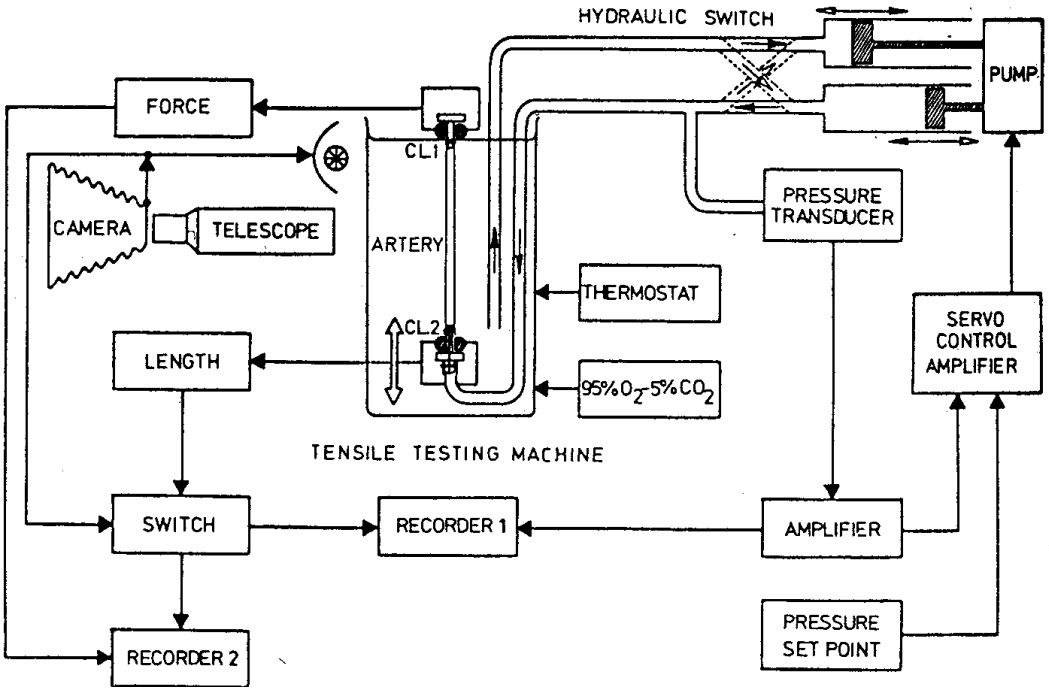

Figure 10.1: Biaxial loading, biaxial measuring apparatus[4].

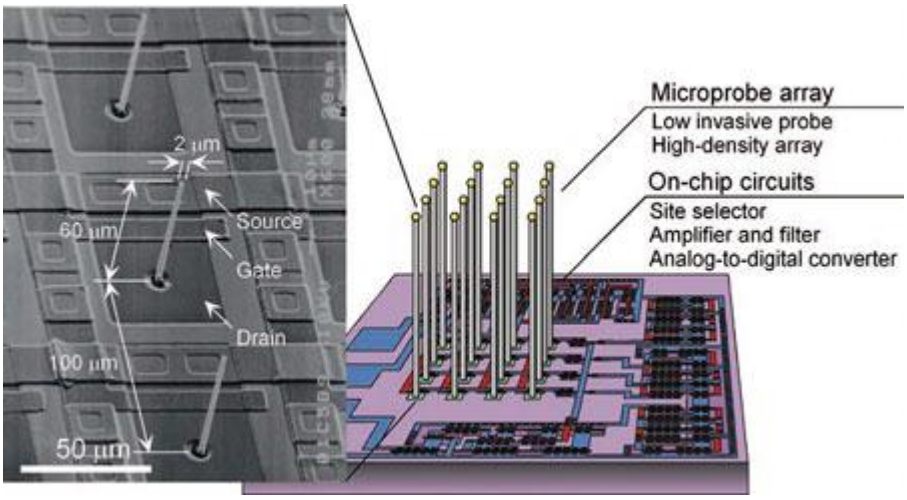

Figure 10.2: Microprobe array based neural interface device[5, 7].

10.5 Devices used

The device shown in figure 10.1 was used by Weizasacker and colleagues [4]. As could be seen from the figure, the artery is mounted in a tank full of saline. After that, it is closed from one end and then stretched to its in vivo length. Pressure is then applied radially and pressure, radius and axial force are recorded in a steady state manner.

The device shown in figure 10.2 could be that is used as an interface between neurons and microelectrodes. It consists mainly of a silicon probe arrays with diameters of 2–3.5 μm and lengths of 60–120 μm. These probes are manufactured by a technique called elective vapour–liquid–solid (VLS) growth and they allow identifying the nerve signal and measure accurately its magnitude.

10.6 References

1. Heltona JC and Davis FJ, *Latin Hypercube Sampling and the Propagation of Uncertainty in Analyses of Complex Systems.* Reliability Engineering and System Safety, 2003. **81** p. 23-69.
2. Iman RL, Helton JC, and Campbell JE, *An Approach to Sensitivity Analysis of Computer Models, Part 1. Introduction, Input Variable Selection and Preliminary Variable Assessment.* Journal of Quality Technology, 1981. **13**(3): p. 174-183.
3. Keramat M and Richard Kielbasa R, *Latin Hypercube Sampling Monte Carlo Estimation of Average Quality Index for Integrated Circuits.* Analog Integrated Circuits And Signal Processing, 1997. **14**(1/2): p. 131-142.
4. Weizsacker HW, Lambert H, and Pascale K, *Analysis of the Passive Mechanical Properties of Rat.* J. Biomech., 1983. **16,**: p. 703-715.
5. Kawanoa T, Harimotoa T, Ishihara A , Takeia K, Kawashimab T, Usuid S, and Ishidaa M, *Electrical Interfacing between Neurons and Electronics Via Vertically Integrated Sub-4microm-Diameter Silicon Probe Arrays Fabricated by Vapor–Liquid–Solid Growth.* Biosensors and Bioelectronics, 2010. **25**(7): p. 1809–1815.
6. Nicholis J , Martin AR, Wallace BG , and Fuchs PA, *From Neuron to Brain: A Cellular and Molecular Approach to the Function of the Nervous System*. 4th ed. 1993 Sunderland: Sinauer 679.
7. Takei K, Kawano T, Kawashima T, Sawada K, Kaneko H, and Ishida M, *Microtube-Based Electrode Arrays for Low Invasive Extracellular Recording with a High Signal-to-Noise Ratio.* Biomedical Microdevices, 2010. **12**(1): p. 1387-2176.

Estimation of Stress-Strain Relationships in Vascular Walls using a Multi-Layer Hyperelastic Modelling Approach

Michel E Mickael[1], Abbas Heydari[2], Roger Crouch[1], and Sherri Johnstone[1]

[1]School of Engineering, Durham University, UK, [2] School of Biological Science, Durham University, UK

Abstract

Determining the stiffness (or compliance) of biological vascular vessels is of importance when investigating pathological conditions, the design of stents, vascular grafts, distal anastomotic connectors in coronary artery bypass surgery, and understanding of biological pressure sensors. This communication is concerned with determining appropriate values of the material constants associated with a layered anisotropic hyperelastic constitutive model to estimate the mean stress for arterial and venous walls. Results show that the values of the material constants, determined from a constrained optimization approach, satisfying equilibrium, give rise to mean stress-strain states which are consistent with responses obtained from the standard averaged model.

1. Introduction

Understanding the stress-strain relationship for cardiovascular vessels could have a major impact on studying diseases such as arteriosclerosis and atherosclerosis. It could also help in designing vascular grafts. The authors are particularly interested in applying such information to investigate baroreceptors. These are pressure sensors that report blood pressure to the CNS. The process of their operation is divided into two main phases[1]. Firstly, blood pressure applied to the vascular wall is transferred into a strain which then controls the opening probability of many mechanosensitive ion channels. These are embedded into the vascular wall[1]. Their exact positions are disputed. Studying stiffness contributions from different layers of the arterial and venous walls, as well as the mean stress for the wall, would help in understanding the function and the process of operation of this type of biosensor. For the arterial wall, there have been various attempts to model the stress-strain profile using different assumptions.

For example, one may use thin-walled cylinder theory to determine the average axial and circumferential stresses given the axial force and internal pressure .In this model, it is assumed that the strain (axial stretch and circumferential stretch) across the wall is constant. Using this simplified approach, the average stress-strain behaviour can be determined. We refer to this approach as the standard averaged model. Alternatively, one could begin with the assumption of a uniform strain field across the wall of the vessel, but now employ a constitutive model (appropriate for the wall material) to determine the stresses. The material constants satisfy structural equilibrium (that is, the sum of the stress-area products equals the applied forces). This is the approach presented here.

2. Modelling Approaches

The arterial and venous wall consists of three concentric cylindrical layers; innermost layer; intima, middle layer; media and outermost layer; adventitia. The layers behave as transversely isotropic homogeneous nearly incompressible hyperelastic materials in which a strain-energy function, W, is assumed to exist [2]. The arterial wall extends passively, but the smooth muscle controls the active tension of the vessel. Forming a model for thin wall arterial response, Holzapfel et al [3] presented a two term strain-energy function that used experimentally obtained elastin and collagen responses to model passive extension. The effect of smooth muscle cells was neglected as it was thought that these do not contribute to the passive stiffness. Only elastin and collagen were considered as the constituents which act during the extension of the arterial wall. However, that model did not consider the specific responses for the individual layers constituting the arterial wall. Von Maltzahn et al [4] measured experimentally the elastic properties of the media and adventitia.

it did not include the role of the intima, which has been proven to be of significant importance [2]. In [5] Demiray and Vito used a two layer model, neglecting the role of the intima. The media was considered orthotropic, while the adventitia was considered isotropic. The relationship between the two layers and the whole structural stress was not presented. In [2] Holzapfel et al presented layer specific strain-energy equations assuming arterial layers. No mean relationship for the stress-strain response of the whole wall was given. The question addressed in this paper is, 'given the axial and circumferential stretches in arteries and veins, how can we develop a model to predict the overall stiffness?' To answer this, a layered approach in conjunction with a hyperelastic anisotropic material model and thin wall theory were used here. This model gives a basis for comparison between different arteries of different species and of different materials. It is assumed that the strain-energy function of the venous wall is of a similar form to that of the arterial wall [6]. The percentage thickness of each layer with respect to the total wall thickness is assumed to be the same for each vessel. Experimental findings by others have revealed the percentage thicknesses to be approximately 27%, 40 % and 33 % for the intima, media and adventitia respectively [2].

3. Experimental Data

There are few papers reporting on the deformation of the arterial wall [2]. Literature containing experiments which compare the response of the whole wall and the single layer response are not available. Some of the data which exists is not in a form useful for the stress–strain analysis. For example, [7] investigates the static pressure-diameter relationship but does not show the axial force relationship with pressure. The arterial experimental data used here were extracted from an investigation carried out by Van Andel et al [8]. That work presented graphs representing the external diameter relationship versus luminal pressure together with the axial force relationship versus the luminal pressure for different arteries. Data for a coronary artery and a mammary artery have been chosen here. A summary of their experimental setup is given. Different arteries were dissected from arteriosclerotic cadavers. Static pressure tests were then carried out after the application of an axial pre-stretch to pre-conditioned arteries. The external diameter and corresponding axial force were then measured.

Experimental data for the vena cava was sourced from Desch et al [6]. We digitised the data sets from those papers using 17 points across the pressure range and imported them into the models for this investigation.

4. Thin Wall Theory

Thin wall theory can be applied when the thickness/ radius ratio is less than a tenth. However, Holzapfel et al in [3] used thin wall theory to represent the circumferential and axial responses. The rationale for this was that as all collagen fibres are embedded in the tangential surface of the tissue, it can be assumed that there are no components in the radial direction [2]. In this case only circumferential and axial stresses become relevant. Thin wall theory offers a simple approximation for the relationship between mean circumferential and axial Cauchy stresses. Its named here the standard model.

5. Hyperelastic Model

Here we describe the form of the hyperelastic constitutive equations. These are based on the theory presented by Holzapfel et al [2]. The equations are used to calculate the specific stress responses for each layer as functions of circumferential and axial stretch. Thin wall theory was applied to calculate the mean wall stress both circumferentially and axially. To find the relationship between the second Piola-Kirchhoff stress tensor, **S**, and Green-Lagrange strain tensor, **E** the concept of a strain-energy function, W is used

$$\mathbf{S} = \frac{\partial W}{\partial \mathbf{E}} \tag{1}$$

The Cauchy stress tensor, **σ**, can be calculated from the second Piola-Kirchhoff stress tensor, **S**, using the inverse Piola transformation. Using the Lagrangian multiplier, a relationship is derived between the total strain-energy and the volumetric, U(J) and isochoric components, W_{ic} (**E**, A_1). Assuming the vascular walls to be incompressible, and that the total strain-energy is a function of the Green-Lagrange strain tensor representing one family of collagen fibres, thus:

$$W\ (\mathbf{E}, \text{A}_1) = \text{U(J)} + W_{\text{ic}}\ (\mathbf{E}\ , \text{A}_1) \tag{2}$$

$$A_1 = a_i \otimes a_i \tag{3}$$

$$a_i = \begin{pmatrix} 0 \\ cos\,\varphi \\ sin\,\varphi \end{pmatrix} \quad (4)$$

φ is the angle between collagen fibre orientation and the circumferential direction. Assuming no change in volume,

$$U = P(J-1) \quad (5)$$

where P has the units of hydrostatic pressure. Thus the Green-Lagrange strain-stretch relationship is given by

$$E_i = \frac{1}{2}(\lambda_i^2 - 1) \quad (6)$$

where λ_i is the principal stretch. For each layer, the strain-energy, W_{ic}, is further divided to two parts representing the response of elastin and collagen. The elastin strain-energy component $W_{iciso}(\mathbf{E})$, is approximated to be

$$W_{iciso}(\mathbf{E}) = \frac{c_1}{2}(I_1 - 3) \quad (7)$$

where , I_1 is the first invariant of stretch and c_1, is a material constant related to the elastin stress response. The collagen component can be described by

$$W_{icaniso}(\mathbf{E}, A_1) = \frac{k_1}{k_2}(e^q - 1) \quad (8)$$

where k_1, and k_2 are material constants related to the collagen stress response. q is a function of the dispersion factor, taken here to be equal one, and I_4 is the fourth stretch invariant. The dispersion factor value represents the amount of dispersion from the ideal alignment of the fibres [2]. A value of unity assumes that there are not any fibres oriented in the φ direction. For a value of zero the fibers are assumed to be isotropically oriented as presented by Demiray et al [5]. Thus for the intima (n)

$$q_n = k_{2n}(I_{4n} - 1)^2 \quad (9)$$

$$I_{4n} = \lambda_\theta^2 cos^2(\varphi_n) + \lambda_z^2 sin^2(\varphi_n) \quad (10)$$

Similar expressions can be obtained the media and adventitia. This paper proposes using stress equilibrium in the wall to calculate the mean wall Cauchy stress components, $\sigma_{t\theta}$ and σ_{tz} in the circumferential and axial directions. h is the wall thickness after deformation.

$$\sigma_{t\theta} = \frac{(\sigma_{\theta n}h_n + \sigma_{\theta m}h_m + \sigma_{\theta a}h_a)}{h} \quad (11)$$

$$\sigma_{tz} = \frac{(\sigma_{zn}h_n + \sigma_{zm}h_m + \sigma_{za}h_a)}{h} \quad (12)$$

6. Results and Discussion

Optimisation of the hyperelastic model data was achieved using the Levenberg–Marquardt method with a root mean square error function provided by Matlab®. Parameter sensitivity analysis was investigated for the material parameters of the coronary artery. Figure1 presents the inferred layer circumferential Cauchy stress-stretch profiles for circumferential Cauchy stresses.

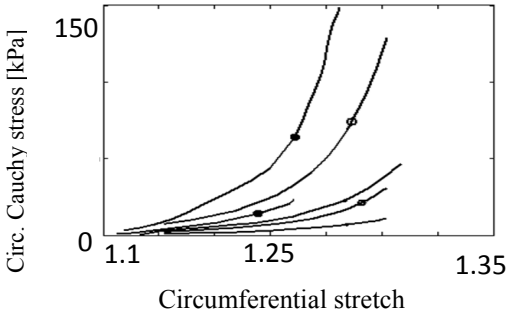

Figure 1: Hyperelastic model estimations of circumferential stress-stretch for coronary artery, for intima (large open symbol), adventitia (middle open symbol) and media (small symbol). An example of a Holzapfel et al coronary model response is indicated by the filled symbols [6].

These stress-strain profiles confirm the layers have the same order of stiffness as Holzapfel et al [2] Von Maltzahn et al [4] and Demiray et al [5] .The model was constrained by relationships which can be explained by experimental evidence; these constraints are as follows:

Circumferentially and Axially:	$k_{intima} > k_{adventitia} > k_{media}$
For the intima:	$k_{axial} > k_{circumferential}$
For the media:	kcircumferential > kaxial
For the adventitia:	kaxial > kcircumferential
Fibre orientation:	φintima > φadventitia> φmedia

k represents the stiffness. Material parameters presented by Holzapfel et al [2], were used as a guide to obtaining the material parameters used here (figure 2).The collagen material parameters are the most sensitive. In terms of layer response, the media possesses the lowest parameters value. The intima, being the stiffest layer has the parameters with highest sensitivity.

The hyperelastic model (figure 3) has been shown to estimate the stress-strain profiles with root mean squared errors of 0.05.

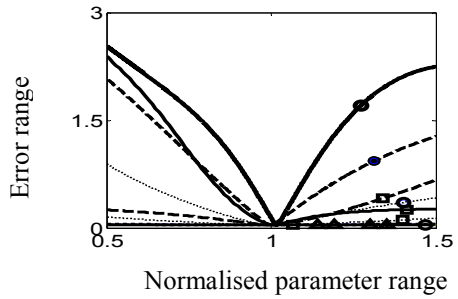

Figure 2: Parameter sensitivity of the coronary artery. A thick continuous line is used for the angle; a thick dashed line for k_2, a thin dashed line for k_1 and c_1 is drawn using a thin continuous line. The intimal layer is represented by a circle, the adventitial layer by a square and medial layer by a triangle.

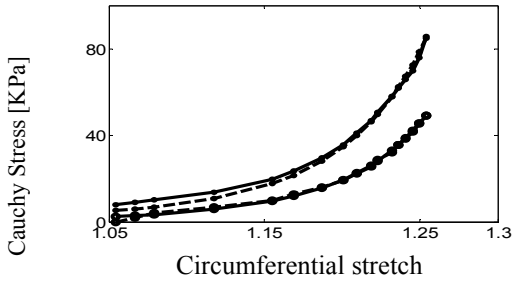

Figure 3: Comparison of the mean stress strain relationships for the axial (small symbol) standard model (dotted) and hyperelastic model (line).

This compares well with Holzapfel et al's [2] prediction of 0.07. At low pressure, the model fit was not so good. It is assumed that elastin is first stretched, while collagen attracts load at higher stretches. Improving the model of the elastin behaviour could increase the quality of the overall fit [9]. collagen contribution to the mean stress is far greater than the elastin for all the three layers [2].This indicates that, in terms of load-carrying capacity, vascular vessels are collagen dominated. Figure 4 shows that the vein is softer than the all arteries investigated both axially and circumferentially. Both the standard and hyperelastic models indicate that the maximum extension ratio for the vena cava is much bigger than that of the arteries (Figure 4). Venous parameters are lower than the arterial ones. These models could be used to design parameters of synthetic stretch receptors and vascular grafts [6] and studying vascular diseases.

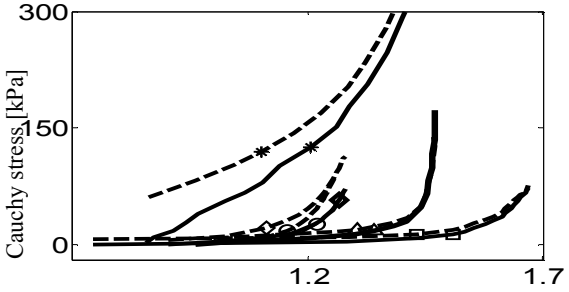

Figure 4: Comparison of mean stresses for abdominal aorta (star) [8], mammary (diamond), coronary (circle), and rat tail artery (triangle) [6] vena cava (square), in both axial (dashed line) and circumferential (continuous line) directions. Axial stretches are 1.66, 1.2, 1.1, 1.29, and 1.91 respectively.

7. Acknowledgements

The author would like to thank the Engineering and Physical Sciences Research Council (ESPRC) for funding this research (EP/F01189X/1) and also thank Dr Susan Pyner , Dr Ritu Kataky for their help and advice .

10. References

[1] Srinivasan R and N. HB., "Modeling the Carotid Sinus Baroreceptor,". *Biophys J. ,* vol. 12, pp. 1171-1182, Sep 1972.

[2] Holzapfel GA*, et al.*, " Determination of layer-specific mechanical properties of human coronary arteries with nonatherosclerotic intimal thickening and related constitutive modelling" *Am J Physiol Heart Circ Physiol,* vol. 289, pp. H2048–H205, 2005.

[3] Holzapfel GA *, et al.*, " New axisymmetrical membrane element for Anisotropic Finite Strain.," *Analysis of Arteries.Comm. num methods in eng. ,* pp. 507-517, 1996.

[4] Von Maltzahn WW and Besdo D. Wiemer W, "Elastic properties of arteries: a nonlinear two-layer cylindrical model," *J Biomech,* vol. 14, pp. 389-397, 1981.

[5] Demiray H and Vito RP, "A layered cylindrical shell model for An aorta " *J Biomech,* vol. 5, pp. 309–311, 1991.

[6] Desch GW and Weizsäcker HW, "A model for passive elastic properties of rat vena cava," *J Biomech,* vol. 2007, pp. 3130–3145.

[7] Gow BS and Hadfield CD, "Changes in the elasticity of canine and human coronary arteries with reference to postmortem," *Circ. Res,* vol. 45, pp. 588-594, 1979.

[8] Van Andel C*, et al.*, "Mechanical properties of porcine and human arteries: Implications for coronary anastomotic connectors," *Ann. Thoracic Surg,* vol. 76, pp. 58-64, 2003.

[9] Watton PN*, et al.*, "Modelling the mechanical response of elastin for arterial tissue," *J Biomech.,* vol. 42, pp. 1320-1325, 2009.

Address School of Engineering , Durham Univesisty DH1 3LE

Mechanical properties of arterial walls: Do they play a role in determining stretch receptor firing rates?

M Mickael, A Heydari, S Pyner, R S Crouch, and S Johnstone

***Abstract*-This paper presents a hyperelastic model which estimates the stress-strain profile in the three layers of the coronary artery: the intima, media and adventitia. The model, based on averaged experimental data confirms that the most elastic layer is the media followed by the adventitia and then the intima. This data was used to investigate the possibility that a contributing factor to the difference in the threshold blood pressures of mechanoreceptors associated with A- and C-fibres in arterial walls is due to their location within the wall. The results suggest that receptors associated with C-fibres could be predominantly located in the more elastic tissue such as the media whilst those associated with A-fibres are in the stiffer layers such as adventitia**.

Key words
Stress, strain, energy, arterial wall, fibres, saturation, sensitivity, coronary artery, baroreceptor, mechanoreceptors, lower threshold

1 INTRODUCTION

This paper presents a mathematical model to aid in the understanding of how blood pressure is measured in arteries and transferred to the central nervous system, CNS, for regulation of the cardiovascular system. The model is then used to investigate whether the location of the receptors which transmit signals to the CNS about blood volume and pressure affects their thresholds.

It has been histologically shown [1] [2] that mechanoreceptors are embedded within arterial and venous walls. These transmit afferent signals to the CNS about blood pressure and volume. Pressure receptors that exist in the arterial system are known as baroreceptors and have been classified into two types: A- and C-fibres. A-fibres are myelinated resulting in higher spike conduction speeds, whereas C-fibres are unmyelinated and slower. However, myelination does not explain the difference in the threshold value of the blood pressure required to activate the many receptor endings nor their sensitivities. It has been shown [3] that A-fibres have a conduction range in the region of 30-90 mmHg whilst type C have a range of 70-140 mmHg.

This investigation explores the relationship between blood pressure and strain energy in each of the three layers of a coronary arterial wall. This is used to test the assumption that the threshold and sensitivity of the firing rate of mechanoreceptors is affected by the material properties of the tissue in which they are embedded.

2 STRUCTURE OF ARTERIAL WALL

Histological data [4] suggests the coronary arterial wall is composed of three layers as shown in Figure 1; the intima(inner layer); media (middle layer) and adventitia (outer layer). For the model, they are assumed to be concentric cylinders which are transversely isotropic, homogeneous, nearly incompressible, hyperelastic materials in which a strain-energy function, *W*, is assumed to exist [5-7].

The histological evidence to support these assumptions is outlined in this section.

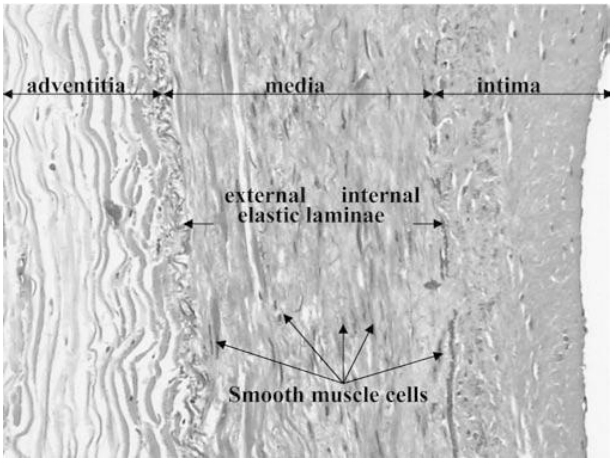

Figure 1: The layered structure of the coronary arterial wall [4]

2.1 INTIMA

The intima is composed of a layer of endothelium cells, a sub-endothelial layer which is formed of dispersed collagen fibers (Type I and III), dispersed smooth muscle cells [8] and elastin. Unlike collagen and smooth muscle cells, elastin is arranged in a three-dimensional network of elastic fibers. It is suggested that it is the mechanically dominant layer [5]. This may be due to the existence of a high content of collagen. It has a typical thickness of 27% with respect to the total wall thickness [5].

2.2 MEDIA

The media consists of a three-dimensional network of bundles of collagen fibrils, elastin and smooth muscle cells [9]. Collagen (Type I and III), and smooth muscle cells, are located in a direction perpendicular to the circumferential direction. This structured arrangement gives the media the ability to resist high loads in the circumferential direction [5]. When under stress, these

fibres are reoriented to the circumferential direction. This is one of the reasons why the media is stiffer in the circumferential direction more than in the axial direction [5]. As a whole, the media is thought to be the most elastic layer [5].

2.3 ADVENTITIA

The adventitia consists mainly of fibroblasts, fibrocytes, and collagen fibers organised in thick bundles. The collagen fibers (Type I)[10] , are arranged within the ground-matrix and form a fibrous tissue. In the adventitial layer the orientation of the collagen fibers is dispersed.

3 EXPERIMENTAL DATA

The arterial experimental data used to validate the model were extracted from an investigation carried out by Van Andel [11]. Graphs representing the external diameter versus luminal pressure together with the axial force versus luminal pressure for different arteries were presented. Firstly, arteries were dissected from different arteriosclerotic cadavers. A constant mechanical response was achieved by preconditioning each artery. An axial pre-stretch was then applied, and static pressure tests performed. Finally, the external diameter and corresponding axial force were measured. A 17 points digitization of the data across the pressure range was carried out such that they could be imported into the models presented in this paper.

4 MATHEMATICAL MODEL

The coronary artery is considered for simplicity as a three layered cylindrical structure [5] with abrupt interfaces. It is assumed that the main stimulus of the mechanoreceptor is the strain-energy which varies through the layered structure in value. Thus, empirical strain-energy formulations based on work by Holzapfel et al [5,6] for each layer are used. Using the assumptions of a uniform strain field across the wall of the vessel, and considering each layer to be a thin wall, a model has been created which can be used to derive the parameters describing the strain-energy in each layer using experimental data for complete three layer arterial walls. Thus, the model can be used to estimate the strain-energy in each layer for a given luminal pressure, such that the effect of firing rate of the stretch receptors can be studied.

4.1 THIN WALL MODEL

Thin wall theory[6,[12] offers a simple approximation for the relationship between mean circumferential and axial Cauchy stresses, σ_θ and σ_z and circumferential stretch, λ_θ using

$$\sigma_\theta = p\left(\frac{r}{h} - \frac{1}{2}\right)\lambda_\theta \tag{1}$$

$$\sigma_z = \frac{\sigma_\theta}{2} + \frac{f}{2\pi rh} \tag{2}$$

assuming a deformed thickness, h, deformed radius, r, a luminal pressure, p, and an axial force, f.

4.2 HYPERELASTIC MODEL

Hyperelastic constitutive equations based on the theory presented by Holzapfel et al [5[13] are used to calculate the specific stress responses for each layer as functions of circumferential and axial stretch. These are related via thin wall theory to calculate the mean wall stress both circumferentially and axially.

4.2.1 RELATIONSHIP BETWEEN STRESS AND STRAIN ENERGY FUNCTION

Equation (3) shows the second Piola-Kirchhoff stress tensor, **S**, as a function of strain-energy function, *W*, and Green-Lagrange strain tensor, **E**.

$$\mathbf{S} = \frac{\partial W}{\partial \mathbf{E}} \tag{3}$$

The second Piola-Kirchhoff stress tensor, **S**, is related to the Cauchy stress tensor, **σ**, using the inverse Piola transformation.

$$\boldsymbol{\sigma} = J^{-1}\mathbf{F}\mathbf{S}\mathbf{F}^{T} \tag{4}$$

where J is the Jacobian; equal to the determinant of the deformation gradient , **F**.

Using the Lagrangian multiplier, a relationship is derived between the total strain-energy and the volumetric, U(J) and isochoric components, W_{ic} ($\mathbf{E}$, A_1). If the arterial wall is assumed to be incompressible, and the total strain-energy is a function of the Green-Lagrange strain tensor representing a particular family of collagen fibres, we have

$$W(\mathbf{E}, \mathbf{A}_1) = U(J) + W_{ic}(\mathbf{E}, \mathbf{A}_1) \tag{5}$$

where

$$\mathbf{A}_1 = a_i \otimes a_i \tag{6}$$

and

$$a_i = \begin{pmatrix} 0 \\ \cos\varphi \\ \sin\varphi \end{pmatrix} \tag{7}$$

φ is the angle between collagen fibre and circumferential directions. Assuming no change in volume,

$$U = P(J - 1) \tag{8}$$

P has the units of hydrostatic pressure. The Green-Lagrange strain-stretch relationship is given by

$$E_i = \frac{1}{2}(\lambda_i^2 - 1) \tag{9}$$

where λ_i is the principal stretch. The circumferential and axial second Piola Kirchhoff stress components, s_θ, and, s_z, respectively, are given by

$$s_\theta = \frac{1}{\lambda_\theta}\frac{\partial W_{ic}}{\partial \lambda_\theta} - \frac{1}{\lambda_\theta^3}\frac{1}{\lambda_z}\frac{\partial W_{ic}}{\partial \lambda_r} \quad (10)$$

$$s_z = \frac{1}{\lambda_z}\frac{\partial W_{ic}}{\partial \lambda_z} - \frac{1}{\lambda_z^3}\frac{1}{\lambda_\theta}\frac{\partial W_{ic}}{\partial \lambda_r} \quad (11)$$

where λ_θ , λ_z, λ_r are the principal stretches in the circumferential, axial and radial directions respectively.

4.2.2 ELASTIN AND COLLAGEN STRAIN-ENERGY FUNCTIONS

For each layer, the strain-energy, W_{ic}, is split into an elastin, $W_{iciso}(\mathbf{E})$, and collagen, $W_{icaniso}(\mathbf{E}, \mathbf{A_1})$, response as shown in Equation (12).

$$W_{ic}(\mathbf{E}, \mathbf{A}_1) = W_{iciso}(\mathbf{E}) + W_{icaniso}(\mathbf{E}, \mathbf{A}_1) \quad (12)$$

where

$$W_{iciso}(\mathbf{E}) = \frac{c_1}{2}(I_1 - 3) \quad (13)$$

with

$$I_1 = \lambda_\theta{}^2 + \lambda_z{}^2 + \lambda_r{}^2 \quad (14)$$

and c_1, is a material constant related to the elastin stress response.

The collagen component is assumed to be of the form

$$W_{icaniso}(\mathbf{E}, A_1) = \frac{k_1}{k_2}(e^q - 1) \quad (15)$$

Where k_1, and k_2 are material constants related to the collagen stress response and

$$q = \rho k_2 (I_4 - 1)^2 + (1 - \rho)(I_1 - 3)^2 \quad (16)$$

Where I_4 is the fourth stretch invariant given by

$$I_4 = \lambda_\theta^2 \cos^2(\varphi) + \lambda_z^2 \sin^2(\varphi) \quad (17)$$

To estimate the parameters in (13) and (15), the stress-stretch relationships must be derived such that they can be optimised using experimental data.

The dispersion factor, ρ, represents the amount of dispersion from the ideal alignment of the fibers [22]. A value of unity assumes that there are not any fibers oriented in the isotropic direction. For a value of zero the fibers are assumed to be isotropically oriented as presented by Demiray et al [18]. In this model, it is assumed to be unity.

4.2.3 CAUCHY STRESS FOR EACH ARTERIAL LAYER

Equations (4), (10) and (11) can now be used to describe each of the three arterial layers, (l) to calculate the Cauchy stress components, $\sigma_{\theta l}$ and σ_{zl} in the circumferential and axial directions respectively. Thus for the intima (l = n),

$$q_n = k_{2n}(I_{4n} - 1)^2 \quad (18)$$

$$I_{4n} = \lambda_\theta^2 \cos^2(\varphi_n) + \lambda_z^2 \sin^2(\varphi_n) \quad (19)$$

$$\sigma_{\theta n} = [c_{1n}\left(1 - \frac{1}{\lambda_\theta^4 \lambda_z^2}\right) + k_{1n} e^{q_n}(I_{4n} - 1)\cos^2(\varphi_n)]\,\lambda_\theta^2 \quad (20)$$

$$\sigma_{zn} = [c_{1n}\left(1 - \frac{1}{\lambda_\theta^2 \lambda_z^4}\right) + k_{1n} e^{q_n}(I_{4n} - 1)\sin^2(\varphi_n)]\lambda_z^2 \quad (21)$$

Similar expressions can be obtained the media layer (l=m) and the adventitia (l=a).

Stress equilibrium in the wall is assumed such that the mean wall Cauchy stress components, $\sigma_{t\theta}$ and σ_{tz} in the circumferential and axial directions can be calculated. These are shown in equations (22) and (23) where h is the wall thickness after deformation.

$$\sigma_{t\theta} = \frac{(\sigma_{\theta n} h_n + \sigma_{\theta m} h_m + \sigma_{\theta a} h_a)}{h} \quad (22)$$

$$\sigma_{tz} = \frac{(\sigma_{zn} h_n + \sigma_{zm} h_m + \sigma_{za} h_a)}{h} \quad (23)$$

It is these stresses that are compared to the complete arterial wall data to estimate the parameters in the elastin and collagen strain-energy functions [14].

4.3 OPTIMISATION

The parameters used to calculate the stresses in equations (20) to (23) were optimised using the *Levenberg–Marquardt* method Constraints based on the physiological response presented in [5] were used.The root mean square error was calculated according to the following equation

$$\varepsilon = \frac{\sqrt{\frac{\chi^2}{N - Q}}}{\sigma_{ref}} \quad (24)$$

Where N is the number of data points and Q is the number of parameters of the strain energy function, σ_{ref} is the sum of all Cauchy stresses for each point divided by the number of all data points.χ^2 is the summation of the difference between the model and the thin wall estimation.

Parameter sensitivity analysis was investigated for the material parameters of the coronary artery. The aim of parameter sensitivity is to decide if variations of the parameter values have a noticeable impact on the results and error estimation and to make sure these values represent the least achievable error.

5 RESULTS AND DISCUSSION

The stretch in a coronary artery as a function of pressure is given in Figure 2. The parameter sensitivity analysis is shown in figure 3. This shows in general that collagen material parameters are significantly more effective than the elastin ones.The estimated circumferential Cauchy and axial stresses are shown in Figures 4a and 4b respectively. Experimental curves obtained from [5] are shown for comparison. These show that the material parameters used in the strain-energy function give results which are in a similar range to experimentally obtained curves. Using these material parameters, the strain-energy as a function of luminal pressure was derived as shown in Figure 5.

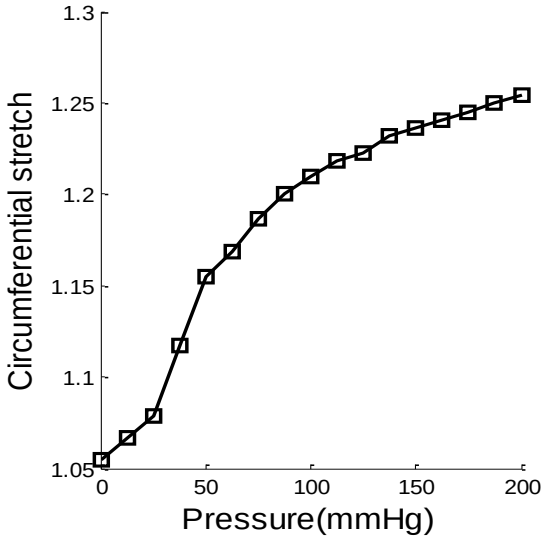

Figure 2. Experimental relationship between circumferential stretch and luminal blood pressure for a coronary artery

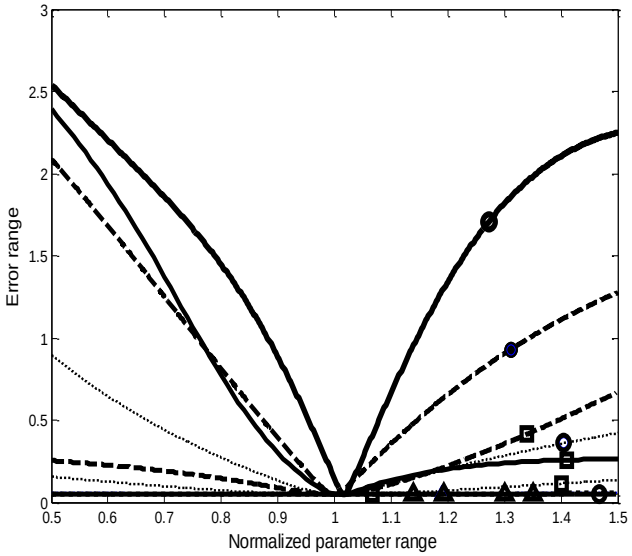

Figure 3: Parameter sensitivity for the twelve parameters of the coronary artery. A thick continuous line is used for the angle; a thick dashed line for k_2, a thin dashed line for k_1 and c_1 is drawn using a thin continuous line. The intimal layer is represented by a circle, the adventitial layer by a square and medial layer by a triangle.

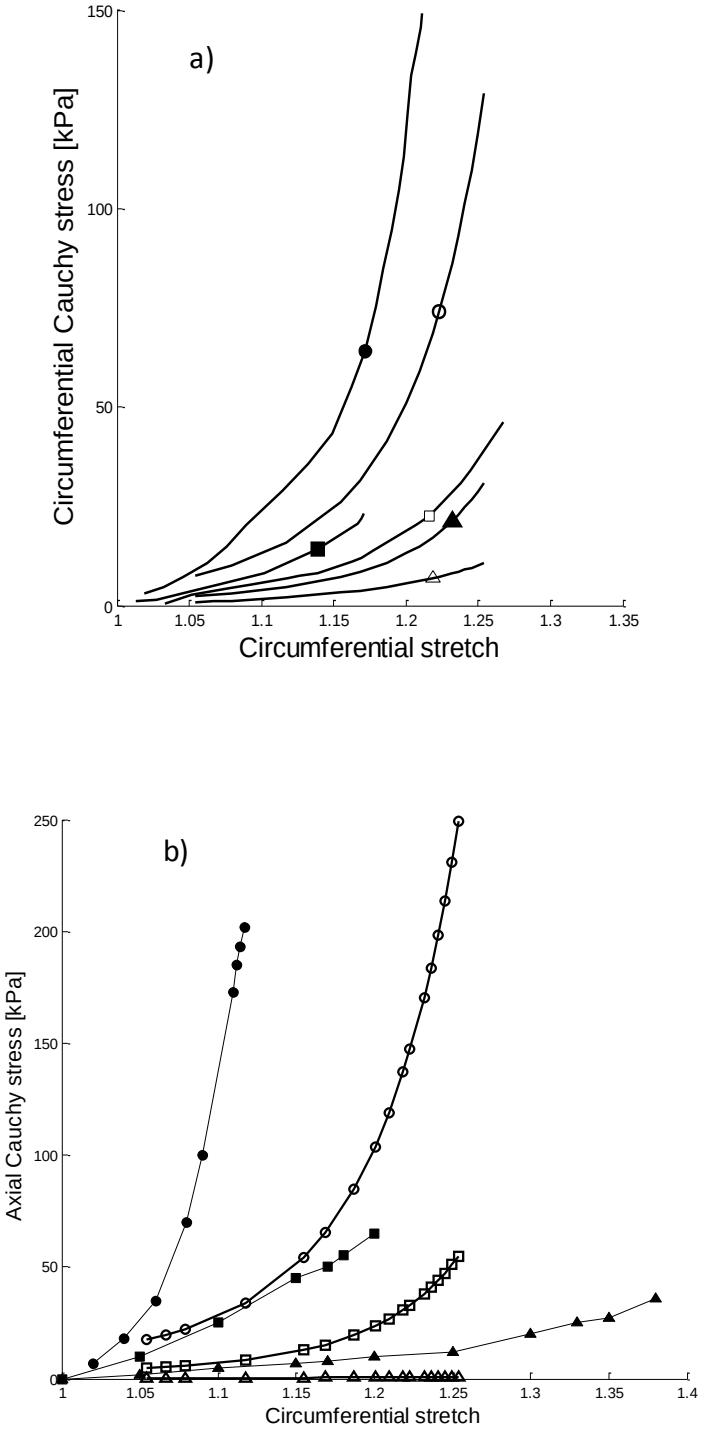

Figure 4. Estimated data calculated from experimental data in [10] and selected experimental data from [5] for coronary artery adventitia (square), media (triangle) and intima (circle) layers. Filled symbols are used for experimental data while empty ones are for model results for a) circumferential and b) axial direction.

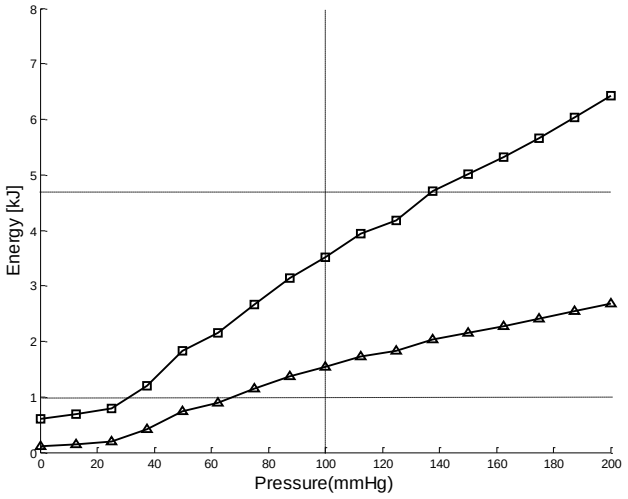

Figure 5: Estimated strain-energy for the adventitia (squares) and media (triangle) as a function of luminal blood pressure for the coronary artery

This figure suggests that at a given blood pressure, for example 100 mmHg, the strain-energy in the intima is highest (not shown) followed by adventitia and media. To investigate the effect of firing rate from mechanoreceptors in each layer, all the receptors were considered to have the same arbitrary threshold strain-energy of around 1 kJ, with saturation occurring around 4.5 kJ. With these limits, the data suggests that mechanoreceptors in the adventitia would have a threshold blood pressure of around 30 mmHg and would saturate at around 140 mmHg. For the media, this scenario suggests receptors here would start firing at around 70 mmHg and do not saturate. Only the media and the adventitia are considered because histological studies [15] [16] suggest that mechanoreceptors do not exist in the intima.

This data is an estimate with root mean square error for the three layers being shown to be as great as 0.05 for the media and the adventitia. However, this study does present some evidence that suggests C-fibres could be predominantly located in the more elastic regions such as the media with A-fibres predominantly in the stiffer regions such as the adventitia. Further experimental studies would be needed to investigate this further.

6 ACKNOWLEDGEMENTS

We would like to thank EPSRC for funding this work and the helpful guidance of Dr Ritu Kataky.

7 REFERENCES

[1] Srinivasan R and N. HB., "Modeling the Carotid Sinus Baroreceptor,". *Biophys J.* , vol. 12, pp. 1171-1182, Sep 1972.

[2] C. T. KAPPAGODA, *et al.*, "ATRIAL RECEPTORS IN THE CAT," *J. Physiol*, vol. 262, pp. 431-446, 1976.

[3] J. Levick, *An introduction to cardiovascular physiology*. London: Hodder, 2003.

[4] Barry M, *et al.*, "Comparative histological and biometric study of the coronary, radial and left internal thoracic arteries," *Surgical and Radiologic Anatomy*, vol. 25, pp. 284-289, 2003.

[5] Holzapfel GA, *et al.*, "Determination of layer-specific mechanical properties of human coronary arteries with nonatherosclerotic intimal thickening and related constitutive modeling. ," *Am. J. Physiol. Heart Circ. Physiol.*
, vol. 289, pp. H2048-2058, 2005 Nov.

[6] Holzapfel GA, *et al.*, " A new axisymmetrical membrane element for anisotropic, finite strain analysis of arteries. ," *Communications in Numerical Methods in Engineering*, vol. 12, pp. 507-517, 1996;.

[7] Bin Feng, *et al.*, "Theoretical and electrophysiological evidence for axial loading about aortic baroreceptor nerve terminals in rats," *Am J Physiol Heart Circ Physiol*, vol. 293, pp. H3659–H3672, ,2007.

[8] Canham PB, *et al.*, "Measurements from light and polarised light microscopy of human coronary arteries fixed at distending pressure," *Cardiovasc. Res.*, vol. 23, pp. 973-982, 1989 Nov

[9] Clark JM, *et al.*, "Structural integration of the arterial wall. I. Relationships and attachments of medial smooth muscle cells in normally distended and hyperdistended aortas,". *Lab. Invest.*, vol. 40, pp. 587-602, 1979 May.

[10] von Der Mark K and Ocalan M, " Immunofluorescent localization of type V collagen in the chick embryo with monoclonal antibodies," *Coll. Relat. Res*, vol. 2, pp. 541-555, 1982 Nov.

[11] van Andel CJ, *et al.*, "Mechanical properties of porcine and human arteries: implications for coronary anastomotic connectors," *Ann. Thorac. Surg.*
, vol. 76, pp. 58-64, 2003Jul.

[12] Fung YC, *et al.*, "Pseudoelasticity of arteries and the choice of its mathematical expression.," *Am. J. Physiol. Heart Circ. Physiol.*, vol. 237, pp. H620-631, 1979 Nov; .

[13] Holzapfel GA, *et al.*, "A New Constitutive Framework for Arterial Wall Mechanics and a Comparative Study of Material Models," *Journal of Elasticity*, vol. 61, pp. 1-48, 2000 Jul

[14] Michel E Mickael, *et al.*, "Estimation of Stress-Strain Relationships in Vascular Walls using a Multi-Layer Hyperelastic Modelling Approach
" presented at the Computers in Cardiology Belfast, 2010.

[15] Kummer Wolfgang, "Three types of neurochemically defined autonomic fibres innervate the carotid baroreceptor and chemoreceptor regions in the guinea-pig," *Anat Embryol*, vol. 181, pp. 477-489, 1990.

[16] MARK W. CHAPLEAU, *et al.*, "Mechanisms Determining Sensitivity of Baroreceptor Afferents in Health and Disease," *Ann N Y Acad Sci.* , vol. 940, pp. 1-19, 2001 Jun.

International Journal for Numerical Methods in Biomedical Engineering

ESTIMATION OF STRESS PROFILES IN THE ANISTROPIC HYPERELASTIC LAYERS OF A CORONARY ARTERIAL WALL USING WHOLE-WALL EXPERIMENTAL DATA

Journal:	*International Journal for Numerical Methods in Biomedical Engineering*
Manuscript ID:	CNM-Jul-10-0078.R2
Wiley - Manuscript type:	Research Article
Date Submitted by the Author:	29-Mar-2011
Complete List of Authors:	mickael, Michel; Durham, engineering Johnstone, Sherri; Durham University, Engineering Crouch, Roger; Durham University, Engineering Heydari, Abbas; Durham University, Biological sciences
Keywords:	stress, strain, layer, parameter, artery, vein

ESTIMATION OF STRESS PROFILES IN THE ANISTROPIC HYPERELASTIC LAYERS OF A CORONARY ARTERIAL WALL USING WHOLE-WALL EXPERIMENTAL DATA

Michel E Mickael[1], Abbas Heydari[2], Roger Crouch[1], Sherri Johnstone[1].

[1]School of Engineering and Computing Sciences, Durham University, Durham, DH1 3LE, UK,[2] School of Biological and Biomedical Sciences, Durham University, Durham, DH1 3LE, UK

SUMMARY

This paper presents a method of estimating the stress-strain behaviour of the three distinct layers of the coronary artery, the intima, media and adventitia. The study involves assuming a constant strain field across three thin layers, in order to estimate the layer anisotropic hyperelastic material parameters using a constrained optimisation method employing whole-wall experimental data. Parameter sensitivity analysis and comparison with experimental data from individual layers suggest that the estimated stress profiles using this simple three layer cylindrical model are consistent with physiological findings.

1 INTRODUCTION

The study of the mechanical properties of cardiovascular blood vessels allows both engineers and clinicians to understand how changes due to disease, lifestyle and ageing can impact on cardiovascular homeostasis. However, there exist several practical barriers to obtaining good quality, detailed, experimental data to assist these investigations [1]. Thus the primary aim of this paper is to propose a simple engineering method to estimate the stress profiles in the intima, media and adventitia layers within vascular walls using experimental data collected from intact arteries. The second aim is to compare the model output against experimental data from layers of arterial tissue [1-2].

All the experimental data used in this investigation were taken from surgically removed arteries and tissue. Although the experimental data were from surgically extracted arteries, the method presented here has the potential to estimate the properties in each layer of tissue from non-surgical clinically derived experimental data, such as that obtained from ultrasonic Doppler techniques[3].

The extra information obtained from the study of arterial layer data (as opposed to whole-wall data) allows the study of certain phenomena; for example , the effect of stiffening of the intima in arteriosclerosis [4] and the effect of material stiffness on mechanoreceptor signalling of changes in blood pressure and volume.

In the first application, if the change in stiffness in the intima can be estimated, then it may be possible to diagnose and hence treat this condition. For the second application, it has been well documented that at least two types of mechanoreceptors exist with different stress-strain thresholds[5]. By studying the stress-strain profile in the layer of tissue in which these receptors are embedded, a better understanding of the signalling mechanism can be obtained. This can assist in studying hypertension.

The first part of this paper (i) defines the biological problem with a review of histological studies of the coronary artery and (ii) discusses the classification of the wall into three layers. Previous experimental and mathematical studies upon which this work is based are then reviewed. Following this, the specific model based on the Holzapfel et al hyperelastic formulation is presented. The authors' approach of assuming a constant strain field across three thin walled layers to formulate the link between the whole-wall stress-strain profile with the individual layers is then described.

The second part of the paper describes the data selected from a series of experimental investigations from two independent research teams [1-2]. The whole-wall data for the coronary artery from [1] was used in the estimation of the material parameters in the proposed model, while the coronary artery layer data from [2] was used to assess the validity of the predictions.

2 ARTERIAL WALLS

Histological studies have shown that arterial walls can be considered as three layers as shown in figure 1 [6]. It can be seen that interface regions separate these three layers: intima, media and adventitia. This section reviews the findings of a number of histological and experimental studies to give an estimation of the physical structure and composition of these layers. Particular attention has been given to coronary arteries as these are the focus of this study. The specific findings from these studies are given in table 1.

In particular, it is suggested that the intima is the mechanically dominant layer in coronary arteries with nonatherosclerotic intimal thickening [1]. This is due to the existence of a high content of collagen. It has been shown that the intima has a typical thickness of 27% with respect to the total wall thickness [1] and comprises a layer of endothelium cells coating a sub-endothelial layer, composed of dispersed collagen fibres (Type I), dispersed smooth muscle cells and elastin [7]. Unlike collagen and smooth muscle cells, elastin is arranged in a three-dimensional network of elastic fibres.

On the basis of the experimental data the media in general is the softest layer over the whole deformation domain [1]. It consists of a three-dimensional network of bundles of collagen fibrils, elastin and smooth muscle cells [8] Collagen (Type III), and smooth muscle cells, are located in the circumferential direction. This structured arrangement gives the media the ability to resist high loads in the circumferential direction [1]. When under tensile stress, these fibres are

reoriented towards the circumferential direction. This is why the media has been shown to be stiffer in the circumferential direction in comparison to the longitudinal direction [9].

The adventitia consists mainly of fibroblasts, fibrocytes, and collagen fibres organized in thick bundles. The collagen fibres (Type I), are arranged within the ground-matrix and form a fibrous tissue [10]. In this layer, the orientation of the collagen fibres is dispersed.

It is worth noting that the intimal thickness as well the other layer thicknesses may differ significantly based on subject, age, disease and location [11]. The intimal thickness as well the other layer thicknesses presented in this study was based on this specific experimental data.

3 REVIEW OF MATHEMATICAL MODELS

The model presented in this paper is based on the assumptions that (i) the arterial wall tissue can be considered as a hyperelastic material, i.e. a strain-energy function exists and (ii) any artery or layer within the artery can be modelled as a thin walled cylindrical vessel. The previous work reviewed here has focussed on deriving phemonologically derived forms of the strain-energy function for thin walled arteries.

Fung et al produced an exponential form of the strain-energy function for a thin-wall whole artery[12]. This model did not fit the experimental data at low pressures. Also, the material parameters in that model did not relate physically to the constituent materials in the arterial tissue. This issue was addressed by Holzapfel et al [13]. Forming a model for thin wall arterial response, Holzapfel et al presented a two term strain-energy function that used experimentally obtained elastin and collagen responses to model passive extension. The effect of smooth muscle cells was neglected , as it was assumed that these do not contribute to the passive stiffness[14-15]. Thus, only elastin and collagen were considered as the constituents which act during the extension of the arterial wall, in response to luminal arterial pressure. However, that model did not consider the specific responses for the individual layers constituting the arterial wall (intima, media and adventitia). The research performed by von Maltzahn et al offers one of the most important contributions to the field [16-18]. In [16] experimental measurements of the elastic properties of media and adventitia were presented. The arterial wall was considered to be orthotropic, but it did not include the role of the intima. In older patients, the intima has been shown to be of significant importance [1]. The strain-energy presented by von Maltzahn et al lacked a coherent relationship with the materials constituting the arterial wall (e.g: elastin and collagen) [18]. Demiray et al introduced another strain-energy function [19]. However, this model lacked any comparison with experimental data and it also assumed the vascular wall to be completely isotropic, i.e. it did not take into consideration collagen fibre anisotropy. Demiray and Vito used a two layer model, neglecting the role of the intima [20]. The media was considered orthotropic, while the adventitia was considered isotropic. No axial force–pressure relationship was presented. Similarly, the relationship between the two layers and the whole structural stress was not presented. Based on work by AJM Spencer [21], Holzapfel et al

presented layer specific strain-energy equations assuming arterial layers, but no relationship for the stress-strain response of the whole-wall was given[1]. Recently [22] Holzapfel et al discussed the role the intima plays in load bearing and the significance of its thickness for nonatherosclerotic intimal thickening cases. Holzapfel et al also covered a complete 3D analysis of residual stress including bending [15]. The study presented in this paper also concentrates on producing a model for subjects with intimal thickening for nonatherosclerotic cases and does not include bending or residual stress.

4 PROPOSED MODEL

The aim of the model proposed in this paper is to be able to estimate the stress-strain relationship in each of the arterial layers, using experimental data from the complete arteries. To achieve this, the arterial wall is modelled as three concentric cylindrical layers (figure 2). The layers are assumed to behave as transversely isotropic homogeneous nearly incompressible hyperelastic materials in which strain-energy functions, *W*, are assumed to exist. These consist of a linear combination of phenomenologically derived collagen and elastin components [1, 12-13, 15, 23-26]. The average stiffness in each layer is estimated using a thin wall approximation. Finally, individual layer stresses are combined to give whole-wall stresses. This is achieved by assuming a constant strain across the entire wall and nominal layer thicknesses of 26.2%, 34.9% and 38.8% for the intima, media and adventitia respectively [1, 27].

In this section we describe the form of the hyperelastic constitutive equations. These are based on the theory presented by Holzapfel et al [1]. Firstly, the strain-energy function is formulated in terms of the principal stretches and the second Piola-Kirchhoff stress tensor. These are then related to material parameters using the collagen and elastin phemonological formulations developed by Holzapfel et al [1]. The assumption of thin wall theory is employed such that the specific stress responses for each thin layer (as functions of circumferential and axial stretch) can be derived. Thin wall theory is finally used again to calculate the whole-wall stress, both circumferentially and axially.

4.1 Formulation of strain-energy function

The strain-energy function, *W*,defined as the strain energy per unit volume in the unloaded reference configuration can be used to find the relationship between the second Piola-Kirchhoff stress tensor, **S**, and Green-Lagrange strain tensor, **E**, as shown in equation (1).

$$\mathbf{S} = \frac{\partial W}{\partial \mathbf{E}} \tag{1}$$

The second Piola-Kirchhoff stress tensor, **S**, does not offer a simple physical interpretation, but it can be used to calculate the (physically more meaningful) Cauchy stress tensor, **σ**, using the following inverse Piola transformation.

$$\boldsymbol{\sigma} = \mathrm{J}^{-1}\mathbf{F}\mathbf{S}\mathbf{F}^{\mathrm{T}} \quad (2)$$

where , J, is the Jacobian; equal to the determinant of the deformation gradient , **F**.

Using the Lagrangian multiplier, a relationship is derived between the total strain-energy and the volumetric, U(J) and isochoric components, W_{ic} (**E**, $\mathbf{A_1}$). Assuming the arterial walls to be incompressible, and that the total strain-energy is a function of the Green-Lagrange strain tensor representing one family of collagen fibres, we have

$$W\,(\mathbf{E}, \mathbf{A}_1) = W_{ic}\,(\mathbf{E_{ic}}, \mathbf{A}_1) \quad (3)$$

where

$$\mathbf{A}_1 = a_1 \otimes a_1 \quad (4)$$

and

$$a_1 = \begin{pmatrix} 0 \\ \cos\varphi \\ \sin\varphi \end{pmatrix} \quad (5)$$

given that, φ, is the angle between collagen fibre orientation and the circumferential direction, using cylindrical coordinates.

Applying Lagrange multiplier

$$\mathbf{S} = \frac{\partial W_{ic}}{\partial \mathbf{E}} + \mathrm{P}\frac{\partial J}{\partial \mathbf{E}} \quad (6)$$

where P has the units of hydrostatic pressure. The isochoric Green-Lagrange strain-stretch relationship is given by

$$\mathrm{E}_i = \frac{1}{2}(\lambda_i^2 - 1) \quad (7)$$

where λ_i is the isochoric principal stretch. The circumferential and axial second Piola Kirchhoff stress components, s_θ, and, s_z, respectively, are given, For thin wall cylinders, we usually assume a plane stress state with zero stresses in the thickness direction , i.e s_r=0

$$\mathrm{s}_\theta = \frac{1}{\lambda_\theta}\frac{\partial W_{ic}}{\partial \lambda_\theta} - \frac{1}{\lambda_\theta^3}\frac{1}{\lambda_z}\frac{\partial W_{ic}}{\partial \lambda_r} \quad (8)$$

where λ_θ , λ_z, λ_r are the principal stretches in the circumferential, axial and radial directions respectively.

$$s_z = \frac{1}{\lambda_z}\frac{\partial W_{ic}}{\partial \lambda_z} - \frac{1}{\lambda_z^3}\frac{1}{\lambda_\theta}\frac{\partial W_{ic}}{\partial \lambda_r} \quad (9)$$

4.2 Collagen and elastin strain-energy functions

For each layer, the strain-energy, W_{ic}, is considered to be the linear combination of elastin and collagen contributions.

$$W_{ic}(\mathbf{E}, \mathbf{A}_1) = W_{iciso}(\mathbf{E_{ic}}) + W_{icaniso}(\mathbf{E_{ic}}, \mathbf{A}_1) \quad (10)$$

The form of the elastin strain-energy component $W_{iciso}(\mathbf{E_{ic}})$, is approximated to be

$$W_{iciso}(\mathbf{E_{ic}}) = \frac{c_1}{2}(I_1 - 3) \quad (11)$$

The first invariant of stretch , I_1, is defined as

$$I_1 = \lambda_\theta^2 + \lambda_z^2 + \lambda_r^2 \quad (12)$$

and c_1, is a material constant related to the elastin stress response.

The form of the collagen contribution can be described by

$$W_{icaniso}(\mathbf{E_{ic}}, A_1) = \frac{k_1}{k_2}(e^q - 1) \quad (13)$$

where k_1, and k_2 are material constants related to the collagen stress response and q is calculated to be

$$q = \rho k_2 (I_4 - 1)^2 + (1 - \rho)(I_1 - 3)^2 \quad (14)$$

where ρ is the dispersion factor. I_4 is the fourth stretch invariant given by

$$I_4 = \lambda_\theta^2 \cos(\varphi)^2 + \lambda_z^2 \sin(\varphi)^2 \quad (15)$$

The dispersion factor value represents the amount of dispersion from the ideal alignment of the fibres [25]. A value of unity assumes that all the fibres are oriented in the φ direction. For a value of zero the fibres are assumed to be randomly isotropically oriented, as presented by Demiray et al [19].

4.3 Thin wall approximation

To estimate the mean stress-strain relationships in each layer and the whole arterial wall, it is assumed that thin wall theory can be applied. Fung et al [12] noted that the arterial wall is not so thin, but it was considered to be thin enough to justify the use of thin wall theory. Fung et al observed that neglecting the variation of stress through the wall thickness will have an effect on the quality of a model prediction [23]. However, no quantitative error estimation was given. Holzapfel et al used thin wall theory to represent the circumferential and axial responses [13].When modelling the layer response, he discussed the usage of different strain-energy forms for each layer . In order to formulate the analytical model, Holzapfel et al made certain assumptions. As all collagen fibres are embedded in the tangential surface of the tissue, it was assumed that there are no components in the radial direction [1, 13, 26]. This supported the use of the thin wall approximation [28]. On comparing circumferential and radial stresses, circumferential stresses appear to be far bigger. Thus this justifies only considering circumferential and axial stresses in this investigation [13]. Although bending and residual stresses are important in some arterial regions, it is not taken into consideration in this study due to lack of experimental data that fits within the scope of this research.

4.3 Layer stress response

Equations (2), (8) and (9) can now be used to describe each of the three arterial layers, *l* to calculate the Cauchy stress components, $\sigma_{\theta l}$ and σ_{zl}, in the circumferential and axial directions respectively. Thus for the intima (*l* = n),

$$\sigma_{\theta n} = \left[c_{1n}\left(1-\frac{1}{\lambda_\theta^4\lambda_z^2}\right)+k_{1n}e^{qn}((1-\rho_n)(I_{1n}-3)\left(1-\frac{1}{\lambda_\theta^2}\right)\rho_n(I_{4n}-1)\cos(\varphi_n)^2)\right]\lambda_\theta^2 \quad (16)$$

$$\sigma_{zn} = \left[c_{1n}\left(1-\frac{1}{\lambda_\theta^2\lambda_z^4}\right)+k_{1n}e^{qn}((1-\rho_n)(I_{1n}-3)\left(1-\frac{1}{\lambda_z^2}\right)+\rho_n(I_{4n}-1)\sin(\varphi_n)^2)\right]\lambda_z^2 \quad (17)$$

Similar expressions can be obtained the media layer (*l*=m) and the adventitia (*l*=a)

4.4 Whole-wall stress response

This paper proposes using stress equilibrium in the wall to calculate the mean wall Cauchy stress components, $\sigma_{t\theta}$ and σ_{tz} in the circumferential and axial directions as shown in equations (18) and (19) where h is the wall thickness after deformation.

$$\sigma_{t\theta} = \frac{(\sigma_{\theta n} h_n + \sigma_{\theta m} h_m + \sigma_{\theta a} h_a)}{h} \quad (18)$$

$$\sigma_{tz} = \frac{(\sigma_{zn} h_n + \sigma_{zm} h_m + \sigma_{za} h_a)}{h} \quad (19)$$

These Cauchy stresses can be related back to luminal blood pressure and axial stress using thin wall theory [12-13] . Assuming a deformed thickness, h, deformed radius, r, a luminal pressure, p, and an axial force, f, we have

$$\sigma_{t\theta} = p\left(\frac{r}{h} - \frac{1}{2}\right) \quad (20)$$

$$\sigma_{tz} = \frac{\sigma_\theta}{2} + \frac{f}{2\pi\, rh} \quad (21)$$

5 EXPERIMENTAL

5.1 Method

To investigate the validity of the assumptions used in the model to relate whole-wall data to layer stress-strain response, experimental data are required. It was found that extensive investigations have already been reported in the literature and repeating these is not the primary purpose of this study. Thus data from peer reviewed journal papers were used. The two particular studies used were both from older nonatherosclerotic patients such that they are directly comparable.

The first part of the experimental investigation was sourcing and extracting the data from research papers in a suitable digital form. Data from whole-wall coronary arteries were used to optimise the layer model parameters using a Levenburg-Marquardt optimiser available in Matlab® and applying the Monte Carlo method. The optimisation was constrained based on experimental and histological findings and a parameter sensitivity analysis was carried out. These techniques were applied to increase the probability of finding the global optimum solution. The resulting estimates of the stress-strain relationships were then compared with the outputs from a range of experiments on layered coronary arterial tissue from an independent study. It should be noted that data from the whole-wall and layered wall stress-strain responses for the same artery would be a suitable next step.

5.2 Data collection

This section describes the data sets used in this investigation. To optimise the model, whole-wall coronary artery data were used. To independently verify the quality of the model estimates, coronary arterial wall layer data were selected.

To optimise the parameters in the layer model proposed in this paper, whole arterial wall data from an investigation carried out by van Andel et al [2] were used. This group published data showing the relationships of external arterial diameter and axial force against luminal blood pressure for a variety of arteries from older noatherosclerotic subjects. Data for a whole-wall coronary artery has been selected for this analysis (figure 3).

The experimental setup reported was as follows [2]. Firstly, the arteries were dissected from cadavers. To establish a constant mechanical response, the arteries were preconditioned before the experiment. An axial pre-stretch was then applied, and pressure applied statically. Finally, the external diameter and corresponding axial force were measured and graphically presented in [2]. To import the data into the algorithm used to optimise the model in this paper, the authors extracted the data from using a 17-point digitisation method across the pressure range.
To assess the validity of the estimated material parameters and resulting stress-strain relationships, selected data were extracted from an extensive investigation on coronary artery layer data from older nonatherosclerotic subjects carried out by Holzapfel et al [1] using the 17-point digitisation technique in Matlab®. Due to the large number of samples in this study, the model outputs are examined in the context of the errors presented in the Holzapfel et al study. A summary of the experimental data used is given in table 2.

5.3 Optimisation

A constrained optimisation of the model parameters was achieved using the Levenberg–Marquardt method with a root mean square error function provided by Matlab®. The constraints were based on the physiological response presented in [1]. The intima stress responses, both axially and circumferentially, were constrained to be stiffer than the adventitia responses. (Stiffness is defined as the ratio of Cauchy stress to the associated extension ratio (stretch)). In the same manner, the adventitia was constrained to be stiffer than the media both circumferentially and axially. Also, the specific layer responses of the intima and adventitia were constrained to be stiffer axially than circumferentially. Whereas, the media was constrained to be stiffer circumferentially than axially. Following the layer dominance for arteries presented in [1] , the media was constrained as the dominant layer circumferentially. The root mean square error was calculated according to the following equation

$$\varepsilon = \frac{\sqrt{\frac{\chi^2}{n_1 - n_2}}}{\sigma_{ref}} \qquad (22)$$

where n_1 is the number of data points and n_2 is the number of parameters of the strain-energy function, σ_{ref} is the sum of all Cauchy stresses for each point divided by the number of all data points. χ^2 is the summation of the stress difference between the model and the thin wall estimation.

The optimisation procedure was repeated ten times from random starting points [29] within the physiological range defined by experimental data in [1]. Each time 50000 solutions with a mean square error less than 0.050 were recorded. From the total data set the probability density functions of all parameter were examined. They were all found to be unimodal, implying a unique set of parameters. Thus, the mean and standard deviation of each parameter were calculated according to the standard Monte Carlo procedure. The optimised parameters used to calculate the stresses in equations (16) to (21) are shown in tables 3 and 4. The collagen fibre angles from the circumferential direction are assumed to be different for each of the three layers in the hyperelastic model [1] as shown in table 4.

Parameter sensitivity analysis was used to assess whether variations of the parameter values have a noticeable impact on the quality of simulation. Parameter sensitivity was carried out according to the following procedure [30-32] . Each parameter was varied ± 50 % across its mean, while the other parameters were kept constant at their optimised values. The error was plotted across the range of normalised parameter values. The parameters intersected at their lowest error point. This procedure is known as one way parameter sensitivity analysis[32] . To ensure the validity of the results a Kolmogorov–Smirnov test was used to compare the statistical distribution of the accepted and the unaccepted ranges. If the statistical distributions were identical, the parameter was deemed to be insensitive.

5.4 Results

Figure 4 shows a graph of the estimated axial and circumferential Cauchy stresses versus luminal pressure for the coronary artery data extracted from [2] . The root mean square error (rms) values were found to be 0.060 and 0.092 respectively indicating a “good” fit in both cases. This results in a total rms error of 0.050, which compares favourably to the averaged layer rms error of 0.080 in [1]. Figure 5 shows estimated stress-strain data for the three layers,(intima, media and adventitia) in the same coronary artery. For comparison a shaded region, showing the range of the experimental data from [1], has been added. A set of experimental curves with similar material constants for a single coronary artery from [1] is also shown for comparison purposes. Figure 6 shows the effect of increasing axial pre-stretch on the maximum strain achieved by the artery. Figure 7 shows graphs of the parameter sensitivity for the coronary artery data. Figure 8 concentrates on comparing the effect of the collagen fibre angle for each layer. Figure 9 shows the whole-wall experimental, estimated results and the estimated layer stress-strain profiles for the same artery.

6 DISCUSSION

This section firstly explores the proposal of using the mathematical model based on layer strain-energy functions for the whole-wall stress-strain estimation. Secondly, the resulting individual layer stress-strain estimations and layer material parameter sensitivity are discussed. Finally the model sensitivity to physiological assumptions is discussed.

6.1 Whole-wall stress-strain estimation

Figure 4 shows the estimated whole-wall stress estimations using the layered model approach. The low mean standard error value of 0.050 indicates the model is a reasonably "good" fit. It is also consistent with the experimental data in that it estimates that the static axial stress response is higher than the circumferential static stress response. However, at low luminal pressures the model fit is not so good. A possible explanation is that at lower pressures only the elastin is under tension and stretches, whilst at higher pressures both the elastin and collagen are under tension and thus both fibre types stretch. Based on this it is suggested that improving the form of the elastin strain-energy function could increase the quality of the overall fit [27] . Further work would be needed to investigate this assumption.

6.2 Layer stress-strain estimation

The inferred layer stress-strain profiles produced in the process of estimating the whole-wall stress-strain profile, as shown in figure 5 and figure 9, are consistent with the experimental layer data in [1] and [16-18, 20]. For example, in figure 9a, it can be seen that in all cases the order of decreasing stiffness is the intima, adventitia and finally the media. This is due to the constrained optimisation process described in Section 5.3.

The layer material parameters optimised to produce the stress-strain profiles have also been compared to those estimated by Holzapfel et al using layer experimental data [1], (Tables 3 and 4). It can be seen that the values estimated by the layer model in this paper for the single coronary artery in [1] are within the range of values for the range of coronary arteries studied by Holzapfel et al [1]. From these it was estimated that the stress-strain profiles are similar to those in [1] for all layers and the adventitia and media in the axial direction. A possible explanation for this is due to the differences in applying the stresses. In the whole-wall artery experiments, biaxial stresses were applied using an axial pre-stretch, whereas in the layered wall experiments, uniaxial stresses were applied. The effect of axial pre-stretch on maximum circumferential stress of a whole arterial wall was further investigated using the three layer model. The results are presented in Figure 6. It can be seen that increasing the axial pre-stretch increases the range of the circumferential strain. This could possibly explain why the intimal response falls outside the experimental range in [1].

6.3 Layer material parameter sensitivity

To investigate the validity of the layer model parameters further, a sensitivity analysis was carried out. The Kolmogorov–Smirnov test indicated that the model was sensitive to all the material parameters within the physiological range.

Figure 7 shows that the minimum error occurs when all the parameters are at the optimised values and there are no other error minima observed within the physiological range. It also suggests that the solution is most sensitive to the predominant angle φ of the dispersed collagen fibres. It is also worth noting that the error range was included for 50% above and below the optimised value. This can be seen in more detail in Figure 8 which shows that the solution is most sensitive to φ in the layers with the highest collagen content and hence the greatest stiffness. This suggests that collagen fibre direction is a major factor in determining the arterial wall stiffness and thus dominates the response in the intima and adventitia, and a less significant effect in the media.

6.4 Model assumptions

In this section the major assumptions used in producing the model are discussed. Factors considered include a thin wall cylinder approximation, abrupt junctions between the layers, a constant strain profile, and a constant ratio of layer thicknesses.

The aim of this study is to produce an analytically derived model such that the effect of material parameters can be studied. In section 4.3 a review of studies using cylindrical thin wall models suggested that analytical solutions for thick wall vessels is far from a trivial task and finite element analysis is a more suitable method [28] . However, the results in this paper based on [13] suggest that a thin wall model does produce results that are consistent with experimental findings. The model is also based on assuming the layers have abrupt junctions. The results of the histological study shown in Figure 1 show that the thickness of the junction regions are relatively small compared with the layer thicknesses and hence this is a reasonable assumption. However, this ignores any effects of the internal elastic lamina and external elastic lamina that separate the media from the intima and adventitia respectively [15] [33]. A model that takes into account inter layer lamina effects may act to improve the goodness of fit of the whole model [34]. The assumption of a constant strain across the three layers is used as this is one of the constraints required for the application of thin wall theory. Finally, the assumption of using fixed layer ratios is addressed. The intimal thickness [1] has been reported to be about 27% of the total thickness for the data used in this study, whilst the adventitial and medial thicknesses are more variable and there is no universal ratio for them. However, the studies show that the media is the largest layer. This suggests that the media varies between 36.5% and 63.0% and the adventitia between 10.0% and 36.5%. Using these extreme values, the model error was found to be 0.050 ± 0.005, which compares favourably with the error presented by Holzapfel et al [1] of 0.067±0.033.

9 CONCLUSIONS

This paper has presented a mathematical model based on a hyperelastic formulation using the condition of stress equilibrium to estimate the stress-strain profiles in both whole and layered arterial walls. The material parameters in the model have been optimised using whole-wall experimental data from studies carried by Holzapfel [1] and van Andel [2]. For the whole-wall estimations of a single coronary artery, the total root mean square error was found to be 0.050 which compares well with previous studies. This suggests the proposed method provides a simple approach to estimating the layer material parameters. A comparison with experimental data from a study on layered data suggested the solutions to the model were physiologically feasible; however, differences in experimental setup prevent this judgement from being completely conclusive.

In optimising the material parameters, it was revealing to find that the errors in the estimated stresses were particularly sensitive to the dominant collagen angle in the stiffest layer, the intima. This suggests the role of collagen content and possibly fibre orientation should be investigated further for conditions such as arteriosclerosis.

9. ACKNOWLEDGEMENTS

The author would like to thank the Engineering and Physical Sciences Research Council (ESPRC) for funding this research (grant number is EP/F01189X/1).The author would also like to thank Dr Susan Pyner and Dr Ritu Kataky for their help and advice during this investigation.

REFERENCES

1. Holzapfel GA, Sommer G, Gasser CT, and Regitnig P, *Determination of Layer-Specific Mechanical Properties of Human Coronary Arteries with Nonatherosclerotic Intimal Thickening and Related Constitutive Modeling.* Am. J. Physiol. Heart Circ. Physiol., 2005. **289**(5): p. H2048-2058.

2. van Andel CJ, Pistecky PV, and Borst C, *Mechanical Properties of Porcine and Human Arteries: Implications for Coronary Anastomotic Connectors.* Ann. Thorac. Surg., 2003. **76**(1): p. 58-64.

3. Wong M, Edelstein J, Wollman J, and Bond MG, *Ultrasonic-Pathological Comparison of the Human Arterial Wall. Verification of Intima-Media Thickness.* Arterioscler. Thromb., 1993. **13**(4): p. 482-486.

4. London GM, Marchais SJ, Guérin AP, and Métivier F, *Arteriosclerosis, Vascular Calcifications and Cardiovascular Disease in Uremia.* Curr. Opin. Nephrol. Hypertens., 2005. **14** (6): p. 525-531.

5. Levick JR, *An Introduction to Cardiovascular Physiology*. 2003, London: Hodder. 384.

6. Barry M, Foulon P, Touati G, Ledoux B, Sevestre H, Carmi D, and Laude M, *Comparative Histological and Biometric Study of the Coronary, Radial and Left Internal Thoracic Arteries.* Surg. Radiol. Anat., 2003. **25**(3): p. 284-289.

7. Canham PB, Finlay HM, Dixon JG, Boughner DR, and Chen A, *Measurements from Light and Polarised Light Microscopy of Human Coronary Arteries Fixed at Distending Pressure.* Cardiovasc. Res., 1989. **23**(11): p. 973-982.

8. Gross, L.; Epstein, E. Z., and Kugel, M. A. Histology of the coronary arteries and their branches in the human heart. Am. J. Path., I934, IO, 253 -274.

9. Sokolis DP, Kefaloyannis EM, Kouloukoussa M, Marinos E, Boudoulas H, and Karayannacos PE, *A Structural Basis for the Aortic Stress-Strain Relation in Uniaxial Tension.* J. Biomech., 2006. **39**(9): p. 1651-1662.

10. von der Mark K and Ocalan M, *Immunofluorescent Localization of Type V Collagen in the Chick Embryo with Monoclonal Antibodies.* Coll. Relat. Res, 1982. **2**(6): p. 541-555.

11. Kawasaki T and Sasayama S, *Non-Invasive Assesment of the Age of Related Changes in Stiffness of Major Branches of the Human Arteries.* Cardiovasc. Res., 1987. **21**(9): p. 678-687.

12. Fung YC, Fronek K, and Patitucci P, *Pseudoelasticity of Arteries and the Choice of Its Mathematical Expression.* Am. J. Physiol. Heart Circ. Physiol., 1979. **237**(5): p. H620-631.

13. Holzapfel GA, Eberlein R, Wriggers P, and Weizsäcker HW, *A New Axisymmetrical Membrane Element for Anisotropic,Finite Strain Analysis of Arteries.* Commun. Num. Meth. Eng., 1996. **12**(8): p. 507-517.

14. Cox RH, *Regional Variation of Series Elasticity in Canine Arterial Smooth Muscles.* Am. J. Physiol. Heart. Circ. Physiol., 1978. **234**(5): p. H542-551.

15. Holzapfel GA, Gasser T, and Ogden R, *A New Constitutive Framework for Arterial Wall Mechanics and a Comparative Study of Material Models.* J. Elast., 2000. **61**(1): p. 1-48.

16. von Maltzahn WW, *Stresses and Strains in the Cone-Shaped Carotid Sinus and Their Effects on Baroreceptor Functions.* J. Biomech., 1982. **15**(10): p. 757-765.

17. von Maltzahn WW, Besdo D, and Wiemer W, *Elastic Properties of Arteries: A Nonlinear Two-Layer Cylindrical Model.* J. Biomech., 1981. **14**(6): p. 389-397.

18. von Maltzahn WW, Warriyar RG, and Keitzer WF, *Experimental Measurements of Elastic Properties of Media and Adventitia of Bovine Carotid Arteries.* J. Biomech., 1984. **17**(11): p. 839-847.

19. Demiray H, *A Note on the Elasticity of Soft Biological Tissues.* J. Biomech., 1972. **5**(3): p. 309-311.

20. Demiray H and Vito RP, *A Layered Cylindrical Shell Model for an Aorta.* Int. J. Engrng. Sci., 1991. **29**(1): p. 47-54.

21. Spencer AJM, ed. *Continuum Theory of the Mechanics of Fibre-Reinforced Composites*. 1992, Springer-Verlag.

22. Holzapfel GA and Ogden R, *Modelling the Layer-Specific Three-Dimensional Residual Stresses in Arteries with an Application to the Human Aorta.* J. R. Soc. Int., 2010. **7**(46): p. 787-799.

23. Chuong CJ and Fung YC, *Three-Dimensional Stress Distribution in Arteries.* J. Biomech. Eng., 1983. **105**(3): p. 268-274.

24. Holzapfel GA, *Nonlinear Solid Mechanics*, ed. Wiley. 2006, Sussex. 455.

25. Holzapfel GA, *Collagen. Structure and Mechanics*, in *Collagen in Arterial Walls: Biomechanical Aspects*, P. Fratzl, Editor. 2008, Springer-Verlag, Heidelberg: New York. p. 285-324.

26. Holzapfel GA, *Biomechanical Behavior of the Arterial Wall and Its Numerical Characterization.* Comp. Biol. Med., 1998. **28**: p. 377-392.

27. Watton PN, Ventikos Y, and Holzapfel GA, *Modelling the Mechanical Response of Elastin for Arterial Tissue.* J. Biomech., 2009. **42**(9): p. 1320-1325.

28. Holzapfel GA and Gasser TC, *A Viscoelastic Model for Fiber-Reinforced Composites at Finite Strains Continuum Basis, Computational Aspects and Applications.* Comput. Methods Appl. Mech. Engr., 2001. **190**(34): p. 4379-4403.

29. Dahl S, Vaughn M, Hu J, Driessen F, Baaijens F, Humphery J, and Niklason L, *A Micostructurally Motivated Model of the Mechanical Behavior of Tissue Engineered Blood Vessels.* Ann. Biomed Eng., 2008. **36**(11): p. 1782-1792.

30. Chang F and Delleur JW, *Systematic Parameter Estimation of Watershed Acidification Model.* Hydrol. Process., 1992. **6**(1): p. 29-44.

31. Jeremy E and O'Hagan OA, *Probabilistic Sensitivity Analysis of Complex Models: A Bayesian Approach.* J. R. Statist. Soc. B, 2004. **66**(3): p. 751-769.

32. Petitti D, *Meta-Analysis,Decision Analysis, and Cost-Effectiveness Analysis*. 2,illustrated ed. 2000: Oxford University Press. 306.

33. Fenner R, *Mechanics of Solids*. 1989, Oxford: Blackwell scientific publications. 615.

34. Kroon M and Holzapfel GA, *A New Constitutive Model for Multi-Layered Collagenous Tissues.* J. Biomech., 2008 **41**(12): p. 2766-2771.

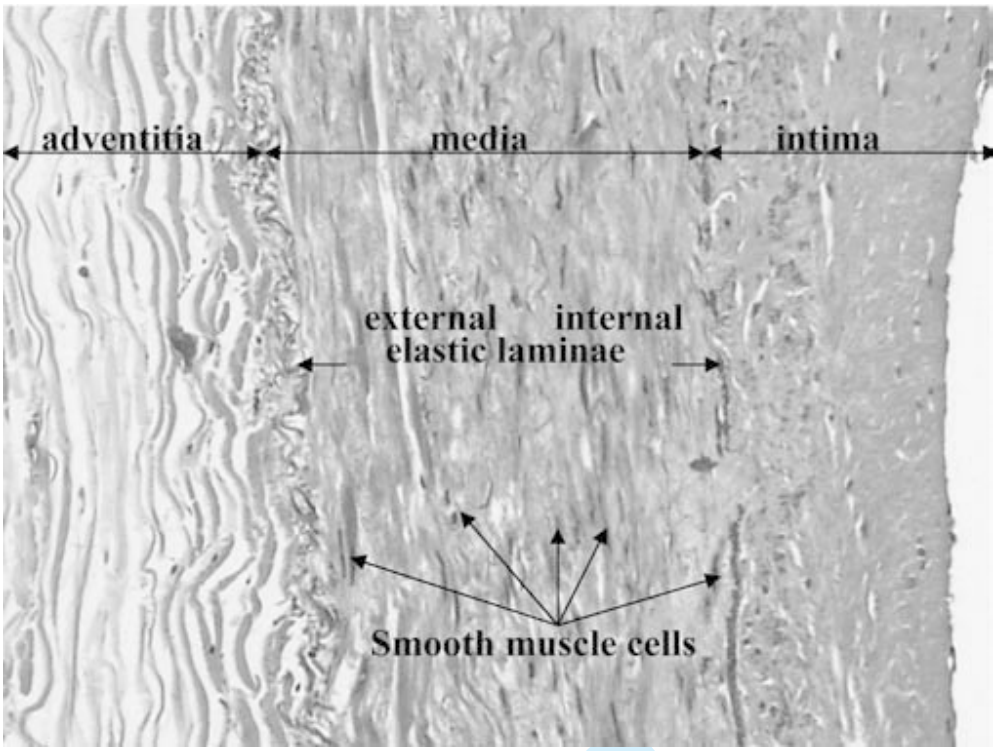

Figure 1: A radial cross section through a coronary arterial wall, showing three layers: intima, media, and adventitia. (Adapted from [6])

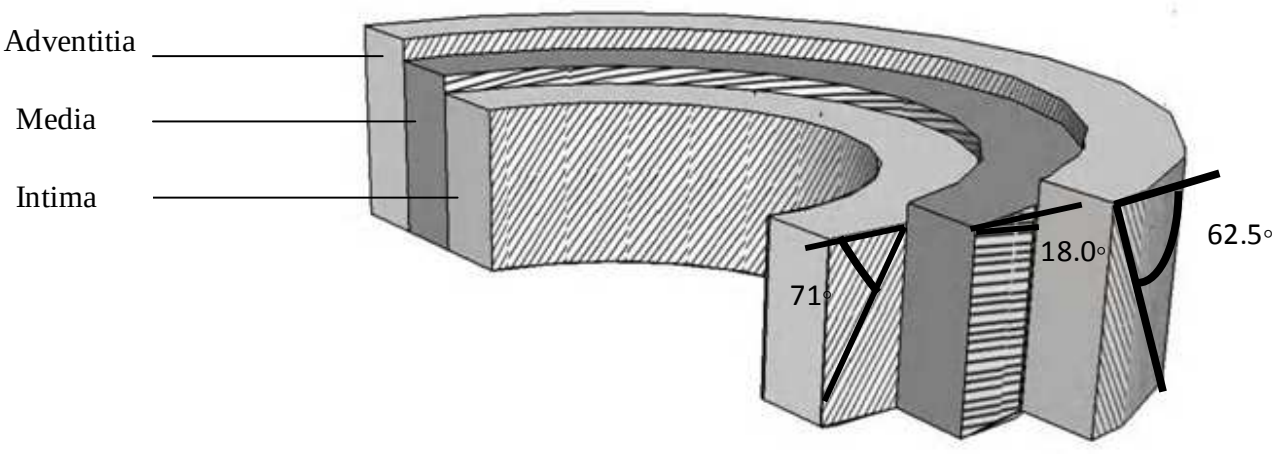

Figure 2: A cross section through the arterial wall showing the intimal, medial and adventitial layers with the optimised collagen fibre angle for each layer.

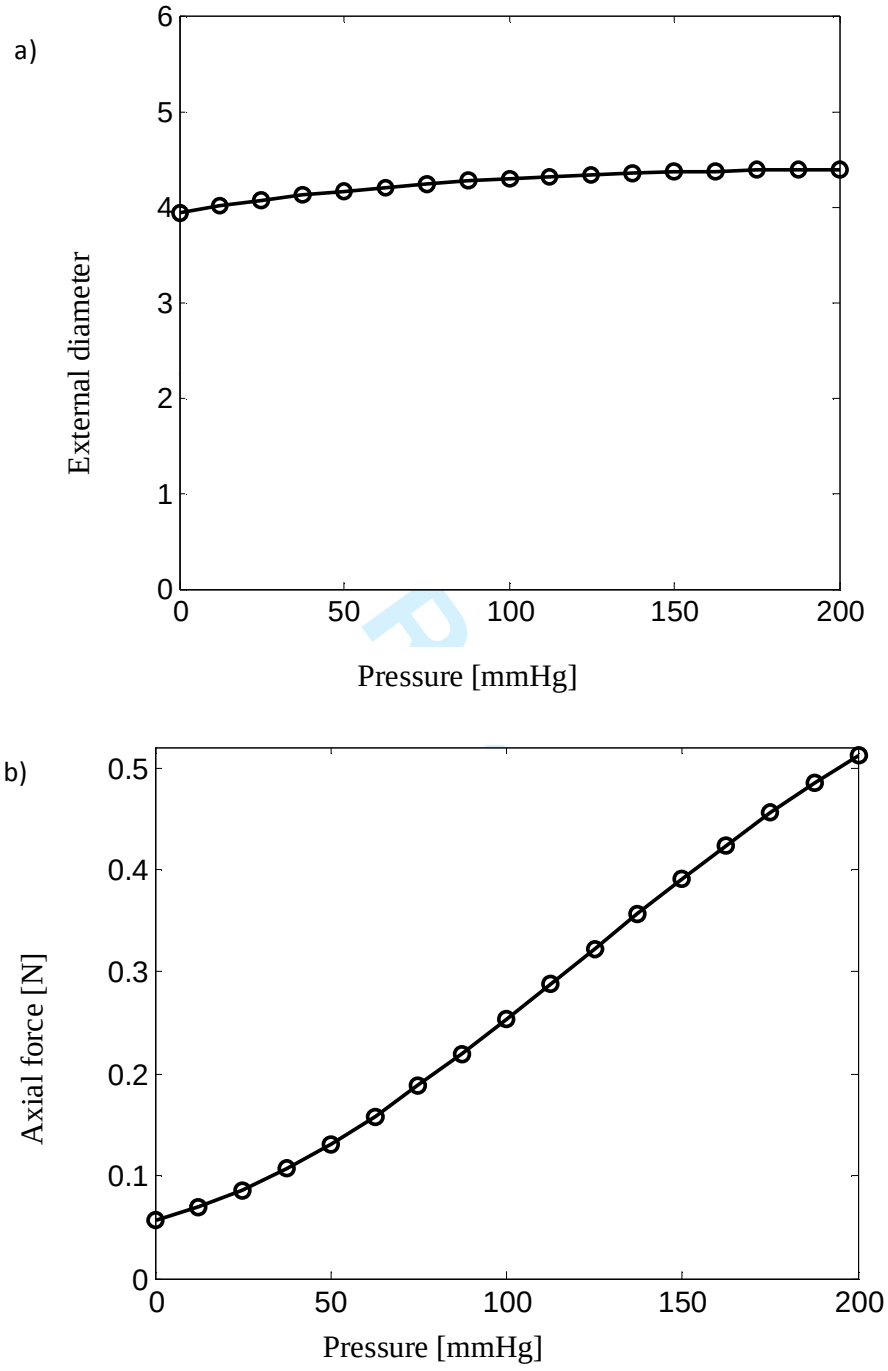

Figure 3: Experimental data for (a) external diameter and (b) axial force for a coronary artery as a function of luminal pressure. Extracted from [2] using 17 point digitisation method.

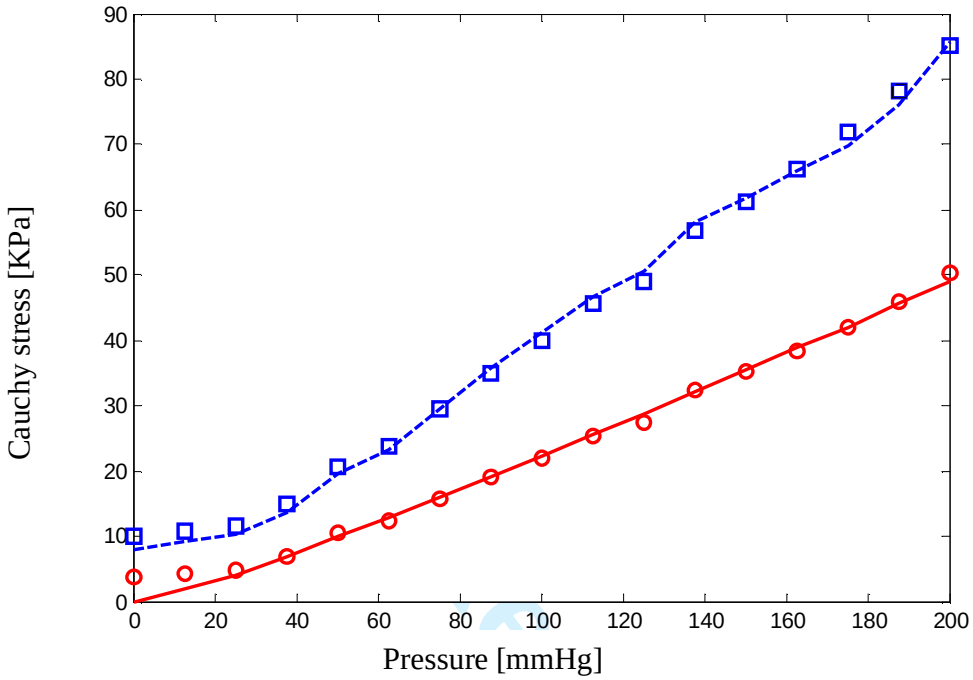

Figure 4: Estimated axial (square) and circumferential stresses (circle) using the hyperelastic layer model proposed in this paper for the coronary artery data extracted from [2] and the corresponding experimental axial (dashed line) and circumferential (continuous line) stresses.

a)

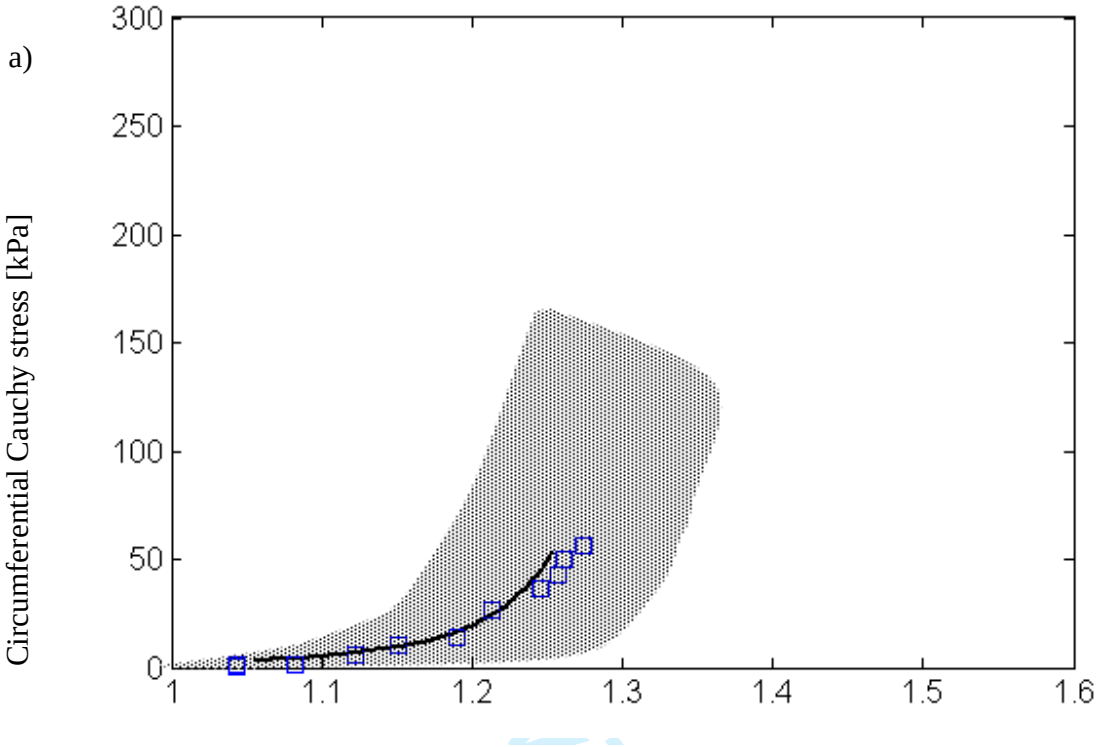

b)

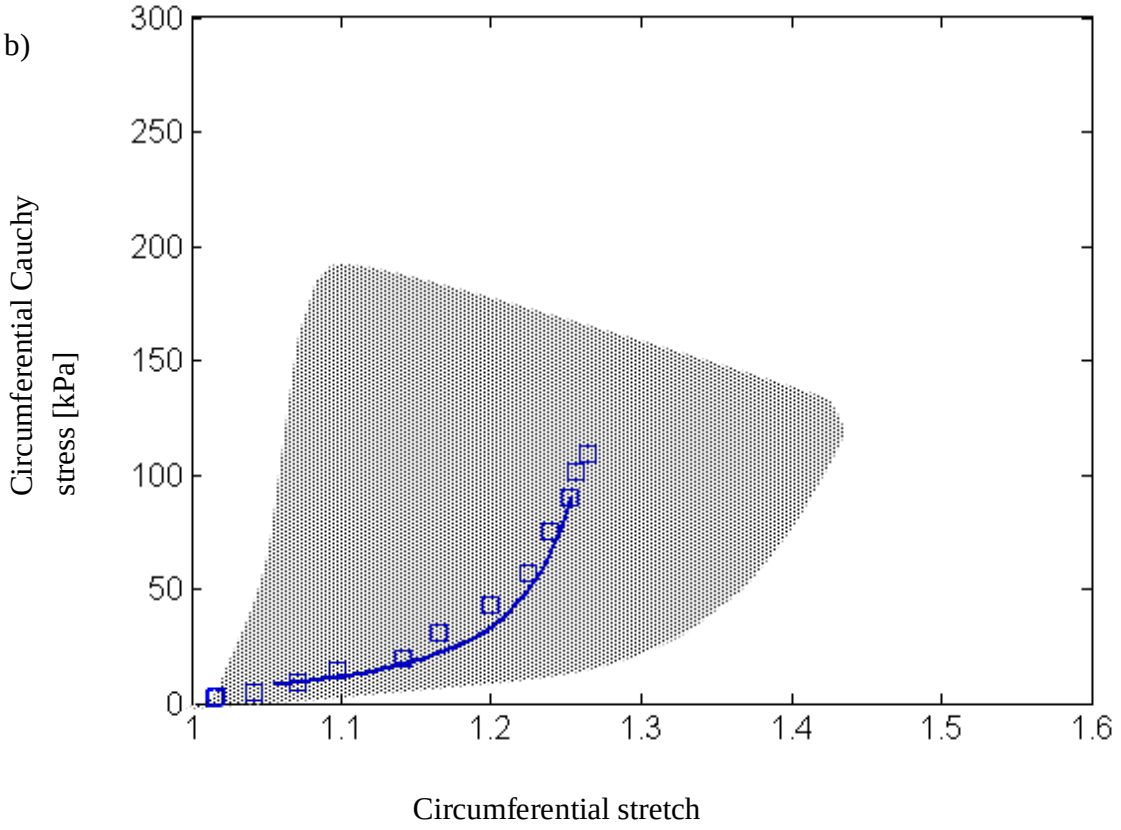

c)

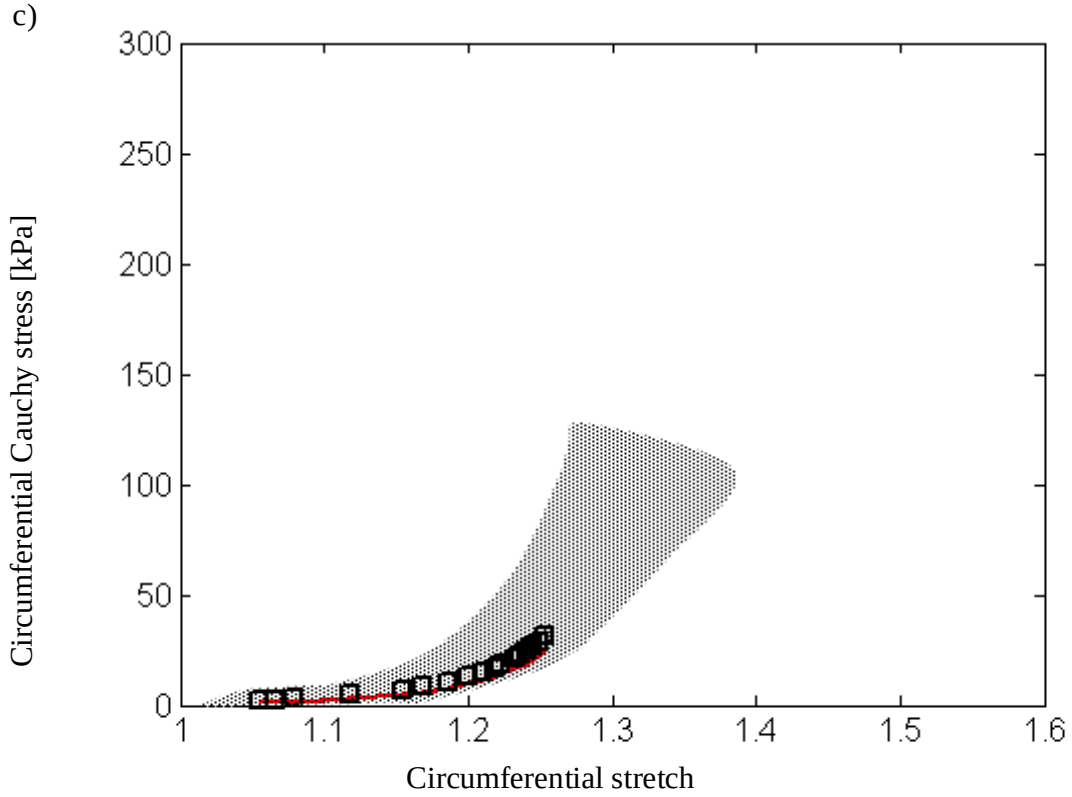

d)

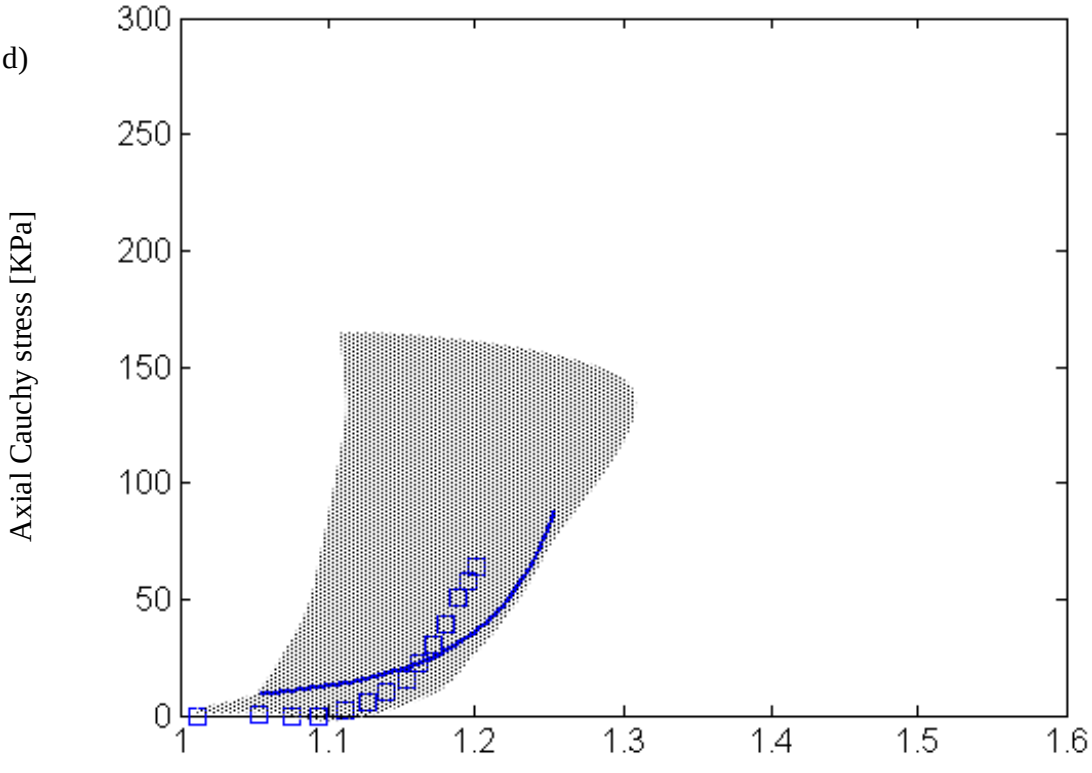

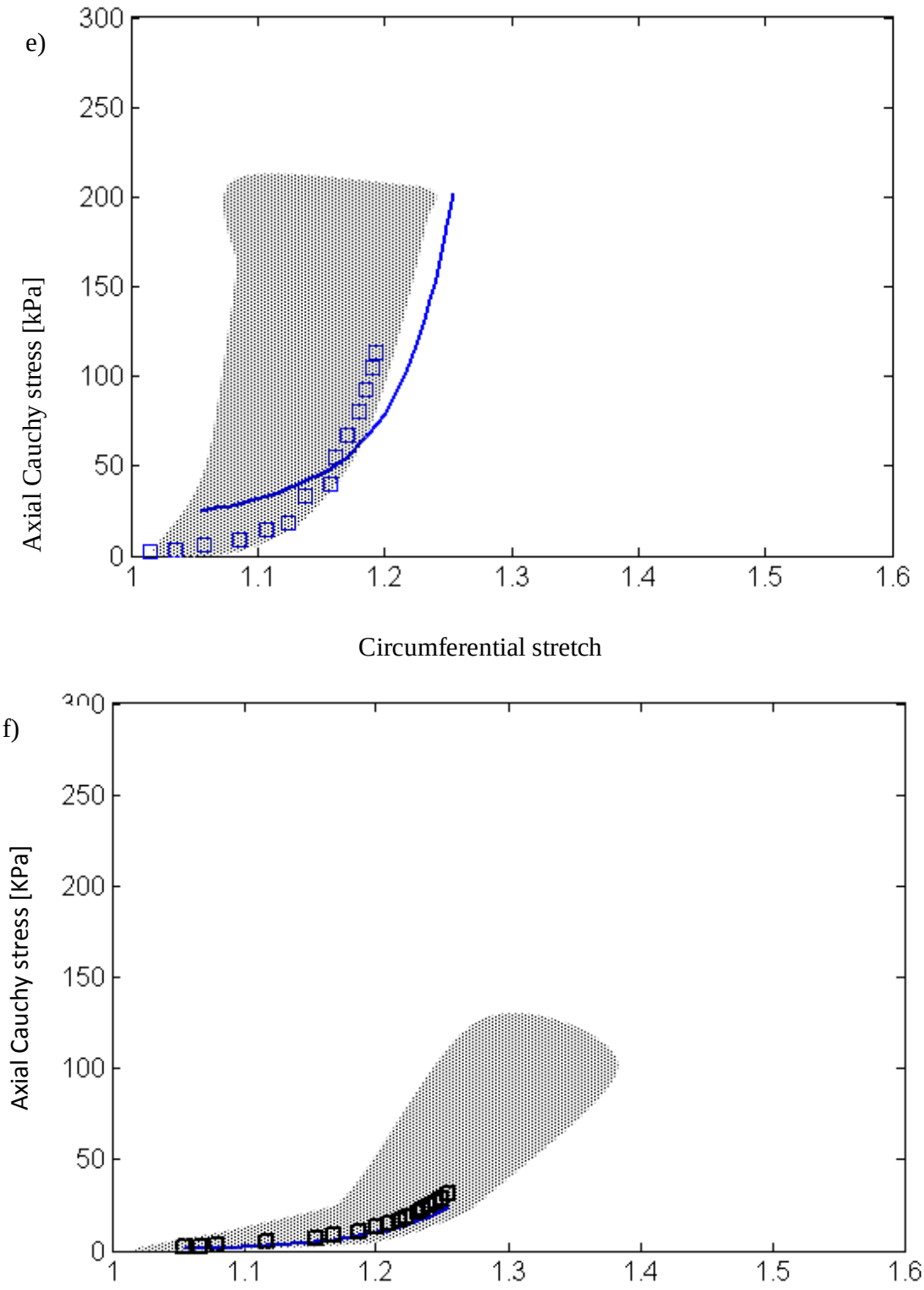

Figure 5: Layer stress (continuous line) for circumferential direction for a) adventitia, b) intima and c) media then in axial direction in d) adventitia e) intima f) media, compared with the experimental range (shaded area) presented in [1] with one data set (square) from the same reference.

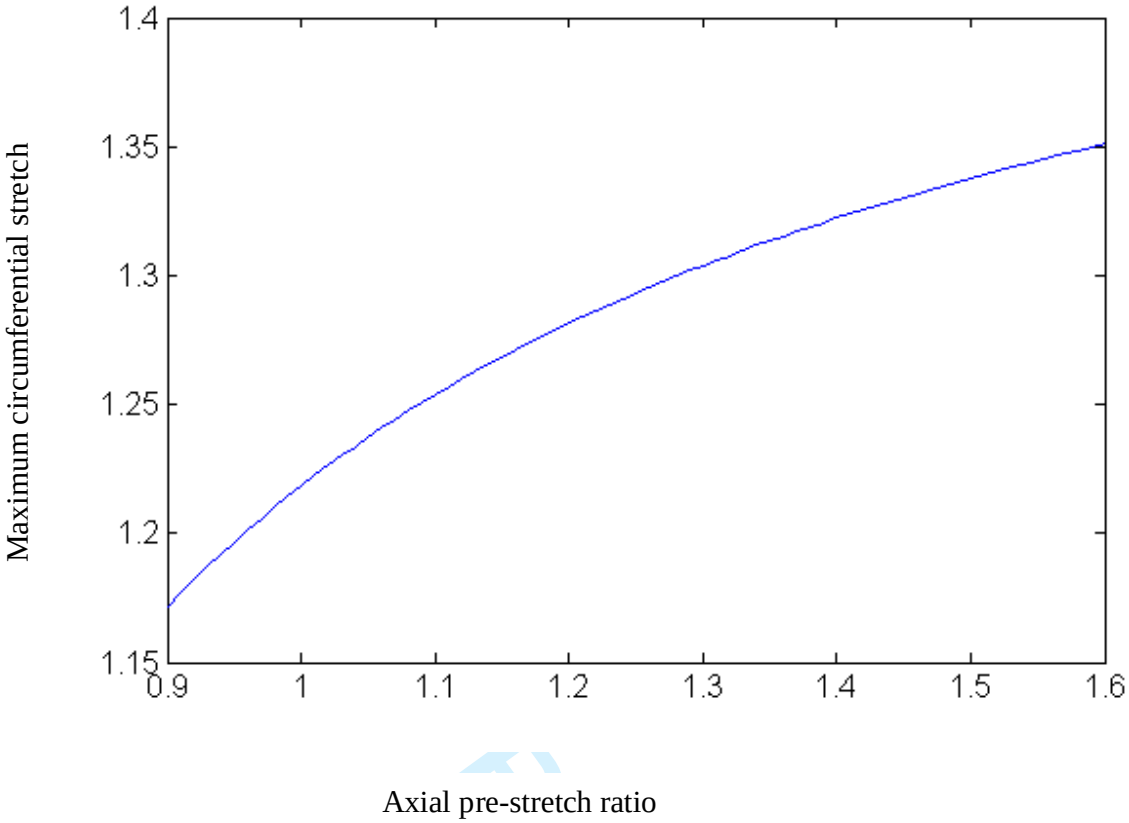

Figure 6: Axial pre-stretch ratio versus maximum stretch ratio.

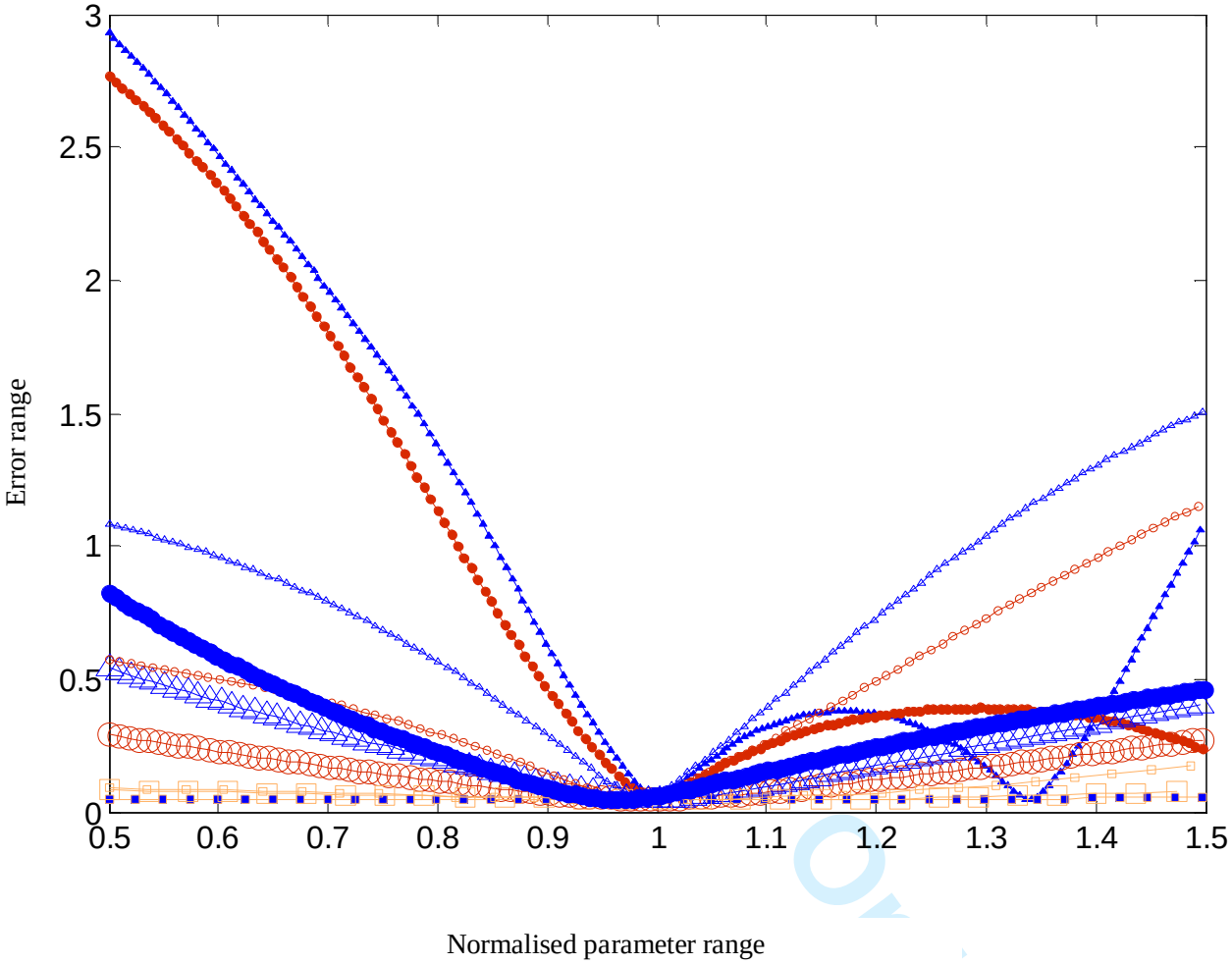

Figure 7: Parameter sensitivity for the fifteen parameters in the model of the coronary artery. A small full symbol is used for φ, k_2 is represented by a small empty symbol, k_1 is represented by a large closed symbol and finally the dispersion is represented by large empty symbol. The intimal layer is represented by a triangle, the adventitial layer by a circle and medial layer by a square. Elastin constants, c_1 are the least significant and are not shown.

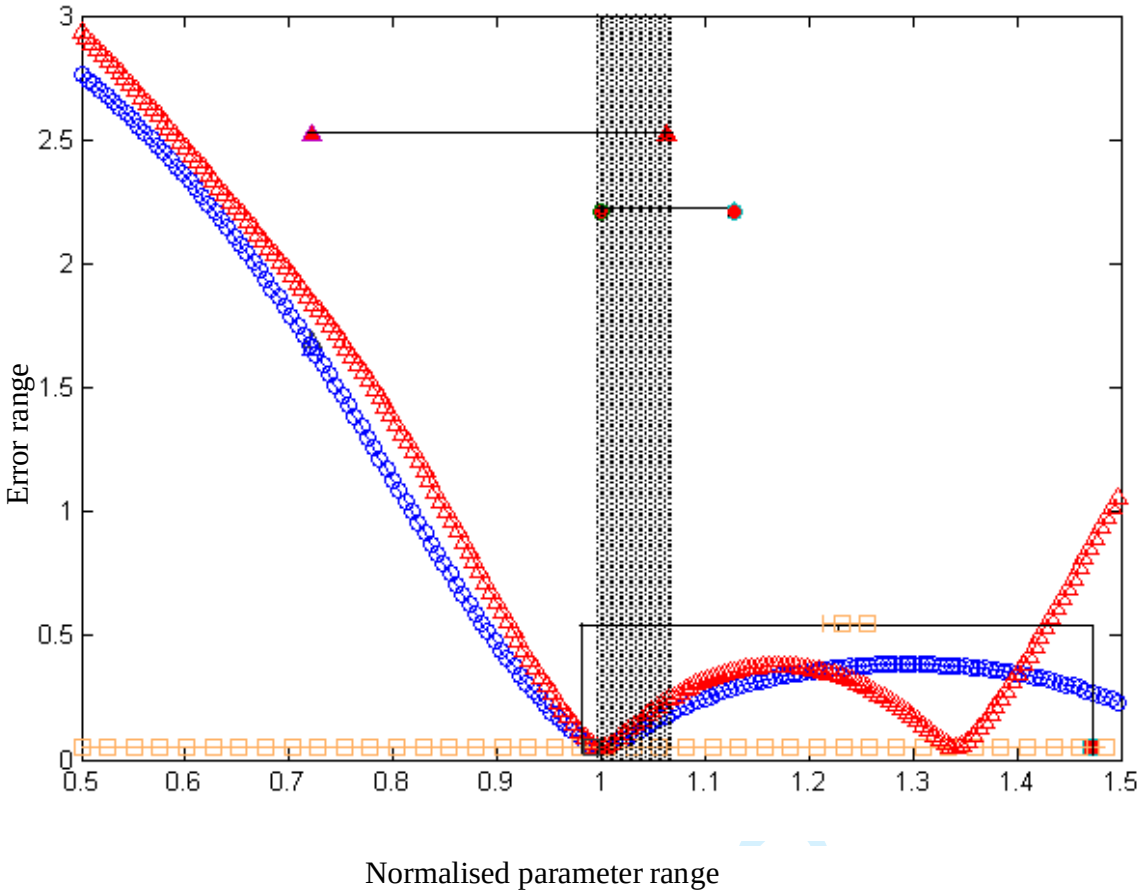

Figure 8: Parameter sensitivity for collagen fibre angles of the coronary artery. The intimal layer is represented by a triangle, the adventitial layer by a circle and medial layer by a square. Each respective physiological range is marked with its symbol and the common physiological range is shaded.

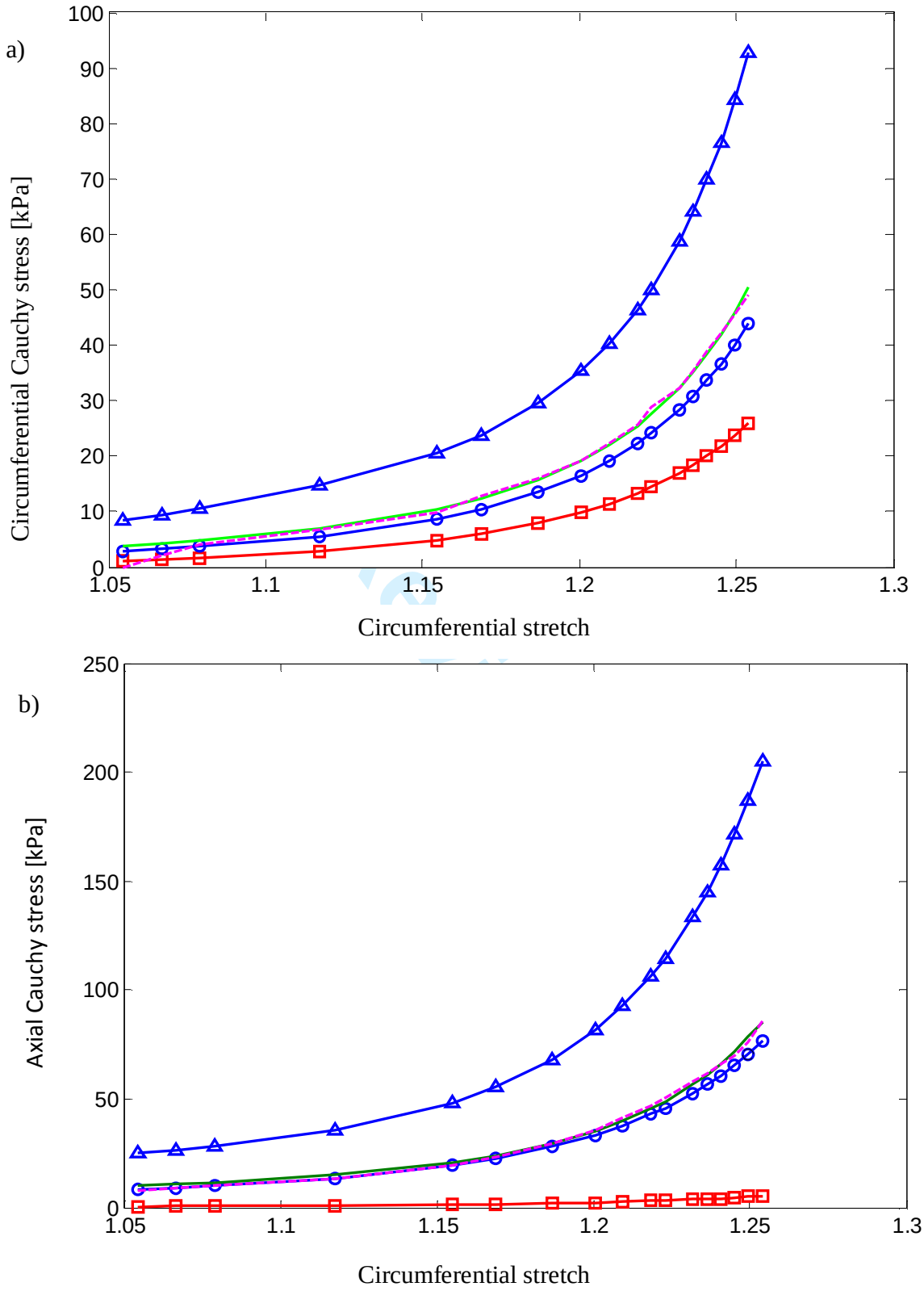

Figure 9: The layer response is compared with the total response in two directions. a) circumferential b) axial, triangle is used for intima, circle for adventitia. The model results are shown in a dashed line and the experimental results are shown in continuous line.

Table 1

Coronary artery characteristics

feature	Intima	Media	Adventitia
Collagen content	Highest	Lowest	Medium
Collagen distribution	Dispersed	Circumferential	Dispersed
Stiffer direction	Longitudinal	Circumferential	Longitudinal
Stiffness	Stiffest	Softest	Medium
Elastin distribution	3-D network of elastic fibres		
Effect of elastin at the curve start	Linear relationship		
Percentage of thickness	27%	40%	33%

Table 2

Coronary artery characteristics

Characteristic	Coronary artery
Anatomy	Cylindrical
External diameter	3.96 mm
Thickness	1.06 mm
Axial pre-stretch	10%

Table 3

Optimised material parameters for the combined layer model and Holzapfel et al's individual layer experiments [1]

Estimated parameter	Model parameter Mean±std (to 2 d.p.)	Holzapfel's parameters Mean±std (to 2 d.p) [1]
k_{2n}	45.41 ± 0.00	170.88 ± 125.47
k_{2m}	9.14 ± 0.08	8.21 ± 3.27
k_{2a}	35.95 ± 0.09	85.03 ±58.94
c_{1n}, [kPa]	8.96 ± 0.47	13.95 ± 5.30
c_{1m} [kPa]	0.33 ± 0.04	0.63 ± 0.36
c_{1a} [kPa]	1.58 ± 0.27	3.78 ± 2.33
k_{1n} [kPa]	7.03 ± 0.52	65.91 ± 122.73
k_{1m} [kPa]	6.28 ± 0.24	5.40 ± 1.78
k_{1a} [kPa]	5.68 ± 0.36	9.64 ± 8.13
ρn	0.64 ± 0.00	0.51 ± 0.14
ρm	0.14 ± 0.01	0.25 ± 0.09
ρa	0.72 ± 0.00	0.55 ± 0.18

Table 4

Estimated collagen fibre angles (from the circumferential direction) for each layer for two vessels

Layer	Model angle Mean ± std (to 2 d.p.)	Holzapfel Model [1] Mean ± std (to 2 d.p.)
Intima	72.49±0.41	60.30 ± 18.20
Media	16.37±1.15	20.61 ± 5.50
Adventitia	62.87±0.42	67.00 ±8.50

Dear Sir,

We would like to thank you for your comments. These comments have proved very valuable and enriching to our research. As advised, we have only concentrated on the collagen types that appear in the coronary artery. We have changed the thickness ratio to agree with what have been suggested. We removed the volumetric portion of the strain energy function. Please find below every point raised and its reply. We are hopeful that after the changes done to our paper, it is raised to the level of acceptance of publication.

Regards

Michel E Mickael

Response to Referee's Comments

1	The summary of the results obtained in [7] (line 46-48) is misleading. According to that paper, collagen is largely of type I in the intima and there is very little SMC in the intima.	Collagen in intima changed to type I as in [1]
2	Reference [8] cited on line 51 is for the aorta so is not appropriate here. As clearly stated in the references including [1] (and now stated in this manuscript) the properties of the coronary arteries differ from elsewhere in the body and with age. Therefore, the authors should focus solely on coronary arteries in this section.	Reference changed to [2]
3	According to reference [7] cited by the authors, the media collagen is largely of type III. In the text line 51, they state types I and III are found in that layer.	Collagen in media changed to type I only[1]
4	The definition of the term softest should be clarified. If the authors mean slope of the stress/strain curve, then the stiffness of the medial layer in the circumferential direction is nearly equal to the of the adventitia up to a stretch of 1.25 (Fig. 7, reference [1]).	Below this table we have shown the analysis we have done to verify the statement used in this paper and by Holzapfel. The graph in Fig. 7 is calculated data. We have performed our analysis on the experimental data. The results do suggest that in general the media is the softest layer.
5	It appears there is a typo in line 52. I think the authors really mean the SMC are aligned in the circumferential direction (not perpendicular to the	Changed

	circumferential direction as they state).	
6	There appears to be a serious error in the selected layer thicknesses on line 109. The authors set the thickness of the individual layers relative to the entire wall thickness of the intima, media, adventitia as [27,40,33] percent respectively (citing [1]) whereas [1] gives the values [27, 36, 40], respectively (page H2051). It appears that the last two are switched. This is an underlying approximation in all the calculations in this paper, so may alter the results.	Changed and updated, initially the separate thickness are given by[3] as follows: 27±0.02, 0.36±0.03 and 0.40±0.03, but it could be noticed that these values when added exceeds unity as each thickness was measured separately after separating the three layers. It is also worth noting that the thickness of the artery increases after being taken out of the body. Thus the value of unity was assumed and the values of the intact thickness were calculated according to the above ratio to be For nominal layer thicknesses of 26.2%, 34.9% and 38.8% for the intima, media and adventitia respectively. The simulations have been repeated with the new values. This has improved the curve fit as can be seen in Figures 2,3 and 4 and has not altered the main findings of this work.
7	There is no need to introduce a volumetric portion of the strain energy function on line 129-130 since the authors are later using the incompressibility assumption. There seems to be some confusion on page 5 about this issue. It would be better if they used the incompressible model from the start.	Changed as advised
8	In (8), the authors have eliminated the Lagrange multiplier (P) without explanation of what the loading is (boundary conditions). Since boundary conditions are needed to eliminate P, great care must be taken. Of possible great significance is that it appears that the Lagrange multiplier was eliminated in equation (8) by setting S_r equal to zero. Namely, there are equations for S_r, S_θ, S_z which all involve the Lagrange multiplier (P). This Lagrange multiplier has been eliminated from (8). Equation (8) will be obtained if S_r is set to zero. However, this cannot be correct, since the authors are considering pressure inflation.	S_r=0 because of the use of the thin wall assumption see (3,4,5) Equations are summarised below this table.
9	From an initial assessment of the results I noted	That is a good observation, the

	that the predicted curves in Fig 5 do not go to zero when stretch reduces to one. This is very strange. It may be related to the errors above.	reason is that the arterial segment is pre-stretched in the axial direction, so when the stretch in the circumferential direction is applied the stress does not come to zero, see equations 16, 17.
10	It should be noted that the results presented in [1] are for uniaxial loading while the authors discuss pressure inflation on pages 8 and 9. It is not clear that this was accounted for in Fig. 5.	Yes, we are aware that the intact arterial experiments are biaxial and the layer experiments are uniaxial, due to difficulties stated by the author (3). We discuss this in lines 303-310.
11	On line 120, it should be stated that W is the strain energy per unit volume in the unloaded reference configuration.	Corrected as advised.

point 4

Evidence supporting the assumption of "the media in general is the softest layer"

The experimental stiffness of the media and adventitia were compared using experimental data given in [2] (figures 2, 3 and 4).

The curves were digitised and the stiffness (gradients of curves in figures 2,3 and 4 were calculated for each artery of the media and adventitia. The stiffness was calculated before and after the knee point on each curve given by (1.15 stretch). The results are shown in figure 1 and table 1. The box plots show the median and the first and third quartiles.

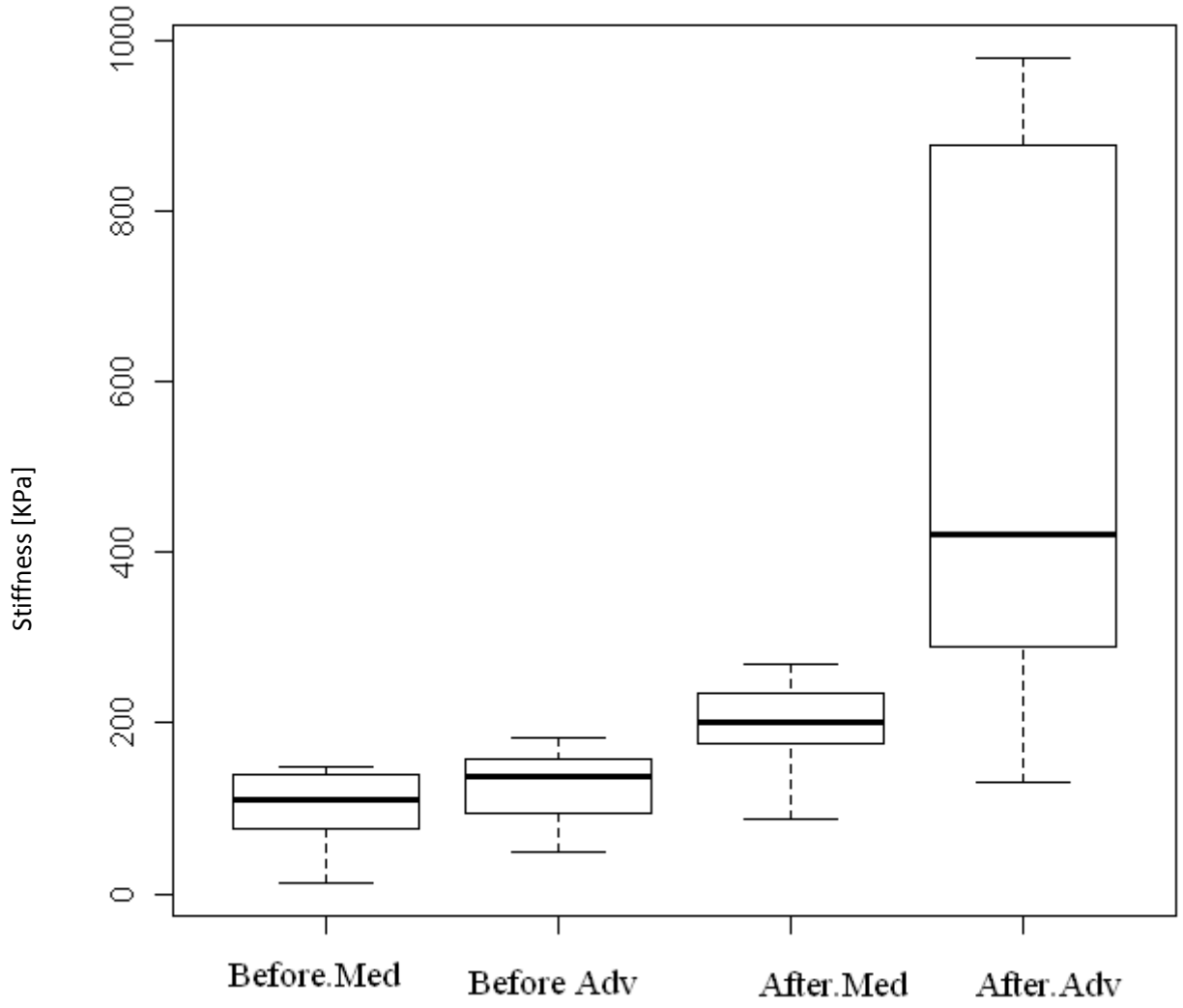

Table showing stiffness estimations in KPa

Artery	before kneepoint media	before kneepoint adventitia	after kneepoint media	after kneepoint adventitia
8	141.0187	180.36	268.6541	420.83
4	148.15	48.1489	201.9438	405.5046
6	137.3442	67.0154	251.9001	130.6419
5	100.566	137.7069	219.0854	877.0304
2	109.3664	123.9843	151.1208	172.88
10	50.9369	182.4311	201.5652	978.5079
7	13.8107	137.7069	87.9107	877.0304

The table shows that the media is less stiff than the adventitia for 71% of the samples before and 86% of the samples after the knee point. The knee point was chosen as a border between the two phases of operation, where phase one, is elastin dominated, and the second phase after 1.15 stretch is dominated by collagen with some elastin contribution.

It is also worth noting that figure 7 of reference [2] is based on the values of the mean of the model of the 13 arteries and not experimental data.

Point 8 Why S_r=0

This is an extract from [5]. Our $S_r = S_{33}$ is this paper's notation.

$$\hat{S}_{AB} = \begin{bmatrix} \frac{1}{\lambda_1}\frac{\partial \hat{W}}{\partial \lambda_1} + \frac{\bar{p}}{\lambda_1^2} & 0 & 0 \\ 0 & \frac{1}{\lambda_2}\frac{\partial \hat{W}}{\partial \lambda_2} + \frac{\bar{p}}{\lambda_2^2} & 0 \\ 0 & 0 & \lambda_1\lambda_2\frac{\partial \hat{W}}{\partial \lambda_3(\lambda_1\lambda_2)} + \bar{p}\lambda_1^2\lambda_2^2 \end{bmatrix}. \quad (15)$$

Furthermore, using the plane stress constraint ($\hat{S}_{33} \overset{!}{=} 0$) the third row of Eq. (15) allows the hydrostatic pressure to be explicitly expressed as

$$\bar{p} = -\frac{1}{\lambda_1\lambda_2}\frac{\partial \hat{W}}{\partial \lambda_3(\lambda_1, \lambda_2)}. \quad (16)$$

Observe that for *membranous structures* the incompressibility condition is already incorporated due to Eq. (9) and the Lagrangian multiplier $\bar{p}$ introduced in Eq. (11) serves here as an arbitrary scalar function to enforce the plane stress condition.

Hence, a back-substitution of the pressure into relations $(15)_1$, $(15)_2$ leads to the following two non-zero components $S_\alpha|_{\alpha=1,2}$, i.e.

$$S_1 := \hat{S}_{11} = \frac{1}{\lambda_1}\frac{\partial \hat{W}}{\partial \lambda_1} - \frac{1}{\lambda_1^3 \lambda_2}\frac{\partial W}{\partial \lambda_3(\lambda_1, \lambda_2)},$$
$$S_2 := \hat{S}_{22} = \frac{1}{\lambda_2}\frac{\partial \hat{W}}{\partial \lambda_2} - \frac{1}{\lambda_1 \lambda_2^3}\frac{\partial W}{\partial \lambda_3(\lambda_1, \lambda_2)}. \tag{17}$$

$$\lambda_3 = \frac{1}{\lambda_1 \lambda_2}. \tag{9}$$

References

1. Canham PB, Finlay HM, Dixon JG, Boughner DR, and Chen A, Measurements from Light and Polarised Light Microscopy of Human Coronary Arteries Fixed at Distending Pressure, Cardiovasc. Res., 1989. 23(11): p. 973-982.
2. Gross L, Epstein EZ, and Kugel, MA, Histology of the Coronary Arteries and their Branches in the Human Heart. Am. J. Path., I934, IO, 253 -274.
3. Holzapfel GA, Sommer G, Gasser CT, and Regitnig P, Determination of Layer-Specific Mechanical Properties of Human Coronary Arteries with Nonatherosclerotic Intimal Thickening and Related Constitutive Modeling. Am. J. Physiol. Heart Circ. Physiol., 2005. 289(5): p. H2048-2058.
4. Holzapfel GA, Eberlein R, Wriggers P, and Weizsäcker HW, A New Axisymmetrical Membrane Element for Anisotropic,Finite Strain Analysis of Arteries. Commun. Num. Meth. Eng., 1996. 12(8): p. 507-517.
5. Holzapfel GA, Eberleinb R, Wriggersb P, Weizsticker H, Large strain analysis of soft biological membranes: Formulation and finite element analysis, Comput. Methods Appl. Mech. Eng., 1996 ,132 :p.45-61.

```
%coronary artery pogram%
clc;
clear;
% Module 1:data input
D=4.94*1e-03;          %D=wall external diameter
H=(D*0.30) ;           %H= wall thickness
%dnew=[4.81 4.83 4.88 4.95 5 5.05 5.06 5.18 5.26 5.3 5.5 6.7 7.75 7.8]*1e-03;
dnew=[4.81 4.83 4.88 4.95 5 5.05 5.1 5.13 5.15 5.18 5.25 5.28 5.3]*1e-03;

l2=1.1;
%Module 2:Thin wall theory
d=(H*(D-H))/l2;
b=((dnew.^2./4)-d).^(0.5);
h=(dnew./2)-b;
r=(dnew-h)/2;
R=(D-H)/2;

sigma=[   0.0350    0.038    0.04   0.05    0.070    0.08510    0.110  0.155 0.23 0.28    0.37 0.46   0.600183  ]*1e05;

s2=[0.029    0.035881    0.045151    0.07    0.0988    0.125   0.17  0.23  0.33  0.4   0.505 0.6  0.75839   ]*1e05;
%sigma=[   0.0570    0.06    0.067   0.0866    0.09    0.1110    0.130    0.195    0.2961    0.600183  0.805   1.2621
1.6741    2.8]*1e05;

%s2=[0.0194    0.03081    0.041151    0.07    0.0988    0.15    0.20    0.35    0.505   0.75839    0.85    1.1    1.2
1.4]*1e05;

%s2=[0.0194    0.03081    0.041151    0.07    0.0988    0.15    0.20    0.35    0.505   0.75839    0.85    1.1    1.2
1.4]*1e05;


%strain=[0.03 0.05 0.06 0.07 0.09 0.1 0.11 0.13 0.14 0.15 0.16 0.17 0.18 0.182];
strain=[0.03 0.05 0.06 0.07 0.09 0.1 0.11 0.12 0.13 0.135  0.14 0.145 0.15 ];

lamda=1./(1-2*strain).^(0.5);
q=((r./h)-(0.5));

p=sigma./q;


%Module 3, assumptions intima=i media=m adventitia=a
hi=0.262*h;
hm=0.349*h;
ha=0.388*h;
%lb=[0.73 0.26 1.09 45.41 4.94 26.09    8650 320 1450 3.9e03 3.625e03 3.7e03 0.37 0.14 0.37];
%ub=[1.37 0.45 1.31 130   13.1 120     19000 900 6000 100e03 7.2e03 17.5e03 0.65 0.34 0.73];
%a=[0.918419836396082,0.41583025021729,1.092130680919774,53.3933731535554,10.8705861753712,48.4858815
885614,13799.3852585224,5196.84278107774,17500;]

%a=[0.88934452774139,0.306473744245994,1.09152905299021,48.6763804123347,9.16139299976272,47.5434477023866,15246.7183041945,4732.33021735782,17500;]
%a=[0.923998924200236,0.295168469396933,1.12290975783508,56.3301427371482,11.6128999579224,31.1578064319077,11128.3487039323,4661.25749407590,17500;]
%a=[0.968559245444828,0.305394898232727,1.25146338797463,58.3736813748610,10.5948874271261,33.4574593590495,13613.2580946418,4779.23430019145,17500;]
%a=[0.968559245444828,0.305394898232727,1.25146338797463,58.3736813748610,10.5948874271261,33.4574593590495,13613.2580946418,4779.23430019145,17500;]
a=[0.918405361868358,0.293391770833512,1.09731791690408,55.2264463401203,11.8045714022707,30.0101014944855,11817.1303875404,4305.55328177654,17500;]

thetai=a(1);
thetam=a(2);
thetaa=a(3);
k2i=a(4);
```

```
k2m=a(5);
k2a=a(6);
c1i=4000;
c1m=400;
c1a=5500;
k1i=a(7);
k1m=3700;
k1a=a(8);
rowi=0.58;
rowm=0.15;
rowa=0.55;

%Module 4: HYPERELASTIC MODEL%
I4m=(lamda.^2).*(cos(thetam)).^2+(l2.^2).*(sin(thetam )).^2;
qm=k2m*((I4m-1).^2);
sm1=[c1m.*(1-(1./((l2.^2).*(lamda).^4)))+k1m* exp(qm).*(I4m-1).*(cos(thetam )).^2].*(lamda.^2);   %circumferential
stress in the media %
sm2=[c1m.*(1-(1./((lamda.^2).*(l2).^4)))+k1m* exp(qm).*(I4m-1).*(sin(thetam  )).^2].*(l2.^2);      %Axial  stress in
the media  %
%module 4b : for adeventitia %
I4a=(lamda.^2).*(cos(thetaa)).^2+(l2.^2).*(sin(thetaa)).^2;
qa=k2a*((I4a-1).^2);
sa1=[c1a.*(1-(1./((l2.^2).*(lamda).^4)))+k1a* exp(qa).*(I4a-1).*(cos(thetaa  )).^2].*(lamda.^2) ;     %circumferential
stress in the adventitia %
sa2=[c1a.*(1-(1./((lamda.^2).*(l2).^4)))+k1a* exp(qa).*(I4a-1).*(sin(thetaa)).^2].*(l2.^2) ;        %Axial stress in the
adventitia %
%module 4 c: for intima%
I4i=(lamda.^2).*(cos(thetai )).^2+(l2.^2).*(sin(thetai)).^2;
qi=k2i*((I4i-1).^2);
si1=[c1i.*(1-(1./((l2.^2).*(lamda).^4)))+k1i* exp(qi).*(I4i-1).*(cos(thetai )).^2].*(lamda.^2);  %circumferential stress
in the intima  %
si2=[c1i.*(1-(1./((lamda.^2).*(l2).^4)))+k1i* exp(qi).*(I4i-1).*(sin(thetai )).^2].*(l2.^2);%Axial  stress in the intima %
%module 5: total stress  calculation%
st1=((si1.*hi+sm1.*hm+sa1.*ha)./(h))            %total circumferentioal stress%
st2=(si2.*hi+sm2.*hm+sa2.*ha)./(h);            %total axial stress
%MODEL 6: Results plotting%
figure(3)
plot(lamda,si1/1000,'g',lamda,sm1/1000,'r',lamda,sa1/1000,'b','LineWidth',2,'Marker','o')
xlabel('Circumferential stretch')
ylabel('Circumferential Cauchy stress [kPa]')
figure(4)
plot(lamda,si2/1000,'g',lamda,sm2/1000,'r',lamda,sa2/1000,'b','LineWidth',2,'Marker','o')
xlabel('Circumferential stretch')
ylabel('Axial Cauchy stress [kPa]')

figure(8)
plot(lamda,(st1/1000),'-ro',lamda,sigma/1000,'--','LineWidth',2)

figure(9)
plot(lamda,st2/1000,'-ro',lamda,s2/1000,'--','LineWidth',2)
xlabel('Circumferential stretch')
ylabel(' Cauchy stress [kPa]')

%figure(9)
%plot(p/133.32,h,'r')
kai=sum((sigma-st1).^2+(s2-st2).^2);
kai1=(kai/22).^0.5;
sigmaref=sum(st1+st2)/34;
eplson1=kai1/sigmaref
%
bai=sum((sigma-st1).^2);
bai1=(bai/5).^0.5;
bigmaref=sum(st1)/17;
```

```
eplsonb=bai1/bigmaref
%kesh kesha mat3rdha 2%
cai=sum((s2-st2).^2);
cai1=(cai/5).^0.5;
cigmaref=sum(st2)/17;
eplsonc=cai1/cigmaref
```

```
%coronary artery program%
clc;
clear;
% Module 1:data input
D=3.96*1e-03;          %D=wall external diameter
H=(D*0.27) ;           %H= wall thickness
p=[0:12.5:200].*133.32   %transumural pressure
dnew=[3.97 3.995 4.02 4.1 4.18 4.21 4.25 4.28 4.3 4.32 4.33 4.35 4.36 4.37 4.38 4.39 4.4]*1e-03;
l2=1.1;
%Module 2:Thin wall theory
d=(H*(D-H))l2;
b=((dnew.^2./4)-d).^(0.5);
h=(dnew./2)-b;
r=(dnew-h)/2;
R=(D-H)/2;
lamda=r./R;
q=((r./h)-(0.5));
sigma=p.q;
sigma21=sigma./2;
f=[ 0.07 0.072 0.073 0.09 0.13 0.15 0.19 0.23 0.265 0.3 0.32 0.37 0.39 0.41 0.43 0.47 0.54];
B=f./(2.*pi.*r.*h);
s2=((sigma21)+B) ;
%Module 3, assumptions intima=i media=m adventitia=a
hi=0.262*h;
hm=0.349*h;
ha=0.388*h;


thetai=a(1);
thetam=a(2);
thetaa=a(3)
k2i=a(4);
k2m=a(5);
k2a=a(6);
c1i=a(7);
c1m=a(8);
c1a=a(9);
k1i=a(10);
k1m=a(11);
k1a=a(12);
rowi=a(13);
rowm=a(14);
rowa=a(15);

%Module 4: HYPERELASTIC MODEL%
I4m=(lamda.^2).*(cos(thetam)).^2+(l2.^2).*(sin(thetam )).^2;
qm=k2m*((I4m-1).^2);
sm1=[c1m.*(1-(1./((l2.^2).*(lamda).^4)))+k1m* exp(qm).*(I4m-1).*(cos(thetam )).^2].*(lamda.^2);   %circumferential
stress in the media %
sm2=[c1m.*(1-(1./((lamda.^2).*(l2).^4)))+k1m* exp(qm).*(I4m-1).*(sin(thetam  )).^2].*(l2.^2);      %Axial  stress in
the media  %
%module 4b : for adeventitia %
I4a=(lamda.^2).*(cos(thetaa)).^2+(l2.^2).*(sin(thetaa)).^2;
qa=k2a*((I4a-1).^2);
sa1=[c1a.*(1-(1./((l2.^2).*(lamda).^4)))+k1a* exp(qa).*(I4a-1).*(cos(thetaa  )).^2].*(lamda.^2) ;     %circumferential
stress in the adventitia %
sa2=[c1a.*(1-(1./((lamda.^2).*(l2).^4)))+k1a* exp(qa).*(I4a-1).*(sin(thetaa)).^2].*(l2.^2) ;        %Axial stress in the
adventitia %
%module 4 c: for intima%
I4i=(lamda.^2).*(cos(thetai )).^2+(l2.^2).*(sin(thetai)).^2;
qi=k2i*((I4i-1).^2);
si1=[c1i.*(1-(1./((l2.^2).*(lamda).^4)))+k1i* exp(qi).*(I4i-1).*(cos(thetai )).^2].*(lamda.^2);  %circumferential stress
in the intima  %
```

```
si2=[c1i.*(1-(1./((lamda.^2).*(l2).^4)))+k1i* exp(qi).*(I4i-1).*(sin(thetai )).^2].*(l2.^2);%Axial  stress in the intima %
%module 5: total stress  calculation%
st1=(si1.*hi+sm1.*hm+sa1.*ha)./(h)          %total circumferentioal stress%
st2=(si2.*hi+sm2.*hm+sa2.*ha)./(h);         %total axial stress
```

```
%coronary artery program%
clc;
clear;
% Module 1:data input
D=3.96*1e-03;          %D=wall external diameter
H=(D*0.27) ;           %H= wall thickness
p=[0:12.5:200].*133.32   %transumural pressure
dnew=[3.97 3.995 4.02 4.1 4.18 4.21 4.25 4.28 4.3 4.32 4.33 4.35 4.36 4.37 4.38 4.39 4.4]*1e-03;
l2=1.1;
%Module 2:Thin wall theory
d=(H*(D-H))l2;
b=((dnew.^2./4)-d).^(0.5);
h=(dnew./2)-b;
r=(dnew-h)/2;
R=(D-H)/2;
lamda=r./R;
q=((r./h)-(0.5));
sigma=p.q;
sigma21=sigma./2;
f=[ 0.07 0.072 0.073 0.09 0.13 0.15 0.19 0.23 0.265 0.3 0.32 0.37 0.39 0.41 0.43 0.47 0.54];
B=f./(2.*pi.*r.*h);
s2=((sigma21)+B) ;
%Module 3, assumptions intima=i media=m adventitia=a
hi=0.262*h;
hm=0.349*h;
ha=0.388*h;
a=[1.265,0.2858,1.097,45.4323,8.988,36.082,8795.973,1514.11,7070.2211,6064.528,5713.593,0.6499,0.168,0.7272]

thetai=a(1);
thetam=a(2);
thetaa=a(3)
k2i=a(4);
k2m=a(5);
k2a=a(6);
c1i=a(7);
c1m=a(8);
c1a=a(9);
k1i=a(10);
k1m=a(11);
k1a=a(12);
rowi=a(13);
rowm=a(14);
rowa=a(15);

%Module 4: HYPERELASTIC MODEL%
I4m=(lamda.^2).*(cos(thetam)).^2+(l2.^2).*(sin(thetam )).^2;
qm=k2m*((I4m-1).^2);
sm1=[c1m.*(1-(1./((l2.^2).*(lamda).^4)))+k1m* exp(qm).*(I4m-1).*(cos(thetam )).^2].*(lamda.^2);   %circumferential
stress in the media %
sm2=[c1m.*(1-(1./((lamda.^2).*(l2).^4)))+k1m* exp(qm).*(I4m-1).*(sin(thetam  )).^2].*(l2.^2);      %Axial  stress in
the media  %
%module 4b : for adeventitia %
I4a=(lamda.^2).*(cos(thetaa)).^2+(l2.^2).*(sin(thetaa)).^2;
qa=k2a*((I4a-1).^2);
sa1=[c1a.*(1-(1./((l2.^2).*(lamda).^4)))+k1a* exp(qa).*(I4a-1).*(cos(thetaa  )).^2].*(lamda.^2) ;     %circumferential
stress in the adventitia %
sa2=[c1a.*(1-(1./((lamda.^2).*(l2).^4)))+k1a* exp(qa).*(I4a-1).*(sin(thetaa)).^2].*(l2.^2) ;        %Axial stress in the
adventitia %
%module 4 c: for intima%
I4i=(lamda.^2).*(cos(thetai )).^2+(l2.^2).*(sin(thetai)).^2;
qi=k2i*((I4i-1).^2);
si1=[c1i.*(1-(1./((l2.^2).*(lamda).^4)))+k1i* exp(qi).*(I4i-1).*(cos(thetai )).^2].*(lamda.^2);  %circumferential stress
in the intima  %
```

```
si2=[c1i.*(1-(1./((lamda.^2).*(l2).^4)))+k1i* exp(qi).*(I4i-1).*(sin(thetai )).^2].*(l2.^2);%Axial  stress in the intima %
%module 5: total stress  calculation%
st1=(si1.*hi+sm1.*hm+sa1.*ha)./(h)            %total circumferentioal stress%
st2=(si2.*hi+sm2.*hm+sa2.*ha)./(h);           %total axial stress
%MODEL 6: Results plotting%
figure(3)
plot(lamda,si1/1000,'y',lamda,sm1/1000,'r',lamda,sa1/1000,'b','LineWidth',2,'Marker','o')
xlabel('Circumferential stretch')
ylabel('Circumferential Cauchy stress [kPa]')
figure(4)
plot(lamda,si2/1000,'y',lamda,sm2/1000,'r',lamda,sa2/1000,'b','LineWidth',2,'Marker','o')
xlabel('Circumferential stretch')
ylabel('Axial Cauchy stress [kPa]')
grid
figure(8)
plot(lamda,st1/1000,'r',lamda,sigma/1000,'b',lamda,st2/1000,'g',lamda,s2/1000,'m','LineWidth',2,'Marker','o')
xlabel('Circumferential stretch')
ylabel(' Cauchy stress [kPa]')
grid
%figure(9)
%plot(p/133.32,h,'r')
kai=sum((sigma-st1).^2+(s2-st2).^2);
kai1=(kai/22).^0.5;
sigmaref=sum(st1+st2)/34;
eplson1=kai1/sigmaref
%
bai=sum((sigma-st1).^2);
bai1=(bai/5).^0.5;
bigmaref=sum(st1)/17;
eplsonb=bai1/bigmaref
%kesh kesha mat3rdha 2%
cai=sum((s2-st2).^2);
cai1=(cai/5).^0.5;
cigmaref=sum(st2)/17;
eplsonc=cai1/cigmaref
```